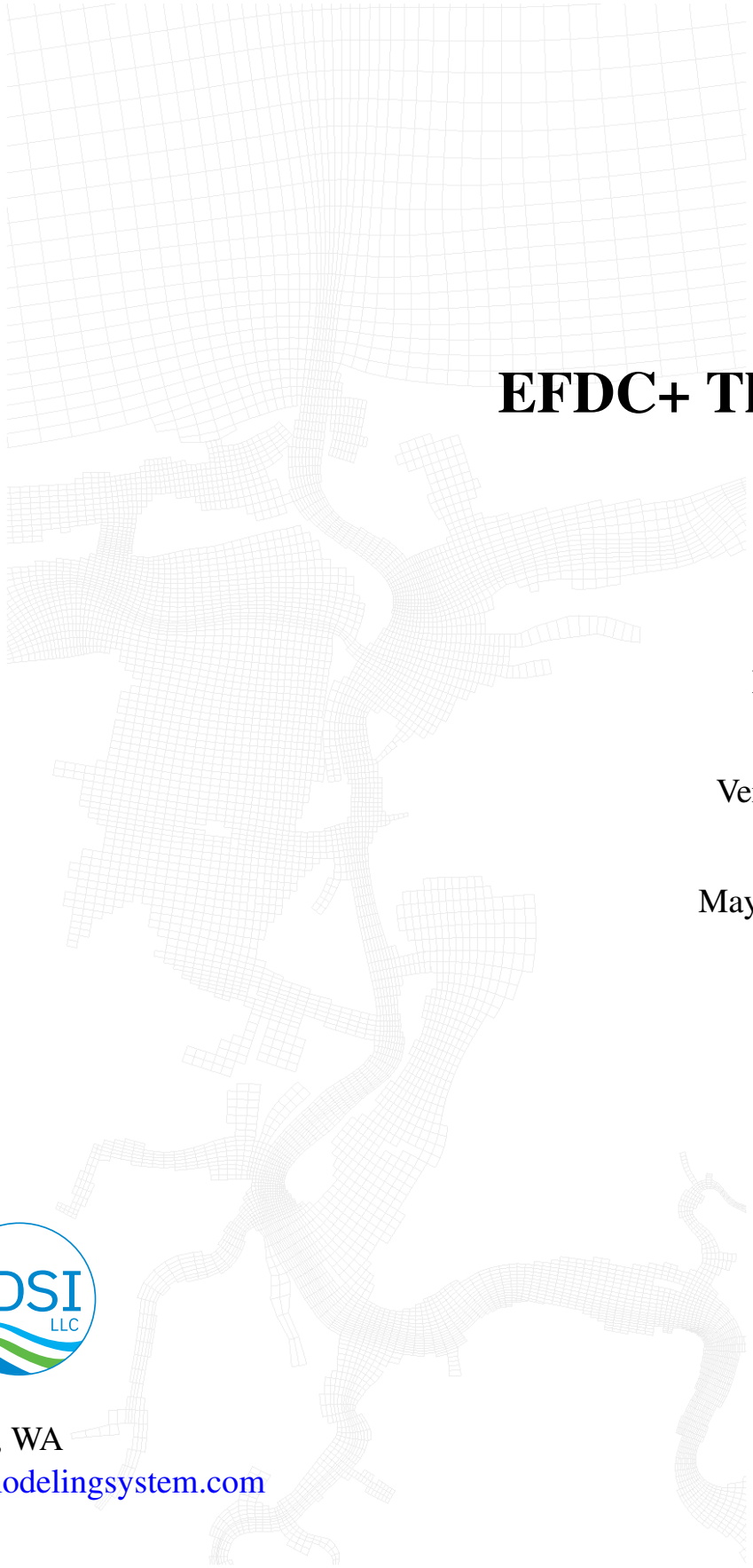

EFDC+ Theory

DSI, LLC

Version 10.2

May 21, 2020

Edmonds, WA
www.eemodelingsystem.com

This page left intentionally blank.

Contents

List of Tables

List of Figures

Chapter 1

INTRODUCTION

The Environmental Fluid Dynamics Code Plus (EFDC+) is an open source, surface water modeling system. EFDC+ encompasses one, two and/or three-dimensional hydrodynamics and water column constituent transport. The hydrodynamics are internally coupled to the multiple modules; sediment erosion/deposition, toxics transport, eutrophication kinetics, sediment diagenesis, oil spill and particle tracking using an integrated, single source code implementation. Worldwide applications in support of environmental assessment, management and regulatory requirements of EFDC+ include hundreds of water bodies such as rivers, lakes, reservoirs, wetlands, estuaries, and coastal ocean regions.

1.1. Development History

EFDC+ is based on the public domain, open source version of EFDC (Hamrick, 1992). EFDC was originally developed at the Virginia Institute of Marine Science (VIMS) and School of Marine Science of The College of William and Mary, by Dr. John M. Hamrick beginning in 1988. The historical evolution of the EFDC model has to a great extent been application driven by a diverse group of EFDC users in the academic, governmental, and private sectors as highlighted in Figure 1.1.

Since 2000, DSI, LLC (DSI) has been providing ongoing enhancement and development of EFDC for various surface water, sediment transport, water and quality projects. This includes adding multiple new features, the theory for which is described in this document. DSIs improvements to the EFDC code had become so extensive that in 2016 the DSI version of EFDC was renamed as EFDC+.

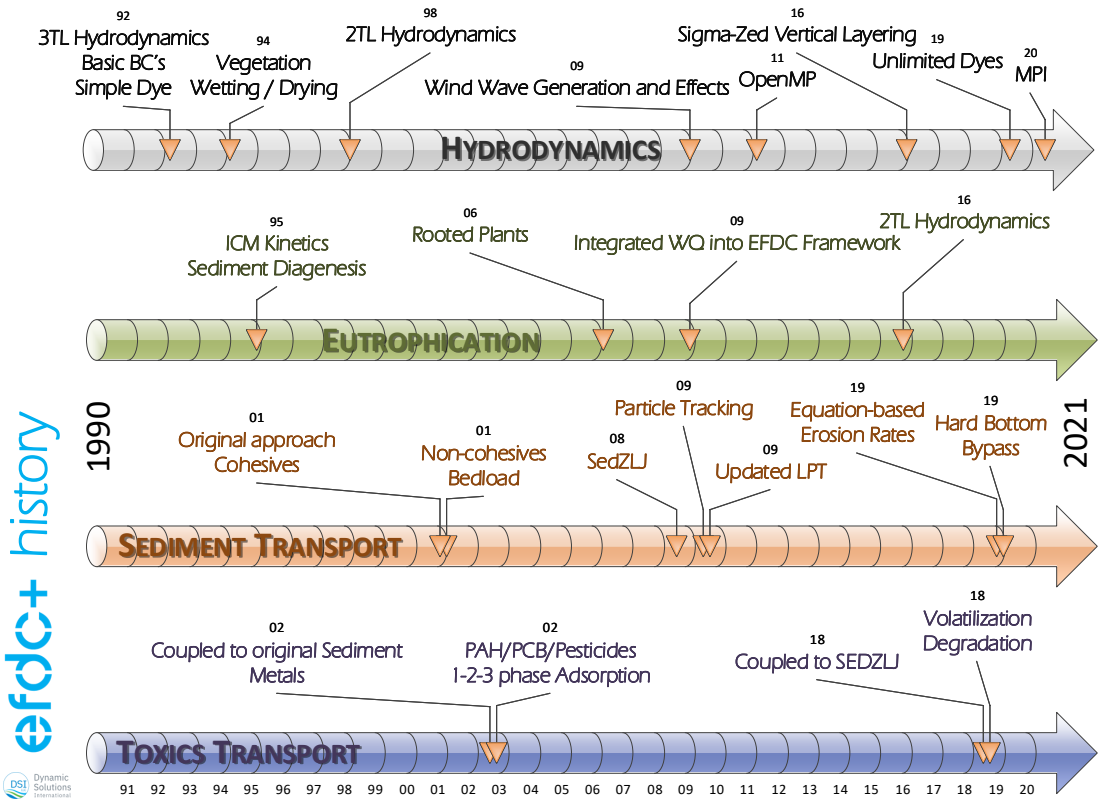

Fig. 1.1. Overview of EFDC+ development history

1.2. EFDC+ Advancements

DSI's EFDC+ code reflects the following key enhancements to the EFDC code:

- **OpenMP - Multithreading:** Integration of OpenMP into the EFDC+ code provides vastly improved model run times. The Intel® OpenMP Runtime Library binds OpenMP threads to physical processing units. EFDC+ typically produces run times up to four times faster on a six-core processor than the conventional single-threaded EFDC model.
- **Dynamic Memory Allocation:** Dynamic allocation eliminates the need to recompile the EFDC+ code for different applications. Previously, due to the limitations of Fortran 77, different maximum array sizes were required to specify the computational grid domain and time series input data sets. Dynamic allocation also helps mitigate array indexing errors and provides better traceability for source code development.
- **Sigma-Zed Layering:** EFDC+ handles the pressure gradient errors that occur in

simulations of models with steep changes in bed elevation. The Sigma-Zed functionality in EFDC+ contrasts the original EFDC code, as the original uses a sigma coordinate transformation in the vertical direction and uses the same number of layers for all cells in the domain. In the EFDC+ Sigma-Zed model, the vertical layering scheme has been modified to allow for the number of layers to vary over the model domain. This approach is computationally efficient and significantly improves the simulation of density stratification.

- **Hydraulic Structures:** Equations governing hydraulic structures such as culverts, weirs, sluice gates, and orifices are implemented in EFDC+. This feature differs from the previous rating curve based approach for a hydraulic structure. Additionally, the modeler can specify rules of operations that depend on the model hydrodynamics.

- **Enhanced Heat Exchange:** EFDC+ includes heat exchange options that use equilibrium temperatures for the water and atmospheric interface, and spatially variable sediment bed temperatures. The eutrophication and sediment transport sub-models water column concentrations are now coupled with the heat submodel by including spatially and temporally varying light extinction.

- **Ice Formation and Melt:** A heat coupled ice formation and melt approach to handle cold climates has been added. Surface processes are controlled by the presence or absence of a dynamically computed ice cover.

- **Multiple Dyes**[1]**:** An unlimited number of user defined dye classes including "Age of Water" can be simulated in EFDC+. Decay and/or growth and settling can be added to any dye class.

- **Lagrangian Particle Tracking (LPT):** An LPT sub-model has been added in EFDC+, that allows for thin and/or tortuous channels, settling, decay and other processes. Oil spill and emergency response simulations are among some of the applications of LPT modeling.

- **SEDZLJ Implementation:** The version of EFDC modified by Sandia National Laboratory (SNL-EFDC+) contains a SEDZLJ model. This model has been further developed in EFDC+ and has undergone significant improvements for mass balance, hard bottom bypass, and computational efficiency. The SEDZLJ model has now been linked to the toxics sub-model.

- **Internal Wind Wave Generation:** A wind generated wave sub-model has been added to EFDC+ to enable the computation of wind wave generated bed shear stress on sediment resuspension and wave induced currents.

[1]This feature is specific to version 10.0 and later.

- **Rooted Plant and Epiphyte Model (RPEM) Module:** A RPEM module has been incorporated into EFDC+ to better simulate water quality interactions with submerged aquatic vegetation (epiphytic algae and macrophytes).
- **External Wave Model Linkage:** Linkage to SWAN (Team, 2019) and other external wave models has been simplified and improved in EFDC+.
- **Marine and Hydro-kinetic (MHK) Linkage:** EFDC+ includes a MHK module for simulation of potential effects of installing and operating turbines and wave energy converters in rivers, tidal channels, ocean currents, and other waterbodies. This code is adapted from SNL-EFDC+ (Grace et al., 2008).
- **Run Continuation:** If the model crashes or the user desires to extend the period of simulation, the EFDC+ model can be configured as a continuation run where the model outputs are seamlessly appended to the previous run.
- **Spatially and Temporally Varying Fields[2]:** Bathymetry and/or other data like roughness and vegetation can be dynamically adjusted during the model run in EFDC+. This allows for dredging scenarios and seasonal vegetation patterns.
- **NetCDF:** EFDC+ can output results in NetCDF file formats for model analysis in other programs.
- **High Frequency Output:** New output snapshot controls are available to target specific periods for high frequency output within the standard regular output frequency.
- **Streamlining:** The code has been converted to Fortran 90 and streamlined for quicker execution times.
- **Model Linkages:** Customized linkage of model results for the Windows-based EFDC_Explorer graphical pre- and post-processor for EFDC+.

1.3. EFDC+ Overview

The EFDC+ is a general-purpose modeling package for simulating three-dimensional (3-D) flow, transport, and biogeochemical processes in surface water systems including: rivers, lakes, estuaries, reservoirs, wetlands, and near-shore to shelf-scale coastal regions. Special enhancements to the hydrodynamics of the code include vegetation resistance, drying and wetting, hydraulic structure representation, wave current boundary layer interaction, and wave-induced currents, refined modeling of wetland and marsh systems, controlled-flow systems, and near-field and far-field discharge dilution from multiple sources.

The structure of the EFDC+ model contains many modules, each of which is highlighted in Figure 1.2.

[2]This feature is specific to version 10.0 and above,

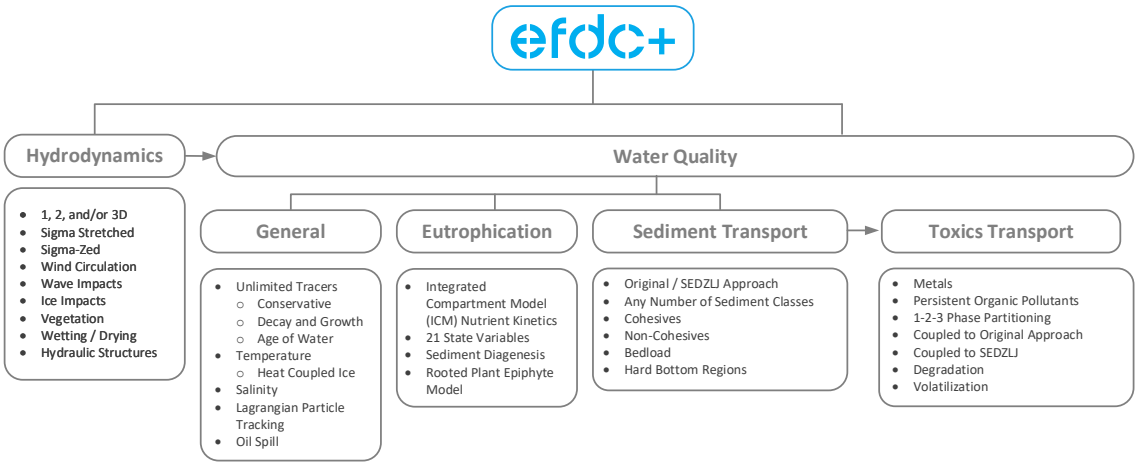

Fig. 1.2. Primary modules of the EFDC+ model.

1.3.1 Hydrodynamics

The EFDC+ hydrodynamic model simulates near field plume, wind generated and externally linked wave models. In the hydrodynamics, temperature and salinity are optionally incorporated to address density effects. The hydrodynamic model is linked to sub models such as dye/age of water, sediments, toxics, water quality and Lagrangian particle tracking as highlighted in Figure 1.2. EFDC+ is a coupled model which solves both the hydrodynamics, transport, and kinetics in an integrated code, thus eliminating the need for external coupling between hydrodynamics and transport modules.

1.3.2 Sediment Transport Modules

EFDC+ supports two separate erosion/deposition approaches:

1. Original EFDC Sediment Transport
2. SEDZLJ Sediment Transport

Both approaches treat the water column transport the same way. The differences in these two approaches are in the way the water column sediment interacts with the sediment bed, i.e. erosion and/or deposition and in the treatment of the sediment bed itself. The first approach is referred to as the “original” sediment transport option, which was added by Hamrick. This approach simulates transports and fate of multiple size classes of cohesive and non-cohesive suspended sediment including bed deposition and resuspension (see Figure 1.2). The SEDZLJ approach (Ji, 2008) uses bed shear and erosion rate data developed from testing sediment cores with the SEDFlume apparatus.

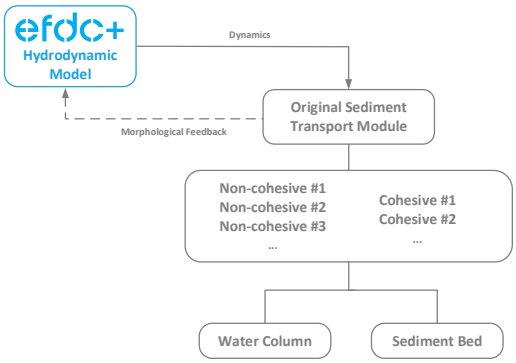

Fig. 1.3. Structure of the original sediment transport model.

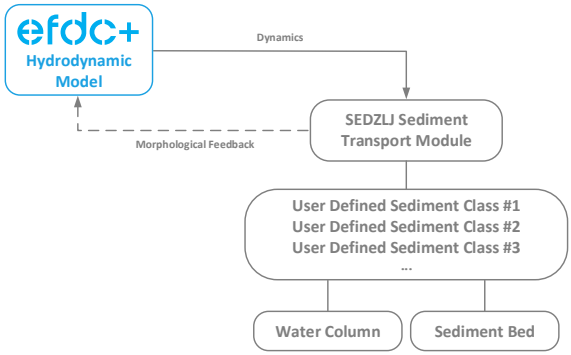

Fig. 1.4. Structure of the EFDC+ SEDZLJ sediment transport model.

1.3.3 Toxics Fate and Transport Module

When the "original" sediment transport capability was added toxic contaminant transport was also added (Tech, 2002). This module allows for optional toxic contaminant partitioning onto water column and sediment bed solids. Prior to 2015, even though multiple partitioning options were available, only one approach could be used for all the toxics included in a simulation. DSI updated the toxic partitioning module to allow each toxic constituent to use its own unique partitioning approach. Figure 1.5 provides a schematic of the basic model approach.

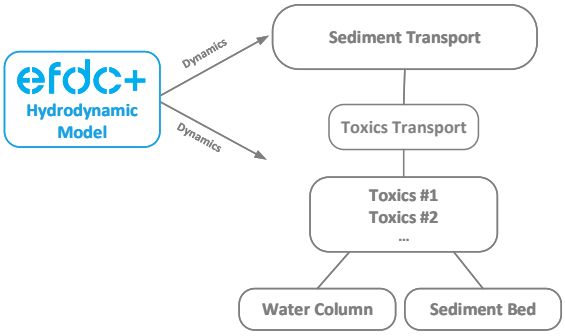

Fig. 1.5. Linkage between hydrodynamic, sediment transport and toxics model.

1.3.4 Lagrangian Particle Tracking Module

Lagrangian Particle Tracking (LPT) was developed as a practical tool for predicting the transport of discrete particles in a system. Specific applications include the tracking of:

1. Floating objects in rivers, lakes and the sea in general

2. Oil spills

3. Particles or water from a specific source

The advantage of this approach is that it is possible to track the progressive movements of each specific particle in greater detail and accurately in comparison with the method of determining average concentration for grid cells. This process is computationally expensive. However, as the computing capacity is getting cheaper, it is getting easier to simulate these models. The movement of solid particles is decided by a field of fluid velocity; therefore, it is necessary to couple it to a fluid flow model.

1.4. Conclusion

EFDC+ is an open source, surface water modeling system developed by DSI, LLC, and is built upon the original EFDC software developed by Hamrick (1992). EFDC+ includes many new features and bug fixes over the original EFDC code. This document describes these new features and provides an overview of the mathematical details in all modules available in EFDC+.

1.4.1 Eutrophication Module

In 1995, a eutrophication sub-model with full sediment diagenesis (Park et al., 1995) was added to EFDC+. The original version of this coupled water quality model was called Hydrodynamic Eutrophication Model Three Dimensional (HEM3D). This original eutrophication model allowed the simulation of 21 state variables. In 2000 the model was modified to include "macroalgae" (Tech et al., 2007). The model simulates spatial and temporal distributions of water quality parameters including dissolved oxygen, suspended algae (three groups), various components of carbon, nitrogen, phosphorus and silica cycles, and fecal coliform bacteria. A sediment diagenesis process model with 27 state variables was also developed for EFDC+. The coupling of the sediment diagenesis model with the water quality model not only enhances the model's predictive capability of water quality parameters but also enables it to simulate the long-term changes in water quality conditions in response to changes in nutrient loadings.

1.4.2 Lagrangian Particle Tracking Module

Lagrangian Particle Tracking (LPT) was developed as a practical tool for predicting the transport of discrete particles in a system. Specific applications include the tracking of:

1. Floating objects in rivers, lakes and the sea in general

2. Oil spills

3. Particles or water from a specific source

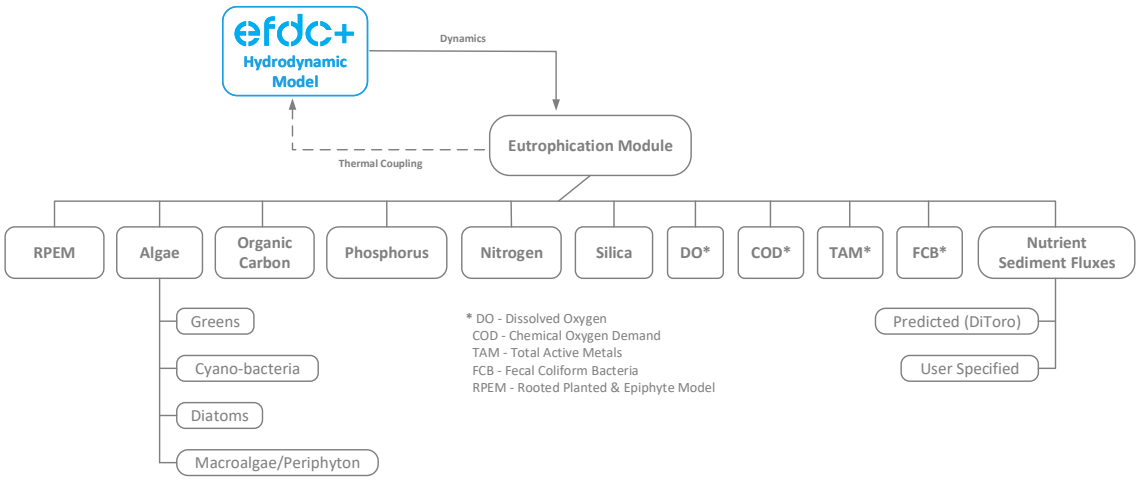

Fig. 1.6. Structure of the EFDC+ water quality model.

The advantage of this approach is that it is possible to track the process of movement for each specific particle in more detail and more accurately in comparison with the method of determining average concentration for grid cells. The unique difficulty for this approach is that when the number of particles is too large due to LPT depending on the speed of computational processing as well as the large amount of memory to be distributed for the variables. Fortunately, nowadays the development of information technology both on hardware and software is considerable and such a problem is completely possible to solve quickly, especially performing calculations in parallel using multi-core processors . The movement of solid particles is decided by a field of fluid velocity; therefore, it is necessary to couple it to a fluid flow model., LLCtprovides an overview of in all available

Chapter 2

HYDRODYNAMICS

The section is primarily based on Hamrick (1992) and Ji (2008) with updates from DSI and others. The basic governing equations for the EFDC+ hydrodynamics are presented and discussed. The primary sources used for this document are:

1. A Three-Dimensional Environmental Fluid Dynamics Computer Code: Theoretical and Computational Aspects (Hamrick, 1992).
2. A User's Manual for the Environmental Fluid Dynamics Computer Code (EFDC), (Hamrick, 1996).
3. A Three-dimensional Hydrodynamic-Eutrophication model (HEM3D): Description of Water Quality and Sediment Processes Submodels (Park et al., 1995).
4. Theoretical and Computational Aspects of Sediment and Contaminant Transport in the EFDC+ Model (Tech et al., 2002).
5. Sandia National Laboratories Environmental Fluid Dynamics Code: Sediment Transport User Manual (Grace et al., 2008).

2.1. Governing Equations

The fundamental principles of the hydrodynamic model in EFDC+ are the laws of conservation for mass, momentum and energy for the flows. With the basic assumption that ambient environmental flows are characterized by horizontal length scales which are orders of magnitude greater than their vertical length scales, the formulation of the governing equations begins with the vertically hydrostatic, boundary layer form of the turbulent equations of motion for an incompressible, variable density fluid. The governing equations of EFDC+ include Navier-Stokes for fluid flow, the advection-diffusion equations for salinity, temperature, dye, toxicants, eutrophication constituents and suspended sediment transport (Hamrick and Wu, 1997; Hamrick, 1992, 1996). In the horizontal direction, the equations are presented in the curvilinear coordinate system and sigma or sigma-Zed (Craig et al.,

2014) transformation (at the bed and at the water surface) for the vertical direction. They are discretized with the finite difference method based on an explicit scheme. Figure 2.1 shows the basic concepts of the EFDC+ model domain.

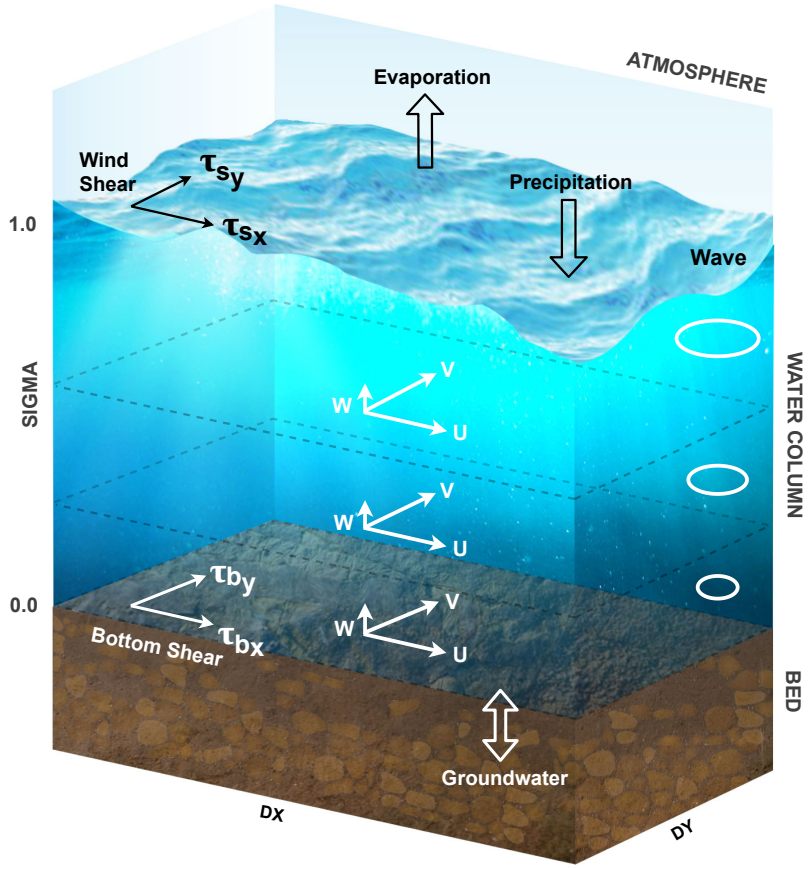

Fig. 2.1. Conceptual overview of the EFDC+ model.

2.1.1 Horizontal and Vertical Coordinate Systems

To accommodate realistic horizontal boundaries, it is convenient to formulate the equations such that the horizontal coordinates, x and y, are curvilinear and orthogonal.

To provide uniform resolution in the vertical direction, aligned with the gravitational vector and bounded by bottom topography and a free surface permitting long wave motion, a time variable mapping or stretching transformation is desirable. The mapping or stretching is given by

$$z = \frac{z^* + h}{\zeta + h} = \frac{z^* + h}{H} \tag{2.1}$$

where

z is the sigma coordinate (dimensionless)

z^* is the vertical coordinate with respect to the vertical reference level (datum) (m)

h is the water depth bellow the vertical reference level (m)

ζ is the water surface elevation above the vertical reference level (m)

and Figure 2.2 provides a schematic of the vertical coordinate system in the physical space in the left panel and the sigma space in the right panel.

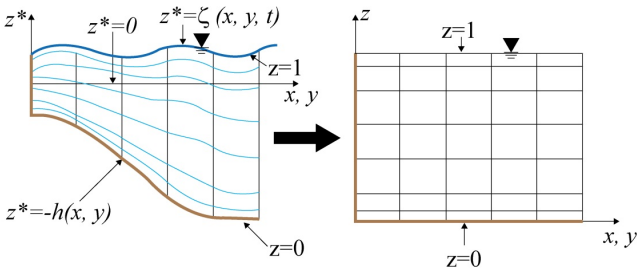

Fig. 2.2. The stretched vertical coordinate system.

EFDC+ supports sigma stretched and sigma-zed (SGZ) grids for the vertical discretization of water column. Details of the sigma transformation may be found in Blumberg and Mellor (1987); Hamrick (1986); Vinokur (1974). Details on the sigma-zed vertical layering options are described in Section 2.1.1.

2.1.2 Basic Hydrodynamic Equations

Transforming the vertically hydrostatic boundary layer form of the turbulent equations of motion and utilizing the Boussinesq approximation for variable density results in the momentum and continuity equations and the transport equations for salinity and temperature in the following form:

The momentum equation in the x direction:

$$\begin{aligned}
&\frac{\partial}{\partial t}(m_x m_y H u)+\frac{\partial}{\partial x}(m_y H u u)+\frac{\partial}{\partial y}(m_x H v u)+\frac{\partial}{\partial z}(m_x m_y w u)\\
&-m_x m_y f H v-\left(v\frac{\partial}{\partial m_y}x-u\frac{\partial m_x}{\partial y}\right)H\\
=&-m_y H\frac{\partial}{\partial x}(g\zeta+p+P_{atm})-m_y\left(\frac{\partial h}{\partial x}-z\frac{\partial H}{\partial x}\right)\frac{\partial p}{\partial z}+\frac{\partial}{\partial x}\left(\frac{m_y}{m_x}HA_H\frac{\partial u}{\partial x}\right)\\
&+\frac{\partial}{\partial y}\left(\frac{m_x}{m_y}HA_H pd[u]y\right)+\frac{\partial}{\partial z}\left(\frac{m_x m_y}{H}A_v\frac{\partial u}{\partial z}\right)-m_x m_y c_p D_p u\sqrt{u^2+v^2}+S_u
\end{aligned}\tag{2.2}$$

The momentum equation in the y direction:

$$\begin{aligned}
&\frac{\partial}{\partial t}(m_x m_y H v) + \frac{\partial}{\partial x}(m_y H u v) \\
&+ \frac{\partial}{\partial y}(m_x H v v) + \frac{\partial}{\partial z}(m_x m_y w v) + m_x m_y f H u + \left(v\frac{\partial m_y}{\partial x} - u\frac{\partial m_x}{\partial y}\right) H u \\
&= -m_x H \frac{\partial}{\partial y}(g\zeta + p + P_{atm}) - m_x\left(\frac{\partial h}{\partial y} - z\frac{\partial H}{\partial y}\right)\frac{\partial p}{\partial z} + \frac{\partial}{\partial x}\left(\frac{m_y}{m_x} H A_H \frac{\partial v}{\partial x}\right) \\
&+ \frac{\partial}{\partial y}\left(\frac{m_x}{m_y} H A_H \frac{\partial v}{\partial y}\right) + \frac{\partial}{\partial z}\left(\frac{m_x m_y}{H} A_v \frac{\partial v}{\partial z}\right) - m_x m_y c_p D_p v\sqrt{u^2+v^2} + S_v
\end{aligned} \tag{2.3}$$

The momentum equation in the z direction:

$$\frac{\partial p}{\partial z} = -gH\frac{\rho - \rho_0}{\rho_0} = -gHb \tag{2.4}$$

The continuity equations (internal and external modes)

$$\frac{\partial}{\partial t}(m_x m_y \zeta) + \frac{\partial}{\partial x}(m_y H u) + \frac{\partial}{\partial y}(m_x H v) + \frac{\partial}{\partial z}(m_x m_y w) = S_h \tag{2.5}$$

$$\frac{\partial}{\partial t}(m_x m_y \zeta) + \frac{\partial}{\partial x}(m_y H U) + \frac{\partial}{\partial y}(m_x H V) = S_h \tag{2.6}$$

The equation of state

$$\rho = \rho(p, S, T, C) \tag{2.7}$$

where

$$U = \int_0^1 u dz, \quad V = \int_0^1 v dz \tag{2.8}$$

$$P = m_y H u, \quad Q = m_x H v \tag{2.9}$$

and

- u, v are the horizontal velocity components in the curvilinear coordinates (m/s)
- x, y are the orthogonal curvilinear coordinates in the horizontal direction (m)
- z is the sigma coordinate (dimensionless)
- t is time (s)
- m_x, m_y are the square roots of the diagonal components of the metric tensor (m)
- m is the Jacobian, $m = m_x m_y (m^2)$
- p is the physical pressure in excess of the reference density hydrostatic pressure (m^2/s^2)
- P_{atm} is the barotropic pressure (Pa)

ρ_o is the reference water density (kg/m^3)

b is the buoyancy

f is the Coriolis parameter (1/s)

A_H is the horizontal momentum and mass diffusivity (m^2/s)

A_v is the vertical turbulent eddy viscosity (m^2/s)

c_p is the vegetation resistance coefficient (dimensionless)

D_p is the projected vegetation area normal to the flow per unit horizontal area (dimensionless)

S_u, S_v are the source/sink terms for the horizontal momentum in the x and y directions, respectively (m^2/s^2)

S_h is the source/sink terms for the mass conservation equation (m^3/s)

S is salinity (ppt)

T is temperature (°C)

C is total inorganic suspended solids (TSS) (g/m^3),

U, V are the depth averaged velocity components in the x and y directions, respectively (m/s)

P, Q are the mass flux components in the x and y directions, respectively (m^2/s).

The vertical velocity, with physical units, in the stretched, dimensionless vertical coordinate z is:

$$w = w^* - z\left(\frac{\partial \zeta}{\partial t} + \frac{u}{m_x}\frac{\partial \zeta}{\partial x} + \frac{v}{m_y}\frac{\partial \zeta}{\partial y}\right) + (1-z)\left(\frac{u}{m_x}\frac{\partial h}{\partial x} + \frac{v}{m_y}\frac{\partial h}{\partial y}\right) \tag{2.10}$$

where,

w is the vertical velocity component in sigma coordinate (m/s)

w^* is the physical vertical velocity (m/s).

The pressure p is the physical pressure in excess of the reference density hydrostatic pressure, $\rho_o g H(1-z)$, divided by the reference density, ρ_o. In the momentum equation (2.2) and (2.3) the momentum source/sink terms S_u and S_v will be later modeled as subgrid scale horizontal diffusion. The density ρ is in general a function of temperature T and salinity S for hydrospheric flows and water vapor for atmospheric flows. Density can be a weak function of pressure but will be treated as an incompressible fluid in the continuity equation under the anelastic approximation (Clark and Hall, 1991; Mellor, 1991). The buoyancy b as defined in equation (2.4), is the normalized deviation of density from the reference value. The continuity equation (2.5) has been integrated with respect to z over the

interval $(0,1)$ to produce the depth integrated continuity equation (2.6) using the vertical boundary conditions, $w = 0$, at $z = (0,1)$, which follows from the kinematic conditions and equation (2.8). It is noted that constraining the free surface displacement to be time independent and spatially constant, yields the equivalent of the rigid lid ocean circulation equations employed by Semtner Jr (1974) and equations similar to the terrain following equations used by Clark (1977) to model mesoscale atmospheric flow.

2.1.3 Equation of State

In case the water density is dependent on temperature and salinity, the UNESCO's equation of state reads

$$\begin{aligned}\rho =& 999.842594 + 6.793952\times10^{-2}T - 9.095290\times10^{-3}T^2 \\ &+ 1.001685\times10^{-4}T^3 - 1.120083\times10^{-6}T^4 + 6.536332\times10^{-9}T^5 \\ &+ \Big(0.824493 - 4.0899\times10^{-3}T + 7.6438\times10^{-5}T^2 \\ &\quad - 8.2467\times10^{-7}T^3 + 5.3875\times10^{-9}T^4\Big)S \\ &+ \Big(-5.72466\times10^{-3} + 1.0227\times10^{-4}T - 1.6546\times10^{-6}T^2\Big)S^{1.5} + 4.8314\times10^{-4}S^2\end{aligned} \tag{2.11}$$

where

ρ is the water density (kg/m^3)

T is the water temperature (°C)

S is the water salinity (ppt)

With the presence of sediment in the water column, the water density and the buoyancy are corrected using a correction factor. The correction factor for the water density is

$$C_{TSS} = 1 - \sum_j^N \rho_{s,j} C_j + \sum_j^N \left(s_j - 1\right) \rho_{s,j} C_j \tag{2.12}$$

where

C_{TSS} is the correction factor that considers the influence of sediment on water density (dimensionless)

$\rho_{s,j}$ is the sediment density of the sediment class j (kg/m^3)

C_j is the concentration of the sediment class j (g/m^3)

s_j is the specific gravity of the sediment class j (dimensionless)

N is the number of sediment classes

2.1.4 Vertical Turbulent Closure

The system of eight equations from equations (2.2) to (2.10) provides a closed system for the variables u, v, w, p, ζ, ρ, and C, provided that the vertical turbulent viscosity and diffusivity, and the source and sink terms are specified. To provide the vertical turbulent viscosity and diffusivity, the second moment turbulence closure model developed by Mellor and Yamada (1982) and modified by Galperin et al. (1988) can be used. The model relates the vertical turbulent viscosity and diffusivity to the turbulent intensity (q) and a turbulent length scale (l), and a Richardson number R_q by:

The vertical turbulent momentum diffusion coefficient is:

$$A_v = \phi_A A_0 q l, \tag{2.13}$$

where ϕ_A is the stability viscosity coefficient and can be defined as:

$$\phi_A = \frac{\left(1 + R_q/R_1\right)}{\left(1 + R_q/R_2\right)\left(1 + R_q/R_3\right)} \tag{2.14}$$

Additionally, the following definitions for variables in equations (2.13) and (2.14) are given as:

$$A_0 = A_1\left(1 - 3C_1 - \frac{6A_1}{B_1}\right) = \frac{1}{B_1^{1/3}} \tag{2.15}$$

$$\frac{1}{R_1} = 3A_2\frac{\left(B_2 - 3A_2\right)\left(1 - \frac{6A_1}{B_1}\right) - 3C_1\left(B_2 + 6A_1\right)}{1 - 3C_1 - \frac{6A_1}{B_1}} \tag{2.16}$$

$$\frac{1}{R_2} = 9A_1A_2 \tag{2.17}$$

$$\frac{1}{R_3} = 3A_2\left[6A_1 + B_2\left(1 - C_3\right)\right]. \tag{2.18}$$

The vertical mass diffusion coefficient is defined as:

$$A_b = \rho_K K_0 q l \tag{2.19}$$

where ϕ_K is the stability diffusivity coefficient given by

$$\phi_K = \frac{1}{\left(1 + R_q/R_3\right)} \tag{2.20}$$

and K_0 is the dimensionless coefficient:

$$K_0 = A_2\left(1 - \frac{6A_1}{B_1}\right) \tag{2.21}$$

The Richardson number is found with the following equation

$$R_q = \frac{gH}{q^2}\frac{l^2}{H^2}\frac{\partial b}{\partial z} \tag{2.22}$$

where

q^2 is the turbulent intensity (m^2/s^2)

l is the turbulent length scale (m)

R_q is the Richardson number

Mellor and Yamada (1982) specify the constants $A_1 = 0.92$, $B_1 = 16.6$, $C_1 = 0.08$, $A_2 = 0.74$, and $B_2 = 10.1$. However, the values of R_1, R_2, R_3 calculated by Galperin et al. (1988) and Kantha and Clayson (1994) are different from Mellor and Yamada (1982) as in Table 2.1.

Table 2.1. Parameters for different turbulent models.

Formulation	K_0	R_1^{-1}	R_2^{-1}	R_3^{-1}
Mellor and Yamada (1982)	0.493928	7.846436	34.676400	6.127200
Galperin et al. (1988)	0.493928	7.760050	34.676440	6.127200
Kantha and Clayson (1994)	0.493928	8.679790	30.192000	6.127200
Kantha (2003)	0.490025	14.509100	24.388300	3.236400

The so-called stability functions ϕ_A and ϕ_K account for the reduced and enhanced vertical mixing or transport in stable and unstable vertically density stratified environments, respectively. The turbulence intensity and the turbulence length scale are determined by a pair of Mellor and Yamada (1982) equations:

$$\begin{aligned}&\frac{\partial}{\partial t}\left(mHq^2\right)+\frac{\partial}{\partial x}\left(Pq^2\right)+\frac{\partial}{\partial y}\left(Qq^2\right)+\frac{\partial}{\partial z}\left(mwq^2\right)\\&=\frac{\partial}{\partial z}\left(m\frac{A_q}{H}\frac{\partial q^2}{\partial z}\right)2m\frac{A_v}{H}\left[\left(\frac{\partial u}{\partial z}\right)^2+\left(\frac{\partial v}{\partial z}\right)^2\right]+2mgA_b\frac{\partial b}{\partial z}-2m\frac{Hq^3}{B_1 l}+S_b\end{aligned} \tag{2.23}$$

$$\begin{aligned}&\frac{\partial}{\partial t}\left(mHq^2l\right)+\frac{\partial}{\partial x}\left(Pq^2l\right)+\frac{\partial}{\partial y}\left(Qq^2l\right)+\frac{\partial}{\partial z}\left(mwq^2l\right)\\&=\frac{\partial}{\partial z}\left[m\frac{A_{ql}}{H}\frac{\partial}{\partial z}\left(q^2l\right)\right]+mlE_1\left\{\frac{A_v}{H}\left[\left(\frac{\partial u}{\partial z}\right)^2+\left(\frac{\partial v}{\partial z}\right)^2\right]+E_3gA_b\frac{\partial b}{\partial z}\right\}\\&-mE_2\frac{Hq^3}{B_1}\left[1+E_4\left(\frac{l}{\kappa Hz}\right)^2+E_5\left(\frac{l}{\kappa H(1-z)}\right)^2\right]+S_l\end{aligned} \tag{2.24}$$

$$\frac{1}{L} = \frac{1}{H}\left(\frac{1}{z} + \frac{1}{1-z}\right), \tag{2.25}$$

where

$E_1 = 1.8,\ E_2 = 1.0,\ E_3 = 1.8,\ E_4 = 1.33,$ and $E_5 = 0.25$ are empirical constants

S_q is the source-sink term for turbulent intensity equation

S_l is the source-sink term for turbulent length scale equation

A_q is the vertical turbulent diffusivity for turbulent intensity equation

A_{ql} is the vertical turbulent diffusivity for turbulent length scale equation.

The vertical diffusivity for turbulence intensity, A_q, is set to $0.2ql$ following Mellor and Yamada (1982). For stable stratification, Galperin et al. (1988) suggested limiting the length scale such that the square root of R_q is less than 0.52. When horizontal turbulent viscosity, A_H and diffusivity are included in the momentum and transport equations, they are determined independently using Smagorinsky (1963) subgrid scale closure formulation:

$$A_H = \Delta x \Delta y \sqrt{\left(\frac{\partial u}{\partial x}\right)^2 + \left(\frac{\partial v}{\partial y}\right)^2 + \frac{1}{2}\left(\frac{\partial u}{\partial y} + \frac{\partial v}{\partial x}\right)^2}, \tag{2.26}$$

where $\Delta x,\ \Delta y$ are the grid sizes in x and y directions, respectively.

The terms S_q and S_l may represent additional source-sink terms such as subgrid scale horizontal turbulent diffusion, wave, and vegetation effects.

2.2. Boundary Conditions and External Forcings

The vertical boundary conditions for the solution of the momentum equations (2.2)-(2.3) are based on the specification of the kinematic shear stresses at the free water surface and at the bed.

Vertical boundary conditions for the turbulent kinetic energy and length scale equations are:

$$q^2 = B_1^{2/3}\sqrt{t_{sx}^2 + t_{sy}^2}, \quad l = 0, \text{ at } z = 1 \tag{2.27}$$

$$q^2 = B_1^{2/3}\sqrt{t_{bx}^2 + t_{by}^2}, \quad l = 0, \text{ at } z = 0 \tag{2.28}$$

Equation (2.28) can become inappropriate under several conditions associated with high near bottom sediment concentrations and/or high frequency surface wave activity.

2.2.1 Bottom Friction

At the bed, the stress components are related to the near bed or bottom layer velocity components by the quadratic resistance formulation:

$$\frac{1}{\rho}\begin{bmatrix}\tau_{xz}\\ t_{yz}\end{bmatrix}=\frac{1}{\rho}\begin{bmatrix}t_{bx}\\ t_{by}\end{bmatrix}=C_b\sqrt{u_1^2+v_1^2}\begin{bmatrix}u_1\\ v_1\end{bmatrix} \tag{2.29}$$

where the subscript 1 denotes bottom layer values. Under the assumption that the near bottom velocity profile is logarithmic at any instant of time, the bottom stress coefficient is given by Nezu (1993).

$$C_b=\left[\frac{\kappa}{\ln(\Delta_1/2z_0)+(\Pi-1)}\right]^2 \tag{2.30}$$

where,

κ is von Karman constant,

Δ_1 is dimensionless thickness of the bottom layer,

$z_o=z_o*/H$ is dimensionless roughness height, and

Π is wake strength parameter. Π varies from 0 at low Reynolds numbers to 0.2 with fully turbulent flow. The Π is assumed to be 0.0.

2.2.2 Vegetation

The vegetation impacts on the turbulent intensity and the turbulent length scale are determined by the transport equations:

$$\begin{aligned}&\partial_t(m_xm_yHq^2)+\partial_x(m_yHuq^2)+\partial_y(m_xHvq^2)+\partial_z(m_xm_ywq^2)\\ =&\partial_z(m_xm_y\frac{A_q}{H}\partial_zq^2)-2m_xm_y\frac{Hq^3}{B_1l}\\ &+2m_xm_y\left(\frac{A_v}{H}\left((\partial_zu)^2+(\partial_zv)^2\right)+gK_v\partial_zb+\partial_pc_pD_p\left(u^2+v^2\right)^{3/2}\right)+Q_q\end{aligned} \tag{2.31}$$

$$\begin{aligned}&\partial_t(m_xm_yHq^2l)+\partial_x(m_yHuq^2l)+\partial_y(m_xHvq^2l)+\partial_z(m_xm_ywq^2l)\\ =&\partial_z\left(m_xm_y\frac{A_{ql}}{H}\partial_z\left(q^2l\right)\right)-m_xm_yE_2\frac{Hlq^3}{lB_1}\left(1+E_4\left(\frac{l}{\kappa Kz}\right)^2+E_5\left(\frac{l}{\kappa H\left(1-z\right)}\right)^2\right)\\ &+m_xm_yl\left(E_1\frac{A_v}{H}\left((\partial_zu)^2+(\partial_zv)^2\right)+E_3gK_v\partial_zb+E_1\eta_pc_pD_p\left(u^2+v^2\right)^{3/2}\right)+Q_l\end{aligned} \tag{2.32}$$

where $(E1, E2, E3, E4, E5) = (1.8, 1.0, 1.8, 1.33, 0.25)$. The second term on the last line of equations (2.31) and (2.32) represents net turbulent energy production by vegetation drag where ν_p is a production efficiency factor having a value less than one. The terms Q_q and Q_l may represent additional source-sink terms such as subgrid scale horizontal turbulent diffusion. The vertical diffusivity, A_q is set to 0.2ql following Mellor and Yamada (1982). For stable stratification, Galperin et al. (1988) suggested limiting the length scale such that the square root of R_q is less than 0.52. When horizontal turbulent viscosity and diffusivity are included in the momentum and transport equations, they are determined independently using Smagorinsky (1963) subgrid scale closure formulation.

2.2.3 Wind Forcings

The influence of wind on hydrodynamics are due to the wind shear stresses exerted on the water surface. At the free surface, the x and y components of the stress are specified by the wind stress:

$$\frac{1}{\rho}\begin{bmatrix} \tau_{xz} \\ t_{yz} \end{bmatrix} = \frac{1}{\rho}\begin{bmatrix} t_{sx} \\ t_{sy} \end{bmatrix} = C_D \frac{\rho_a}{\rho} W_s \begin{bmatrix} U_w \\ V_w \end{bmatrix} \tag{2.33}$$

$$W_s = \sqrt{U_w^2 + V_w^2} \tag{2.34}$$

where

W_s, U_w and V_w are the wind velocity and $x-$ and $y-$ components of the wind velocity (m/s) at 10 meters above the water surface, respectively,

C_D is the wind drag coefficient, and

ρ_a and ρ_w are air and water densities, respectively.

EFDC+ provides three options for wind drag. In case of magnitude sheltering and no directional sheltering, the original wind drag coefficient can be calculated as

$$C_D = \begin{cases} 3.83111\times10^{-5}W_s^{-3} - 0.000308715W_s^{-2} \\ \quad +0.00116012W_s^{-1} + 0.000899602, & W_s < 5m/s \\ -5.37642\times10^{-6}W_s^3 + 0.000112556W_s^2 \\ \quad -0.000721203W_s + 0.00259657, & 5m/s = W_s < 7m/s \\ -3.99677\times10^{-7}W_s^2 + 7.32937\times10^{-5}W_s \\ \quad +0.000726716, & W_s = 7m/s \end{cases} \tag{2.35}$$

A second option is from European Centre for Medium-Range Weather Forecasts (ECMWF) which has determined a wind speed-dependent drag coefficient based on the wave age-dependent surface roughness computed with their coupled atmospheric wave model (Hersbach, 2011). The wind speed-dependent formulation is given by

$$C_{DN} = [c_1 + c_2 (U_{10N})^{p_1}] / (U_{10N})^{p_2} \tag{2.36}$$

where $c_1 = 1.03x10^{-3}$, $c_2 = 0.04x10^{-3}$, $p_1 = 1.48$, and $p_2 = 0.21$.

2.2.4 Wave Action

The action of short waves on the field velocity of flow in a large water body could be an important aspect that may not be ignored, especially in estuaries and coastal areas. As is commonly known, both longshore currents and undertow are generated by waves. The asymmetry of wave velocity in its orbital plane is one of the causes of mass transport, such as sediment. Waves may be generated either by local wind or by distant storms with longer time periods. In this document, wind-induced wave theory is presented as applied in EFDC+. In EFDC+, there are two options to include wave effects; 1) by an internal wind-generated waves sub-model inside EFDC+, and 2) by providing wave parameters are computed by an external wave model such as SWAN (Team, 2019), REF/DIF (Kirby et al., 1994), and STWAVE (Smith et al., 2001).

In the case of waves, apart from the forces from currents, it is also necessary to add the forces from waves for the whole water column, such as radiation stresses or stresses due to the roller in breaking waves (Mengguo and Chongren, 2003). However, EFDC+ only considers radiation stresses. The additional wave-induced momentum exerted on the flow field can be accounted for through wave radiation stresses (Longuet-Higgins and Stewart, 1964):

$$S_{xx} = n\cos^2\theta + n - \frac{1}{2}E \tag{2.37}$$

$$S_{xy} = S_{yx} = (n\cos\theta\sin\theta)\,E \tag{2.38}$$

$$S_{yy} = n\sin^2\theta + n - \frac{1}{2}E \tag{2.39}$$

where

S_{xx}, S_{xy}, S_{yx}, S_{yy} are the components of wave radiation stresses

E is the wave energy (kg/s^2)

$$E = \frac{1}{8}\rho g H_S^2 \tag{2.40}$$

where

H_s is the wave height (m)

θ is the radian measure of the wave direction angle with respect to the x axis (counterclockwise)

k is the wave number

$$k = \frac{2\pi}{L} \tag{2.41}$$

where

L is the wavelength (m)

C is the wave celerity (m/s)

and

$$n = \frac{1}{2}\left[1 + \frac{2kH}{\sinh(2kH)}\right] \tag{2.42}$$

In general, the wavelength, L (m), can be computed by solving the non-linear equation for the dispersion relation shown in equation (2.43).

$$L = \frac{gT^2}{2p}\tanh\left(\frac{2p}{L}H\right) \tag{2.43}$$

This dispersion relation can be solved for the wavelength using approximations or iterative methods, for example, EFDC+ computes wavelength by using an approximate formula (Hunt, 1979):

$$L \approx T\sqrt{\frac{1}{d}gH}, \tag{2.44}$$

where

$$d = \gamma + \frac{1}{(1 + 0.6522\gamma + 0.4622\gamma^2 + 0.0864\gamma^4 + 0.0675\gamma^5)}, \tag{2.45}$$

and

$$\gamma = \omega^2\frac{H}{g} \tag{2.46}$$

where ω is the wave angular frequency (1/s)

$$\omega = \frac{2\pi}{T}. \tag{2.47}$$

The regime of flow is determined through the wave Reynolds number R_w, and the relative bed roughness r :

$$R_w = \frac{U_b A}{\nu}, \quad r = \frac{A}{k_s} \tag{2.48}$$

in which A is the semi-orbital excursion, k_s the Nikuradse equivalent sand grain roughness, and U_b is the wave maximum orbital velocity near the bed.

$$A = \frac{H_s}{2\sinh(kH)} \tag{2.49}$$

$$U_b = A\omega = \frac{\omega H_s}{2\sinh(kH)} \tag{2.50}$$

The bottom friction, the bed forms (such as ripples) and the characteristics of bed materials are strongly interdependent in case of wave actions. The friction coefficient due to waves according to Swart (1974) is given in equation (2.51).

$$f_w = \begin{cases} exp\left(5.21r^{-0.19} - 6.0\right) & r > 1.57 \\ 0.3r & r = 1.57 \end{cases} \tag{2.51}$$

2.2.5 Local Wind-Generated Waves

The force applied by wind constitutes an important mechanism which drives the hydrodynamic processes as well as sediment transport in lakes, estuaries, and coastal areas. Wind effects can not only induce the flow current through the vertical boundary conditions at water surface, but also generate surface waves with wave height of several meters. Consequently, the calculation of the total bed shear stress should take the wave factor into account.

Waves with periods of 3 to 25 seconds are primarily caused by winds. Therefore, wind-generated waves play an important role in hydrodynamic modeling. The advantage of this wind-wave sub-model is that it can be easily incorporated into the source code of a hydrodynamic model instead of running a separate wave model. This means that the changes in hydrodynamic parameters are immediately updated in the wave calculations. Additionally, the calculation time is reduced compared to other wave models.

The theoretical basis and tests of the wind wave sub-model that is incorporated into EFDC+ is presented in detail. The mathematical formulae are empirical equations called the SMB (Sverdrup, Munk and Bretschneider) model (Ji, 2008). The model calibration is based on the experiment of Cox et al. (1996) for a wave flume. Another verification of the sub-model is the comparison of wave heights computed by the model with those generated by SWAN (Team, 2019) for the same wind condition in Caloosahatchee Estuary.

The basic assumptions of the SMB model for wind-generated waves are; a) the duration of wind blowing along one direction is long enough to attain the equilibrium condition, and b) the wind speed and water depth are spatially uniform over the fetch. The main wave parameters can be determined including wave height, wave direction and wave period. For the SMB model, the wave direction is the same as the wind direction. This means that the effects of refraction, diffraction and reflection are not considered. Wave height and period can be defined as:

$$H_s = 0.283a\frac{W_s^2}{g}\tanh\left(\frac{0.0125}{\alpha}\left(\frac{gF}{W_s^2}\right)^{0.42}\right) \tag{2.52}$$

$$T_p = 7.54\beta\frac{W_s}{g}\tanh\left(\frac{0.077}{\beta}\left(\frac{gF}{W_s^2}\right)^{0.25}\right) \tag{2.53}$$

where

$$\alpha = \tanh\left\{0.53\left(\frac{gH}{W_s^2}\right)^{0.75}\right\} \tag{2.54}$$

$$\beta = \tanh\left\{0.833\left(\frac{gH}{W_s^2}\right)^{0.375}\right\} \tag{2.55}$$

in which

H_s is the wave height (m)

T_p is the wave period (s)

H is the water depth (m)

W_s is the wind velocity (m/s)

F is the fetch length from the land boundary to the cell in the upwind direction (m); F is calculated for 16 directions

2.2.6 Harmonic Forcings

The open boundary conditions in EFDC+ support a combination of forcings defined as a time series and harmonic forcings. This allows to model the situations in estuaries or coastal areas where the influences of tides and river flows or storm surges may happen.

The harmonic representation of a time series $\zeta(t)$ can be approximated as a combination of sine and cosine functions:

$$\zeta(t) = \zeta_0(t) + a_0 + \sum_{k=1}^{N}\left[a_k\cos(\omega_k t) + b_k\sin(\omega_k t)\right] \tag{2.56}$$

where

t is the time (s)

$\zeta_0(t)$ is the residual signal other than the periodic components (m)

a_0 is the mean value of the periodic components (m)

N is the number of the harmonic constituents

a_k, b_k are the harmonic constant of the constituent k (m)

ω_k is the angular speed of constituent k (radians/s)

Here,

$$\omega_k = \frac{2\pi}{T_k} \tag{2.57}$$

where T_k is the period constituent k (s).

Equation (2.56) can be also rewritten in another common form as

$$\zeta(t) = \zeta_0(t) + a_0 + \sum_{k=1}^{N} A_k \cos(\omega_k t - \phi_k) \tag{2.58}$$

where A_k is the amplitude of the harmonic constituent k (m):

$$A_k = \sqrt{a_k^2 + b_k^2} \tag{2.59}$$

and ϕ_k is the phase lag the harmonic constituent k (radians):

$$f_k = \arctan\left(\frac{b_k}{a_k}\right) \tag{2.60}$$

2.2.7 Hydraulic Structures

Hydraulic structures can be modeled in EFDC+ by rating curves or hydraulic equations. A rating curve is a lookup table which presents a relationship between the flow rate through a structure and the water heads. Depending on the actual water heads of the structure at a certain time step, the flow rate is determined using the lookup table. EFDC+ allows a variety of rating curves by which the flow discharge can be determined from; a) upstream water depth, b) the head difference (between upstream and downstream), c) the head difference and flow accelerations, d) the upstream and downstream water surface elevations, e) upstream water depth for a low chord structure, and f) head difference for a low chord structure.

The last two types of rating curves use low chord structures such as bridges. With the low chord structures, when flows are below the deck, they may be bi-directional, i.e., flows can be going upstream or downstream. However, once the bridge is overtopped, flows only go from upstream to downstream.

2.2.7.1 Rating Curves

If the flow through a structure is uni-directional, i.e., the flow direction is from upstream to downstream of the structures only. The rating curve is a lookup table which composes of a single column for water head and a corresponding single column for flow rate.

If the flow through a structure is bi-directional, the rating curve is a two-dimensional lookup table where the flow rates can be determined based on both upstream and downstream water surface elevations.

Beside using lookup tables, EFDC+ can also simulate internally different types of hydraulic structures. This allows the user to model hydraulic structures rapidly and with ease in EFDC+. The built-in modeling codes for hydraulic structures inside EFDC+ includes culverts, weirs, sluice gates, and orifices.

2.2.7.2 Culverts

Flow rate through a culvert or sluice gate is calculated in EFDC+ based on the water levels at both sides of the structure at its configuration. In a tidal region, the water levels on two sides of the structure are constantly changing, which can result in bi-directional flows. The characteristics of flow through a culvert are complicated and are determined by the inlet geometry, slope, shape, size, roughness, approach, and headwater and tailwater conditions. Dill (2011) described six different types of culvert flows based on the location of the control section within the culvert and the relative elevations of the headwater, tailwater, and culvert invert and crown elevations. The discharge through a culvert can be expressed as:

$$Q = AV = AC\sqrt{RS} = K\sqrt{S} \tag{2.61}$$

where Q is the flow discharge (m^3/s), A is the cross-sectional flow area (m^2), R is the hydraulic radius (m), S is the culvert slope (fraction), K is the conveyance (m^3/s), and C is the Chézy coefficient ($m^{0.5}/s$) which can be calculated by using the Manning's formula

$$C = \frac{1}{n}R^{\frac{1}{6}} \tag{2.62}$$

where n is Manning's roughness coefficient.

Four distinct conditions arise depending on elevation of the tailwater and headwater compared to the height of the culvert. The handling of these conditions are described in case "a" through "d" below:

a) If the tailwater is greater than the culvert height or the headwater is greater than 1.5 times the culvert height, the culvert outlet is submerged, and the culvert is assumed to flow full. The slope is estimated as the difference in headwater and tailwater elevation divided by the culvert length, L (m), the conveyance is determined for the full culvert, and discharge is calculated by equation (2.61).

b) If both the inlet and outlet are not submerged, the critical depth (y_c) is computed, assuming free flow through the culvert inlet. In this case, it is assumed the approach velocity is negligible so that total energy at the culvert inlet is equal to the headwater. Thus,

$$H_{HW} = y_c + \frac{V_c^2}{2g} \tag{2.63}$$

where

H_{HW} is the headwater (m),
V_c is the critical velocity (m/s)
y_c is the critical depth (m)
g is acceleration due to gravity

In the case of critical flow through the culvert:

$$\frac{V_c^2}{2g} = \frac{D}{2} \tag{2.64}$$

where D is the hydraulic depth (m):

$$D = \frac{A}{T} \tag{2.65}$$

and T is the flow top width (m). Combining equations (2.63) and (2.64) yields an expression for the critical depth,

$$y_c = H_{HW} - \frac{D}{2} \tag{2.66}$$

where H_{TW} is the tailwater (m).

Once the critical depth is determined, the critical velocity V_c, critical discharge Q_{cr}, and critical slope S_{cr} are also calculated. The critical discharge represents the maximum possible flow through the culvert for the given headwater as shown in equation (2.67)

$$Q_{cr} = V_c A \tag{2.67}$$

If the culvert slope is greater than the critical slope, the culvert can convey more flow than the inlet will allow. As such, the inlet controls the flow and the discharge is assumed to be equal to the critical discharge Q_{cr} calculated as equation (2.67).

c) If the culvert slope is less than the critical slope, the control section may be at the culvert outlet or downstream of the culvert. The critical depth is then compared to the tailwater, and if the tailwater is greater than the critical depth, the tailwater elevation is used to determine the flow area and hydraulic radius, and the flow through the culvert is calculated using the equation (2.61).

d) If the tailwater depth is less than the critical depth, but the slope is less than the critical slope, it is assumed that uniform flow will occur within the culvert. In this case potential energy is balanced by head loss due to friction in the culvert and conservation of energy between the control section and inlet can be expressed as;

$$H_{HW} = y_n + \frac{V^2}{2g} \tag{2.68}$$

where y_n is the normal depth (m) in the culvert and V is the average velocity at the control section. It is also assumed that the approach velocity is negligible, and the slope is small such that the normal depth is approximately equal to the vertical depth.

Equation (2.61) can be re-written as an expression of the velocity head at the control section as;

$$V = \frac{1}{n} R^{\frac{2}{3}} \sqrt{S} \tag{2.69}$$

Combining equations (2.68) and (2.69) yields an equation for the normal depth

$$y_n = H_{HW} - \frac{1}{2g} \frac{1}{n^2} R^{\frac{4}{3}} S \tag{2.70}$$

Because R is a function of depth, an adaptive procedure is employed to determine the normal depth. In culverts that experience bi-directional flow, the slope may be adverse or zero. In either case, the assumption of uniform flow is problematic because the water surface slope cannot be equal to the culvert slope. In this case, the water surface slope, as determined from the difference in headwater and tailwater elevations, is used in the equation (2.70).

2.2.7.3 Weirs

A general formula for free flow through a weir can be expressed as

$$Q = C_d W \sqrt{2g H_{HW}^3} \tag{2.71}$$

where W is the width of weir (m) and C_d is the weir discharge coefficient. This coefficient depends on the type of weir (broad crested or sharp-/narrow-crested, ogee), shape of opening (rectangular, triangular, trapezoidal), and other weir parameters.

For submerged flow through a weir, an adjustment factor is applied to the equation (2.71) to account for the submergence, and is given by the equation (2.72) (Villemonte, 1947).

$$Q = \left(1 - \frac{H_{TW}}{H_{HW}}\right)^{0.385} C_d W \sqrt{2g H_{HW}^3} \tag{2.72}$$

2.2.7.4 Sluice Gates

Flow through a sluice gate can be characterized by two basic parameters; the tranquility of the flow (i.e., subcritical or supercritical flow), and the water depth (i.e., gate is submerged or not). For supercritical weir flow, the equation (2.73) is used

$$Q = C_1 W \sqrt{g \left(\frac{2}{3} H_{HW}\right)^3} \tag{2.73}$$

and for subcritical weir flow, equation (2.74) is used.

$$Q = C_2 W H_{TW} \sqrt{2g\left(H_{HW} - H_{TW}\right)} \tag{2.74}$$

where

C_1 is the supercritical discharge coefficient

C_2 is the subcritical discharge coefficient

H_{HW} is the headwater (m)

H_{TW} is the tailwater (m)

W is the width of the gate (m)

g is acceleration due to gravity

When the water surface is determined to be below the top of the gate, the gate is modeled as a broad crested weir and equation (2.71) is used. When the gate is submerged, the appropriate equation for either free sluice flow (supercritical) or submerged orifice flow (subcritical) is applied. To determine the flow through the sluice gate at a given model time step, the headwater is compared to the tailwater.

For free sluice flow the equation (2.75) is used:

$$Q = C_3 A \sqrt{2gH_{HW}} \tag{2.75}$$

Similarly, for submerged orifice flow equation (2.76) is used.

$$Q = C_4 A \sqrt{2g\left(H_{HW} - H_{TW}\right)} \tag{2.76}$$

where

C_3 is the discharge coefficient for free sluice flow,

C_4 is the discharge coefficient for submerged orifice flow, and

A is the gate opening (m^2).

If the ratio of tailwater to headwater is less than 0.64, equation (2.72) for supercritical flow is applied. If the ratio of tailwater to headwater is greater than 0.68, equation (2.73) for subcritical flow is applied. This is either a free sluice for supercritical flow, or a submerged orifice for subcritical flow. In cases when the tailwater to headwater ratio is between 0.64 and 0.68 both discharges are computed and a weighted average of the two is used.

2.2.7.5 Orifices

If the headwater is lower than the opening of a orifice, the flow through the orifice is treated as weir flow, and the equation (2.71) is used. If the tailwater is higher than the opening of an orifice, then equation (2.76) submerged flow through the orifice is applied.

If the headwater is higher than the opening of an orifice but the tailwater is lower than the opening of an orifice, the free jet flow through the orifice is calculated as

$$Q = C_2 A \sqrt{2g\left(H_{HW} + 0.5B\right)} \tag{2.77}$$

where B is the height of orifice opening (m), and H_{HW} is calculated based on the center line of the orifice.

2.3. Numerical Solution for the Equations of Motion

The equations of motion, shown previously in equations (2.2) and (2.3) will be solved in a region subdivided into six faced cells. The projection of the vertical cell boundaries to a horizontal plane forms a curvilinear, orthogonal grid in the orthogonal coordinate system (x,y). In a vertical (x,z) or (y,z) plane, the cells bounded by the same constant z surfaces will be referred to as celllayers. The equations will be solved using a combination of finite volume and finite difference techniques, with the variable locations shown in Figure 2.3.

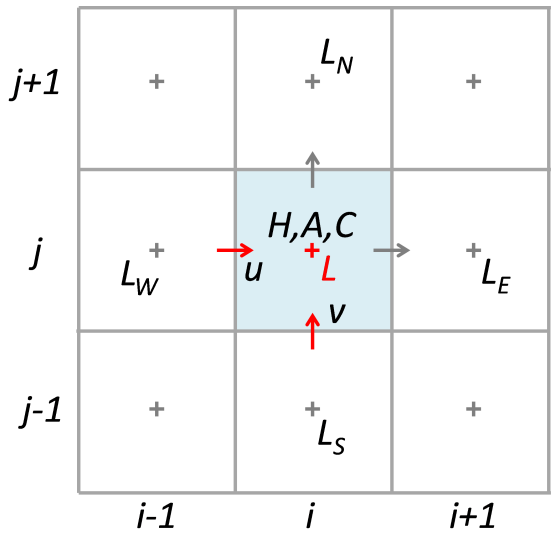

Fig. 2.3. Free surface displacement centered horizontal grid.

The staggered grid location of variables is often referred to as the Arakawa C grid (Arakawa and Lamb, 1977) or the MAC grid (Peyret and Taylor, 1983). To proceed, it is convenient to modify equations (2.2) and (2.3) by eliminating the vertical pressure gradients using equation (2.4). After some manipulation, the horizontal momentum equations are given in the equations (2.78) and (2.79).

$$\begin{aligned}
&\frac{\partial}{\partial t}\left(m_x m_y H u\right)+\frac{\partial}{\partial x}\left(m_y H u u\right)+\frac{\partial}{\partial y}\left(m_x H v u\right)+\frac{\partial}{\partial z}\left(m_x m_y w u\right)\\
&\quad-\left(v\frac{\partial m_y}{\partial x}-u\frac{\partial m_x}{\partial y}\right)Hv-m_x m_y f H v\\
&=-m_y H\frac{\partial p}{\partial x}-m_y H g\frac{\partial \zeta}{\partial x}+m_y H g b\frac{\partial h}{\partial x}-m_y H g b z\frac{\partial H}{\partial x}+\frac{\partial}{\partial z}\left(\frac{m_x m_y A_v}{H}\frac{\partial u}{\partial z}\right)+S_u
\end{aligned} \tag{2.78}$$

$$\begin{aligned}
&\frac{\partial}{\partial t}\left(m_x m_y H v\right)+\frac{\partial}{\partial x}\left(m_y H u v\right)+\frac{\partial}{\partial y}\left(m_x H v v\right)+\frac{\partial}{\partial z}\left(m_x m_y w v\right)\\
&\quad+\left(v\frac{\partial m_y}{\partial x}-u\frac{\partial m_x}{\partial y}\right)Hu+m_x m_y f H u\\
&=-m_x H\frac{\partial p}{\partial y}-m_x H g\frac{\partial \zeta}{\partial y}+m_x H g b\frac{\partial h}{\partial y}-m_x H g b z\frac{\partial H}{\partial y}+\frac{\partial}{\partial z}\left(\frac{m_x m_y A_v}{H}\frac{\partial v}{\partial z}\right)+S_v
\end{aligned} \tag{2.79}$$

First, the vertical discretization of equations (2.78) and (2.79) is performed. The equations are integrated with respect to z over a cell layer assuming that vertically defined variables (at the cell or layer centers) are constant. Additionally, these variables must be defined vertically at the cell layer interfaces or boundaries. Using the notation for mass fluxes,

$$P_k = m_y H u_k, Q_k = m_x H v_k \tag{2.80}$$

equations (2.78) and (2.79) are redefined as;

$$\begin{aligned}
&\frac{\partial}{\partial t}\left(m_x P_k \Delta_k\right)+\frac{\partial}{\partial x}\left(P_k u_k \Delta_k\right)+\frac{\partial}{\partial y}\left(Q_k u_k \Delta_k\right)+m\left[(wu)_k-(wu)_{k-1}\right]\\
&\quad-\left(v_k\frac{\partial m_y}{\partial x}-u_k\frac{\partial m_x}{\partial y}\right)Hv_k\Delta_k-m_y f Q_k\Delta_k\\
&=-\frac{1}{2}m_y H Delta_k\frac{\partial}{\partial x}\left(p_k+p_{k-1}\right)-m_y H\Delta_k g\frac{\partial \zeta}{\partial x}+m_y H\Delta_k g b_k\frac{\partial h}{\partial x}\\
&\quad-0.5 m_y H\Delta_k g b_k\left(z_k+z_{k-1}\right)\frac{\partial H}{\partial x}+m\left[(\tau_{xz})_k-(\tau_{xz})_{k-1}\right]+(S_u\Delta)_k
\end{aligned} \tag{2.81}$$

$$\begin{aligned}
&\frac{\partial}{\partial t}\left(m_y Q_k \Delta_k\right)+\frac{\partial}{\partial x}\left(P_k v_k \Delta_k\right)+\frac{\partial}{\partial y}\left(Q_k v_k \Delta_k\right) \\
&+m\left[(wv)_k-(wv)_{k-1}\right]+\left(v_k\frac{\partial m_y}{\partial x}-u_k\frac{\partial m_x}{\partial y}\right)Hu_k\Delta_k+m_x f P_k\Delta_k \\
=&-\frac{1}{2}m_x H\Delta_k\frac{\partial}{\partial y}\left(p_k+p_{k-1}\right)-m_x H\Delta_k g\frac{\partial \zeta}{\partial y}+m_x H\Delta_k g b_k\frac{\partial h}{\partial y} \\
&-0.5m_x H\Delta_k g b_k\left(z_k+z_{k-1}\right)\frac{\partial H}{\partial y}+m\left[(t_{yz})_k-m(t_{yz})_{k-1}\right]+(S_v\Delta)_k
\end{aligned} \tag{2.82}$$

where Δk is the vertical cell or layer thickness, and the turbulent shear stresses at the cell layer interfaces are defined by:

$$(\tau_{xz})_k=\frac{2}{H}(A_v)_k\frac{u_{k+1}-u_k}{\Delta_{k+1}+\Delta_k} \tag{2.83}$$

$$(t_{yz})_k=\frac{2}{H}(A_v)_k\frac{v_{k+1}-v_k}{\Delta_{k+1}+\Delta_k} \tag{2.84}$$

If there are K cells in the z direction, the hydrostatic equation can be integrated from a cell layer interface to the surface to give:

$$p_k=gH\left(\sum_{j=k}^{K}b_j\Delta_j-b_k\Delta_k\right)+p_s \tag{2.85}$$

where p_s is the physical pressure at the free surface or under the rigid lid divided by the reference density. The continuity equation (2.5) is also integrated with respect to z over a cell or layer to give:

$$\frac{\partial}{\partial t}\left(m\zeta\Delta_k\right)+\frac{\partial}{\partial x}\left(P_k\Delta_k\right)+\frac{\partial}{\partial y}\left(Q_k\Delta_k\right)+m\left(w_k+w_{k-1}\right)=S_h \tag{2.86}$$

The numerical solution of the vertically discrete momentum equations (2.78) and (2.79) proceeds by splitting the external depth integrated mode (associated with external long surface gravity waves from) the internal mode (associated with vertical current structure).

The external mode equations are obtained by summing equations (2.78) and (2.79) over K cells or layers in the vertical utilizing equation (2.85), and are given by:

$$\frac{\partial}{\partial t}\left(m_x\hat{P}\right)+\sum_{k=1}^{K}\left[\frac{\partial}{\partial x}\left(P_k u_k\Delta_k\right)+\frac{\partial}{\partial y}\left(Q_k u_k\Delta_k\right)-\left(v_k\frac{\partial m_y}{\partial x}-u_k\frac{\partial m_x}{\partial y}\right)Hv_k\Delta_k-m_y f Q_k\Delta_k\right]$$
$$=-m_yHg\frac{\partial\zeta}{\partial x}-m_yH\frac{\partial p_s}{\partial x}+m_yHg\hat{b}\frac{\partial h}{\partial x}-m_yHg\left[\sum_{k=1}^{K}\left(\beta_k\Delta_k+\frac{1}{2}\left(z_k+z_{k-1}\right)b_k\Delta_k\right)\right]\frac{\partial H}{\partial x}$$
$$-m_ygH^2\frac{\partial}{\partial x}\left(\sum_{k=1}^{K}\beta_k\Delta_k\right)+m\left[\left(\tau_{xz}\right)_K-\left(\tau_{xz}\right)_0\right]+\hat{S}_u \tag{2.87}$$

$$\frac{\partial}{\partial t}\left(m_x\hat{Q}\right)+\sum_{k=1}^{K}\left[\frac{\partial}{\partial x}\left(P_k v_k\Delta_k\right)+\frac{\partial}{\partial y}\left(Q_k v_k\Delta_k\right)-\left(v_k\frac{\partial m_y}{\partial x}-u_k\frac{\partial m_x}{\partial y}\right)Hu_k\Delta_k-m_x f P_k\Delta_k\right]$$
$$=-m_xHg\frac{\partial\zeta}{\partial y}-m_xH\frac{\partial p_s}{\partial y}+m_xHg\hat{b}\frac{\partial h}{\partial y}-m_xHg\left[\sum_{k=1}^{K}\left(\beta_k\Delta_k+\frac{1}{2}\left(z_k+z_{k-1}\right)b_k\Delta_k\right)\right]\frac{\partial H}{\partial y}$$
$$-m_xgH^2\frac{\partial}{\partial y}\left(\sum_{k=1}^{K}\beta_k\Delta_k\right)+m\left[\left(\tau_{yz}\right)_K-\left(\tau_{yz}\right)_0\right]+\hat{S}_u \tag{2.88}$$

$$\frac{\partial}{\partial t}(m\zeta)+\frac{\partial}{\partial x}\bar{P}+\frac{\partial}{\partial y}\bar{Q}=S_h \tag{2.89}$$

where the over bar indicates an average over the depth as reiterated in equation (2.90). Additionally, equation (2.91) is introduced to simplify equations (2.87) and (2.88).

$$\hat{P}=m_yH\hat{u},\hat{Q}=m_xH\hat{v} \tag{2.90}$$

$$\beta_k=\sum_{j=k}^{K}b_j\Delta_j-\frac{1}{2}b_k\Delta_k \tag{2.91}$$

The depth integrated continuity equation, equation (2.89), follows from equation (2.6) and provides the continuity constraint for the external mode. Consistent with the form of equation (2.89) the external mode variables will be chosen to be the free surface displacement, ζ, and the volumetric transports $P=m_yHu$ and $Q=m_xHv$. Details of the solution of the external mode equations (2.87) to (2.89) are presented in Section 2.4.

Several formulations are possible for the internal mode equations. Equations (2.78) and (2.79) have K degrees of freedom for each of the horizontal velocity components.

However, the summation of these equations over K cells or layers in the vertical to form the external mode equations (2.87) and (2.88) effectively removes a degree of freedom since the constraints:

$$\sum_{k=1}^{K} u_k \Delta_k = \hat{u} \tag{2.92}$$

$$\sum_{k=1}^{K} v_k \Delta_k = \hat{v} \tag{2.93}$$

must be satisfied. One approach to the internal mode is to solve equations (2.78) and (2.79) using the free surface slopes, or the surface pressure gradients in the rigid lid case, from the external solution and distribute the error such that equations (2.92) and (2.93) are satisfied. A second approach is to form equations for the deviations of the velocity components from their vertical means by subtracting the external equations (2.87) and (2.88) from the layer integrated equations (2.78) and (2.79). However, it will still be necessary to satisfy the constraints (2.92) and (2.93). The approach proposed herein is to reduce the systems of K layer averaged equations (2.81) and (2.82) to systems of $K-1$ equations and use equations (2.92) and (2.93) to provide the K^{th} equation consistent with the actual degrees of freedom.

The internal mode equations are formed by first dividing equations (2.81) and (2.82) by the cell layer thickness (Δk). Next, the equations for cell layer k is subtracted from the equations for cell layer $k+1$. The resulting equation from these two operations is divided by the average thickness ($\Delta_{k+1,k}$) of the two cell layers resulting in:

$$\begin{aligned}
&\frac{\partial}{\partial t}\left(m_x \frac{P_{k+1}-P_k}{\Delta_{k+1,k}}\right) + \frac{\partial}{\partial x}\left(\frac{P_{k+1}u_{k+1}-P_k u_k}{\Delta_{k+1,k}}\right) + \frac{\partial}{\partial y}\left(\frac{Q_{k+1}u_{k+1}-Q_k u_k}{\Delta_{k+1,k}}\right) \\
&+ \frac{m}{\Delta_{k+1,k}}\left[\frac{(wu)_{k+1}-(wu)_k}{\Delta_{k+1}} - \frac{(wu)_k-(wu)_{k-1}}{\Delta_k}\right] - m_y f \frac{Q_{k+1}-Q_k}{\Delta_{k+1,k}} \\
&- \frac{1}{\Delta_{k+1,k}}\left[\left(v_{k+1}\frac{\partial m_y}{\partial x} - u_{k+1}\frac{\partial m_x}{\partial y}\right) H v_{k+1} - \left(v_k \frac{\partial m_y}{\partial x} - u_k \frac{\partial m_x}{\partial y}\right) H v_k\right] \\
&= m_y H \frac{b_{k+1}-b_k}{\Delta_{k+1,k}} g\left(\frac{\partial h}{\partial x} - z_k \frac{\partial H}{\partial x}\right) + \frac{1}{2}\frac{m_y H^2}{\Delta_{k+1,k}} g\left(\Delta_{k+1}\frac{\partial b_{k+1}}{\partial x} + \Delta_k \frac{\partial b_k}{\partial x}\right) \\
&+ \frac{m}{\Delta_{k+1,k}}\left[\frac{(\tau_{xz})_{k+1}-(\tau_{xz})_k}{\Delta_{k+1}} - \frac{(\tau_{xz})_k-(\tau_{xz})_{k-1}}{\Delta_k}\right] + \frac{(S_u)_{k+1}-(S_u)_k}{\Delta_{k+1,k}}
\end{aligned} \tag{2.94}$$

$$\begin{aligned}
&\frac{\partial}{\partial t}\left(m_y\frac{Q_{k+1}-Q_k}{\Delta_{k+1,k}}\right)+\frac{\partial}{\partial x}\left(\frac{P_{k+1}v_{k+1}-P_kv_k}{\Delta_{k+1,k}}\right)+\frac{\partial}{\partial y}\left(\frac{Q_{k+1}v_{k+1}-Q_kv_k}{\Delta_{k+1,k}}\right)\\
&+\frac{m}{\Delta_{k+1,k}}\left[\frac{(wv)_{k+1}-(wv)_k}{\Delta_{k+1}}-\frac{(wv)_k-(wv)_{k-1}}{\Delta_k}\right]+m_xf\frac{P_{k+1}-P_k}{\Delta_{k+1,k}}\\
&+\frac{1}{\Delta_{k+1,k}}\left[\left(v_{k+1}\frac{\partial m_y}{\partial x}-u_{k+1}\frac{\partial m_x}{\partial y}\right)Hu_{k+1}-\left(v_k\frac{\partial m_y}{\partial x}-u_k\frac{\partial m_x}{\partial y}\right)Hu_k\right] \qquad (2.95)\\
&=m_xH\frac{b_{k+1}-b_k}{\Delta_{k+1,k}}g\left(\frac{\partial h}{\partial y}-z_k\frac{\partial H}{\partial y}\right)+\frac{1}{2}\frac{m_xH^2}{\Delta_{k+1,k}}g\left(\Delta_{k+1}\frac{\partial b_{k+1}}{\partial y}+\Delta_k\frac{\partial b_k}{\partial y}\right)\\
&+\frac{m}{\Delta_{k+1,k}}\left[\frac{(\tau_{yz})_{k+1}-(\tau_{yz})_k}{\Delta_{k+1}}-\frac{(\tau_{yz})_k-(\tau_{yz})_{k-1}}{\Delta_k}\right]+\frac{(S_v)_{k+1}-(S_v)_k}{\Delta_{k+1,k}}
\end{aligned}$$

$$\Delta_{k+1,k}=\frac{1}{2}\left(\Delta_{k+1}+\Delta_k\right) \qquad (2.96)$$

Inspection of equations (2.94) and (2.95) reveals that they could have also been obtained by differentiating the horizontal momentum equations (2.78) and (2.79) with respect to z and introducing a finite difference discretion in z. Using equations (2.83) and (2.84) to relate the shear stresses to the velocity differences across the interior interfaces suggests that the equations (2.94) and (2.95) be interpreted as a system of $K-1$ equations for either the $K-1$ interfacial velocity differences or the $K-1$ interior interfacial shear stresses. Details of the solution of the internal mode equations (2.94) and (2.95) will be presented in Section 2.5.

The solution of the vertical velocity, w, employs the continuity equations. Dividing equation (2.86) by Δk, and subtracting equation (2.88) yields

$$w_k=w_{k-1}-\frac{\Delta_k}{m}\left[\frac{\partial}{\partial x}\left(P_k-\hat{P}\right)+\frac{\partial}{\partial y}\left(Q_k-\hat{Q}\right)\right]. \qquad (2.97)$$

Since $w_o=0$, the solution proceeds from the first cell layer to the surface. Provided the constraints (equations (2.92) and (2.93)) are satisfied, the surface velocity at $k=K$ will be zero and satisfy the boundary condition.

2.4. Computational Aspects of the Three Time Level External Mode Solution

The formulation of a computational algorithm for the numerical solution of the external mode equations (2.87) to (2.89) begins by introducing modified variables and reorganizing the equations to give:

$$\frac{\partial \hat{P}}{\partial t} = -\frac{m_y}{m_x} Hg \frac{\partial \zeta}{\partial x} - \frac{m_y}{m_x} H \frac{\partial p_s}{\partial x} + \frac{m_y}{m_x} Hg \left(\hat{b} \frac{\partial h}{\partial x} - \hat{B} \frac{\partial H}{\partial x} - H \frac{\partial \hat{\beta}}{\partial x} \right)$$
$$- \frac{1}{m_x} \sum_{k=1}^{K} \Delta_k \left(\frac{\partial}{\partial x} (P_k u_k) + \frac{\partial}{\partial y} (Q_k u_k) \right) + \frac{1}{m_x} \sum_{k=1}^{K} \Delta_k \left[\left(v_k \frac{\partial m_y}{\partial x} - u_k \frac{\partial m_x}{\partial y} \right) H v_k + m_y f Q_k \right]$$
$$+ \frac{1}{m_x} \sum_{k=1}^{K} \left[\frac{\partial}{\partial x} \left(\frac{m_y}{m_x} H A_{Hk} \Delta_k \frac{\partial u_k}{\partial x} \right) + \frac{\partial}{\partial y} \left(\frac{m_x}{m_y} H A_{Hk} \Delta_k \frac{\partial u_k}{\partial y} \right) \right]$$
$$+ m_y (\tau_{xz})_K - m_y (\tau_{xz})_0 + \frac{1}{m_x} \hat{S}_u \tag{2.98}$$

$$\frac{\partial \hat{Q}}{\partial t} = -\frac{m_x}{m_y} Hg \frac{\partial \zeta}{\partial y} - \frac{m_x}{m_y} H \frac{\partial p_s}{\partial y} + \frac{m_x}{m_y} Hg \left(\hat{b} \frac{\partial h}{\partial y} - \hat{B} \frac{\partial H}{\partial y} - H \frac{\partial \hat{\beta}}{\partial y} \right)$$
$$- \frac{1}{m_y} \sum_{k=1}^{K} {}_k \left(\frac{\partial}{\partial x} (P_k v_k) + \frac{\partial}{\partial y} (Q_k v_k) \right) + \frac{1}{m_y} \sum_{k=1}^{K} \Delta_k \left[\left(v_k \frac{\partial m_y}{\partial x} - u_k \frac{\partial m_x}{\partial y} \right) H u_k + m_x f P_k \right]$$
$$+ \frac{1}{m_y} \sum_{k=1}^{K} \left[\frac{\partial}{\partial x} \left(\frac{m_y}{m_x} H A_{Hk} \Delta_k \frac{\partial v_k}{\partial x} \right) + \frac{\partial}{\partial y} \left(\frac{m_x}{m_y} H A_{Hk} \Delta_k \frac{\partial v_k}{\partial y} \right) \right]$$
$$+ m_x (\tau_{yz})_K - m_x (\tau_{yz})_0 + \frac{1}{m_y} \hat{S}_v \tag{2.99}$$

$$\frac{\partial \zeta}{\partial t} + \frac{1}{m} \left(\frac{\partial \hat{P}}{\partial x} + \frac{\partial \hat{Q}}{\partial y} \right) = S_h \tag{2.100}$$

where

$$\hat{\beta} = \sum_{k=1}^{K} \beta_k \Delta_k \tag{2.101}$$

$$\hat{\beta} = \sum_{k=1}^{K} \left[\beta_k \Delta_k + \frac{1}{2} (z_k + z_{k-1}) b_k \Delta_k \right]. \tag{2.102}$$

Equations (2.98) and (2.99) now equate the time rate of change of the external or depth integrated volumetric transports to the pressure gradients associated with the free surface slope, atmospheric pressure and buoyancy, the advective accelerations, the Coriolis and curvature accelerations, the free surface and bottom tangential stresses, and the general source,

sink terms. The staggered location of variables on the computational grid, Figure 2.3, allows most horizontal spatial derivatives in equations (2.98) to (2.100) to be represented by second order accurate central differences and results in conservation of volume, mass, momentum and energy in the limit of exact integration of the equations in time (Haltiner and Williams, 1980; Simons et al., 1973). When a variable is not located at a point required for implementation of central difference operators, averaging in either or both spatial directions is appropriate. The use of the spatial averaging scheme of Arakawa and Lamb (1977) to represent the Coriolis and curvature accelerations also guarantees energy conservation.

Following the introduction of discrete finite difference and averaging representations in space, equations (2.98) to (2.100), for a horizontal grid of L cells, may be viewed as a system of $3L$ ordinary differential equations in time for the volumetric transport and the free surface displacement. The numerous techniques available to solve these equations generally fall within the categories of explicit and semi-implicit. The most frequently used explicit scheme is the three-time level leapfrog scheme where the time derivatives are approximated between the time levels $n+1$ and $n-1$, and the remaining terms are evaluated at time level n. Although computationally simple to implement, the maximum time step is restricted by the Courant-Fredrick-Levy condition based on the gravity wave phase speed. An alternate approach allowing larger time steps is the semi-implicit three-time level scheme (Madala and Piacseki, 1977), which when implemented for equations (2.98) to (2.100) is

$$\begin{aligned}
\hat{P}^{n+1} = \hat{P}^{n-1} &- \Delta t\left(\frac{m_y}{m_x}H\right)^u g d_x^u\left(\zeta^{n+1}+\zeta^{n-1}\right) - 2\Delta t\left(\frac{m_y}{m_x}H\right)^u d_x^u p_s \\
&+ 2\Delta t\left(\frac{m_y}{m_x}H\right)^u g\left(\hat{b}^u d_x^u h - \hat{B}^u d_x^u H - H^u d_x^u \hat{\beta}\right) \\
&- 2\Delta t\left(\frac{1}{m_x}\right)^u \sum_{k=1}^{K}\Delta_k\left[d_x^u\left(P_k u_k\right) + d_y^u\left(Q_k u_k\right)\right] \\
&+ 2\Delta t\left(\frac{1}{m_x}\right)^u \sum_{k=1}^{K}\Delta_k\left[\left(v_k\frac{\partial m_y}{\partial x} - u_k\frac{\partial m_x}{\partial y}\right)Hv_k + m_y f Q_k\right]^u \\
&+ 2\Delta t m_y^u\left[\left(t_{xz}^{n-1}\right)_K - \left(t_{xz}^{n-1}\right)_0\right]^u \\
&+ 2\Delta t\left(\frac{1}{m_x}\right)^u \sum_{k=1}^{K}\Delta_k\left[\frac{\partial}{\partial x}\left(m_y H t_{xx}^{n-1}\right) + \frac{\partial}{\partial y}\left(m_x H t_{xy}^{n-1}\right)\right. \\
&\qquad \left. + \frac{\partial}{\partial y}\left(m_x H t_{xy}^{n-1}\right) - \frac{\partial}{\partial x}\left(m_y H t_{yy}^{n-1}\right)\right]_k^u
\end{aligned} \tag{2.103}$$

$$\begin{aligned}\hat{Q}^{n+1} &= \hat{Q}^{n-1} - \Delta t\left(\frac{m_x}{m_y}H\right)^v g\delta_y^u\left(\zeta^{n+1}+\zeta^{n-1}\right) - 2\Delta t\left(\frac{m_x}{m_y}H\right)^v \delta_y^u p_s \\ &+ 2\Delta t\left(\frac{m_x}{m_y}H\right)^v g\left(\hat{b}^v d_y^v h - \hat{B}^v\delta_y^v H - H^v\delta_y^v\hat{\beta}\right) \\ &- 2\Delta t\left(\frac{1}{m_y}\right)^u \sum_{k=1}^{K}\Delta_k\left[d_x^v\left(P_k v_k\right) + d_y^v\left(Q_k v_k\right)\right] \\ &- 2\Delta t\left(\frac{1}{m_y}\right)^v \sum_{k=1}^{K}\Delta_k\left[\left(v_k\frac{\partial m_y}{\partial x} - u_k\frac{\partial m_x}{\partial y}\right)Hu_k + m_x f P_k\right]^v \\ &+ 2\Delta t m_x^v\left[\left(\tau_{yz}^{n-1}\right)_K - \left(\tau_{yz}^{n-1}\right)_0\right]^v \\ &+ 2\Delta t\left(\frac{1}{m_y}\right)^v \sum_{k=1}^{K}\Delta_k\left[\frac{\partial}{\partial x}\left(m_y H t_{yx}^{n-1}\right) + \frac{\partial}{\partial y}\left(m_x H t_{yy}^{n-1}\right)\right. \\ &\left.\frac{\partial}{\partial y}\left(m_x H t_{xx}^{n-1}\right) - \frac{\partial}{\partial x}\left(m_y H t_{yx}^{n-1}\right)\right]_k^v\end{aligned} \tag{2.104}$$

$$\zeta^{n+1} - \zeta^{n-1} + \Delta t\left(\frac{1}{m}\right)^\zeta\left[\delta_x^\zeta\left(\hat{P}^{n+1}+\hat{P}^{n-1}\right) + \delta_y^\zeta\left(\hat{Q}^{n+1}+\hat{Q}^{n-1}\right)\right] = S_h\Delta t \tag{2.105}$$

where Δt indicates the time step. All terms in equations (2.103) to (2.105) are understood to be evaluated at the center time level n except those evaluated at the forward and backward time levels, $n+1$ and $n-1$, which are denoted by superscripts. The u, v, and ζ superscripts indicate that a variable is evaluated, or that a spatial derivative is centered, at the corresponding spatial point.

The subscript of the spatial central difference operator δ indicates direction. The grid cells are presumed to be bounded in the horizontal by lines of constant integer values of the dimensionless orthogonal coordinates x and y, resulting in the central spatial differences having the forms given in equations (2.106) and (2.107).

$$\delta_x\left(\phi_{i,j,k}\right) = \frac{1}{\Delta x}\left(\phi_{i+\frac{1}{2},j,k} - \phi_{i-\frac{1}{2},j,k}\right) \tag{2.106}$$

$$\delta_y\left(\phi_{i,j,k}\right) = \frac{1}{\Delta y}\left(\phi_{i,j+\frac{1}{2},k} - \phi_{i,j-\frac{1}{2},k}\right) \tag{2.107}$$

Application of these finite difference operators to the advective accelerations is illustrated by,

$$\delta_x^u\left(P_{i,j,k}u_{i,j,k}\right) = \frac{1}{\Delta x}\left(P_{i+\frac{1}{2},j,k}u_{i+\frac{1}{2},j,k} - P_{i-\frac{1}{2},j,k}u_{i-\frac{1}{2},j,k}\right), \tag{2.108}$$

where the constant y dependence of the variables is implied. Since the u type variables are located at integer values of x, averaging is necessary to obtain values at half intervals. Averaging both the transport and the velocity yields,

$$\delta_x^u \left(P_{i,j,k} u_{i,j,k} \right) = \frac{1}{\Delta x} \left(\frac{P_{i+1,j,k} + P_{i,j,k}}{2} \frac{u_{i+1,j,k} + u_{i,j,k}}{2} - \frac{P_{i,j,k} + P_{i-1,j,k}}{2} \frac{u_{i,j,k} + u_{i-1,j,k}}{2} \right), \tag{2.109}$$

which is consistent with a central difference approximation of the non-conservative form of this portion of the advective acceleration. Averaging the transport and allowing the velocity to be advected from the upwind direction gives,

$$\begin{aligned} \delta_x^u \left(P_{i,j,k} u_{i,j,k} \right) = & \frac{1}{\Delta x} \left[\max \left(\frac{P_{i+1,j,k} + P_{i,j,k}}{2}, 0 \right) u_{i,j,k}^{n-1} - \max \left(\frac{P_{i,j,k} + P_{i-1,j,k}}{2}, 0 \right) u_{i-1,j,k}^{n-1} \right] \\ & + \frac{1}{\Delta x} \left[\min \left(\frac{P_{i+1,j,k} + P_{i,j,k}}{2}, 0 \right) u_{i+1,j,k}^{n-1} - \min \left(\frac{P_{i,j,k} + P_{i-1,j,k}}{2}, 0 \right) u_{i,j,k}^{n-1} \right] \end{aligned} \tag{2.110}$$

which is consistent with an upwind or backward difference approximation of the non-conservative form of this portion of the advective acceleration. In equation (2.110), the transport is still at time level n, while the velocity is at time level $n-1$, for both stability and accuracy (Smolarkiewicz and Clark, 1986). The preference for the use of equation (2.109) or equation (2.110) will generally depend upon the physical situation being simulated. The central difference form introduces no numerical diffusion, but may produce solution fields which exhibit cell to cell spatial oscillations. These oscillations can be eliminated by the addition of horizontal diffusion terms to the momentum equations. Specification of the horizontal diffusivity allows the degree of spatial smoothing to be controlled. The upwind difference form introduces numerical diffusion and does not produce spatial oscillations in the solution field. The Coriolis and curvature terms in equations (2.103) and (2.104) are discretized using an energy conserving spatial averaging and differencing (Arakawa and Lamb, 1977; Haltiner and Williams, 1980). For example, the Coriolis and curvature term in equation (2.103) is given by:

$$\left[m_y f Q_k + \left(v_k \frac{\partial m_y}{\partial x} - u_k \frac{\partial m_x}{\partial y} \right) H v_k \right]^u = \frac{1}{2} \left[(RH)^{\zeta}_{i+\frac{1}{2},j} v^{\zeta}_{i+\frac{1}{2},j,k} + (RH)^{\zeta}_{i-\frac{1}{2},j} v^{\zeta}_{i-\frac{1}{2},j,k} \right] \tag{2.111}$$

$$R^{\zeta}_{i+\frac{1}{2},j} = (mf)_{i+\frac{1}{2},j} + \frac{(m_y)_{i+1,j} - (m_y)_{i,j}}{\Delta x} v^{\zeta}_{i+\frac{1}{2},j,k} - \frac{(m_x)_{i+\frac{1}{2},j+\frac{1}{2}} - (m_x)_{i+\frac{1}{2},j-\frac{1}{2}}}{\Delta y} u^{\zeta}_{i+\frac{1}{2},j,k} \tag{2.112}$$

$$v^{\zeta}_{i+\frac{1}{2},j,k} = \frac{1}{2}\left(v_{i+\frac{1}{2},j+\frac{1}{2},k} + v_{i+\frac{1}{2},j-\frac{1}{2},k}\right) \tag{2.113}$$

$$u^{\zeta}_{i+\frac{1}{2},j,k} = \frac{1}{2}\left(u_{i+1,j,k} + u_{i,j,k}\right) \tag{2.114}$$

where the variables locations are shown in Figure 2.4.

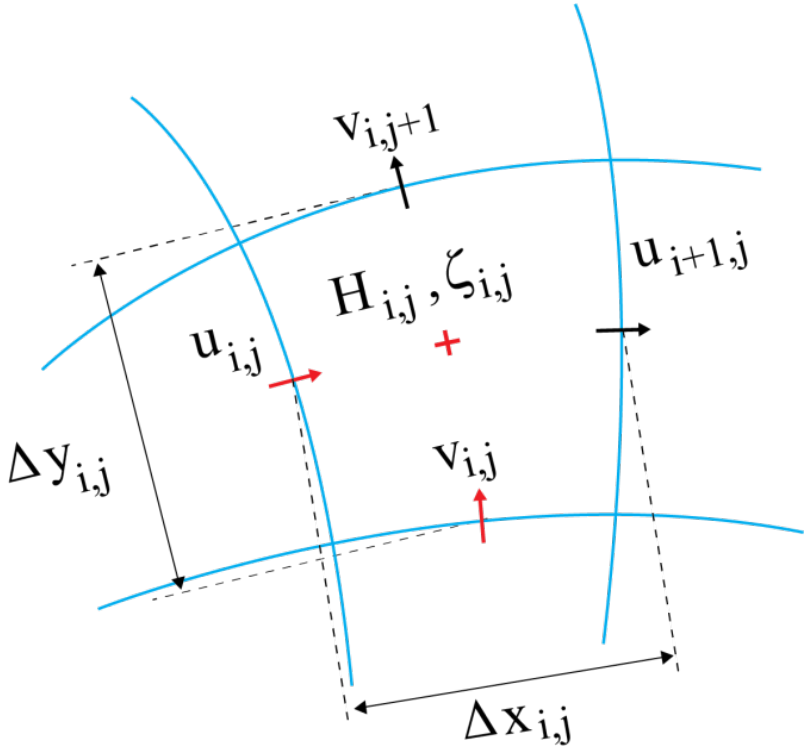

Fig. 2.4. U-centered grid in the horizontal (x, y) plane.

Since the bottom tangential stresses in equations (2.103) and (2.104) must be supplied from the internal mode solution which follows the external solution, it is lagged at the backward time level. The general source, sink term has been replaced by horizontal diffusion terms having the form proposed by Mellor and Blumberg (1985). The horizontal stress tensors are shown in equations (2.115) to (2.117).

$$(\tau_{xx})_k = 2A_H \frac{1}{m_x}\frac{\partial u_k}{\partial x} \tag{2.115}$$

$$(\tau_{xy})_k = (t_{yx})_k = 2A_H\left(\frac{1}{m_x}\frac{\partial v_k}{\partial x} + \frac{1}{m_y}\frac{\partial u_k}{\partial y}\right) \tag{2.116}$$

$$(t_{yy})_k = 2A_H \frac{1}{m_y}\frac{\partial v_k}{\partial y}. \tag{2.117}$$

The horizontal diffusion coefficient, A_H, is often specified as a minimum constant value necessary to smooth cell to cell spatial oscillations in the solution field when the central difference form of the advective acceleration, equation (2.109) is used. When the horizontal turbulent diffusion is used to represent subgrid scale mixing, A_H may be determined as suggested by (Smagorinsky, 1963).

The solution scheme for equations (2.103) to (2.105) requires first, the evaluation of all terms in the three equations at time levels n and $n-1$. On boundaries where the transports are specified, the specified values at time level $n+1$ are inserted into equation (2.105). Equations (2.103) and (2.104) are then used to eliminate the unknown transports at time level $n+1$, from equation (2.105). The result is a discrete Helmholtz type elliptic equation for the free surface displacement at time level $n+1$, having the general form

$$\zeta^{n+1} - g\Delta t^2 \left(\frac{1}{m}\right)^{\zeta} \left[\delta_x^{\zeta}\left(H\frac{m_y}{m_x}\right)^{u}\delta_x^{u}\zeta^{n+1} + \delta_x^{\zeta}\left(H\frac{m_x}{m_y}\right)^{v}\delta_y^{v}\zeta^{n+1}\right] - \phi = 0 \tag{2.118}$$

with the term ϕ containing all previously evaluated terms and transport boundary conditions. For cells where the free surface displacement is specified, equation (2.118) is replaced by an equation which enforces the specified boundary condition at time level $n+1$. For the rigid lid case where the free surface displacement is constant in time and space, equation (2.118) is modified to give an equation for the unknown surface pressure p_s, by eliminating the first term, replacing $g\zeta$ in the discrete elliptic operator by p_s, and appropriately modifying the last term. In the computer code, the system of equations corresponding to equation (2.118) is solved by a reduced system conjugate gradient scheme with a multicolor or red-black ordering of the cells (Hageman and Young, 1981). The conjugate gradient iterations continue until the sum of the squared residuals is less than a specified value. The free surface displacements or surface pressures are then substituted into equations (2.103)-(2.104) to determine the transports at time level $n+1$. Since the solution of equation (2.118) is approximate, equation (2.105) may not be identically satisfied upon substitution of the time level $n+1$ transports and free surface displacement. To ensure that the equation (2.105) is identically satisfied in the case of a dynamic free surface, it is solved for a revised value of the time level $n+1$, free surface displacement after introduction of the time level $n+1$ transports. For the rigid lid case, an external divergence error is calculated and compensated for by adding appropriate volumetric source or sink terms to equation (2.105) during the next time step.

2.5. Computational Aspects of the Three-Time Level Internal Mode Solution

The internal mode equations (2.94) and (2.95) are solved using a fractional step scheme (Peyret and Taylor, 1983) with the first step being explicit and the second step being im-

plicit. Figure 2.5 illustrates the location variables in the x, z plane for the x component of the internal mode equations.

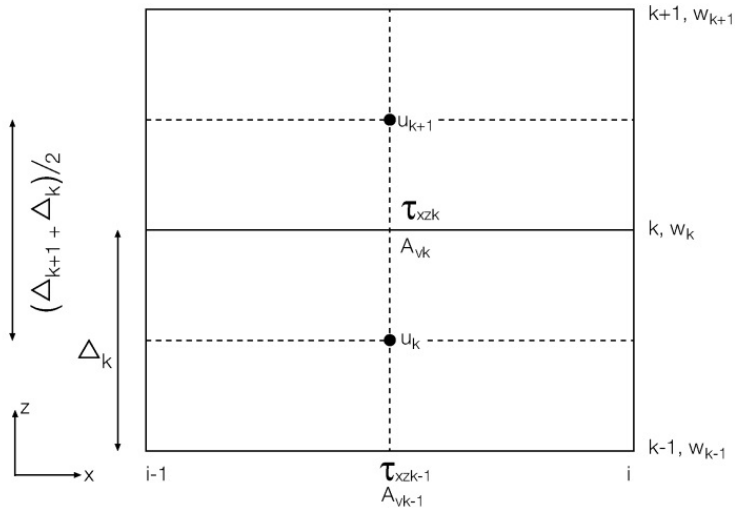

Fig. 2.5. U-centered grid in the vertical (x,z) plane.

The computational equations for the three-time level explicit step are;

$$
\begin{aligned}
(P_{k+1}-P_k)^{**} = {} & (P_{k+1}-P_k)^{n-1} \\
& -2\Delta t\left(\frac{1}{m_x}\right)^u\left[\delta_x^u\left(P_{k+1}u_{k+1}-P_ku_k\right)+\delta_y^u\left(Q_{k+1}u_{k+1}-Q_ku_k\right)\right] \\
& -2\Delta t\left(\frac{1}{m_x}\right)^u\left[\frac{(Wu)_{k+1}-(Wu)_k}{\Delta_{k+1}}-\frac{(Wu)_k-(Wu)_{k-1}}{\Delta_k}\right]^u \\
& +2\Delta t\left(\frac{1}{m_x}\right)^u\left[m_yfQ_{k+1}-m_yfQ_k\right]^u \\
& +2\Delta t\left(\frac{1}{m_x}\right)^u\left[\left(v_{k+1}\frac{\partial m_y}{\partial x}-u_{k+1}\frac{\partial m_x}{\partial y}\right)Hv_{k+1}-\left(v_k\frac{\partial m_y}{\partial x}-u_k\frac{\partial m_x}{\partial y}\right)Hv_k\right]^u \\
& +2\Delta t\left(\frac{m_y}{m_x}H\right)^u g\left[(b_{k+1}-b_k)^u\delta_x^u\left(h-z_kH\right)+\frac{1}{2}H^u\delta_x^u\left(b_{k+1}\Delta_{k+1}+b_k\Delta_k\right)\right] \\
& +2\Delta t\left(\frac{1}{m_x}\right)^u\left[(S_u)_{k+1}-(S_u)_k\right]^u
\end{aligned}
\tag{2.119}
$$

$$
\begin{aligned}
(Q_{k+1}-Q_k)^{**} = {} & (Q_{k+1}-Q_k)^{n-1} \\
& - 2\Delta t\left(\frac{1}{m_y}\right)^v \left[\delta_y^v\left(P_{k+1}v_{k+1}-P_kv_k\right)+\delta_y^v\left(Q_{k+1}v_{k+1}-Q_kv_k\right)\right] \\
& - 2\Delta t\left(\frac{1}{m_y}\right)^v \left[\frac{(Wv)_{k+1}-(Wv)_k}{\Delta_{k+1}}-\frac{(Wv)_k-(Wv)_{k-1}}{\Delta_k}\right]^v \\
& - 2\Delta t\left(\frac{1}{m_y}\right)^v \left[m_xfP_{k+1}-m_xfP_k\right]^v \\
& - 2\Delta t\left(\frac{1}{m_y}\right)^v \left[\left(v_{k+1}\frac{\partial m_y}{\partial x}-u_{k+1}\frac{\partial m_x}{\partial y}\right)Hu_{k+1}-\left(v_k\frac{\partial m_y}{\partial x}-u_k\frac{\partial m_x}{\partial y}\right)Hu_k\right]^v \\
& + 2\Delta t\left(\frac{m_x}{m_y}H\right)^v g\left[(b_{k+1}-b_k)^v\delta_y^v\left(h-z_kH\right)+\frac{1}{2}H^v\delta_y^v\left(\Delta_{k+1}b_{k+1}+\Delta_kb_k\right)\right] \\
& + 2\Delta t\left(\frac{1}{m_y}\right)^v \left[(S_v)_{k+1}-(S_v)_k\right]^v
\end{aligned}
\tag{2.120}
$$

$$
W \;=\; m_xm_yw \;=\; mw, \tag{2.121}
$$

where the superscript ** denotes the provisional solution, and all the terms that don't have a specified time level are at the centered time level n. The horizontal volume transport, P and Q are defined by the equation (2.80), and W is the vertical volume transport. The horizontal difference operations on the horizontal advection terms are identical to those presented in Section 2.3, equations (2.108) to (2.110). The vertical momentum flux terms may be represented in forms consistent with central or upwind differencing as shown in equations (2.122) and (2.123).

$$
(Wu)^u_{i,j,k} = \frac{W_{i-\frac{1}{2},j,k}+W_{i+\frac{1}{2},j,k}}{2}\,\frac{u_{i,j,k}+u_{i,j,k+1}}{2} \tag{2.122}
$$

$$
(Wu)^u_{i,j,k} = \max\left(\frac{W_{i-\frac{1}{2},j,k}+W_{i+\frac{1}{2},j,k}}{2},0\right)u^{n-1}_{i,j,k}+\min\left(\frac{W_{i-\frac{1}{2},j,k}+W_{i+\frac{1}{2},j,k}}{2},0\right)u^{n-1}_{i,j,k+1} \tag{2.123}
$$

where the advected velocity is in the upwind form, equation (2.123) is evaluated at time level $n-1$ for stability. The horizontal difference operations on the buoyancy and mean and total depths are central difference operators defined by equations (2.106) and (2.107). The inclusion of horizontal diffusion in the source, sink terms in equations (2.119) and (2.120) would follow from its inclusion in equations (2.103) and (2.104). The Coriolis and curvature terms are averaged and differenced by the energy conserving scheme presented in the Section 2.3, equations (2.111) to (2.114). The stability of the explicit fractional step

(Equations (2.119) and (2.120)) is governed by the stability of the discretization of the horizontal and vertical advective accelerations, which will be discussed in Section 2.5, and the discretization of the Coriolis and curvature terms. The results of the Fourier stability analysis of the external mode scheme, with respect to the Coriolis acceleration, can be shown to apply to the internal mode scheme as well.

The computational equations for the second step of the three-time level scheme are:

$$\frac{(P_{k+1}-P_k)^{n+1}}{m_y^u\Delta_{k+1,k}} = \frac{(P_{k+1}-P_k)^{**}}{m_y^u\Delta_{k+1,k}} + 2\Delta t\left[\frac{(\tau_{xz})_{k+1}-(\tau_{xz})_k}{\Delta_{k+1}\Delta_{k+1,k}} - \frac{(\tau_{xz})_k-(\tau_{xz})_{k-1}}{\Delta_k\Delta_{k+1,k}}\right]^{n+1} \tag{2.124}$$

$$\frac{(Q_{k+1}-Q_k)^{n+1}}{m_x^v\Delta_{k+1,k}} = \frac{(Q_{k+1}-Q_k)^{**}}{m_x^v\Delta_{k+1,k}} + 2\Delta t\left[\frac{(t_{yz})_{k+1}-(t_{yz})_k}{\Delta_{k+1}\Delta_{k+1,k}} - \frac{(t_{yz})_k-(t_{yz})_{k-1}}{\Delta_k\Delta_{k+1,k}}\right]^{n+1} \tag{2.125}$$

Using equations (2.83) and (2.84), the turbulent shear stresses are related to the horizontal transports by:

$$(\tau_{xz})_k^{n+1} = \left(\frac{A_v^u}{H^u}\right)_k^n\left(\frac{1}{m_y^uH^u}\frac{P_{k+1}-P_k}{\Delta_{k+1,k}}\right)^{n+1} \tag{2.126}$$

$$(t_{yz})_k^{n+1} = \left(\frac{A_v^v}{H^v}\right)_k^n\left(\frac{1}{m_x^vH^v}\frac{Q_{k+1}-Q_k}{\Delta_{k+1,k}}\right)^{n+1} \tag{2.127}$$

Equations (2.126) and (2.127) could be used to eliminate the turbulent shear stresses from equations (2.124) and (2.125) to give a pair of $K-1$ systems of equations for the transport differences between layers, however, the resulting equations are poorly conditioned. Instead, equations (2.126) and (2.127) are used to eliminate the horizontal transport differences at time level $n+1$ from equations (2.124) and (2.125) to give a pair of $K-1$ equations for the turbulent shear stresses.

$$\begin{aligned}-\frac{1}{\Delta_k\Delta_{k+1,k}}(\tau_{xz})_{k-1}^{n+1} + \left[\frac{1}{\Delta_k\Delta_{k+1,k}} + \frac{(H^u)^{n+1}}{2\Delta t}\left(\frac{H^u}{A_v^u}\right)_k^n + \frac{1}{\Delta_{k+1}\Delta_{k+1,k}}\right](\tau_{xz})_k^{n+1} \\ -\frac{1}{\Delta_{k+1}\Delta_{k+1,k}}(\tau_{xz})_{k+1}^{n+1} = \frac{1}{2\Delta t m_y^u}\frac{(P_{k+1}-P_k)^{**}}{\Delta_{k+1,k}}\end{aligned} \tag{2.128}$$

$$\begin{aligned}-\frac{1}{\Delta_k\Delta_{k+1,k}}(t_{yz})_{k-1}^{n+1} + \left[\frac{1}{\Delta_k\Delta_{k+1,k}} + \frac{(H^v)^{n+1}}{2\Delta t}\left(\frac{H^v}{A_v^v}\right)_k^n + \frac{1}{\Delta_{k+1}\Delta_{k+1,k}}\right](t_{yz})_k^{n+1} \\ -\frac{1}{\Delta_{k+1}\Delta_{k+1,k}}(t_{yz})_{k+1}^{n+1} = \frac{1}{2\Delta t m_x^v}\frac{(Q_{k+1}-Q_k)^{**}}{\Delta_{k+1,k}}\end{aligned} \tag{2.129}$$

These equations are diagonally dominant and well conditioned, and can be solved independently at each of the horizontal velocity locations. Since equations (2.128) and (2.129) represent fully implicit, backward difference in time, schemes for one dimensional parabolic diffusion equations, the solutions are unconditionally stable (Fletcher, 1988). Given the solutions of the equations (2.128) and (2.129), the shear stresses, the $K-1$ transport differences, $P_{k+1}-P_k$, and $Q_{k+1}-Q_k$, are determined from equations (2.126) and (2.127) and combined with the continuity constraints, equations (2.92) and (2.93), to form a pair of K equations for the horizontal transports in each cell layer. To illustrate, the horizontal transports in the surface cell layer are determined analytically and given as

$$P_k = \hat{P} + \sum_{k=1}^{K-1} \left(\sum_{j=1}^{k} \Delta_j \right) (P_{k+1} - P_k) \,. \tag{2.130}$$

A similar expression can be derived for Q_K. Working down from the surface using the $K-1$ transport differences allows the remaining transports to be determined. It is noted for later use that the bottom cell layer transports can be expressed in terms of the depth integrated transports and the transport differences using:

$$P_1 = \hat{P} - \sum_{k=1}^{K-1} \left(1 - \sum_{j=1}^{k} \Delta_j \right) (P_{k+1} - P_k), \tag{2.131}$$

and an identical equation for Q_1.

The solution of equations (2.128) and (2.129) requires specification of bottom and surface stresses at $k=0$ and $k=K$, respectively. On the free surface, $(k=K)$ the surface wind stress components are specified. On the bottom fluid-solid boundary, $(k=0)$ the bottom stress must be specified. The simplest approach to specifying the bottom stress components utilizes the velocity component in the bottom cell layer and the quadratic friction relations shown in equations (2.132) and (2.132).

$$(\tau_{xz})_0^{n+1} = C_b \left(\sqrt{(u_1)^2 + (v_1^u)^2} \right)^n \left(\frac{P_1}{m_y^u H^u} \right)^{n+1} \tag{2.132}$$

$$(t_{yz})_0^{n+1} = C_b \left(\sqrt{(u_1^v)^2 + (v_1)^2} \right)^n \left(\frac{Q_1}{m_x^v H^v} \right)^{n+1} \tag{2.133}$$

Assuming a logarithmic velocity profile between the solid bottom and the middle of the bottom cell layer gives the bottom stress coefficient:

$$C_b = \frac{\kappa^2}{\left[\ln \left(\frac{\Delta_1 H}{2 z_0^*} \right) \right]^2} \tag{2.134}$$

where z_o^* is the dimensional bottom roughness height. Inserting equation (2.131) and a corresponding equation for Q_1 into equations (2.132) and (2.133), respectively allows the bottom stresses at time level $n+1$ to be expressed in terms of the depth integrated transport components, known from the external mode solution, and the unknown transport differences at time level $n+1$. However, the transport differences at time level $n+1$ are related to the shear stress components by equations (2.126) and (2.127), allowing the bottom stresses to be expressed in terms of the depth integrated transports and the internal shear stresses by:

$$(\tau_{xz})_0^{n+1} = C_b\left(\sqrt{(u_1)^2+\left(v_1^u\right)^2}\right)^n\left[\left(\frac{\hat{P}}{m_y^u H^u}\right)^{n+1} - \sum_{k=1}^{K-1}\left(1-\sum_{j=1}^{k}\Delta_j\right)\frac{\Delta_{k+1,k}(\tau_{xz})_k^{n+1}}{\left(\frac{A_v^u}{H^u}\right)_k^n}\right], \tag{2.135}$$

and a similar expression for the y component. Inserting equation (2.135) and the corresponding y component equation for the bottom stress components into the $k=1$ pair of equations (2.128) and (2.129) results in a nearly tri-diagonal system with a fully populated first row. The systems of equations are still efficiently solved using a tri-diagonal equation solver and the Sherman-Morrison formula (Press et al., 1986).

The internal mode solution is completed by the determination of the vertical velocity using:

$$w_k = w_{k-1} - \frac{\Delta_k}{m^\zeta}\left[\delta_x^\zeta\left(P_k-\hat{P}\right)+\delta_y^\zeta\left(Q_k-\hat{Q}\right)\right] \tag{2.136}$$

which follows from the equation (2.97). The solution of equation (2.136), where all variables are at time level $n+1$, proceeds from $k=1$ since $w_o=0$. A two time level correction step is also periodically inserted into the internal mode time integration on the same time step as the external mode correction. The computational equations follow directly from the three time level equations using the details of the external mode presented in Section .

2.6. Vertical Layering Options

This section summarizes the vertical coordinate options in EFDC+. It supplements the theoretical and computational description of the basic EFDC+ hydrodynamic and transport model components. The EFDC+ model was originally formulated with a sigma stretched vertical coordinate. Later, more efficient vertical layering options, namely sigma-zed options have been implemented to reduce the error due to the horizontal pressure gradients and to reduce the number of computational cells.

2.6.1 Sigma Coordinate System

A sigma coordinate system is a topographically conformal vertical coordinate system which is widely used in three-dimensional hydrodynamic models. In this vertical coordinate system, the number of vertical levels in the water column is the same everywhere in the domain irrespective of the depth of the water column (Figure 2.6(a)). This can resolve the water column equally well and equally efficiently in both shallow and deep regions of a computational domain simultaneously and it is suitable for a water body with complicated geometry and large changes in bottom elevation. The transformation of the governing equations using sigma-coordinate in the vertical is described in the Section 2.1.

In the sigma coordinate formulation, the number of vertical layers is the same at all horizontal locations in the model grid. Although this formulation is widely accepted, conceptually attractive and adequate for a large range of applications, there are numerous application classes where a traditional z or physical vertical grid is desirable, such as deep reservoirs with rapid and large lateral bathymetric changes. There are also applications where the ability to use a combination of sigma and physical z vertical layering in different regions of the horizontal domain would be desirable. An example would be a deep navigation channel in an otherwise shallow estuary. The sigma stretched vertical grid formulation may also be subject to internal pressure gradient errors (Mellor et al., 1994) providing another motivation for having alternative options to the sigma formulation.

2.6.2 Sigma-Zed Approach (SGZ)

The standard sigma grid used for the transformation of the vertical coordinate introduces a well-known error in the horizontal gradient terms including the concentration, velocity, and pressure (Mellor et al., 1994). In general, this error is significant only in the regions with steeply varying bathymetry. In order to overcome this weakness, two new vertical layering approaches that are computationally efficient have been developed and applied to the EFDC+ model (Craig et al., 2014). The vertical layering scheme has been modified to allow the number of layers to vary over the model domain based on the water depth. Consequently, each cell can have a different number of layers. The z coordinate system varies for each cell face, matching the number of active layers to the adjacent cells (face matching of layering is a fundamental difference with the GVC approach). Such a transformation is referred to as the sigma-zed (SGZ) coordinate. The differences in the two optional SGZ approaches relate to the sigma layer thickness computed for each cell. Figure 2.6 shows a schematic demonstrating the layering options. Panel (a) represents a standard sigma stretch grid with 10 layers. Panels (b) represents the specified bottom approach which allows a user specified number of layers in each horizontal cell. Figure 2.6(c) represent SGZ options with uniform layering where the bottom of each vertical layer are aligned in the horizontal direction. It should be noted that, in SGZ coordinate the number of vertical layers can be very large, but the computational time is shorter in comparison with a similarly configured sigma (SIG) coordinate model.

For SGZ transformation, the equations are still the same as the standard sigma trans-

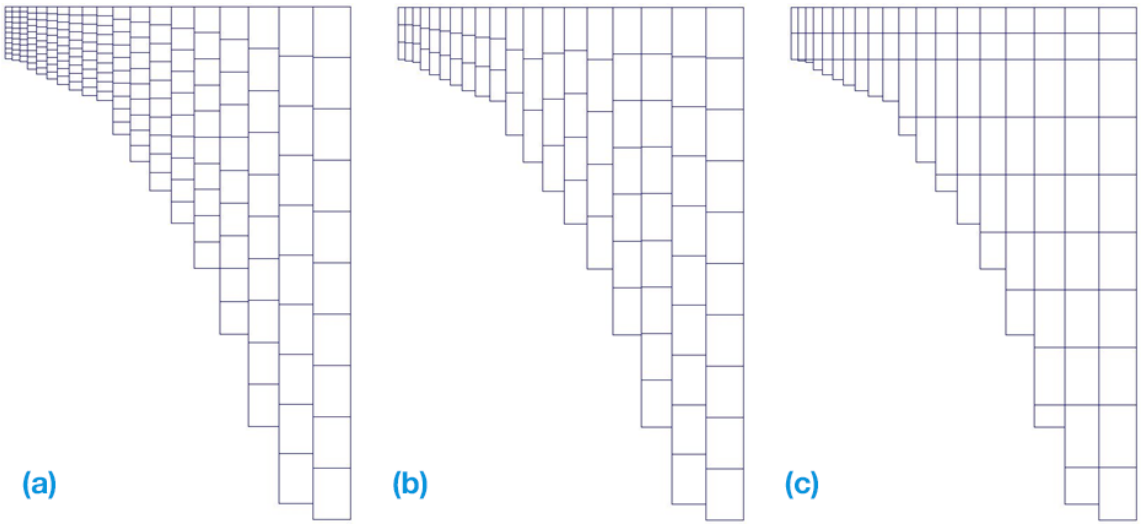

Fig. 2.6. An illustration of EFDC+ Layering options for a model with $K = 10$. (a) Standard Sigma (SIG), (b) SGZ-Specified Bottom, and (c) SGZ-Uniform Layering.

formation, however, the number of layers at each cell differs based on a factor determined based on the ratio between bed elevation and the minimum elevation. In addition, the thickness of layers at each cell must satisfy

$$\sum_{k=n}^{KC} \Delta_k = 1, \tag{2.137}$$

in which KC is the maximum number of layers, n the index of bottom layer and Δk the thickness of layer k.

For the original sigma the index of the bed layer always is equal to $n = 1$ while in the SGZ this value can be varied in the range $1 \leq n \leq K$ depending on the number of layers due to the rescaling. This requirement improves the accuracy of the horizontal gradient calculation for the variable $C_{i,j,k}$ of the cell $L(i, j)$ at layer k :

$$pd[C_{i,j,k}]x = \frac{C_{i,j,k} - C_{i-1,j,k}}{\Delta x}. \tag{2.138}$$

When sediment transport is simulated and bed morphology is considered, the determination of the new indices of bottom layers should be implemented at every time step. This is because currently the ratios between water depths and the maximum are changing due to erosion or deposition compared to the previous time step. Therefore, an update of layering for the whole domain is important and necessary for SGZ. However, the re-layering is only an optional approach.

The other necessary modification for SGZ coordinate system is the treatment on wet/dry in 3-D calculation of the horizontal gradient when the number of layers at cell $L(i-1, j)$

is less than that at cell $L(i, j)$. It should be noted that this problem does not appear for SIG coordinates, because the number of layers is the same for every cell. This means that the SIG model requires more calculation time and is therefore one of the weak points of the SIG coordinate system which is overcome with SGZ.

2.6.3 Verification of SGZ Approach

A modification of the vertical coordinate system algorithm in EFDC+ with SGZ transformation has been successfully implemented. It has been tested for many computation domains with different hydrodynamic regimes, such as the application to Lake Washington (Seattle, WA, USA), which has steep bottom gradients and sharp thermoclines.

In this test, two EFDC+ options including the original sigma (SIG) and sigma-zed (SGZ), were applied with the same model conditions. Some parameters in the model for the two options are presented in Table 2.2.

Table 2.2. Input parameters for the Lake Washington Model With Two Different Layering Options

Options	Time (days)	Time step (seconds)	Number of layers	Thermal model
Standard sigma stretched grid (SIG)	120	5	55	Yes
Sigma-Zed grid (SGZ)	120	5	2 - 55	Yes

In order to investigate the influence of horizontal gradient terms on the vertical profiles of temperature as well as the accuracy between SIG and SGZ models, comparisons between the model outputs versus the data were conducted for every day during the summer 2008 simulation period. Eight representative vertical profiles, starting at the beginning of the simulation and ending on October 15, are presented in Figure 2.7 for the SIG model and Figure 2.8 for the SGZ model. These figures suggest that the temperature profile generated by the SGZ model replicates the observed data better than the SIG model.

2.7. Near-Field Discharge Dilution and Mixing Zone Analysis

The calculation procedure of the jet/plume submodel is mainly based on Lee and Cheung (1990). The trajectory of a group of plume particles is traced in time using a Lagrangian formulation. The plume puff gains mass as ambient fluid is entrained and mixed within it, but once entrained, the new mass becomes an indistinguishable part of the plume puff. In the simplest version, the plume is assumed to be essentially a cylindrical segment whose radius grows as mass is entrained. The initial plume mass is identified as the mass issuing form a diffuser with radius b_0 :

$$M_0 = \rho_0 \pi b_0^2 h_0, \tag{2.139}$$

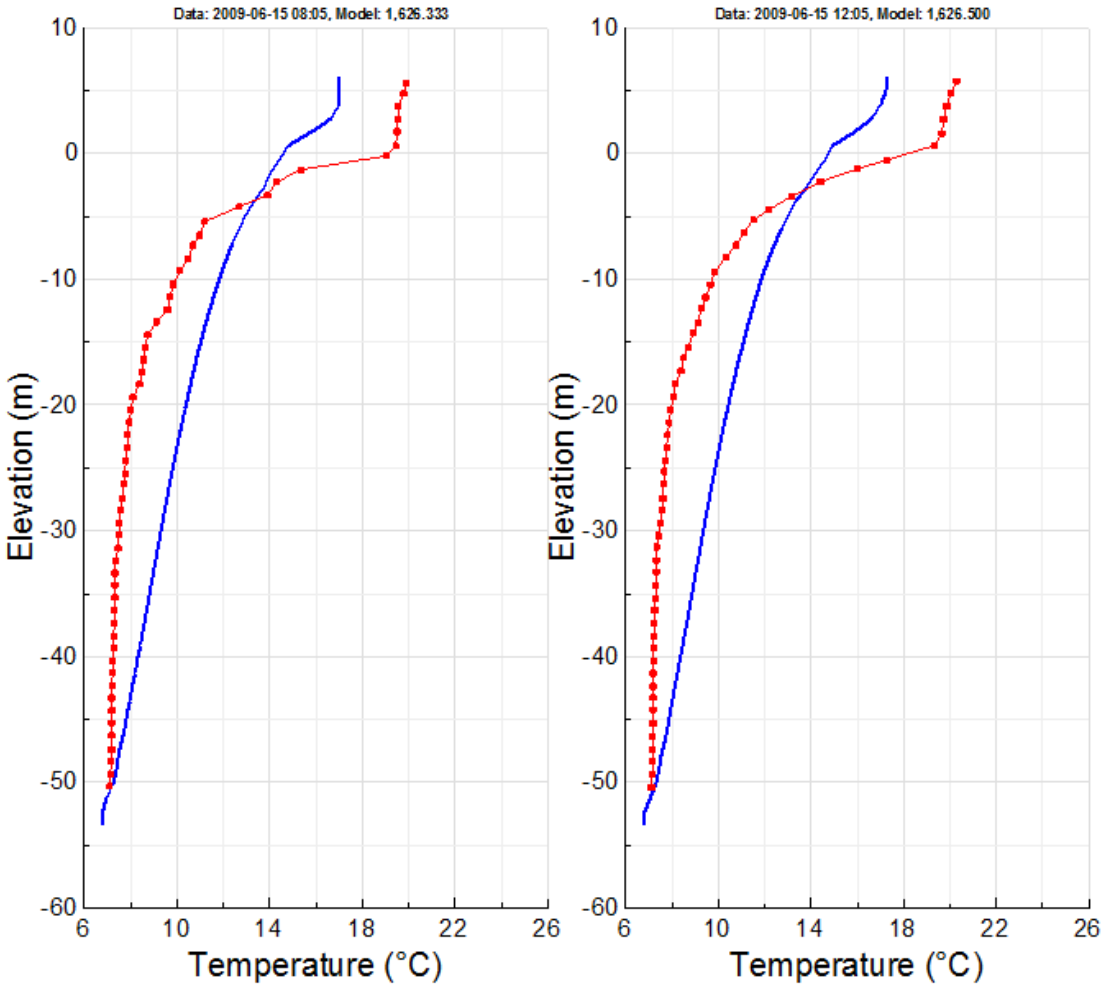

Fig. 2.7. Comparison of the vertical profile of temperature between data (red) and SIG model (blue).

where h_0 is the length of the plume mass and is chosen to be comparable to b_0. For example, $h_0 = r$ and $b_0 = r$, where r is the radius of the diffuser.

$$h_0 = V_0 \Delta t \tag{2.140}$$

The increment in the plume mass at the time step n^{th} is evaluated as the sum of the plume mass increment due to the shear-induced entrainment and the forced entrainment.

$$\Delta M_n = \Delta M_s + \Delta M_f \tag{2.141}$$

In equation (2.141) ΔM_s is the increase in mass due to shear entrainment, and ΔM_f is the increase in mass due to forced entrainment. A schematic of a rising plume discharged into a water body is shown in Figure 2.9.

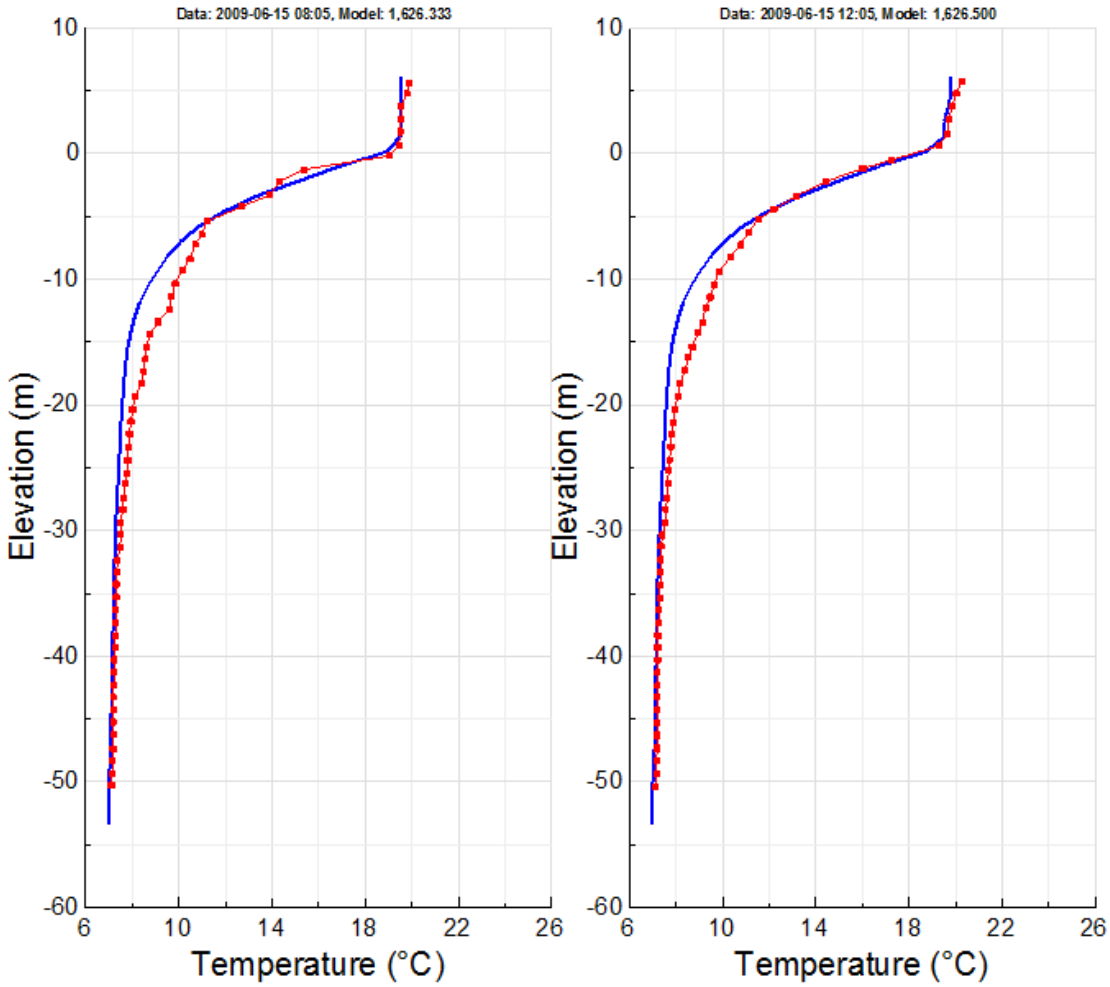

Fig. 2.8. Comparison of the vertical profile of temperature between data (red) and SGZ model (blue).

2.7.1 Shear-Induced Entrainment

The increase in mass of the plume element is due to turbulent entrainment of the ambient flow. Close to the discharge point, or in a very weak current, shear-induced entrainment dominates. In general, however, the forced entrainment of the cross flow dominates, except very close to the source. In the model, assuming the total entrainment is a function of the horizontal currents and a shearing action of the plume relative to the currents, the increase in mass due to shear entrainment, ΔM_s, is written as

$$\Delta M_s = \rho_a 2\pi b_n h_n E \left| V_n - u_a \cos\phi_n \cos\theta_n \right| \Delta t. \tag{2.142}$$

In which the subscript n denotes the value of plume element at n^{th} step of calculation,

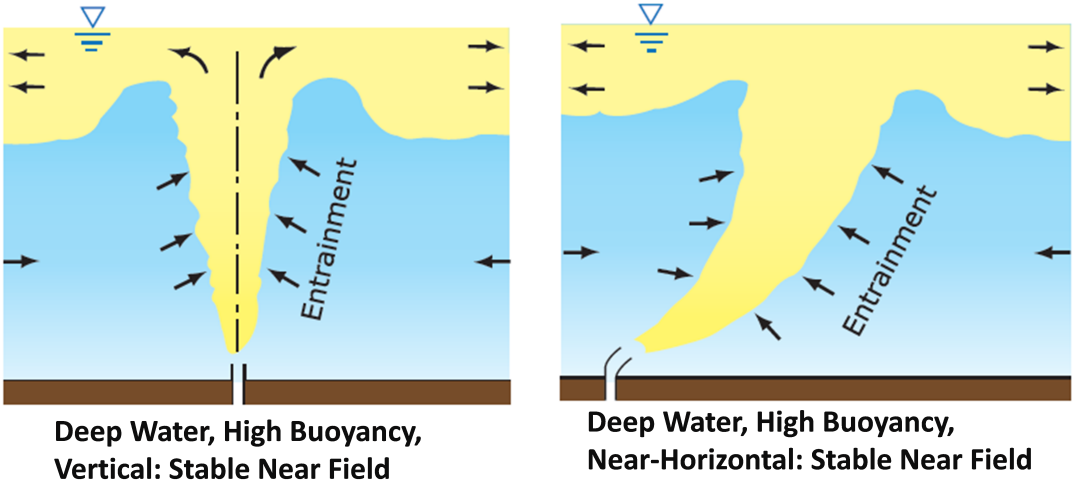

Fig. 2.9. Near field Jet Plume mixing.

the subscript a denotes the local ambient value, E is the entrainment coefficient which is dependent on the local densimetric Froude number F_1 and jet orientation

$$E = \sqrt{2}\frac{0.057 - 0.554\frac{\sin\theta_n}{F_1^2}}{1 + 5\frac{u_a \cos\phi_n \cos\theta_n}{|V_n - u_a \cos\phi_n \cos\theta_n|}}, \tag{2.143}$$

where F_1 is the local densimetric Froude number

$$F_1 = \alpha\frac{|V_n - u_a \cos\phi_n \cos\theta_n|}{\sqrt{g\frac{\Delta\rho_n}{\rho_a}b_n}}, \tag{2.144}$$

and α is a proportionality constant.

2.7.2 Forced Entrainment

Experimental observations by Chu and Goldberg (1984) and Stuart Churchill (1975) have shown that the transfer of horizontal momentum is complete beyond a few jet diameters. We assume that all the ambient flow on the downdrift side of the plume is entrained into the plume element. This forced entrainment of the ambient flow into an arbitrarily inclined plume element can be formulated as

$$\Delta M_f = \rho_a u_a \left[2b\Delta s\sqrt{1 - \cos^2\phi\cos^2\theta} + \pi b\Delta b\cos\phi\cos\theta + \frac{1}{2}\pi b^2\Delta(\cos\phi\cos\theta)\right] \tag{2.145}$$

In the equation 2.145, the first term represents the forced entrainment due to the projected plume area normal to the cross flow; the second term is a correction due to the growth of plume radius; and the third term is a correction fue to the curvature of the trajectory.

An initial estimate of ΔM_f can be obtained as

$$\Delta M_f = \rho_a u_a h_n b_n \left[2\sqrt{\left(\sin^2\phi + \sin^2\theta - \sin^2\phi\sin^2\theta\right)_n} + \pi\left(\frac{\Delta b}{\Delta s}\cos\phi\cos\theta\right)_n + \frac{\pi b_n}{2}\frac{(\cos\phi\cos\theta)_n - (\cos\phi\cos\theta)_{n-1}}{\Delta s_n}\right]\Delta t \tag{2.146}$$

2.7.3 Model Implementation

At the n^{th} step, consider a plume element located at $(x_n,\ y_n,\ z_n)$ with the velocity $(u_n,\ v_n,\ w_n)$ and its magnitude V_n. The jet axis makes an angle of ϕ_n with the horizontal plane, and θ_n is the angle between the x-axis and the projection of the jet axis on the horizontal plane. The half-width or radius of the plume element is b_n; h_n is the thickness, defined as proportional to the magnitude of the local jet velocity, $h_n = V_n\Delta t$. The mass of the plume element is then given by

$$M_n = \rho_n \pi b_n^2 h_n \tag{2.147}$$

Given the increase in mass due to turbulent entrainment, ΔM_n, the plume element characteristics at the next step are obtained by applying conservation of mass, horizontal and vertical momentum, energy, and tracer mass to the discrete element. For completeness, the self-explanatory equations of the generalized Lagrangian model, essentially similar to its original two-dimensional counterpart (Winiarski and Frick, 1976) are summarized as follows:

Mass conservation

$$M_{n+1} = M_n + \Delta M_n \tag{2.148}$$

$$M_{n+1} = \rho_{n+1}\pi b_{n+1}^2 h_{n+1} \tag{2.149}$$

The concentration of the tracer, salinity, temperature and water density

$$C_{n+1} = \frac{M_n C_n + \Delta M_n C_a}{M_{n+1}} \tag{2.150}$$

$$S_{n+1} = \frac{M_n S_n + \Delta M_n S_a}{M_{n+1}} \tag{2.151}$$

$$T_{n+1} = \frac{M_n T_n + \Delta M_n T_a}{M_{n+1}} \tag{2.152}$$

$$\rho_{n+1} = \rho\left(S_{n+1}, T_{n+1}\right) \tag{2.153}$$

The horizontal momentum

$$u_{n+1} = \frac{M_n u_n + \Delta M_n u_a}{M_{n+1}} \tag{2.154}$$

$$v_{n+1} = \frac{M_n v_n}{M_{n+1}} \tag{2.155}$$

The vertical momentum

$$w_{n+1} = \frac{M_n w_n + \Delta M_{n+1}\left(\frac{\Delta\rho}{\rho}\right)_{n+1} g\Delta t}{M_{n+1}} \tag{2.156}$$

$$(Mw)_{n+1} = (Mw)_n + (\Delta\rho V)_{n+1} g\Delta t \tag{2.157}$$

where

$$V_{n+1} = \sqrt{u_{n+1}^2 + v_{n+1}^2 + w_{n+1}^2} \tag{2.158}$$

$$U_{n+1} = \sqrt{u_{n+1}^2 + v_{n+1}^2} \tag{2.159}$$

The new thickness and radius of the plume element

$$h_{n+1} = \frac{V_{n+1}}{V_n} h_n \tag{2.160}$$

$$b_{n+1} = \sqrt{\frac{M_{n+1}}{\pi\rho_{n+1} h_{n+1}}} \tag{2.161}$$

The jet orientation

$$\phi_{n+1} = \arctan\left(\frac{w_{n+1}}{U_{n+1}}\right) \tag{2.162}$$

$$\theta_{n+1} = \arctan\left(\frac{v_{n+1}}{u_{n+1}}\right) \tag{2.163}$$

The new location of the plume element

$$x_{n+1} = x_n + u_{n+1}\Delta t \tag{2.164}$$

$$y_{n+1} = y_n + v_{n+1}\Delta t \tag{2.165}$$

$$z_{n+1} = z_n + w_{n+1}\Delta t \tag{2.166}$$

The distance along the trajectory

$$\Delta s_{n+1} = V_{n+1}\Delta t \tag{2.167}$$

The time step Δt can be fixed or variable; its is chosen via a "prediction-correction" procedure to attain a prescribed fractional change in mass (typically of the order of 1%) at each step.

Chapter 3

TRANSPORT MODEL FOR CONSERVATIVE CONSTITUENTS

3.1. Introduction

This section summarizes the theoretical and computational aspects of the transport formulations for passive scalar transport used in EFDC+. Theoretical and computational aspects for the EFDC+ generic transport model components are presented in Hamrick (1992).

3.2. Basic Equation of Advection-Diffusion Transport

The generic transport equation for a dissolved or suspended material is shown in equation (3.1):

$$\frac{\partial}{\partial t}(m_x m_y HC) + \frac{\partial}{\partial x}(m_y HuC) + \frac{\partial}{\partial y}(m_x HvC) + \frac{\partial}{\partial z}(m_x m_y wC) - \frac{\partial}{\partial z}(m_x m_y w_{sc} C) = \frac{\partial}{\partial x}\left(\frac{m_y}{m_x} HA_H \frac{dC}{dx}\right) + \frac{\partial}{\partial y}\left(\frac{m_x}{m_y} HA_H \frac{dC}{dy}\right) + \frac{\partial}{\partial z}\left(\frac{m_x m_y}{H} A_b \frac{dC}{dz}\right) + S_C \quad (3.1)$$

where

- x, y are the orthogonal curvilinear coordinates in the horizontal direction (m)
- z is the sigma coordinate (dimensionless)
- t is time (s)
- m_x, m_y are the square roots of the diagonal components of the metric tensor (m)
- m is the Jacobian $m = m_x m_y$ (m^2)
- C is the concentration or intensity of transport constituent (g/m^3 for concentration of dissolved/suspended material, °C for temperature, ppt for salinity)

H is the total water depth (m)

u, v are the horizontal velocity components in the curvilinear coordinates (m/s)

w is the vertical velocity component (m/s)

A_H is the horizontal turbulent eddy diffusivity (m^2/s)

A_b is the vertical turbulent eddy diffusivity (m^2/s)

w_{sc} is a positive settling velocity when C represents a suspended material

S_c is the source/sink term for the constituent that includes subgrid scale horizontal diffusion and thermal sources and sinks.

3.3. Numerical Solution for Transport Equations

In this section, solutions techniques for the transport equations for salinity, temperature, turbulence intensity, and turbulence length scale are presented. Stability and accuracy aspects of the advection schemes common to the transport equations and the external and internal horizontal momentum equations are also discussed. The salinity transport equation (3.2) is used as a generic example and the location of variables is shown in Figure 3.1.

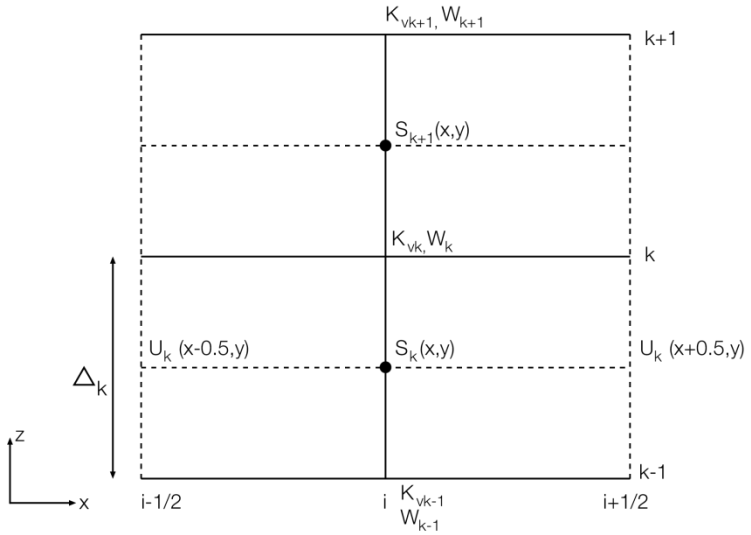

Fig. 3.1. S-centered grid in the vertical (x,z)-plane

The salinity transport equation (3.2) is integrated over a cell layer to give:

$$\frac{\partial}{\partial t}(mHC_k)+\frac{\partial}{\partial x}(P_kC_k)+\frac{\partial}{\partial y}(Q_kC_k)+\frac{(WC)_k-(WC)_{k-1}}{d_k}- \frac{m}{d_k}\left[\left(\frac{A_b}{H}\frac{dC}{dz}\right)_k-\left(\frac{A_b}{H}\frac{dC}{dz}\right)_{k-1}\right]-(S_C)_k=0 \quad (3.2)$$

where P_k, Q_k, and W_k are defined by equations (2.80) and (2.121). The source, sink, advection, and vertical diffusion portions of equation (3.2) are treated in separate fractional steps, as was done for the internal mode momentum equations in Section 2.4.

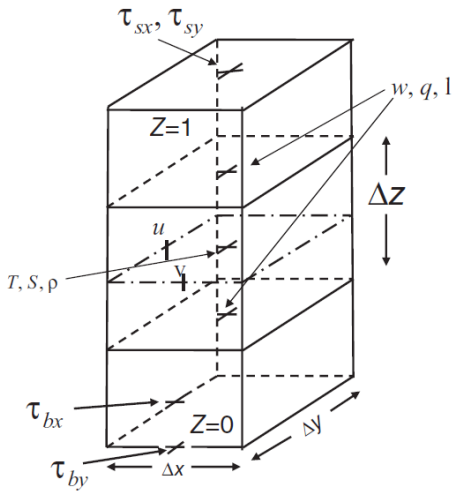

Fig. 3.2. Sigma coordinate and variable center (Ji, 2008).

The three time level fractional step sequence is given by:

$$C_k^* = C_k^{n-1} + \frac{2dt}{mH^{n-1}}(S_C)_k^{n-1} \tag{3.3}$$

$$(mH)^{n+1}C_k^{**} = (mH)^{n-1}C_k^* - 2dt\left[d_x^d(P_kC_k) + d_y^d(Q_kC_k) + \frac{(WC)_k - (WC)_{k-1}}{d_k}\right] \tag{3.4}$$

$$(HC_k)^{n+1} - 2dt\left\{\left[\left(\frac{A_b}{H}\right)_k^n \frac{(C_{k+1}-C_k)^{n+1}}{d_k d_{k+1,k}}\right] - \left[\left(\frac{A_b}{H}\right)_{k-1}^n \frac{(C_k - C_{k-1})^{n+1}}{d_k d_{k,k-1}}\right]\right\} = H^{n+1}C_k^{**} \tag{3.5}$$

The source, sink step (see equation (3.3)) is explicit and involves no changes in cell volumes. When the source, sink term represents horizontal turbulent diffusion, it is evaluated at time level $n-1$, for stability (Fletcher, 1988). The advection step, equation (3.4), is explicit and involves changes in cell volumes. The vertical diffusion step, equation (3.5), which involves no changes in cell volumes, is fully implicit and unconditionally stable (Fletcher, 1988).

Rearranging equation (3.5), the vertical diffusion step, gives:

$$-\frac{2dt}{d_k d_{k,k-1}}\left(\frac{A_b}{H}\right)^n_{k-1} C^{n+1}_{k-1} + \left[\frac{2dt}{d_k d_{k,k-1}}\left(\frac{A_b}{H}\right)^n_{k-1} + H^{n+1} + \frac{2dt}{d_k d_{k+1,k}}\left(\frac{A_b}{H}\right)^n_{k}\right] C^{n+1}_{k} - \frac{2dt}{d_k d_{k+1,k}}\left(\frac{A_b}{H}\right)^n_{k} C^{n+1}_{k+1} = H^{n+1} C^{**}_k \quad (3.6)$$

For salinity, temperature, and suspended sediment concentration, the generic variable C is defined vertically at cell layer centers, and the diffusivity is defined at cell layer interfaces. Equation (3.6) then represents a system of K equations and the boundary conditions are generally of the specified flux type. Specified surface and bottom flux boundary conditions are most conveniently incorporated in the surface and bottom cell layer source and sink terms allowing A_b at the bottom boundary, $k = 0$, and the surface boundary, $k = k+1$, to be set to zero making equation (3.6) tri-diagonal. For turbulence intensity and turbulence length scale, equations (2.23) and (2.24), the generic variable C is defined vertically at cell layer interfaces and the diffusivity is defined at cell layer centers. Equation (3.6) then represents a system of $K-1$ equations for the variables at internal interfaces with the variable values at the free surface and bottom being provided as boundary conditions. For the turbulence intensity and length scale, the boundary conditions are:

$$q^2_0 = B_1^{2/3}\sqrt{t^2_{bx}+t^2_{by}}, l_0 = 0, \text{ at} z = 0 \quad (3.7)$$

$$q^2_K = B_1^{2/3}\sqrt{t^2_{sx}+t^2_{sy}}, l_K = 0, \text{ at} z = 1 \quad (3.8)$$

where τ_b and τ_s are the bottom and surface stress vectors, respectively. Insertion of these boundary conditions results in equation (3.6) representing tri-diagonal systems of $K-1$ equations for the turbulence intensity and length scale.

Without loss of generality, the notation used in analyzing the three time level advection step, equation (3.4), is simplified by replacing the double and single asterisk intermediate time level indicators by $n+1$ and $n-1$, respectively to give:

$$(mHC_k)^{n+1} = (mHC_k)^{n-1} - 2\frac{dt}{dx}\left[(PC)_{i+\frac{1}{2},j,k} - (PC)_{i-\frac{1}{2},j,k}\right] - 2\frac{dt}{dy}\left[(QC)_{i,j+\frac{1}{2},k} - (QC)_{i,j-\frac{1}{2},k}\right] - 2\frac{dt}{d_k}\left[(WC)_k - (WC)_{k-1}\right] \quad (3.9)$$

where the horizontal central difference operators have been expanded about the cell volume centroid (x,y), according to equations (2.106) and (2.107). The cell face fluxes can be represented consistent with centered in time and space differencing as was illustrated by equations (2.108), (2.109) and (2.122) or forward in time and backward or upwind in space as was illustrated by equations (2.110) and (2.123) for the x momentum fluxes. For the centered in time and space form, equation (3.9) becomes:

$$
\begin{aligned}
(mHC_k)^{n+1} = (mHC_k)^{n-1} - \\
\frac{dt}{dx}\left[\tilde{P}_{i+\frac{1}{2},j,k}\left(C_{i+1,j,k}+C_{i,j,k}\right) - \tilde{P}_{i-\frac{1}{2},j,k}\left(C_{i,j,k}+C_{i-1,j,k}\right)\right] - \\
\frac{dt}{dy}\left[\tilde{Q}_{i,j+\frac{1}{2},k}\left(C_{i,j+1,k}+C_{i,j,k}\right) - \tilde{Q}_{i,j-\frac{1}{2},k}\left(C_{i,j,k}+C_{i,j-1,k}\right)\right] - \\
\frac{dt}{d_k}\left[\tilde{W}_{i,j,k}\left(C_{i,j,k+1}+C_{i,j,k}\right) - \tilde{W}_{i,j,k-1}\left(C_{i,j,k}+C_{i,j,k-1}\right)\right] \qquad (3.10)
\end{aligned}
$$

The transports in equation (3.10) are evaluated at the centered time level when used in the external and internal momentum equations, and are averaged to the centered time level using

$$\tilde{P}_k = \frac{1}{2}\left(P_k^{n+1} + P_k^{n-1}\right) \qquad (3.11)$$

when used in the transport equations for scalar variables.

Chapter 4

DYE MODULE

The dye constituent in EFDC+ represents a dilute substance in the water column that does not impact the hydrodynamics (i.e. no impact on thermal physical properties such as density and viscosity) or any other water column process (e.g. light extinction). This constituent can be used as a tracer, with or without decay, or it can be used to compute the age of water in days.

The dye is transported in the water column as determined by the equation (4.1).

$$\frac{\partial}{\partial t}(m_x m_y HC) + \frac{\partial}{\partial x}(m_y HuC) + \frac{\partial}{\partial y}(m_x HvC) + \frac{\partial}{\partial z}(m_x m_y wC) - \frac{\partial}{\partial z}(m_x m_y w_{sc} C)$$
$$= \frac{\partial}{\partial x}\left(\frac{m_y}{m_x} HA_H \frac{dC}{dx}\right) + \frac{\partial}{\partial y}\left(\frac{m_x}{m_y} HA_H \frac{dC}{dy}\right) + \frac{\partial}{\partial z}\left(\frac{m_x m_y}{H} A_b \frac{dC}{dz}\right) + \frac{dC}{dt} + S_C \quad (4.1)$$

4.1. Decay

The dye constituent can be configured to decay with a zeroth or first order approach, as shown in the equations 4.2 and 4.3, respectively.

$$\frac{dC}{dt} = -K \quad (4.2)$$

$$\frac{dC}{dt} = -KC \quad (4.3)$$

In equations 4.2 and 4.3, C is the dye concentration in g/m^3, K is the first order decay rate in 1/s and t is time is seconds.

Additionally, dye decay rate can be a function of water temperature using the equation (4.4).

$$\frac{dC}{dt} = -K\theta^{(T-T_{ref})}C \quad (4.4)$$

4.2. Age of Water

As mentioned, the dye constituent may be used to calculate the age of water (in days). With this option, a zero-order kinetic rate approach is used:

$$\frac{dC}{dt} = -K \tag{4.5}$$

where C is "age" in days, t is time in days and K is in units of 1/day. By averaging cell ages over all or parts of the model domain, residence times can be computed. If the model is run sufficiently long enough to achieve a dynamic steady state, the hydraulic residence time can be computed.

Chapter 5

TEMPERATURE AND HEAT TRANSFER MODULE

5.1. Introduction

This chapter presents an overview of heat transfer implemented in EFDC+, including the energy equation and heat transfer options. Additional details are given regarding the sub-models for water column temperature, surface and bed heat exchanges, thermal power plant cooling water, and ice formation and melt.

5.2. Basic Equation of Heat Transfer

The basic equation for heat transfer in curvilinear and sigma coordinates is given as follows (Ji, 2008):

$$\frac{\partial}{\partial t}(mHT)+\frac{\partial}{\partial x}(PT)+\frac{\partial}{\partial y}(QT)+\frac{\partial}{\partial z}(mwT)=\frac{\partial}{\partial z}\left(\frac{m}{H}A_b\frac{\partial T}{\partial z}\right)+\frac{\partial I}{\partial z}+S_T \qquad (5.1)$$

where

x, y are the orthogonal curvilinear coordinates in the horizontal direction (m)

z is the sigma coordinate (dimensionless)

t is time (s)

m_x, m_y are the square roots of the diagonal components of the metric tensor (m)

$m = m_x m_y$ is the Jacobian (m^2)

T is temperature (°C)

H is the total water depth (m)

P,Q are the mass flux components (m^2/s) in the x and y directions, respectively, which were defined in (2.9)

u, v are the horizontal velocity components in the curvilinear coordinates (m/s)

w is the vertical velocity component (m/s)

A_b is the vertical turbulent eddy viscosity (m^2/s)]

I is the short wave solar radiation (M/m^2)

S_T is the source/sink term for heat exchanges (J/s)

To solve the equation (5.1), the hydrodynamic transport (u, v, w), and the turbulent mixing A_b, are provided by the hydrodynamic module in EFDC+ model. For the short wave solar radiation, the depth distribution is exponential and can be expressed as Beer's Law:

$$I(D) = I_s e^{(-K_e D)} \tag{5.2}$$

where

$I(D)$ is the solar radiation at depth D below the surface (M/m^2)

I_S is the solar radiation at the surface ($D = 0$) (M/m^2)

D $=H(1-z)$ is the depth below water surface (m)

K_e is the light extinction coefficient (1/m)

Solar radiation that penetrates the surface of water is absorbed by water. The absorption heats the water column and radiation penetration depends on the light extinction coefficient (K_e). The light extinction coefficient (also referred to as the light attenuation coefficient) is the measure for the reduction (absorption) of light intensity within a water column. The solar radiation at the surface I_s is a function of location, time of the year, time of day, meteorological conditions, and other insignificant factors.

5.3. Surface Heat Exchange

5.3.1 Equilibrium Temperature

A computed equilibrium temperature can be used for the surface heat exchange in EFDC+. The approach used here is based on the equilibrium temperature computation approach in the CE-QUAL-W2 (Wells and Cole, 2000). Equilibrium temperature submodel is fully linked with ice submodel that incorporates ice growth and ice melt processes.

Because some of the terms in the term-by-term heat balance equation are surface temperature dependent and others are measurable or computable input variables, the most direct route to simplify computation is to define an equilibrium temperature, T_e, as the temperature at which the net rate of surface heat exchange is zero.

Linearization of the term-by-term heat balance along with the definition of equilibrium temperature allows for expression of the net rate of surface heat exchange, H_n, as:

$$H_{aw} = -K_{aw} \left(T_w - T_e \right) \tag{5.3}$$

where

H_{aw} is the rate of surface heat exchange (M/m^2)

K_{aw} is the coefficient of surface heat exchange (W/m^2/$^\circ C$)

T_w is the water surface temperature ($^\circ C$)

T_e is the equilibrium temperature ($^\circ C$)

Seven separate heat exchange processes are summarized in the coefficient of surface heat exchange and equilibrium temperature. The definition of the coefficient of surface heat exchange can be shown to be the first term of a Taylor series expansion by considering the above equation as:

$$H_{aw} = \frac{dK_{aw}}{dT_s} \left(T_s - T_e \right) \tag{5.4}$$

where the derivative of H_{aw} with respect to surface temperature is evaluated from equation (5.3) to give K_{aw}, the coefficient of surface heat exchange. All approximations of the individual surface heat exchange terms enter into the evaluation of the coefficient of surface heat exchange and the equilibrium temperature.

5.3.2 Full Heat Balance

At the water surface ($z = 1$), the boundary condition for the temperature transport equation (5.1) is:

$$-\frac{\rho c_p A_b}{H}\frac{\partial T}{\partial z} = H_L + H_E + H_C \tag{5.5}$$

where

ρ is the water density (kg/m^3)

c_p is the water specific heat

A_b is the vertical turbulent mass mixing coefficient (m^2/s)

H is the water depth (m)

H_L is the surface heat exchange due to long wave back radiation (M/m^2)

H_E is the surface heat exchange due to evaporation/condensation (M/m^2)

H_C is the surface heat exchange flux due to convection (M/m^2)

Based on the approach proposed by **?** and Hamrick (1992) the following is applied to the temperature boundary condition at water surface:

$$H_L = \varepsilon\sigma T_s^4 \left(0.39 - 0.05\sqrt{e_a}\right)\left(1 + B_c C\right) + 4\varepsilon\sigma T_s^3 \left(T_s - T_a\right) \tag{5.6}$$

$$H_E = c_e \rho_a L_E W_s \left(e_s - e_a\right) \frac{0.622}{P_a} \tag{5.7}$$

$$H_C = c_h \rho_a c_{pa} W_s \left(T_s - T_a\right) \tag{5.8}$$

where

- ε is the emissivity of the waterbody ($\varepsilon = 0.97$)
- σ is the Stefan–Boltzmann constant ($\sigma = 5.67 \times 10^{-8}$ W/m^2/K^4)
- e_a is the actual vapor pressure (mb)
- C is the cloud fraction ($C = 0$: cloudless, $C = 1$: full cloud coverage)
- B_c is an empirical constant ($B_c = 0.8$)
- T_s is the water surface temperature ($^\circ C$)
- T_a is the air temperature ($^\circ C$)
- c_4, c_h are the turbulent exchange coefficients ($c_e = 1.1 \times 10^{-3}$)]
- ρ_a is the atmospheric density ($\rho_a = 1.2\ kg/m^3$)
- c_{pa} is the specific heat of air ($c_{pa} = 1005\ J/kg/K$)
- L_E is the latent heat of evaporation ($L_E = 2.501 \times 10^6\ J/kg$)
- W_s is the wind speed (m/s)
- e_s is the saturation vapor pressure at surface water temperature (mb)
- P_a is the atmospheric pressure (mb)

5.3.3 Solar Radiation

The light extinction coefficient (also called light attenuation coefficient) is the measure for the reduction (absorption) of light intensity within a water column. The light field in the water column is governed by:

$$\frac{\partial I}{\partial z^*} = -K_{ess} I \tag{5.9}$$

where

- I is the short wave solar radiation or light intensity (M/m^2)
- K_{ess} is the light extinction coefficient ($1/m$)

$z*$ is the depth below the water surface (m).

Integration of equation (5.9) gives:

$$I = I_{ws}\exp\left(-\int_0^{z^*} K_{ess}dz^*\right) \tag{5.10}$$

The solar radiation at the surface I_0 is a function of location, time of the year, time of day, meteorological conditions, and other insignificant factors. The light intensity at the water surface I_{ws}, is given by:

$$I_{sw} = I_0 S_f \min\left\{\exp\left[-K_{e,me}\left(H_{rps}-H\right)\right],1\right\}\min\left\{\exp\left[-K_{e,ice}H_{ice}\right],1\right\} \tag{5.11}$$

where

I_0 is the solar radiation at the Earth's surface (M/m^2)

S_f is the tree canopy and/or terrain shading factor (dimensionless)

H_{ice} is the ice thickness (m)

$K_{e,ice}$ is the light extinction coefficient for ice cover (1/m)

$K_{e,me}$ is the light extinction coefficient for emergent shoots (1/m)

H_{rps} is the rooted plant shoot height (m), and

H is the water column depth (m)

In EFDC+, depending on which heat exchange option has been selected, light extinction is treated differently. The different heat exhcange options are listed below.

- **Term by Term Heat Exchange**: EFDC+ computes the net extinction coefficient for each cell and layer at every time step.
- **Term by Term Heat Exchange (Legacy)**: The extinction coefficient is constant spatially and temporally. This is consistent with legacy versions of EFDC+.
- **Equilibrium Temperature**: EFDC+ computes the net extinction coefficient for each cell and layer at every time step.

5.3.3.1 Term by Term Heat Exchange

EFDC+ computes the net extinction coefficient for each cell and layer at every time step using equation (5.10).

5.3.3.2 Term by Term Heat Exchange (Legacy)

The extinction coefficient is constant spatially and temporally. This is consistent with previous implementations of EFDC+. To solve the equation (5.1), the hydrodynamic transport (u, v, w), and the turbulent mixing A_b, are provided by the EFDC+ model. The depth distribution of the solar radiation heating is an exponential function and is expressed as:

$$I = rI_{sw}\exp\left[-\beta_f H\left(1-z\right)\right] + \left(1-r\right)I_{sw}\exp\left[-\beta_s H\left(1-z\right)\right] \tag{5.12}$$

where

I is the solar radiation at water depth z (M/m^2)

I_{sw} is the incident solar radiation at water surface $(z=1)$ (M/m^2)

β_f is the fast scale attenuation coefficients $(1/m)$

β_s is the slow scale attenuation coefficients $(1/m)$

r is the distribution fraction between 0 and 1

5.3.3.3 Equilibrium Temperature

The extinction coefficient can vary spatially and temporally as described in the Full Heat Exchange option. If the Equilibrium Temperature heat exchange option is selected, the light extinction is handled the same as with the Full Heat Balance option with the exception of the addition of a constant fraction of the solar radiation is always adsorbed in the top layer, regardless of how thick it is or what the extinction coefficient is. This is described by the Beer's law with the additional term β :

$$H_s(z) = \left(1-\beta\right)H_s\exp\left(-\eta z\right) \tag{5.13}$$

where

$H_s(z)$ is the short wave radiation at depth z (M/m^2)

β is the fraction absorbed at the water surface (dimensionless)

K_e is the extinction coefficient $(1/m)$

H_s is the short wave radiation reaching the water surface (M/m^2)

5.3.4 Light Extinction Factors

The standard EFDC+ term by term full heat balance surface heat exchange processes are the same as the full heat balance (legacy) option. The major difference between these two options is that the standard EFDC+ full heat balance uses variable light extinction factors. Total light extinction in the model is given by:

$$K_{e,SS} = K_{e,b} + K_{e,TSS}TSS + K_{e,POC}POC + K_{e,DOC}DOC + K_{e,Chl}\sum Chl + K_{e,RPS}RPS \quad (5.14)$$

This equation also applies for the equilibrium temperature (CE-QUAL-W2 method) option. When using the EFDC+ full heat balance or equilibrium temperature option, the heat module and the WQ module use the same light extinction factor (K_e). For the full heat balance (legacy) option they are decoupled.

If the legacy version of the surface heat exchange option is used, then light extinction is constant in time and space. However, the user must specify $K_{e,(fast)}$, $K_{e,(slow)}$, and $FACT(fast)$. The latter term is the fraction of the SR that is attenuated "fast", i.e. using $K_{e,(fast)}$,
where

$K_{e,SS}$ is the total light extinction coefficient $(1/m)$

$K_{e,TSS}$ is the light extinction coefficient for total inorganic suspended solid $(1/m$ per $g/m^3)$

$K_{e,b}$ is the background light extinction $(1/m)$

$K_{e,TSS}$ is the light extinction coefficient for total inorganic suspended solid $(1/m$ per $g/m^3)$

TSS is the inorganic suspended solid concentration (g/m^3) provided from the sediment transport module

POC is the total Particulate Organic Carbon concentration (Labile and Refractory) (g/m^3) provided from the water quality module

$K_{e,POC}$ is the light extinction factor as a function of POC concentrations $(1/m$ per $g/m^3)$

DOC is the Dissolved Organic Carbon concentration (Labile and Refractory) (g/m^3) provided from the water quality module

$K_{e,DOC}$ is the light extinction factor as a function of DOC concentrations $(1/m$ per $g/m^3)$
$CChl_{RPE}$ is the carbon-to-chlorophyll ratio for epiphytes (g C per mg Chl)

$K_{e,Ckl}$ is the light extinction coefficient for algae chlorophyll $(1/m$ per mg Chl per $m^2)$

B_m is the concentration of algae group m (g C per ml)

$CChl_m$ is the carbon-to-chlorophyll ratio in algal group m (g C per mg Chl)

$K_{e,RPS}$ is the light extinction coefficient for rooted plant shoots $(1/m$ per gm C per $m^2)$

RPS is the concentration of plant shoots (g C per m^2)

If only hydrodynamics and temperature is simulated in the EFDC+ model, then background light extinction coefficient will be used. If hydrodynamics, temperature and TSS

is simulated, then the total light extinction coefficient is a function of background extinction coefficient and light extinction coefficient due to TSS. If a full water quality model is simulated with TSS, then the total light extinction coefficient is the function of background extinction, TSS, POC, DOC and $Chl-a$.

Full heat balance with variable light extinction option is fully coupled with ice submodel and accounts for the ice melt and ice growth. Finally, the surface heat exchange coefficients for evaporative and conductive exchange can be spatially variable.

5.4. Bed Heat Exchange

Sediment-water interface heat exchange with water is generally small compared to surface heat exchange and is frequently neglected. However, including sediment bed heat exchange can improve the simulation of temperature in deep lakes and reservoirs. The heat exchange between the sediment bed and the bottom layer of the water column can be described as

$$H_b = -\left(K_{b,v}U + K_{b,c}\right)\left(T_w - T_b\right) \tag{5.15}$$

$$U = \sqrt{u_1^2 + v_1^2} \tag{5.16}$$

where

H_b is the sediment bed-water heat exchange (M/m^2)

$K_{b,v}$ is the convective heat exchange coefficient $(W-s/m^2-^\circ C)$

$K_{b,c}$ is the conductive heat exchange coefficient $(W/m^2-^\circ C)$

u_1 is the u component water velocity in layer 1 (m/s)

v_1 is the v component water velocity in layer 1 (m/s)

T_w is the water temperature in layer 1 $(^\circ C)$

T_b is the sediment bed temperature $(^\circ C)$

Typical applications have used a value of 0.3 W/m^2-°C for $K_{b,c}$ that is approximately two orders of magnitude smaller than the surface heat exchange coefficient. $K_{b,c}$ is often not used (i.e. equal to zero) but can be in the range of 0 to 10. Average yearly air temperature is a good initial estimate of T_b.

Optionally, the bed temperature (T_b) can change with time due to the heat exchange.

$$\frac{\delta\left(D_b T_b\right)}{\delta t} = -\left(K_{b,v}U + K_{b,c}\right)\left(T_b - T_w\right) \tag{5.17}$$

where D_B is the sediment bed-thermal thickness (m). Selection of the thermal thickness is subject to initial approximation and subsequent calibration. The larger the thermal thickness is, the slower the bed temperature will change.

5.5. Ice Formation and Melt

A robust ice sub-model has been implemented in EFDC+ which is based on the CE-QUAL-W2 (Wells and Cole, 2000) ice module. With this model:

1. Ice formation and melt is simulated by EFDC+ using a coupled heat approach.
2. Ice dynamics (i.e. movement of ice block/chunks) have not yet been implemented.

5.5.1 Heat Balance

The heat balance for the water-to-ice air system is given by:

$$\rho_i L_f \frac{dh}{dt} = h_{ai}(T_i - T_e) - h_{wi}(T_w - T_m) \tag{5.18}$$

where

ρ_i is the density of ice (kg/m^3)

L_f is the latent heat of fusion of ice (J/kg)

dh/dt is the change in ice thickness (h) with time (t) (m/s)

h_{ai} is the coefficient of ice-to-air heat exchange ($W/m^2/^\circ C$)

H_{wi} is the coefficient of water-to-ice heat exchange through the melt layer ($W/m^2/^\circ C$)

T_I is the ice temperature ($^\circ C$)

T_{ei} is the equilibrium temperature of ice to air heat exchange ($^\circ C$)

T_w is the water temperature below ice ($^\circ C$)

T_m is the melt temperature ($^\circ C$)

Formation of ice requires lowering the surface water temperature to the freezing point by normal surface heat exchange processes. With further heat removal, ice begins to form on the water surface. This is indicated by a negative water surface temperature. The negative water surface temperature is then converted to equivalent ice thickness and equivalent heat is added to the heat source and sink term for water. The thickness of ice formation is calculated as

$$\theta_0 = -\frac{T_{wn}\rho_w c_{pw} h}{\rho_i L_f} \tag{5.19}$$

where

θ_0 is the thickness of initial ice formation during a time step (m)

T_{wn} is the local temporary negative water temperature ($^\circ C$)

h is the layer thickness (m)

ρ_w is the density of water (kg/m^3), c_{pw} is the specific heat of water ($J/kg/^\circ C$)

ρ_i is the density of ice (kg/m^3)

L_f is the latent heat of fusion (J/kg)

5.5.2 Ice Surface Temperature

The ice surface temperature is given by the equations:

$$T_s^n \frac{\theta^{n-1}}{K_i} \left[H_{sn}^n + H_{an}^n - H_{br}(T_s^n) - H_c(T_s^n)\right] \tag{5.20}$$

$$H_{sn} + H_{an} - H_{br} - H_e - H_c + q_i = \rho_i L_f \frac{d\theta_{ai}}{dt}, \quad \text{for } T_s = 0^\circ C \tag{5.21}$$

$$q_i = K_i \frac{T_f - T_s(t)}{\theta(t)} \tag{5.22}$$

where

K_i is the thermal conductivity of ice ($W/m/^\circ C$)

T_f is the freezing point temperature ($^\circ C$)

n is the time level

q_i is the heat flux through ice (M/m^2)

H_n is the net rate of heat exchange across the water surface (M/m^2)

H_s is the incident short wave solar radiation (M/m^2)

H_a is the incident long wave radiation (M/m^2),

H_{sr} is the reflected short wave solar radiation (M/m^2)

H_{ar} is the reflected long wave radiation (M/m^2)

H_{br} is the back radiation from the water surface (M/m^2)

H_e is the evaporative heat loss (M/m^2)

H_c is the heat conduction (M/m^2)

5.5.3 Freezing Temperature

The freezing temperature relationship is described as below.

$$T_f = \begin{cases} -0.0545\,TDS\,, & TDS < 35 \text{ ppt} \\ -0.3146 - 0.0417\,TDS - 0.000166\,TDS^2\,, & TDS > 35 \text{ ppt} \end{cases} \tag{5.23}$$

where

T_f is the freezing point temperature ($^\circ C$)

TDS is the total dissolved solids (ppt)

5.5.4 Ice Melt at Air/Water Interface

The ice melt at the air/water interface is described by the equation below:

$$rho_i c_{pi} \frac{T_s(t)}{2} \theta(t) = \rho_i L_f \Delta\theta_{ai} \tag{5.24}$$

where

c_{pi} is the specific heat of ice ($J/kg/^\circ C$)

θ_{ai} is the ice melt at the air-ice interface ($1/m$)

5.5.5 Ice Growth/Melt at Bottom of Ice

The ice growth/melt at the bottom of the ice is described by the equation below:

$$q_i - q_{iw} = \rho_i L_f \frac{d\theta_{iw}}{dt} \tag{5.25}$$

where

q_i is the heat flux through the ice (M/m^2)

q_{iw} is the heat flux at the ice/water interface (M/m^2)

θ_{iw} is the ice growth/melt at the ice-water interface

$$\Delta\theta_{iw}^n = \frac{1}{\rho_i L_f} \left[K_i \frac{T_f - T_s^n}{\theta^{n-1}} - h_{wi} \left(T_w^n - T_f \right) \right] \tag{5.26}$$

5.5.6 Solar Radiation at Bottom of Ice

Solar radiation at the bottom of the ice is given by the equation below:

$$H_{ps} = H_s\,(1-\alpha_i)\,(1-\beta_i)\exp\left[-\gamma_i\theta(t)\right] \tag{5.27}$$

where

H_{ps} is the solar radiation absorbed by water under ice cover (M/m^2)

H_s is the incident solar radiation (M/m^2)

α_i is the ice albedo

β_i is the fraction of the incoming solar radiation absorbed in the ice surface

γ_i is the ice extinction coefficient $(1/m)$

5.6. Thermal Power Plant Cooling Water

EFDC+ has features specifically designed for thermal simulation of a power plant's cooling systems. In EFDC+, the cooling water withdrawal from a nearby river or lake and discharge from the plant are represented by the withdrawal and return boundaries. The user can add them by specifying the flow rate Q at the withdrawal and return cells (Hamrick and Mills, 2000).

Heat energy added to or removed from a receiving waterbody can be estimated using:

$$H_T = Q_c\rho c_p\Delta T \tag{5.28}$$

where

H_{WR} is the rate of heat energy exchange due to temperature rise/fall (J/s)

Q_C is the withdrawal flow rate (m^2/s)

ρ is the water density (kg/m^3)

c_p is the specific heat of water $(c_p = 2400J/kg/^\circ C)$

ΔT is the temperature difference between the discharged water and the receiving water $(^\circ C)$

So, for any industrial process that uses once-through cooling water we can define the following:

Q_{cool} is the process water flow rate that is being pumped from the water body. The sign convention is positive for a standard withdrawal. The thermal sinks and sources H_T are specified in the transport equation for heat:

$$H_{intake} = -Q_{cool}\rho c_p T_1 \tag{5.29}$$

$$H_{discharge} = Q_{cool}\rho c_p (T_1 + \Delta T) \tag{5.30}$$

where

H_{intake} is the heat removed from the withdrawal cell or intake

$H_{discharge}$ is the heat added back to the water body at the power plant discharge location

T_1 is the ambient intake temperature ($^\circ C$)

ΔT is the temperature rise of a power plant

5.7. Thermal Power Plant Forced Evaporation

The Forced Evaporation (FE) Analysis capability has been developed to quantify increased evaporation induced by increased water temperatures due to releases from thermoelectric power plants. These power plants withdraw cooling waters, which once run through the plant and are returned to rivers or lakes at a higher temperature than the ambient water temperature. This higher temperature water causes additional evaporation (forced evaporation) from the waterbody. This additional evaporation is counted as water consumption by regulators as it is no longer available to downstream users.

Evaporation is dependent on wind speed, atmospheric humidity, and water temperature. There are a number of methods to compute FE using different wind functions as listed in Table 5.1. Using these various evaporation methods, the model is first run with the power plant, and then run again without the power plant. EE then subtracts the output from two models and displays the difference which is the consumption of water from the power plant. Once temperature is activated and the correct Surface Heat Exchange option has been selected, the user can choose which evaporation approach is desired. Even if evaporative losses are not a major concern, the evaporative mass fluxes should normally be activated for most models.

Heat flux due to evaporation is always included for the Full Heat and the Equilibrium Temperature (W2) options.

EFDC+/EFDC_Explorer Forced Evaporation (FE) toolset results have been compared to the Electric Power Research Institute's (EPRI) FE estimates. EPRI's once through cooling FE analysis for river discharges is based on a USGS report on water consumption by thermoelectric power plants (Diehl et al., 2013; EPRI, 2014).

Table 5.1. List of Evaporation Calculation Methods

IEAVAP	Evaporation Approach	General Usage
0	Do Not Include Evaporation	
1	Use Evaporation from ASER	Measured or Externally Estimated
2	EFDC+ Original	
3	Ward (1980)	Cooling Lake
4	Harbeck Jr (1964)	Cooling Lake
5	Brady et al. (1969)	Cooling Pond
6	Anderson et al. (1954)	Large Lake
7	Webster and Sherman (1995)	Lakes
8	Fulford and Sturm (1984)	Rivers
9	Gulliver and Stefan (1984)	Streams
10	Edinger et al. (1974)	Lakes/Rivers
11	Ryan et al. (1974)	Lakes/Rivers

Chapter 6

SEDIMENT TRANSPORT MODULE

6.1. Introduction

This chapter presents the transport equations of suspended sediment that are part of EFDC+. This includes the basic theory for the two transport options available in EFDC+. The two sediment transport options available are:

1. The "Original" sediment transport model that is based on the Hamrick's work (Tech et al., 2007).
2. The Ziegler, Lick, and Jones (SEDZLJ) sediment transport model that is based on the SEDiment dynamics work (Jones and Lick, 2000; Ziegler and Lick, 1988, 1986).

6.2. Governing Equations for Suspended Sediment Transport

6.2.1 Suspended Sediment Transport

The water column equation for suspended sediment transport is derived from the generic transport equation (3.1) for a dissolved or suspended material. For the EFDC+ implementation, the physical horizontal diffusion terms in equation (3.1) are omitted due to small inherent numerical diffusion encountered. This yields the following from of the suspended sediment transport equation:

$$\frac{\partial}{\partial t}\left(mHC_j\right)+\frac{\partial}{\partial x}\left(PC_j\right)+\frac{\partial}{\partial y}\left(QC_j\right)+\frac{\partial}{\partial z}\left(mwC_j\right)-\frac{\partial}{\partial z}\left(mw_{s,j}C_j\right) = \frac{\partial}{\partial z}\left(m\frac{A_b}{H}\frac{\partial}{\partial z}C_j\right)+S^E_{s,j}+S^I_{s,j} \quad (6.1)$$

where,

C_j represents the concentration of the j^{th} sediment class,

$S^E_{s,j}$ is the external source-sink term, and

$S^I_{s,j}$ is the internal source-sink term.

The source term has been split into two terms so that the external source-sink term could include point and nonpoint source loads. Whereas the internal source-sink term can now include reactive decay of organic sediments or the exchange of mass between sediment classes. The mass exchange would occur if floc formation and destruction are simulated.

The boundary conditions for the equation (6.1) in the vertical direction are as follows:

$$-\frac{A_b}{H}\frac{\partial}{\partial z}C_j - w_{s,j}C_j = J_{jo} \quad \text{at } z = 0 \tag{6.2}$$

$$-\frac{A_b}{H}\frac{\partial}{\partial z}C_j - w_{s,j}C_j = 0 \quad \text{at } z = 1 \tag{6.3}$$

where, J_{jo} is the net water column-bed exchange flux defined as positive into the water column.

6.2.2 Numerical Solution

The general procedure follows that for the salinity transport equation, which uses a high order upwind difference discretization scheme for the advective terms, described in Hamrick (1992). The numerical solution of equation (6.1) utilizes a fractional step procedure. The first step advances the concentration due to advection and external sources and sinks having corresponding volume fluxes by

$$H^{n+1}C^* = H^nC^n + \frac{\Delta t}{m}\left(S^E_{s,j}\right)^{n+1/2} - \frac{\Delta t}{m}\left[\frac{\partial}{\partial x}\left(P^{n+\frac{1}{2}}C^n\right) + \frac{\partial}{\partial y}\left(Q^{n+\frac{1}{2}}C^n\right) + \frac{\partial}{\partial z}\left(mw^{n+\frac{1}{2}}C^n\right)\right] \tag{6.4}$$

where the superscripts n and $n+1$ denote the old- and new-time levels and the superscript $*$ denotes the intermediate fractional step results. The portion of the source and sink term, associated with volumetric sources and sinks is included in the advective step for consistency with the continuity constraint. This source-sink term, as well as the advective field (u, v, w,) is defined as intermediate in time between the old and new time levels consistent with the temporal discretization of the continuity equation. Note that the sediment class subscripts have been dropped for clarity. The advection step uses the anti-diffusive MPDATA scheme (Smolarkiewicz and Clark, 1986) with optional flux corrected transport (Smolarkiewicz and Grabowski, 1990).

The second fractional step or settling step is given by

$$C^{**} = C^* + \frac{\Delta t}{H^{n+1}}\frac{\partial}{\partial z}\left(w_sC^{**}\right) \tag{6.5}$$

Equation (6.5) is solved by a fully implicit upwind difference scheme

$$C_{k,c}^{**} = C_{k,c}^{*} + \frac{\Delta t}{\Delta_z H^{n+1}} \left(w_s C^{**}\right)_{k,c} \tag{6.6}$$

$$C_k^{**} = C_k^{*} + \frac{\Delta t}{\Delta_1 H^{n+1}} \left(w_s C^{**}\right)_{k+1} - \frac{\Delta t}{\Delta_k H^{n+1}} \left(w_s C^{**}\right)_k \text{ with } 2 \le k \le KC-1 \tag{6.7}$$

$$C_1^{**} = C_1^{*} + \frac{\Delta t}{\Delta_z H^{n+1}} \left(w_s C^{**}\right)_2 \tag{6.8}$$

where,

C_k is the concentration in each layer (g/m^3),

$C-1$ is the bottom layer concentration, and

k is the layer index.

The solution starts at $k = KC$ and marches downward to the bottom layer. The implicit solution includes an optional anti-diffusion correction across internal water column layer interfaces. The third fractional step accounts for water column-bed exchange by resuspension and deposition through the following,

$$C_1^{***} = C_1^{**} + \frac{\Delta t}{\Delta_z H^{n+1}} L_0 J_0^{***} \tag{6.9}$$

where L_0 is a flux limiter such that only the current top layer of the bed can be completely resuspended in single time step. For resuspension and deposition of suspended non-cohesive sediment, the bed flux is given by

$$J_0^{***} = \frac{w_s}{v} \left(\mu C_{eq} - C_1^{***}\right) \tag{6.10}$$

which will be further discussed in the next section. For cohesive sediment resuspension, the bed flux is specified as a function of the bed stress and bed geomechanical properties. For cohesive sediment deposition, the bed flux is typically given by

$$J_0^{***} = -P_d w_s C_1^{***} \tag{6.11}$$

where, P_d is a probability of deposition. The representation of the water column bed exchange by a distinct fractional step is equivalent to a splitting of the bottom boundary condition equation (6.2) such that the bed flux is imposed at the intermediate step between settling and vertical diffusion.

The remaining step is an implicit vertical turbulent diffusion step corresponding to,

$$C^{n+1} = C^{***} + \Delta t \frac{\partial}{\partial z} \left[\left(\frac{A_b}{H^2} \right)^{n+1} \frac{\partial}{\partial z} C^{n+1} \right] \tag{6.12}$$

with zero diffusive fluxes at the bed and water surface.

6.2.3 Definitions

The void ratio, ε, is defined as the ratio of the volume of voids, ϕ, to the total volume of the soil (dimensionless).

$$\varepsilon = \frac{\phi}{1-\phi} \tag{6.13}$$

The bulk density ρ_b is defined as the dry weight of soil per unit volume of soil (kg/m^3). The relationship between dry and bulk density is represented by,

$$\rho_d = \rho_s \frac{(\rho_b - \rho_w)}{(\rho_s - \rho_w)} \tag{6.14}$$

where ρ_s is the solids or grain density (kg/m^3) and ρ_w is the water density (kg/m^3).

6.3. Original EFDC+ Sediment Transport

The original implementation of sediment transport involves the transport of both non-cohesive and cohesive sediments.

6.3.1 Non-Cohesive Sediments

6.3.1.1 Settling Velocity

Non-cohesive inorganic sediments settle as discrete particles where hindered settling and multiphase interactions are important in regions of high sediment concentration near the bed. At low concentrations, the settling velocity for the j^{th} non-cohesive sediment class corresponds to the settling velocity of a discrete particle,

$$w_{sj} = w_{soj} \tag{6.15}$$

where w_{soj} is the discrete particle settling velocity that depends on the sediment density, effective grain diameter, and fluid kinematic viscosity. A piece-wise relation for w_{soj} by Rijn (1984) is as follows,

$$w_{soj} = \sqrt{g' d_j} \begin{cases} \frac{R_{dj}}{18}\,, & d \le 100\ \mu\text{m} \\ \frac{10}{R_{dj}}\left(\sqrt{1+0.01R_{dj}^2}-1\right)\,, & 100\mu m < d_j \le 1000\ \mu\text{m} \\ 1.1\,, & d_j > 1000\mu\text{m} \end{cases} \tag{6.16}$$

where g' is the reduced gravitational acceleration and represented as,

$$g' = g\left(\frac{\rho_{sj}}{\rho_w} - 1\right) \tag{6.17}$$

and R_{dj} is the sediment grain densimetric Reynolds number and calculated as,

$$R_{dj} = \frac{d_j \sqrt{g' d_j}}{\nu} \tag{6.18}$$

At higher concentrations and hindering settling conditions, the settling velocity is less than the discrete velocity and can be expressed in the form,

$$w_{sj} = \left(1 - \sum_i^I \frac{C_i}{\rho_{si}}\right)^n w_{soj} \tag{6.19}$$

where ρ_s is the sediment particle density with values of n ranging from 2 (Cao et al., 1996) to 4 (Rijn, 1984). The expression (6.16) is approximated to within 5 percent by

$$w_{sj} = \left(1 - n\sum_i^I \frac{C_i}{\rho_{si}}\right) w_{soj} \tag{6.20}$$

for total sediment concentrations up to $200,000\, mg/l$. For total sediment concentrations less than $25,000\, mg/l$, neglecting the hindered settling correction results in less than a 5% error in the settling velocity. This is well within the range of uncertainty in parameters used to estimate the discrete particle settling velocity.

6.3.1.2 Deposition, Resuspension, and Bedload

Non-cohesive sediment is transported as bedload and suspended load. The initiation of both modes of transport begins with erosion or resuspension of sediment from the bed when the bed stress τ_b, exceeds a critical stress referred to as the Shield's stress τ_{cs}.The Shield's stress depends upon the density and diameter of the sediment particles and the kinematic viscosity of the fluid and can be expressed in empirical dimensionless relationships of the form:

$$\theta_{csj} = \frac{\tau_{csj}}{g' d_j} = \frac{u^2_{*csj}}{g' d_j} = f\left(R_{dj}\right) \tag{6.21}$$

Useful numerical expressions of the relationship of equation (6.19), provided by Rijn (1984) are:

$$\theta_{csj} = \begin{cases} 0.24\left(R_{dj}^{2/3}\right)^{-1}, & R_{dj}^{2/3} < 4 \\ 0.14\left(R_{dj}^{2/3}\right)^{-0.64}, & 4 \le R_{dj}^{2/3} < 10 \\ 0.04\left(R_{dj}^{2/3}\right)^{-0.1}, & 10 \le R_{dj}^{2/3} < 20 \\ 0.013\left(R_{dj}^{2/3}\right)^{0.29}, & 20 \le R_{dj}^{2/3} < 150 \\ 0.055, & R_{dj}^{2/3} \ge 150 \end{cases} \tag{6.22}$$

A number of approaches have been used to distinguish whether a particular sediment size class is transported as bedload or suspended load under specific local flow conditions characterized by the bed stress or bed shear velocity:

$$u_* = \sqrt{\tau_b} \tag{6.23}$$

The approach proposed by Rijn (1984) is used in the EFDC+ model and is as follows. When the bed velocity is less than the critical shear velocity

$$u_{*csj} = \sqrt{\tau_{csj}} = \sqrt{g' d_j \theta_{csj}} \tag{6.24}$$

no erosion or resuspension takes place and there is no bedload transport. Sediment in suspension under this condition will deposit to the bed as will be subsequently discussed.

When the bed shear velocity exceeds the critical shear velocity but remains less than the settling velocity,

$$u_{*csj} < u_* < w_{soj} \tag{6.25}$$

sediment will be eroded from the bed and transported as bedload. Sediment in suspension under this condition will deposit to the bed. When the bed shear velocity exceeds both the critical shear velocity and the settling velocity, bedload transport ceases and the eroded or resuspended sediment will be transported as suspended load. For grain diameters less than approximately 1.3×10^{-4} m (130μm), the settling velocity is less than the critical shear velocity and sediment resuspend from the bed when the bed shear velocity exceeds the critical shear velocity will be transported entirely as suspended load. For grain diameters greater than 1.3×10^{-4} m, eroded sediment can be transported by bedload in the region corresponding to equation (6.25) and then as suspended load when the bed shear velocity exceeds the settling velocity.

In the EFDC+ model, the preceding set of rules are used to determine the mode of transport of multiple size classes of non-cohesive sediment. Bedload transport is determined using a general bedload transport rate formula:

$$\frac{q_B}{\rho_s d \sqrt{g' d}} = \phi\left(\theta, \theta_{cs}\right) \tag{6.26}$$

where q_B is the bedload transport rate (mass per unit time per unit width) in the direction of the near bottom horizontal flow velocity vector. The function ϕ depends on the Shield's parameter:

$$\theta = \frac{\tau_b}{g' d_j} = \frac{u_*^2}{g' d_j} \tag{6.27}$$

and the critical Shield's parameter defined by the equations (6.21) and (6.22). A number of bedload transport formulas explicitly incorporate the settling velocity. However, since both the critical Shield's parameter and the settling velocity are unique functions of the sediment grain densimetric Reynolds number, the settling velocity can also be expressed as

a function of the critical Shield's parameter with equation (6.27) remaining an appropriate representation.

A number of bedload formulations developed for riverine prediction (Ackers and White, 1973; Laursen, 1958; Yang, 1973; Yang and Molinas, 1982) do not readily conform to equation (6.27) and were not incorporated as options in the EFDC+ model. Two widely used bedload formulations which do conform to equation (6.27) are found in Meyer-Peter and Müller (1948) and Bagnold (1956) and their derivatives in Reid and Frostick (1994), which have the general form

$$\$(\theta,\theta_{cs}) = \phi\,(\theta-\theta_{cs})^{\alpha}\left(\sqrt{\theta}-\gamma\sqrt{\theta_{cs}}\right)^{\beta} \tag{6.28}$$

where,

$$\phi = \phi\,(\theta_{cs}) \quad \text{or} \quad \phi = \phi\,(R_d) \tag{6.29}$$

The Meyer-Peter and Muller formulations are typified by

$$\Phi = \phi\,(\theta-\theta_{cs})^{3/2} \tag{6.30}$$

while Bagnold formulations are typified by

$$\Phi = \phi\,(\theta-\theta_{cs})\left(\sqrt{\theta}-\gamma\sqrt{\theta_{cs}}\right) \tag{6.31}$$

with Bagnold's original formula having γ equal to zero. The Meyer-Peter and Muller formulation has been extended to heterogeneous beds by Suzuki et al. (1998), while Bagnold's formula has been similarly extended by (van Niekerk et al., 1992). The bedload formulation by Rijn (1984) having the form

$$\begin{aligned}\Phi &= \phi\,(\theta-\theta_{cs})^{2.1}\\ \phi &= \frac{0.053}{R_d^{1/5}\theta_{cs}^{2.1}}\end{aligned} \tag{6.32}$$

has been incorporated into the CH3D-SED model and modified for heterogeneous beds by Spasojevic and Holly Jr (1994). Equation (6.32) can be implemented in the EFDC+ model with an appropriately specified ϕ. A modified formulation of the Einstein bedload function (Einstein, 1950) which conforms to equations (6.27) and (6.28) has been presented by Rahmeyer (1999) and will be later incorporated into the EFDC+ model.

The procedure for coupling bedload transport with the sediment bed in the EFDC+ model is as follows. First, the magnitude of the bedload mass flux per unit width is calculated according to equation (6.27) at horizontal model cell centers, denoted by the subscript C. The cell center flux is then transformed into cell center vector components using

$$q_{bcx} = \frac{u}{\sqrt{u^2+v^2}} q_{bc}$$
$$q_{bcy} = \frac{v}{\sqrt{u^2+v^2}} q_{bc} \tag{6.33}$$

where, u and v are the cell center horizontal velocities near the bed. Cell face mass fluxes are determined by downwind projection of the cell center fluxes

$$q_{bfx} = (q_{bcx})_{upwind}$$
$$q_{bfy} = (q_{bcy})_{upwind} \tag{6.34}$$

where the subscript *upwind* denotes the cell center upwind of the x normal and y normal cell faces. The net removal or accumulation rate of sediment material from the deposited bed underlying a water cell is then given by:

$$m_x m_y J_b = (m_y q_{bfx})_e - (m_y q_{bfx})_w + (m_x q_{bfy})_n - (m_x q_{bfy})_s \tag{6.35}$$

where,

J_b is the net removal rate ($gm/m^2 - sec$) from the bed,

m_x and m_y are x and y dimensions of the cell, and

e, w, n, s represent the compass direction subscripts, which define the four cell faces.

The implementation of equations (6.33) through (6.35) in the EFDC+ code includes logic to limit the out fluxes equation (6.34) over a time step, such that the time integrated mass flux from the bed does not exceed bed sediment available for erosion or resuspension.

Under conditions when the bed shear velocity exceeds the settling velocity and critical Shield's shear velocity, non-cohesive sediment will be resuspended and transported as suspended load. When the bed shear velocity falls below both the settling velocity and the critical Shield's shear velocity, suspended sediment will deposit to the bed.

A consistent formulation of these processes can be developed using the concept of a near bed equilibrium sediment concentration. Under steady, uniform flow and sediment loading conditions, an equilibrium distribution of sediment in the water column tends to be established, with the resuspension and deposition fluxes canceling each other. Using a number of simplifying assumptions, the equilibrium sediment concentration distribution in the water column can be expressed analytically in terms of the near bed reference or equilibrium concentration, the settling velocity, and the vertical turbulent diffusivity. For unsteady or spatially varying flow conditions, the water column sediment concentration distribution varies in space and time in response to sediment load variations, changes in hydrodynamic transport, and associated nonzero fluxes across the water column-sediment bed interface. An increase or decrease in the bed stress and the intensity of vertical turbulent mixing will result in net erosion or deposition, respectively, at a particular location or time.

To illustrate how an appropriate suspended non-cohesive sediment bed flux boundary condition can be established, consider the approximation to the sediment transport equation (6.1) for nearly uniform horizontal conditions

$$\frac{\partial}{\partial t}(HC) = \frac{\partial}{\partial z}\left(\frac{A_b}{H}\frac{\partial C}{\partial z} + w_z C\right) \tag{6.36}$$

Integrating equation (6.36) over the depth of the bottom hydrodynamic model layer gives

$$\frac{\partial}{\partial t}\left(\Delta H\bar{C}\right) = J_0 - J_\Delta \tag{6.37}$$

where the over bar denotes the mean over the dimensionless layer thickness Δ. Subtracting equation (6.37) from equation (6.36) gives

$$\frac{\partial}{\partial t}\left(HC'\right) = \frac{\partial}{\partial z}\left(\frac{A_b}{H}\frac{\partial C}{\partial z} + w_z C\right) - \left(\frac{J_0 - J_\Delta}{\Delta}\right) \tag{6.38}$$

Assuming that the rate of change of the deviation of the sediment concentration from the mean is small

$$\frac{\partial}{\partial t}\left(HC'\right) << \frac{\partial}{\partial t}\left(H\bar{C}\right) \tag{6.39}$$

allows equation (6.36) to be approximated by

$$\frac{\partial}{\partial z}\left(\frac{A_b}{H}\frac{\partial C}{\partial z} + w_z C\right) = \left(\frac{J_0 - J_\Delta}{\Delta}\right) \tag{6.40}$$

Integrating equation (6.37) once gives

$$\frac{A_b}{H}\frac{\partial C}{\partial z} + w_z C = \left(J_0 - J_\Delta\right)\frac{z}{\Delta} - J_0 \tag{6.41}$$

Very near the bed, equation (6.41) can be approximated by

$$\frac{A_b}{H}\frac{\partial C}{\partial z} + w_z C = -J_0 \tag{6.42}$$

Neglecting stratification effects and using the results of Section 5.3.2, the near bed diffusivity is approximately

$$\frac{A_b}{H} = K_o q\frac{l}{H} \cong u_* \kappa z \tag{6.43}$$

Introducing equation (6.43) into (6.42) gives

$$\frac{\partial C}{\partial z} + \frac{R}{z}C = -\frac{R}{z}\frac{J_o}{w_s} \tag{6.44}$$

where,

$$R = \frac{w_s}{u_* \kappa} \tag{6.45}$$

is the Rouse parameter. The solution of equation (6.44) is

$$C = -\frac{J_o}{w_s} + \frac{C_0}{z^R} \tag{6.46}$$

The constant of integration is evaluated using

$$C = C_{eq} \text{ at } z = z_{eq} \text{ and } J_o = 0 \tag{6.47}$$

which sets the near bed sediment concentration to an equilibrium value, defined just above the bed under no net flux condition. Using equation (6.47), equation (6.46) becomes

$$C = \left(\frac{z_{eq}}{z}\right)^R C_{eq} - \frac{J_o}{w_s} \tag{6.48}$$

For non-equilibrium conditions, the net flux is given by evaluating equation (6.48) at the equilibrium level

$$J_o = w_s \left(C_{eq} - C_{ne}\right) \tag{6.49}$$

where C_{ne} is the actual concentration at the reference equilibrium level. Equation (6.49) clearly indicates that when the near bed sediment concentration is less than the equilibrium value, a net flux from the bed into the water column occurs. Likewise when the concentration exceeds equilibrium, a net flux to the bed occurs. For this case, when C_{ne} is greater than C_e

$$J_o = -w_s C_{ne} \left(1 - \frac{C_{eq}}{C_{ne}}\right) \tag{6.50}$$

and the term inside the parenthesis in the equation (6.50) can be considered as the deposition factor which does not exceed unity.

For the relationship equation (6.49) to be useful in a numerical model, the bed flux must be expressed in terms of the model layer mean concentration. For a three-dimensional

$$J_o = w_s \left(\bar{C}_{eq} - \bar{C}\right) \tag{6.51}$$

where,

$$\begin{aligned} \bar{C}_{eq} &= \frac{\ln\left(\Delta z_{eq}^{-1}\right)}{\left(\Delta z_{eq}^{-1} - 1\right)} C_{eq}\,, \quad R = 1 \\ \bar{C}_{eq} &= \frac{\left(\Delta z_{eq}^{-1}\right)^{1-R} - 1}{(1-R)\left(\Delta z_{eq}^{-1} - 1\right)} C_{eq}\,, \quad R \neq 1 \end{aligned} \tag{6.52}$$

defines an equivalent layer mean equilibrium concentration in terms of the near bed equilibrium concentration. The corresponding quantities in the numerical solution bottom boundary condition equation (6.9) are

$$\begin{aligned} w_r C_r &= w_s \bar{C}_{eq} \\ P_d w_s &= w_s \end{aligned} \tag{6.53}$$

If the dimensionless equilibrium elevation, z_{eq} exceeds the dimensionless layer thickness, equation (6.33) can be modified to

$$\begin{aligned} \bar{C}_{eq} &= \frac{\ln\left(M\Delta z_{eq}^{-1}\right)}{\left(M\Delta z_{eq}^{-1}-1\right)} C_{eq}\,, \quad R=1 \\ \bar{C}_{eq} &= \frac{\left(M\Delta z_{eq}^{-1}\right)^{1-R}-1}{(1-R)\left(M\Delta z_{eq}^{-1}-1\right)} C_{eq}\,, \quad R\neq 1 \end{aligned} \tag{6.54}$$

where the over bars in equations (6.51) and (6.53) implying an average of the first M layers above the bed.

For two-dimensional depth averaged model application, a number of additional considerations are necessary. For depth average modeling, the equivalent of equation (6.41) is

$$\frac{A_b}{H}\frac{\partial C}{\partial z} + w_s C = -J_o\,(1-z) \tag{6.55}$$

Neglecting stratification effects and using the results of the sediment boundary layers, the diffusivity is

$$\frac{A_b}{H} = K_o q \frac{1}{H} \cong u_* \kappa z\,(1-z)^{\lambda} \tag{6.56}$$

Introducing equation (6.56) into equation (6.55) gives

$$\frac{\partial C}{\partial z} + \frac{R}{z\,(1-z)^{\lambda}} C = -\frac{R\,(1-z)^{1-\lambda}}{z}\frac{J_o}{w_s} \tag{6.57}$$

A closed form solution of equation (6.57) is possible for λ equal to zero. Although the resulting diffusivity is not as reasonable as the choice of λ equal to one, the resulting vertical distribution of sediment is much more sensitive to the near bed diffusivity distribution than the distribution in the upper portions of the water column. For λ equal to zero, the solution of equation (6.57) is

$$C = -\left(1 - \frac{Rz}{(1+R)}\right)\frac{J_o}{w_s} + \frac{C_0}{z^R} \tag{6.58}$$

Evaluating the constant of integration using equation (6.56) gives

$$C = \left(\frac{z_{eq}}{z}\right)^R C_{eq} - \left(1 - \frac{Rz}{(1+R)}\right)\frac{J_o}{w_s} \tag{6.59}$$

For non-equilibrium conditions, the net flux is given by evaluating equation (6.59) at the equilibrium level

$$J_o = w_s \left(\frac{1+R}{1+R\left(1-z_{eq}\right)}\right)\left(C_{eq} - C_{ne}\right) \tag{6.60}$$

where C_{ne} is the actual concentration at the reference equilibrium level. Since z_{eq} is on the order of the sediment grain diameter divided by the depth of the water column, equation (6.60) is essentially equivalent to equation (6.49). To obtain an expression for the bed flux in terms of the depth average sediment concentration, equation (6.59) is integrated over the depth to give

$$J_o = w_s \left(\frac{2\left(1+R\right)}{2+R\left(1-z_{eq}\right)}\right)\left(\bar{C}_{eq} - \bar{C}\right) \tag{6.61}$$

where,

$$\begin{aligned} \bar{C}_{eq} &= \frac{\ln\left(z_{eq}^{-1}\right)}{\left(z_{eq}^{-1}-1\right)} C_{eq}, \quad R = 1 \\ \bar{C}_{eq} &= \frac{\left(z_{eq}^{R-1}-1\right)}{\left(1-R\right)\left(z_{eq}^{-1}-1\right)} C_{eq}, \quad R \neq 1 \end{aligned} \tag{6.62}$$

The corresponding quantities in the numerical solution bottom boundary condition equation (6.9) are

$$\begin{aligned} w_r s_r &= w_s \left(\frac{2\left(1+R\right)}{2+R\left(1-z_{eq}\right)}\right)\bar{C}_{eq} \\ P_d w_s &= \left(\frac{2\left(1+R\right)}{2+R\left(1-z_{eq}\right)}\right) w_s \end{aligned} \tag{6.63}$$

When multiple sediment size classes are simulated, the equilibrium concentrations given by equations (6.52), (6.54), and (6.62) are adjusted by multiplying by their respective sediment volume fractions in the surface layer of the bed.

The specification of the water column-bed flux of non-cohesive sediment has been reduced to specification of the near bed equilibrium concentration and its corresponding reference distance above the bed. Garcia and Parker (1991) evaluated seven relationships,

derived by combinations of analysis and experiment correlation, for determining the near bed equilibrium concentration as well as proposing a new relationship. All of the relationships essentially specify the equilibrium concentration in terms of hydrodynamic and sediment physical parameters

$$C_{eq} = C_{eq}(d, \rho_s, \rho_w, w_s, u_*, \nu) \tag{6.64}$$

including the sediment particle diameter, the sediment and water densities, the sediment settling velocity, the bed shear velocity, and the kinematic molecular viscosity of water. Garcia and Parker concluded that the representations of Smith and McLean (1977) and Rijn (1984) as well as their own proposed representation perform acceptably when tested against experimental and field observations.

Smith and McLean's formula for the equilibrium concentration is

$$C_{eq} = \rho_s \frac{0.65\gamma_o T}{1+\gamma_o T} \tag{6.65}$$

where γ_o is a constant equal to 2.4×10^{-3} and T is given by

$$T = \frac{\tau_b - \tau_{cs}}{\tau_{cs}} = \frac{u_*^2 - u_{*cs}^2}{u_{*cs}^2} \tag{6.66}$$

where,

τ_b is the bed stress, and

τ_{cs} is the critical Shields stress.

The use of Smith and McLean's formulation requires that the critical Shields stress be specified for each sediment size class. Van Rijn's formula is

$$C_{eq} = 0.015\rho_s \frac{d}{z_{eq}^*} T^{3/2} R_d^{-1/5} \tag{6.67}$$

where,

$z_{eq}^* = H z_{eq}$ is the dimensional reference height, and

R_d is a sediment grain Reynolds number.

When van Rijn's formula is select for use in EFDC+, the critical Shields stress in internally calculated using relationships from Rijn (1984). Van Rijn suggested setting the dimensional reference height to three grain diameters. In the EFDC+ model, the user specifies the reference height as a multiple of the largest non-cohesive sediment size class diameter.

Garcia and Parker (1991) general formula for multiple sediment size classes is

$$C_{jeq} = \rho_s \frac{A\left(\lambda Z_j\right)^5}{\left(1+3.33A\left(\lambda Z\right)^5\right)} \tag{6.68}$$

$$Z_j = \frac{u_*}{w_{sj}} R_{dj}^{3/5} F_H \tag{6.69}$$

$$F_H = \left(\frac{d_j}{d_{50}}\right)^{1/5} \tag{6.70}$$

$$\lambda = 1 + \frac{\sigma_\phi}{\sigma_{\phi o}}\left(\lambda_o - 1\right) \tag{6.71}$$

where,

- A is a constant equal to 1.3×10^{-7},
- d_{50} is the median grain diameter based on all sediment classes,
- λ is a straining factor,
- F_H is a hiding factor, and
- σ_ϕ is the standard deviation of the sedimentological phi scale of sediment size distribution.

Garcia and Parker (1991) formulation is unique in that it can account for armoring effects when multiple sediment classes are simulated. For simulation of a single non-cohesive size class, the straining factor and the hiding factor are set to one. The EFDC+ model has the option to simulate armoring with Garcia and Parker's formulation. For armoring simulation, the current surface layer of the sediment bed is restricted to a thickness equal to the dimensional reference height.

6.3.2 Cohesive Sediments

6.3.2.1 Settling Velocities

The settling of cohesive inorganic sediment and organic particulate material is an extremely complex process. Inherent in the process of gravitational settling is the process of flocculation, where individual cohesive sediment particles and particulate organic particles aggregate to form larger groupings or flocs having settling characteristics significantly different from those of the component particles (Burban et al., 1989, 1990; Gibbs, 1985; Mehta et al., 1989). Floc formation is dependent upon the type and concentration of the suspended material, the ionic characteristics of the environment, and the fluid shear and turbulence intensity of the flow environment. Progress has been made in first principles mathematical modeling of floc formation or aggregation, and disaggregation by intense flow shear (Lick and Lick, 1988; Tsai et al., 1987). However, the computational cost of

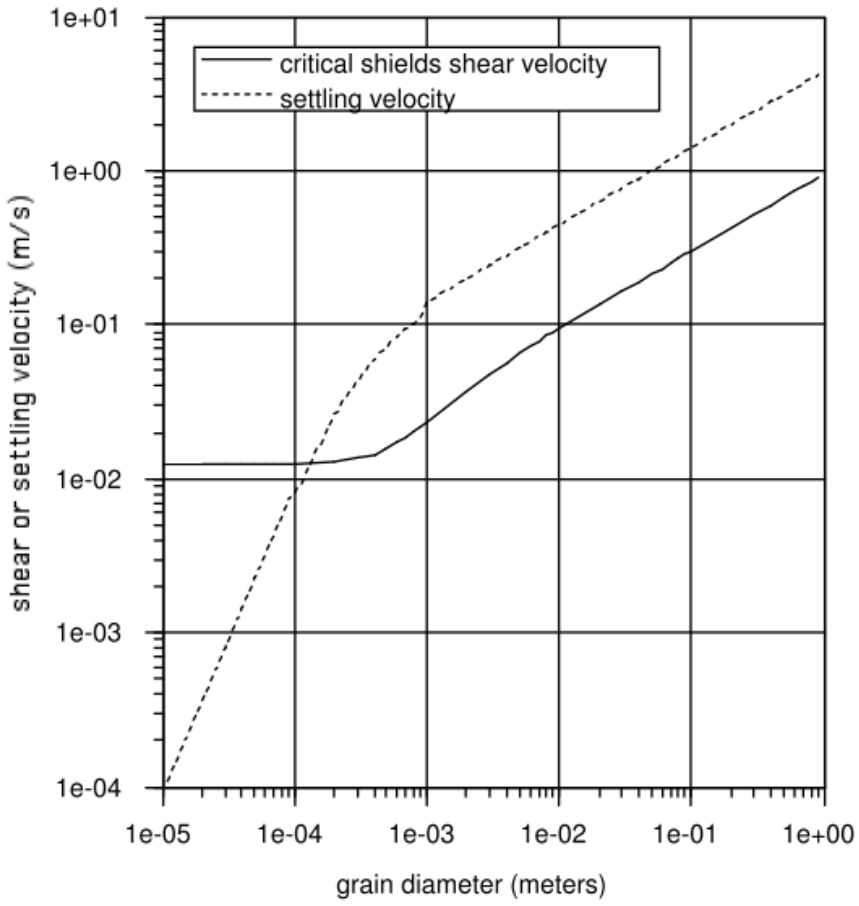

Fig. 6.1. Critical Shield's shear velocity and settling velocity as a function of sediment grain size

such approaches precludes direct simulation of flocculation in operational cohesive sediment transport models currently.

An alternative approach, which has been applided with reasonable success, is the parameterization of the settling velocity of flocs in terms of cohesive and organic material fundamental particle size d, concentration S, and flow characteristics such as vertical shear of the horizontal velocity du/dz, shear stress $A_v du/sz$, or turbulence intensity in the water column or near the sediment bed q. This has allowed semi-empirical expressions having the functional form

$$w_{se} = w_{se}\left(d, C, \frac{du}{dz}, q\right) \tag{6.72}$$

to be developed to represent the effective settling velocity. The following settling approaches are available in EFDC+.

6.3.2.1.1 Option 1

Hwang and Mehta (1989) proposed the following

$$w_s = \frac{aC''}{(C^2 + b^2)^m} \tag{6.73}$$

based on observations of settling at six sites in Lake Okeechobee. This equation has a general parabolic shape with the settling velocity decreasing with decreasing concentration at low concentrations and decreasing with increasing concentration at high concentration. Least squares analysis for the parameters a, m, n, in equation (6.73) was shown to agree well with observational data. Equation (6.73) does not have a dependence on flow characteristics, but is based on data from an energetic field condition having both currents and high frequency surface waves.

6.3.2.1.2 Option 2

The formulation given by Shrestha and Orlob (1996) and as subsequently modified by Mehta et al. (1989) has the form

$$cw_s = C^{\alpha} \exp(-4.21 + 0.147G) \tag{6.74}$$

$$\alpha = 1.11075 + 0.0386G \tag{6.75}$$

where,

$$G = \sqrt{\left(\frac{\partial u}{\partial z}\right)^2 + \left(\frac{\partial v}{\partial z}\right)^2} \tag{6.76}$$

is the magnitude of the vertical shear of the horizontal velocity. It is noted that all of these formulations are based on specific dimensional units for input parameters and predicted settling velocities and that appropriate unit conversion are made internally in their implementation in the EFDC+ model.

6.3.2.1.3 Option 3

Ziegler and Nisbet (1994, 1995) proposed a formulation to express the effective settling as a function of the floc diameter d_f

$$w_s = a d_f^b \tag{6.77}$$

with the floc diameter given by:

$$d_f = \sqrt{\frac{\alpha_f}{C\sqrt{\tau_{xz}^2 + \tau_{yz}^2}}} \tag{6.78}$$

where,

C is the sediment concentration

α_j is an experimentally determined constant

τ_{xz} and τ_{yz} are the x and y components of the turbulent shear stresses at a given position in the water column

Other quantities in equation (6.78) have been experimentally determined to fit the relationships:

$$a = B_1 \left(C \sqrt{\tau_{xz}^2 + \tau_{yz}^2} \right)^{-0.85} \tag{6.79}$$

$$b = -0.8 - 0.5 \log \left(C \sqrt{\tau_{xz}^2 + \tau_{yz}^2} - B_2 \right) \tag{6.80}$$

where B_1 and B_2 are experimental constants.

6.3.2.1.4 Option 4

Generalized approach to compute settling velocities based on shear stress is as follows:

$$w_s = \begin{cases} 1.510 \times 10^{-5} (C')^{0.45} , & C' < 40 \\ 8 \times 10^{-5} , & 40 \leq C' \leq 400 \\ 0.893 \times 10^{-6} (C')^{0.75} , & C' > 400 \end{cases} \tag{6.81}$$

$$C' = \tau C \tag{6.82}$$

where, τ is shear stress (cm^2/s^2), and C is total cohesive concentration (g/m^3).

6.3.2.1.5 Option 5

The following approach for settling velocities are based on the Housatonic River approach combining Burban & Lick with site specific regressions.

$$w_s = \begin{cases} \frac{1.270}{86400 (C')^{0.79}} , & C' < 3.8 \\ \frac{3.024}{86400 (C')^{0.14}} , & C' \geq 3.8 \end{cases} \tag{6.83}$$

$$C' = \tau C \tag{6.84}$$

where, τ is shear stress (cm^2/s^2) and C is total cohesive concentration (g/m^3).

6.3.2.1.6 Option 6

Generalized approach to compute settling velocities based on shear stress is as follows:

$$w_s = \begin{cases} 2.32 \times 10^{-5}(C')^{0.5}, & C' < 100 \\ 3.68 \times 10^{-5}(C')^{0.4}, & C' \geq 100 \end{cases} \tag{6.85}$$

$$C' = \tau C \tag{6.86}$$

where, τ is shear stress (cm^2/s^2) and C is total cohesive concentration (g/m^3).

6.3.2.1.7 Option 7

Generalized approach to compute settling velocities based on shear stress is as follows:

$$w_s = 0.0052(C')^{0.470138} \tag{6.87}$$

$$C' = \tau C \tag{6.88}$$

where, τ is shear stress (m^2/s^2) and C is total cohesive concentration (g/m^3).

6.3.2.1.8 Option 8

A modified Shrestha and Orlob (1996) approach to compute settling velocities based on shear stress is as follows:

$$w_s = a\left(\frac{C}{2650}\right)^{0.3333} \tag{6.89}$$

$$a = \begin{cases} \frac{0.06}{\sqrt{\tau}}, & \tau \geq 0.1 \\ 0.1, & \tau \leq 0.1 \end{cases} \tag{6.90}$$

where, τ is shear stress (m^2/s^2) and C is total cohesive concentration (g/l).

6.3.2.2 Deposition

Water column-sediment bed exchange of cohesive sediments and organic solids is controlled by the near bed flow environment and the geomechanics of the deposited bed. Net deposition to the bed occurs as the flow-induced bed surface stress decreases. The most widely used expression for the depositional flux is:

$$J_o^d = \begin{cases} -w_s C_d \left(\frac{\tau_{cd}-\tau_b}{\tau_{cd}}\right) = -w_s P_d C_d & \tau_b \leq \tau_{cd} \\ 0, & \tau_b \geq \tau_{cd} \end{cases} \tag{6.91}$$

where,

τ_b is the stress exerted by the flow on the bed,

τ_{cd} is a critical stress for deposition which depends on sediment material and floc physiochemical properties (Mehta et al., 1989), and

C_d is the near bed depositing sediment concentration.

The probability of deposition P_d is based on the linear term, $(\tau_{cd} - \tau_b)/\tau_{cd}$. The critical deposition stress is generally determined from laboratory or *in situ* field observations and values ranging from 0.06 to 1.1 N/m^2 have been reported in the literature. Given this wide range of reported values, in the absence of site specific data, the depositional stress and is generally treated as a calibration parameter. The depositional stress is an input parameter in the EFDC+ model.

6.3.2.3 Erosion

Cohesive bed erosion occurs in two distinct modes, mass erosion and surface erosion. Mass erosion occurs rapidly when the bed stress exerted by the flow exceeds the depth varying shear strength τ_s, of the bed at a depth H_{me}, below the bed surface. Surface erosion occurs gradually when the flow-exerted bed stress is less than the bed shear strength near the surface but greater than a critical erosion or resuspension stress τ_{ce}, which is dependent on the shear strength and density of the bed. A typical scenario under conditions of accelerating flow and increasing bed stress would involve first the occurrence of gradual surface erosion, followed by a rapid interval of mass erosion, followed by another interval of surface erosion. Alternately, if the bed is well consolidated with a sufficiently high shear strength profile, only gradual surface erosion would occur. Transport into the water column by mass or bulk erosion can be expressed in the form

$$J_o^r = w_r C_r = \frac{m_{me}\,(\tau_s \leq \tau_b)}{T_{me}} \tag{6.92}$$

where,

J_o is the erosion flux,

W_{Cr} represents the numerical boundary condition equation (6.9),

m_{me} is the dry sediment mass per unit area of the bed having a shear strength,

τ_s less than the flow-induced bed stress, and

τ_b and T_{me} is a somewhat arbitrary time scale for the bulk mass transfer.

The time scale can be taken as the numerical model integration time step (Shrestha and Orlob, 1996). Observations by Hwang and Mehta (1989) have indicated that the maximum rate of mass erosion is on the order of $0.6\,gs^{-1}m^{-2}$ which provides a means of estimating the transfer time scale in equation (6.92). The shear strength of the cohesive sediment bed is generally agreed to be a linear function of the bed bulk density (Hwang and Mehta, 1989; Mehta et al., 1982; Villaret and Paulic, 1986).

$$\tau_s = a_s \rho_b + b_s \tag{6.93}$$

For the shear strength in N/m^2 and the bulk density in g/cm^3, Hwang and Mehta (1989) give a_s and b_S values of 9.808 and -9.934, respectively for bulk density greater than $1.065\, g/cm^3$. The EFDC+ model currently implements Hwang and Mehta (1989) relationship, but can be readily modified to incorporate other functional relationships.

Surface erosion is generally represented by relationships of the form

$$J_o^r = w_r C_r = \frac{dm_e}{dt}\left(\frac{\tau_b - \tau_{ce}}{\tau_{ce}}\right)^{\alpha}, \quad \tau_b \geq \tau_{ce} \tag{6.94}$$

or

$$J_o^r = w_r C_r = \frac{dm_e}{dt}\exp\left(-\beta\left(\frac{\tau_b - \tau_{ce}}{\tau_{ce}}\right)^{\gamma}\right), \quad \tau_b \geq \tau_{ce} \tag{6.95}$$

where

$\frac{dm_e}{dt}$ is the surface erosion rate per unit surface area of the bed,

τ_{ce} is the critical stress for surface erosion or resuspension.

The critical erosion rate and stress and the parameters α, β, and γ are generally determined from laboratory or *in situ* field experimental observations. Equation (6.94) is more appropriate for consolidated beds, while (6.95) is appropriate for soft partially consolidated beds. The base erosion rate and the critical stress for erosion depend upon the type of sediment, the bed water content, total salt content, ionic species in the water, pH and temperature (Mehta et al., 1989) and can be measured in laboratory and sea bed flumes.

Surface erosion rates ranging from 0.005 to $0.1\, gs^{-1}m^{-2}$ have been reported in the literature, and it is generally accepted that the surface erosion rate decreases with increasing bulk density. The critical erosion stress is related to but generally less than the shear strength of the bed, which in turn depends upon the sediment type and the state of consolidation of the bed. Experimentally determined relationships between the critical surface erosion stress and the dry density of the bed of the form

$$\tau_{ce} = c\rho_s^d \tag{6.96}$$

have been presented (Mehta et al., 1989).

The EFDC+ model allows for a user defined constant critical stress for surface erosion or the use of a computed τ_{ce} based on one of the following options.

6.3.2.3.1 Option 1

Hwang and Mehta (1989) proposed the relationship

$$\tau_{ce} = \begin{cases} a(\rho_b - \rho_l)^b + c, \ \rho_b > 1.065 \\ 0, \ \rho_b \leq 1.065 \end{cases} \tag{6.97}$$

between the critical surface erosion stress and the bed bulk density with $a = 0.883$, $b = 0.2$, $c = 0.05$, and $\rho_l = 1.065$ for the stress in N/m^2 and the bulk density in g/cm^3.

6.3.2.3.2 Options 2 and 3

Sanford and Maa (2001) proposed the relationship

$$\tau_{ce} = \tau_{ci} \frac{(1+VR_r)}{(1+VR_b)} \tag{6.98}$$

where

τ_{ci} is the reference critical surface erosion rate (m^2/s^2)

VR_r and VR_b are the void ratios of the reference and the bed, respectively (dimensionless).

6.3.2.3.3 Options 4 and 5

This option is governed by the relationship:

$$\tau_{ce} = \tau_{ci} \tag{6.99}$$

where τ_{ci} is the reference critical surface erosion rate (m^2/s^2).

6.3.2.3.4 Option 99

The Housatonic River relationship is

$$\tau_{ce} = \begin{cases} \frac{0.2}{1000}, L \leq 265 \ \frac{0.4}{1000}, & L > 265 \end{cases} \tag{6.100}$$

where L is the EFDC+ linear cell index. This is a hardwired option for the Housatonic River.

6.3.3 Consolidation of Mixed Cohesive and Non-Cohesive Sediment Beds

This section presents a methodology for representing consolidation of sediment beds containing both cohesive and non-cohesive sediments. The methodology allows for both cohesive and non-cohesive sediment in any bed layer and is based on the following assumptions. First, it is assumed that during the consolidation step, a fraction of the bed pore water volume per unit horizontal area is associated with each sediment type or

$$\left(\frac{\varepsilon H_{bed}}{1+\varepsilon}\right) = (\psi_{wc} + \psi_{wn}) H_{bed} \tag{6.101}$$

where,

H_{bed} is the bed thickness (m)

ψ is the volume fraction of water with the subscripts

wc and wn denoting cohesive and non-cohesive sediment, respectively.

Likewise, the volume of sediment per unit horizontal area can be fractionally partitioned between cohesive and non-cohesive

$$\left(\frac{H_{bed}}{1+\varepsilon}\right) = (\psi_{sc} + \psi_{sn}) H_{bed} \tag{6.102}$$

Following the Lagrangian formulation of the previous section, the total volume of sediment and the fractional sediment volume in a bed layer remain constant during a consolidation step.

$$\frac{\partial}{\partial}(H_{bed}\psi_{sc}) = \frac{\partial}{\partial}(H_{bed}\psi_{sn}) = 0 \tag{6.103}$$

Fractional void ratios can also be defined

$$\varepsilon_c = \frac{\psi_{wc}}{\psi_{sc}} \tag{6.104}$$

$$\varepsilon_n = \frac{\psi_{wn}}{\psi_{sn}} \tag{6.105}$$

and using equations (6.101) and (6.102), the void ratio of the mixture is

$$\varepsilon = \frac{\psi_{sc}\varepsilon_c + \psi_{sn}\varepsilon_n}{\psi_{sc} + \psi_{sn}} \tag{6.106}$$

which is the sediment volume weighted average of the void ratios of the two sediment types.

The second assumption is that during the consolidation time step, the fraction of water associated with non-cohesive sediment remains constant, as does the fractional void ratio. This is equivalent to the assuming that the portion of the bed layer associated with non-cohesive sediment is incompressible, and that the pore water associated the non-cohesive sediment is specified by ε_n.

Consistent with the preceding assumptions, the thickness of the bed layer can be divided into cohesive and non-cohesive fractions $H_{bed,c}$ and $H_{bed,n}$, respectively.

$$\begin{aligned} H_{bed,c} &= (\psi_{wc} + \psi_{sc}) H_{bed} = (1+\varepsilon_c)\,\psi_{sc} H_{bed} \\ H_{bed,n} &= (\psi_{wn} + \psi_{sn}) H_{bed} = (1+\varepsilon_n)\,\psi_{sn} H_{bed} \end{aligned} \tag{6.107}$$

The hydraulic conductivity of the layer can be expressed by

$$K = \frac{\left(H_{bed,c} + H_{bed,n}\right)}{\left(\frac{H_{bed,c}}{K_c} + \frac{H_{bed,n}}{K_n}\right)} \tag{6.108}$$

which is equivalent to an infinite number of alternating infinitesimal cohesive and non-cohesive sublayers of proportional thickness comprising the mixed bed layer. Equation (6.108) can be written as

$$\frac{K}{(1+\varepsilon)} = \frac{1}{\left(f_{sc}\frac{(1+\varepsilon_c)}{K_c} + f_{sn}\frac{(1+\varepsilon_n)}{K_n}\right)} \tag{6.109}$$

where,

$$\begin{aligned} f_{sc} &= \frac{\psi_{sc}}{(\psi_{sc}+\psi_{sn})} \\ f_{sn} &= \frac{\psi_{sn}}{(\psi_{sc}+\psi_{sn})} \end{aligned} \tag{6.110}$$

are the time invariant total cohesive and non-cohesive sediment fractions in the bed layer. Likewise, equation (6.106) can be written as

$$\varepsilon = f_{sc}\varepsilon_c + f_{sn}\varepsilon_n \tag{6.111}$$

The final assumption for the mixed material consolidation formulation is that changes in effective stress are due entirely to changes in the cohesive void ratio. Under this assumption, the specific discharge can be written as

$$q = -\left(\frac{K}{1+\varepsilon}\right)_{k+\frac{1}{2}} \frac{2\lambda_{k+\frac{1}{2}}}{(\Delta_{k+1}+\Delta_k)}\left[(f_{sc}\varepsilon_c)_{k+1} - (f_{sc}\varepsilon_c)_k\right] + \left(\frac{K}{1+\varepsilon}\right)_{k+\frac{1}{2}}\left(\frac{\bar{\rho}_s}{\rho_w} - 1\right)_{k+\frac{1}{2}} \tag{6.112}$$

and

$$\lambda_{k+\frac{1}{2}} = -\frac{1}{g\rho_w}\left(\frac{\sigma_{e,k+1} - \sigma_{e,k}}{(f_{sc}\varepsilon_c)_{k+1} - (f_{sc}\varepsilon_c)_k}\right) \tag{6.113}$$

When the depositional void ratio is specified for the surface layer specific discharge becomes

$$q_{w:kt+} = -\left(\frac{2\lambda_{kt+}}{\Delta_{kt}}\right)\left(\frac{K}{1+\varepsilon}\right)_{kt+}\left[(\varepsilon_c)_{dep} - (\varepsilon_c)_k\right] + \left(\frac{\bar{\rho}_s}{\rho_w} - 1\right)_{kt+}\left(\frac{K}{1+\varepsilon}\right)_{kt+} \tag{6.114}$$

When the zero excess pore pressure boundary condition at the bed surface is used

$$q_{w:kt+} = \left(\frac{K}{1+\varepsilon}\right)_{Kt} \frac{2}{\Delta_{Kt}} \left(\lambda^* f_{sc} \varepsilon_c^{n+1}\right)_{Kt} + \left(\frac{K}{1+\varepsilon}\right)_{Kt} \left(\frac{\bar{\rho}_s}{\rho_w} - 1\right)_{Kt} - \left(\frac{K}{1+\varepsilon}\right)_{Kt} \frac{2}{\Delta_{Kt}} \left(\frac{\sigma_e^n}{g\rho_w} + \lambda^* f_{sc} \varepsilon^*\right)_{Kt} \quad (6.115)$$

The equation for updating the void ratio is modified using equation (6.111) to give

$$(f_{sc}\varepsilon_c)_k^{**} = (f_{sc}\varepsilon_c)_k^* + \frac{\Delta t}{2} \left(\frac{1+\varepsilon}{H_{bed}}\right)_k^{**} (q_{w:k-} q_{w:k+}) \quad (6.116)$$

Thus the mixed bed layer consolidation formulation essentially solves of the space and time evolution of $f_{sc}\varepsilon_c$ with the continuum constitutive relationship for λ given by

$$\lambda = -\frac{1}{f_{sc}} \frac{\partial}{\partial \varepsilon} \left(\frac{\sigma}{g\rho_w}\right) \quad (6.117)$$

The formulation has the desirable characteristic of reducing to the well established cohesive formulation in the absence of non-cohesive material. The solution for $f_{sc}\varepsilon_c$ proceeds by introducing equations (6.102) and (6.104) or (6.105) into (6.106) and solving the resulting tri-diagonal system of equations. The new specific discharges are then directly calculated using equations (6.102) and (6.104) or (6.105) and used to update the layer thickness

$$H_{bed,k}^{n+1} = H_{bed,k}^* + \Delta t \left(q_{w:k-} - q_{w:k+}\right) \quad (6.118)$$

The ratio $H_{bed}/(1+\varepsilon)$ can then be updated

$$\left(\frac{H_{bed}}{1+\varepsilon}\right)_k^{n+1} = \left(\frac{H_{bed}}{1+\varepsilon}\right)_k^* \quad (6.119)$$

Followed by the solution of equation (6.111) for the cohesive void ratio

$$\varepsilon_c = \frac{\varepsilon - f_{sn}\varepsilon_n}{f_{sc}} \quad (6.120)$$

6.4. SEDZLJ Sediment Transport

6.4.1 Overview

The EFDC+ model was extended in James et al. (2010) to include measured erosion rates from an erosion rate measurement flume referred to as SEDFlume (Jones and Lick, 2001). The mathematical framework for the unified treatment of erosion, deposition and bedload transport is referred to as the SEDZLJ model. This section of the EFDC+ theory document provides a summary of the theory of SEDZLJ and larger is taken from Grace et al. (2008); James et al. (2010); Jones and Lick (2001).

A SEDFlume consists of a straight flume with an open bottom through which a rectangular cross-section core tube containing sediment can be inserted. The main components of the flume are the core tube and sediment, the test section, the inlet section for uniform, fully-developed, turbulent flow, the flow exit section, the water storage tank, and the pump (which forces water through the system). A schematic of the SEDFlume is shown in Figure 6.2. Data produced from these tests produce erosion rates, critical shear stress, and bulk density by depth in a core.

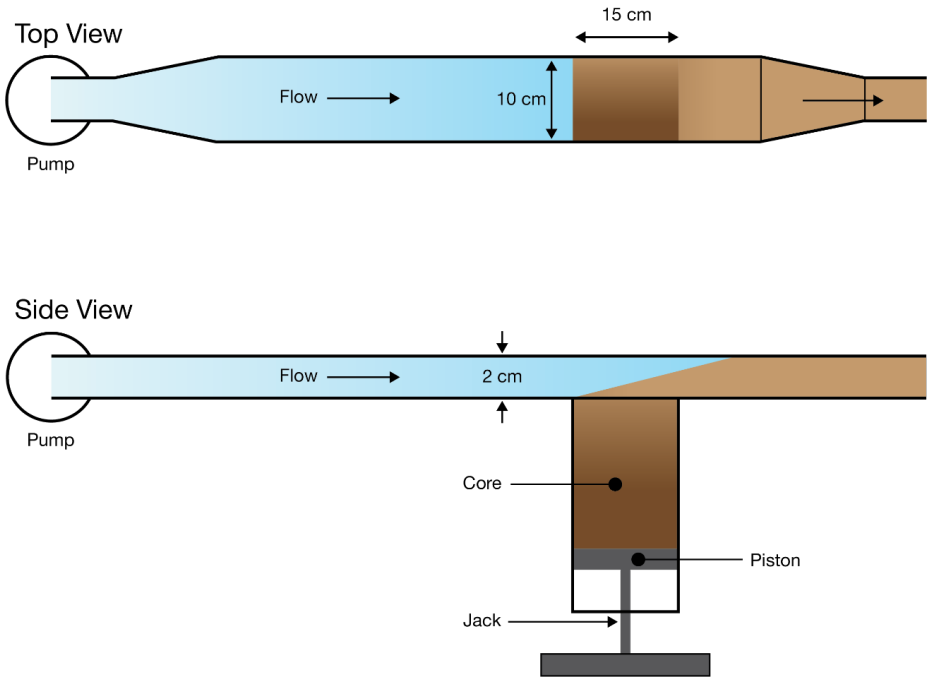

Fig. 6.2. Schematic of the SEDFlume apparatus.

6.4.2 Introduction

Most models are calibrated using hind casting techniques which can have limitations when extending the simulation to future conditions. The most typically available sediment transport indicator measured in aquatic systems is the suspended sediment concentration. Unfortunately, many different combinations of erosion and deposition rates can be used to reach the same suspended sediment concentration. This can be illustrated as follows. In the steady state, an equilibrium exists between erosion and deposition. Deposition is generally described as $D = Pw_sC$ where P is a probability of deposition, w_s is the settling speed of the sediment particles, and C is the sediment concentration in the water. Equilibrium then gives

$$E - Pw_sC = 0 \tag{6.121}$$

This can be solved for the sediment concentration, which is

$$C = \frac{E}{Pw_s} \tag{6.122}$$

From this equation, it is seen that any suspended sediment concentration can be matched with an infinite number of erosion rates and deposition parameters by adjusting both accordingly. For example, the observed value of C can be obtained by high values of E and high values of Pw_s or by low values of E and low values of Pw_s. In other words, measurements of suspended sediment concentrations are not sufficient to determine erosion and/or deposition, parameters essential for predicting sediment and contaminant transport and fate. Historically, the erosion was constrained by theoretical relationships between shear stress and grain sizes, however there was still a range of parameters that would produce the same suspended concentrations. In order to predict erosion and deposition accurately, these quantities should be determined as functions of sediment characteristics and hydrodynamic variables by means of experiments or theory based on experiments.

6.4.3 SEDZLJ Model

6.4.3.1 Bed Shear Stress

The bottom stress is represented by τ_b given by

$$\tau_b = c_f V \tag{6.123}$$

where V is the velocity magnitude (cm/s) and c_f is a bottom shear stress friction factor calculated using a log-layer distribution of velocity. c_f is given by

$$c_f = \begin{cases} \frac{\kappa^2}{\left(\ln \frac{H}{2z_b}\right)^2} & \text{for } H \geq H_{min} \\ 0.0 & \text{for } H < H_{min} \end{cases} \tag{6.124}$$

where,

κ is von Karman's constant (κ=0.42),

z_b is bottom skin friction based on the d_{50} at the sediment surface (m), and

H_{min} is the minimum depth to allow shear computations (m).

The bottom roughness is assumed to be equal to the average particle diameter of the surface of the sediment bed at any given location. As the bottom roughness increases or as the depth of water decreases, c_f increases.

6.4.3.2 Erosion Rates

Results of a typical application of SEDFlume are shown in Figure 6.3, where erosion rates, E, in units of cm/s are plotted as a function of depth (cm) with shear stress τ (N/m^2). Erosion rates are generally highest at the surface and decrease with depth; they also increase with shear stress. In general, information of this type for sediments throughout the system is necessary for accurate predictions of sediment transport (Jones and Lick, 2000). Availability of this type of data is assumed and is used in the present model.

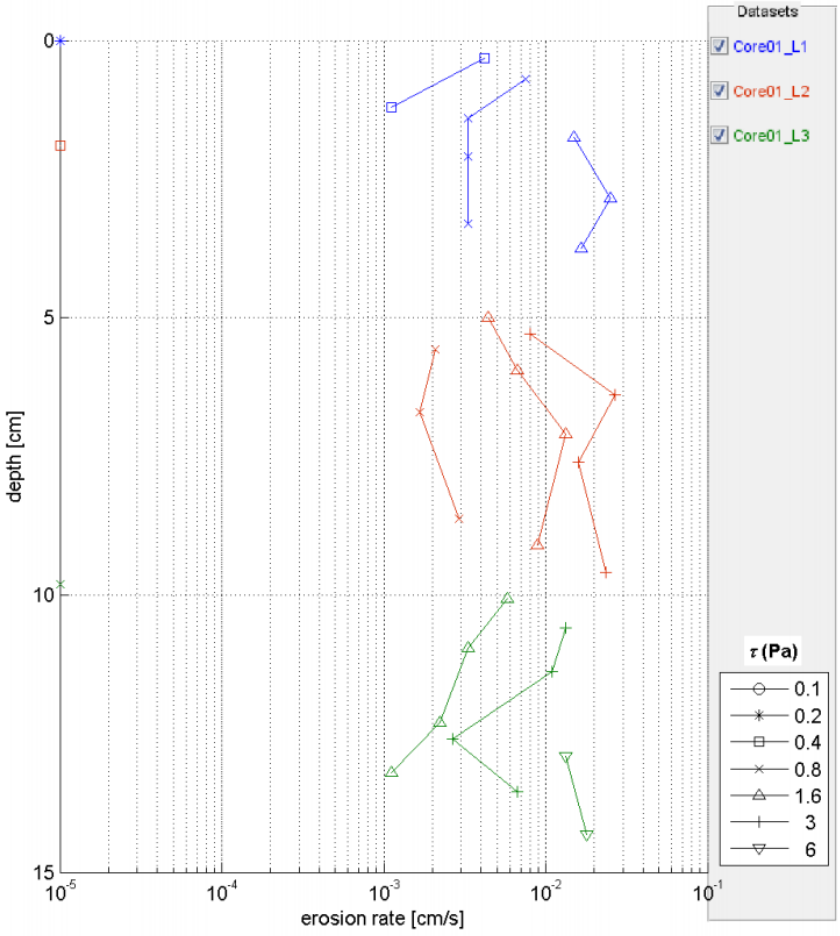

Fig. 6.3. SEDFlume data for Conowingo Reservoir (DNR Maryland).

Information on erosion rates is generally reported in units of cm/s. In order to convert this to a mass flux in units of g/cm^2/s which is needed in the modeling, the mass of solids within a sediment volume is needed. This quantity, for a sediment consisting of solids and water only (i.e. no gas), can be determined in terms of the bulk density of the sediments ρ, as follows:

$$\rho = \rho_s x_s + \rho_w x_w = \rho_s x_s + \rho_w (1 - x_s) \tag{6.125}$$

where,

ρ_s is the density of solids (g/cm^3),

x_s is the volume fraction of the solids,

ρ_w is the density of water (g/cm^3), and

x_w is the volume fraction of water.

Since $x_w = 1 - x_s$, the mass of solids per unit volume is $x_s\rho_s$ and can be determined from the above equation as

$$x_s\rho_s = \frac{\rho_s(\rho - \rho_w)}{\rho_s - \rho_w} = \frac{2.6}{1.6}(\rho - 1) \tag{6.126}$$

where it is assumed that $\rho_s = 2.6\, g/cm^3$ and $\rho_w = 1.0\, g/cm^3$. Once the bulk density of the sediments is known, the erosion rate in units of $g/cm^2 s$ can be determined by multiplying the erosion rate in units of cm/s by $x_s\rho_s$.

As indicated above, erosion rates change as a function of depth. This variation is incorporated into the sediment bed model through a discrete layering system where the erosion rate is defined at each layer interface, and the particle size distribution and bulk density are defined as constant throughout the layer. Any number and thickness of layers required to approximate the variation of sediment properties with depth can be introduced as necessitated by field data.

The sediment transport model developed herein can incorporate erosion rate data collected in the field that are typically spatially discrete and at specific depths, but can be interpolated where no direct data are available. The total erosion rate is interpolated across sediment layer thicknesses and shear stresses. Linear interpolation is used to calculate an erosion rate at a specified shear stress τ as

$$E(\tau) = \left(\frac{\tau_{i+1} - \tau}{\tau_{i+1} - \tau_i}\right) E_i + \left(\frac{\tau - \tau_i}{\tau_{i+1} - \tau_i}\right) E_{i+1} \tag{6.127}$$

where, subscript i denotes data for a shear stress less than τ and $i+1$ denotes measured data for a shear stress greater than τ, with $\tau_i < \tau < \tau_{i+1}$.

Because E often changes rapidly with depth, the logarithmic interpolation between data points best represents erosion rates as a function of depth

$$\ln[E(T)] = \left(\frac{T_0 - T}{T_0}\right) \ln(E^j) + \frac{T}{T_0} \ln\left(E^{j+1}\right) \tag{6.128}$$

where T is the actual layer thickness, T_0 is the initial layer thickness, and the superscripts j and $j+1$ denote data for the interface at the top and the bottom of the specific layer where the erosion rate is required, respectively. Equations (6.127) and (6.128) are combined so that the erosion rates may be calculated as a function of shear stress and depth.

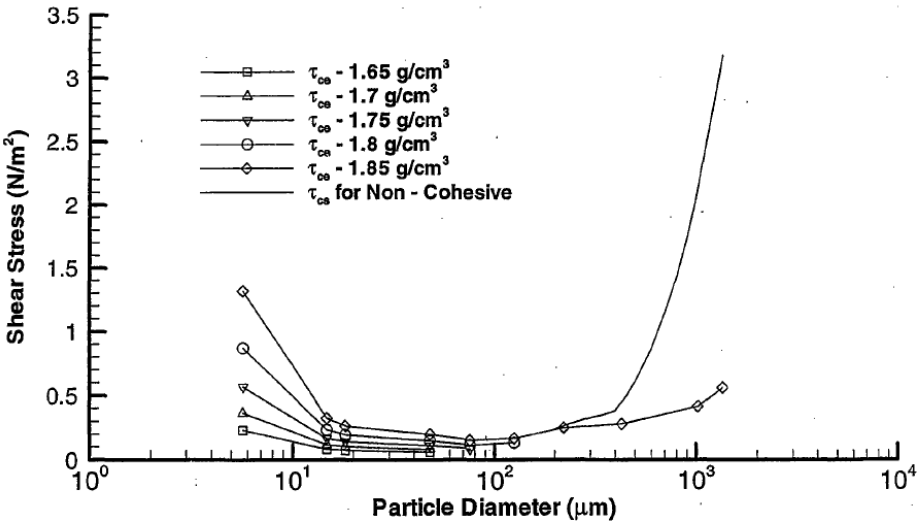

Fig. 6.4. Critical shear stresses for erosion and suspension of quartz particles.

6.4.3.2.1 Critical Shear Stress for Erosion

In addition to erosion rates, another parameter of significance in modeling is the critical stress for erosion, τ_{ce}. This quantity can be understood and quantified as follows. Consider the flow of water over a sediment bed. As the rate of flow is increased starting from rest, there is a range of velocities (or shear stresses) at which the movement of the easiest-to-move particles (generally the smallest) is first noticeable to an observer. These eroded particles then travel a relatively short distance until they come to rest in a new location. This initial motion tends to occur only at a few isolated spots. As the flow velocity and shear stress increase further, more particles participate in this process of erosion, transport, and deposition, and the movement of the particles becomes more sustained.

Because of this gradual increase in sediment erosion as the shear stress increases, it is difficult to precisely define a critical velocity or critical shear stress at which sediment erosion is first initiated. More quantitatively and with less ambiguity, a critical shear stress for erosion can be defined as the shear stress at which a small, but accurately measurable, rate of erosion occurs. Roberts et al. (1998) defined this rate as $10^{-6}\ m/s$, represented by approximately $1\ mm$ of erosion in $15\ minutes$, though different rates have been used to define τ_{ce}.

Critical shear stresses for erosion as a function of particle diameter d, are shown in Figure 6.4. For $d > 200\,\mu m$, the sediments behave in a non-cohesive manner, i.e., they consolidate rapidly and they erode particle by particle. For $d < 200\,\mu m$, cohesive effects between particles become significant. The sediments consolidate relatively slowly with time, and the critical stresses depend not only on particle diameter but also on the bulk density of the sediments. For these cohesive sediments, τ_{ce} increases as d decreases and as bulk density increases.

For non-cohesive sediment beds, the curve of Shields (1936), or any approximation

thereof Rijn (1984), could be used to define the critical shear stress for erosion. Soulsby et al. (1997) approximated the critical shear for erosion as

$$\tau_{ce} = \rho g d \theta = \rho g d \left\{ \frac{0.3}{1+1.2d_*} + 0.055\left[1-\exp\left(-0.02d_*\right)\right] \right\} \tag{6.129}$$

$$d_* = d\left[\left(\rho_{sd}/\rho_w - 1\right) g/v^2\right]^{1/3} \tag{6.130}$$

where,

- g is the acceleration due to gravity,
- d the sediment particle diameter,
- d_* is the non-dimensional particle diameter,
- v the kinematic fluid viscosity, and
- θ the critical Shields parameter, represented by the algebraic fit shown in the parenthesis in equation (6.129)

6.4.3.2.2 Erosion into Suspended Load versus Bedload

As bottom sediments are eroded, a fraction of the sediments are suspended into the overlying water and are transported as suspended load; the rest of the eroded sediments move by rolling and/or saltation in a thin layer near the bed in what is called bedload. The fraction in each of the transport modes depends on the particle size and shear stress.

For fine-grained particles (which are generally cohesive), erosion occurs both as individual particles and in the form of chunks or small aggregates of particles. The individual particles move as suspended load. The aggregates tend to move downstream near the bed but generally seem to disintegrate into small particles in the high stress boundary layer near the bed as they move downstream. These disaggregated particles then move as suspended load. For this reason, it is assumed here that fine-grained sediments less than about $200\,\mu m$ are completely transported as suspended load.

Coarser, non-cohesive particles (defined here as those particles with diameters greater than about $200\,\mu m$) can be transported both as suspended load and bedload, with the fraction in each dependent on particle diameter and shear stress. For particles of a particular size, the shear stress at which suspended load (or sediment suspension) is initiated is defined as $\tau_{cs}(N/m^2)$. This shear stress τ_{cs}, can be defined from the Rijn (1984) formulations as

$$\tau_{cs} = \begin{cases} \frac{1}{\rho_w}\left(\frac{4w_s}{d_*}\right)^2, & \text{for } d \le 400\ \mu m \\ \frac{1}{\rho_w}(0.4w_s)^2, & \text{for } d > 400\ \mu m \end{cases} \tag{6.131}$$

where,

d_* is the non-dimensional particle diameter calculated from $d_* = d\left[\frac{(\rho_s-\rho)}{\rho}\frac{g}{\nu^2}\right]^{1/3}$ where d is the particle diameter (cm), and

w_s is the particle settling speed (cm/s)

For $\tau^b > \tau_{cs}$, sediments are transported both as bedload and suspended load with the fraction in suspended load f, increasing with τ^b from $f = 0$ until f reaches 1. For τ^b greater than this, sediments are transported completely as suspended load.

The settling speed can be determined from Cheng (1997) and Rijn (1984) or user specified. Cheng's formula for settling speed is

$$w_s = \frac{\nu}{d}\left(\sqrt{25+1.2d_*^2}-5\right)^{1.5} \tag{6.132}$$

where ν is the kinematic fluid viscosity (cm^2/s).

Since Cheng's formula is based on the observations of the settling of real sediment particles, it produces settling speeds lower than Stoke's law. This is because real sediments are often irregular in shape and have a greater hydrodynamic resistance to settling than perfect spheres as in Stoke's law.

Rijn (1984) computed the settling velocity as

$$w_s = \begin{cases} \frac{1}{18}\left[\frac{(s-1)gD_s^2}{\nu}\right], & D_s < 100\,\mu\text{m} \\ 10\frac{\nu}{D_s}\left\{\left[1+\frac{0.01(s-1)gD_s^3}{\nu^2}\right]^{0.5}-1\right\}, & 100\,\mu\text{m} \le D_s < 1000\,\mu\text{m} \\ 1.1\left[(s-1)\,gD_s\right]^{0.5}, & D_s \ge 1000\,\mu\text{m} \end{cases} \tag{6.133}$$

where,

D_s is the representative particle size (m), s is the specific density

g is the acceleration due to gravity (m/s^2), and

ν is the kinematic viscosity coefficient and w_s is in m/s.

Guy et al. (1966) performed detailed flume measurements of suspended load and bedload transport for sediments ranging in median diameter d_{50}, from 190 μm to 930 μm. They found that, as the ratio of shear velocity (defined as $u_* = \sqrt{\tau^b/\rho_w}$) to settling velocity increases, the proportion of suspended load to total load transport, q_s/q_t increases. An approximation of their data can be made with the following function:

$$\frac{q_s}{q_t} = \begin{cases} 0, & \tau^b < \tau_{cs} \\ \frac{\ln(u_*/w_s)-\ln\left(\sqrt{\tau_{cs}/\rho_w}/w_s\right)}{\ln(4)-\ln\left(\sqrt{\tau_{cs}/\rho_w}/w_s\right)}, & \tau^b > \tau_{cs} \text{ and } \frac{u_*}{w_s} < 4 \\ 1, & \frac{u_*}{w_s} > 4 \end{cases} \tag{6.134}$$

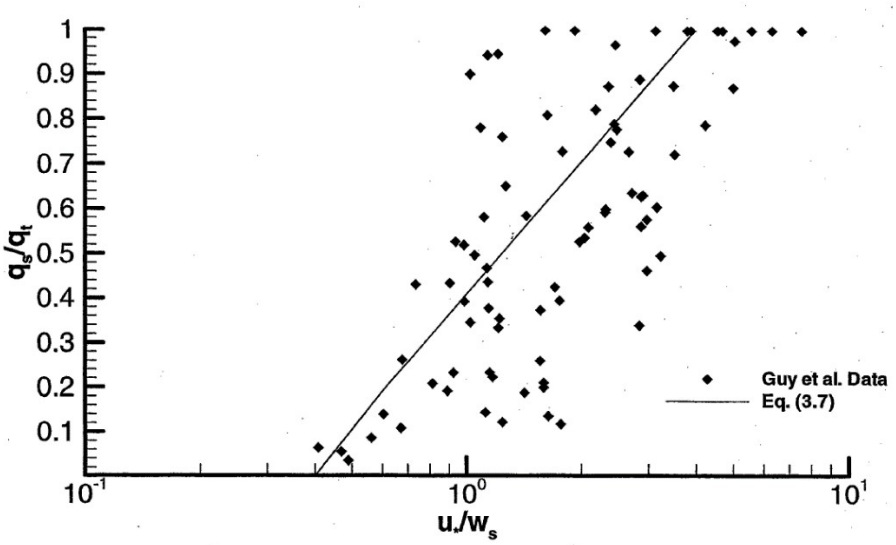

Fig. 6.5. Results from flume measurements of suspended load and bedload (Guy et al., 1966).

This approximation is used here. The original data is shown with the result given by the above equation in Figure 6.5.

Although sediments in nature have a continuous size distribution, physical quantities in numerical models are inherently discrete; hence, sediment particle sizes are discretized. The discretization of particle size classes j is done by measuring the different sediment sizes in a site-specific sediment core and grouping into appropriate size classes. The sediment bed in the model is described as the product of the particle size class and the corresponding mass fraction. By multiplying the total erosion flux of a particular size class j by q_s/q_t, the erosion flux of that class into suspended load $E_{s,j}$ can be calculated. The corresponding erosion flux into bedload $E_{b,j}$ is also calculated by multiplying the total erosion flux of the size class by the factor $(1-q_s/q_t)$. Thus, the erosion flux for any size class j is

$$E_{s,j} = \begin{cases} 0, & \tau^b < \tau_{\text{ce}} \\ \frac{q_s}{q_t} f_j E\,, & r\tau^b \geq \tau_{\text{ce}} \end{cases} \tag{6.135}$$

$$E_{b,j} = \begin{cases} 0, & \tau^b < \tau_{\text{ce}} \\ \left(1 - \frac{q_s}{q_t}\right) f_j E, & \tau^b \geq \tau_{\text{ce}} \end{cases} \tag{6.136}$$

where, f_j is the mass fraction of the j^{th} sediment size class.

6.4.3.3 Suspended Load

For suspended sediments, the three-dimensional, time dependent transport equation in the water over the bed is shown in equation (6.1). The net sediment flux into suspension

Q_s, is calculated as the total erosion flux into suspended load $E_{s,j}$, minus the deposition flux from suspended load $D_{s,j}$, for each sediment size class j

$$Q_{s,j}=E_{s,j}-D_{s,j} \tag{6.137}$$

where,

$$Q_s=\sum_j Q_{s,j} \tag{6.138}$$

In a quiescent fluid where no shear stress is present, the deposition flux for suspended sediments can be described as the product of the settling speed of the sediment and the concentration of the sediment in the overlying water. However, in flowing water, the deposition is affected by the fluid turbulence, quantified as shear stress. In this case, a probability of deposition for each size class j, P_k, can be included in the formulation to account for the effects of the shear stress to yield

$$D_{sj}=P_j w_{sj} C_{sj} \tag{6.139}$$

This probability would be unity in the case of quiescent flow and decrease as the flow, turbulence, and shear stress increase. The probability for suspended load deposition seems to differ for cohesive and non-cohesive particle sizes. For cohesive particles, size classes with effective diameters less than 200 μm, Krone (1962) found that the probability of deposition varied approximately as

$$P_j = \begin{cases} 0 & \text{for } \tau^b \tau_{cs,j} \\ \left(1-\frac{\tau^b}{\tau_{cs,j}}\right) & \text{for } \tau^b > \tau_{cs,j} \end{cases} \tag{6.140}$$

For larger non-cohesive particles, size classes with an effective diameter greater than 200 μm, Gessler (1967) showed that the probability of deposition could be described with a Gaussian distribution, or error function given by

$$P_j(Y)=\text{erf}\left(\frac{Y}{2}\right)=\frac{2}{\sqrt{\pi}}\int_0^{Y/2}\exp\left(-\xi^2\right)\,\text{d}\xi \tag{6.141}$$

where,

$$Y=\frac{1}{\sigma}\left(\frac{\tau_{cs,j}}{\tau^b}-1\right) \tag{6.142}$$

where, $\tau_{cs,j}$ is the critical shear stress for suspension for size class j and σ is the standard deviation for shear stress variation, which Gessler (1967) determined to be about 0.57.

An approximation to this function for $Y>0$ with an error of less than 0.001% is found to be (Abramowitz, 1964; Dwight, 1947)

$$P_j=1-F(Y)(0.4632X-0.1202X^2+0.9373X^3) \tag{6.143}$$

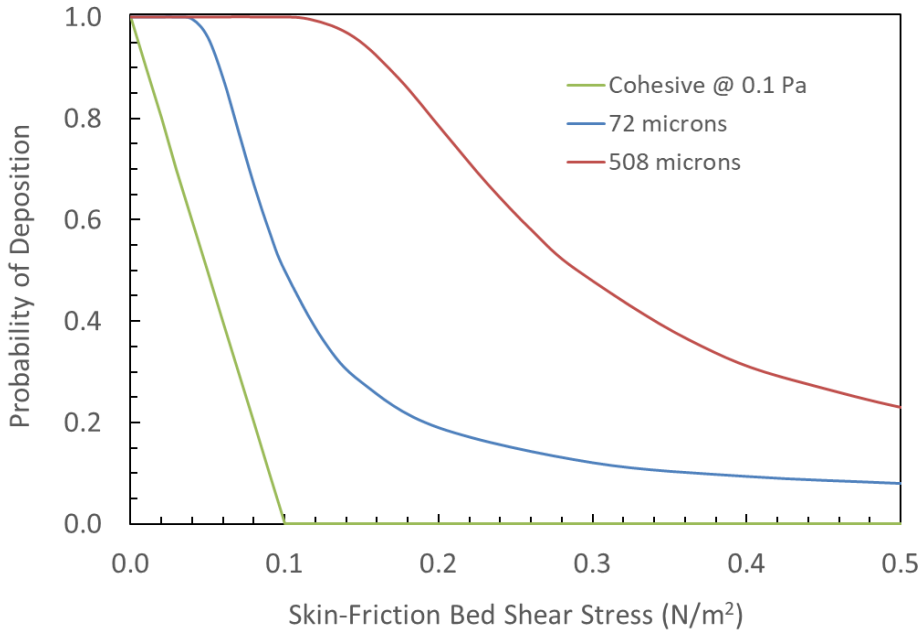

Fig. 6.6. Sample probability distributions for cohesive and non-cohesive particles.

where,

$$F(Y)=\frac{1}{(2\pi)^{1/2}}e^{-\frac{1}{2}Y^2} \tag{6.144}$$

$$X=\frac{1}{(1+0.33267Y)} \tag{6.145}$$

When $Y<0$

$$P_j=1-P(|Y|) \tag{6.146}$$

Figure 6.6 shows sample probability distributions using the formulations for cohesive and non-cohesive particles.

6.4.3.4 Bedload

For the description of bedload transport, the Rijn (1984) approach is used. To calculate the concentration of particles moving in bedload, a mass balance equation can be written as

$$\frac{\partial(mC_b)}{\partial t}=\frac{\partial(mq_{bx})}{\partial x}+\frac{\partial(mq_{by})}{\partial y}+Q_b \tag{6.147}$$

where,

C_b is the bedload concentration (g/cm^2),

q_b is the horizontal bedload flux in the x or y directions ($g/s/cm$),

m is the cell area (cm^2), and

Q_b is the net vertical flux of sediments between the sediment bed and bedload (g/s).

This equation is solved using a central difference approximation for the fluxes in the x and y directions. The horizontal bedload flux in general is calculated as

$$q_b = u_b C_b \tag{6.148}$$

where u_b is the bedload velocity (cm/s) in the direction of interest. The bedload velocity and thickness can be calculated from Rijn (1984) using formulations as follows

$$u_b = 1.5 T^{0.6} [(\rho_s - 1)\, g d]^{0.5} \tag{6.149}$$

$$h_b = 3 d d_*^{0.6} T^{0.9} \tag{6.150}$$

The transport parameter T, is calculated as

$$T = \frac{\tau^b - \tau_{ce}}{\tau_{ce}} \tag{6.151}$$

The flux of sediments between the bottom sediments and bedload Q_b, is calculated as the erosion of sediments into bedload E_b, minus the deposition of sediments from bedload D_b, and is

$$Q_b = E_b - D_b \tag{6.152}$$

where D_b is given by,

$$D_b = P w_s C_b \tag{6.153}$$

In steady state equilibrium, the concentration of sediments in bedload, C_e, is due to a dynamic equilibrium between erosion and deposition, i.e.,

$$E_b = P w_s C_e \tag{6.154}$$

From this, the probability of deposition can be written as

$$P = \frac{E_b}{w_s C_e} \tag{6.155}$$

The erosion rate can be determined from SEDFlume, while the settling speed can be calculated from equation (6.133). The equilibrium concentration C_e, has been investigated by several authors; the formulation by Rijn (1984) will be used here and is calculated as

$$C_e = 0.117 \frac{\rho_s T}{d_*} \tag{6.156}$$

Once E_b, w_s, and C_e are known as a function of particle diameter and shear stress, P can be calculated from equation (6.155). It is then assumed that this probability is also valid for the non-steady case so that the deposition rate can be calculated in this case also.

The equilibrium concentration C_e, is based on experiments with uniform sediments. In general, the sediment bed contains and must be represented by more than one size class. In this case; the erosion rate for a particular size class is given by $f_j E_b$, it follows that the probability of deposition for size class j is then given by

$$P_j = \frac{f_j E_b}{w_{sj} f_j C_{ej}} = \frac{E_b}{w_{sj} C_{ej}} \tag{6.157}$$

In equation (6.157), it is implicitly assumed that there is a dynamic equilibrium between erosion and deposition for each size class j.

6.4.3.5 Bed Armoring

A decrease in sediment erosion rates with time, or bed armoring, can occur due to (1) the consolidation of cohesive sediments with depth and time, (2) the deposition of coarser sediments on the sediment bed during a flow event, and (3) the erosion of finer sediments from the surficial sediment, leaving coarser sediments behind, again during a flow event. The consolidation of sediments and subsequent change in erosion rates with of depth can be determined by SEDFlume in situ measurements. The consolidation of sediment and increase of erosion rates with time can be determined approximately from consolidation studies, again by means of SEDFlume.

Here we are concerned about bed armoring due to processes (2) and (3). In order to describe these processes, it is assumed in the present model that a thin mixing layer, or active layer, is formed at the surface of the bed. The existence and properties of this have been discussed by previous researchers (Parker et al., 2000; van Niekerk et al., 1992). The presence of this active layer permits the interaction of depositing and eroding sediments to occur in a discrete layer without allowing deposited sediments to affect the undisturbed sediments below. The authors in van Niekerk et al. (1992) have suggested that the thickness Ta, can be approximated by

$$T_a = 2 d_{50} \frac{\tau^b}{\tau_{ce}} \tag{6.158}$$

This formulation takes into account the deeper penetration of turbulence into the bed with increasing shear stress. In the present calculations, d_50 is approximated by the average diameter in the interest of computational efficiency.

Since the active layer is kept at a constant thickness T_a, three possible states of the active layer must be considered. The first state is a net erosion of the active layer, where there may

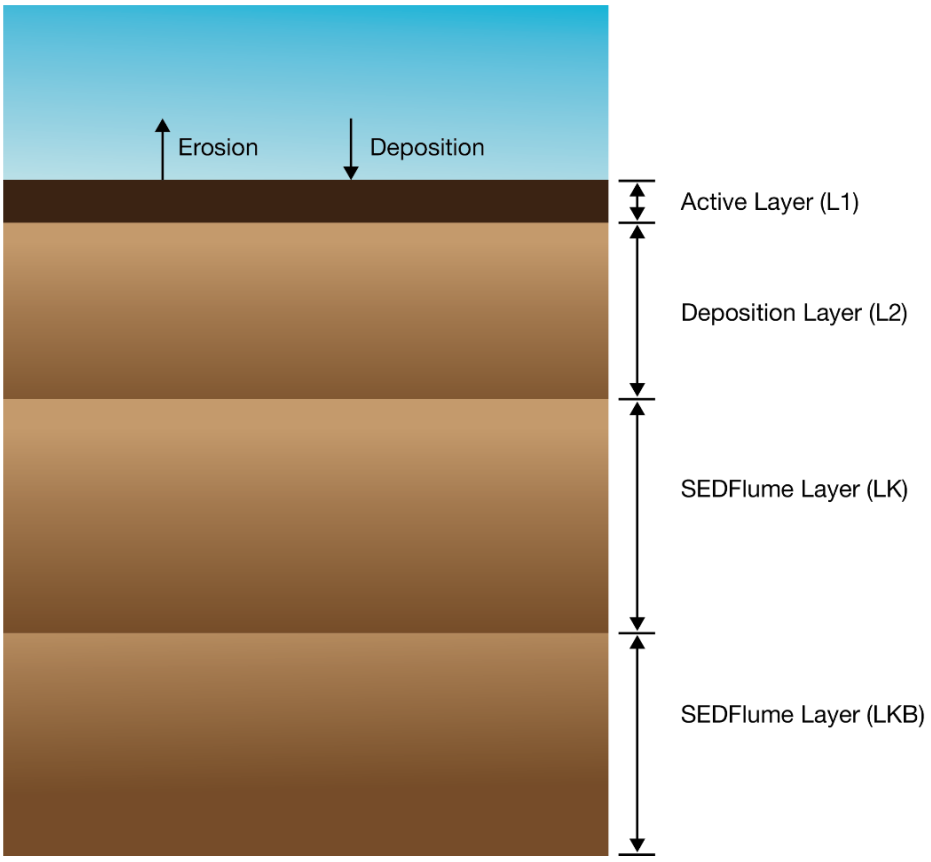

Fig. 6.7. Diagram of SEDflume layering system.

be deposition occurring but the net flux is erosional. If the thickness of the active layer after this net erosion is T, then a thickness of material equal to $T_a - T$ is added to the active layer so that a thickness of T_a can be maintained. This material is added from the layer below in size class proportions equivalent to that in the layer below. The second possible state of the active layer is a net depositional state where the thickness of the active layer exceeds T_a. In this case, the excess material $T - T_a$, is put into a new deposited material layer just below the active layer, but above the parent bed. This material is added to the deposited layer in size class proportions equal to the active layer. The third state of the active layer is where T is equal in thickness to T_a. In this case, no action is taken. Figure 6.7 shows a diagram of the layering system.

The erosion rates for this active layer are dependent on its average particle size. Figure 6.8 shows the erosion rate vs. particle diameter for quartz sediment. It is seen that as the particle diameter increases beyond 200 μm, the erosion rate decreases. This demonstrates how bed coarsening affects erosion rates. A dataset of this type can be constructed utilizing laboratory and field cores to determine erosion rates as a function of particle size for any particular site. The erosion rate for an active or deposited layer can then be calculated from the average particle size of the layer with an interpolation similar to equation (6.127) with

particle size in place of thickness.

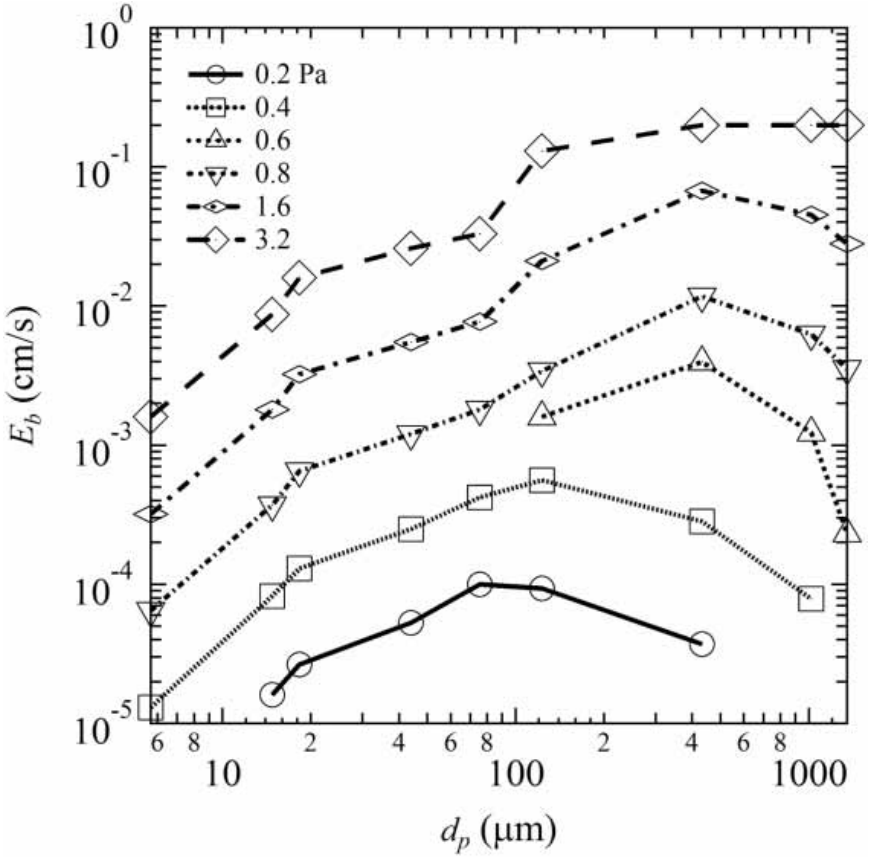

Fig. 6.8. Erosion rates versus particle size and shear stress for a bulk density of $1.9\,g/cm^2$, adapted from Roberts et al. (1998) by James et al. (2010). Model uses interpolated data to estimate erosion rates at $1\,Pa$.

Chapter 7

TOXIC CONTAMINANT TRANSPORT AND FATE MODULE

7.1. Introduction

This chapter presents processes associated with toxics and their mathematical modeling. It starts with the basic equations and their numerical aspects then follows by characteristics of toxic organic chemicals and metals, and the absorption and deabsorption processes.

7.2. Basic Equations

The transport of an absorptive contaminant in the water column is governed by transport equations for the contaminant dissolved in the water phase, for the contaminant absorbed to material effectively dissolved in the water phase, and for the contaminant absorbed to suspended particles. For the portion of the contaminant dissolved directly in the water phase

$$\frac{\partial}{\partial t}(mHC_w)+\frac{\partial}{\partial x}(m_yHuC_w)+ \frac{\partial}{\partial y}(m_xHvC_w)+\frac{\partial}{\partial z}(mwC_w)= \frac{\partial}{\partial z}\left(m\frac{A_b}{H}\partial_z C_w\right)+mH\left(\sum_i\left(K^i_{dS}S^i\partial^i_S\right)+\sum_j\left(K^j_{dD}D^j\partial^j_D\right)\right)- mH\sum_i\left(K^i_{aS}S^i\right)\left(\partial_w\frac{C_w}{\partial}\right)\left(\hat{\partial}^i_S-\partial^i_S\right)- mH\sum_j\left(K^j_{aD}D^j\right)\left(\partial_w\frac{C_w}{\partial}\right)\left(\hat{\partial}^j_D-\partial^j_D\right)+S^E_C+S^I_C \quad (7.1)$$

where,

C_w is the mass of water dissolved contaminant per unit total volume ($\mu g/l$),

S^i is the mass of sediment class i (g/m^3),

D^j is the mass of the dissolved substance (i.e. DOC) (g/m^3),

χ_S is the mass of contaminant absorbed to sediment class i per mass of sediment (mg/g),

χ_D is the mass of contaminant absorbed to dissolved material j per unit mass of dissolved material (i.e. absorbed to DOC) (mg/g),

ϕ is the porosity (dimensionless),

ψ_w is the fraction of the water dissolved contaminant available for absorption (dimensionless),

K_a is the absorption rate of sediment (S) or dissolved material (D) ($/s$),

K_d is the deabsorption rate ($/s$),

S_C^E is the external source/sink of the contaminant (mg/s), and

S_C^I is the internal source/sink of the contaminant (mg/s) due to degradation, volatilization and conversions to/from other contaminants (mg/s).

7.2.1 Contaminant Partitioning

The absorption kinetics are based on the Langmuir isotherm (Chapra et al., 1997) with $\hat{\chi}$ denoting the saturation absorbed mass per carrier mass. The sediment and dissolved material concentrations S and D are defined as mass per unit total volume.

Introducing absorbed concentrations defining absorbed mass per unit total volume

$$C_D^j = D^j \chi_D^j \tag{7.2}$$

$$C_S^i = S^i \chi_S^i \tag{7.3}$$

The EFDC+ absorbed contaminant transport formulation currently employees equilibrium partitioning with the absorption and deabsorption terms

$$\left(K_{sD}^j D^j\right)\left(\psi_w \frac{C_w}{\phi}\right)\left(\widehat{\chi}_D^j - \chi_D^j\right) = K_{dD}^j C_D^j \tag{7.4}$$

$$\left(K_{aS}^i S^i\right)\left(\psi_w \frac{C_w}{\phi}\right)\left(\widehat{\chi}_S^i - \chi_S^i\right) = K_{dS}^i C_S^i \tag{7.5}$$

Solving equations (7.4) and (7.5) for the absorbed to water phase concentration ratios gives

$$\frac{C_D^j}{C_w} = \frac{f_D^j}{f_w} = P_D^j \frac{D^j}{\phi} P_D^j = P_{Do}^j \left(1 + P_{Do}^j \left(\frac{C_w}{\widehat{\chi}_D^j \phi}\right)\right)^{-1} P_{Do}^j = \frac{\psi_w K_{aD}^j \widehat{\chi}_D^j}{K_{dD}^j} \tag{7.6}$$

$$\frac{C_S^i}{C_w} = \frac{f_S^i}{f_w} = P_S^i \frac{S^i}{\phi} P_S^i = P_{So}^i \left(1 + P_{So}^i \left(\frac{C_w}{\widehat{\chi}_S^i \phi}\right)\right)^{-1} P_{So}^i = \frac{\psi_w K_{aS}^i \widehat{\chi}_S^i}{K_{dS}^i} \tag{7.7}$$

where, P denotes the partition coefficient, and P_o is its linear equilibrium value. For linear equilibrium partitioning, P is set to P_o, which in effect approximates

$$\left(1 + P_{So}^i \left(\frac{C_w}{\widehat{\chi}_S^i \phi}\right)\right)^{-1}$$

terms in equations (7.6) and (7.7) as unity. Requiring the mass fractions to sum to unity

$$f_w + \sum_i f_S^i + \sum_j f_D^j = 1 \tag{7.8}$$

gives

$$\begin{aligned} f_w &= \frac{C_w}{C} \\ &= \frac{\phi}{\phi + \sum_i P_S^i S^i + \sum_j P_D^j D^j} f_D^j \\ &= \frac{C_D^j}{C} \\ &= \frac{P_D^j D^j}{\phi + \sum_i P_S^i S^i + \sum_j P_D^j D^j} f_S^i \\ &= \frac{C_S^i}{C} \\ &= \frac{P_S^i S^i}{\phi + \sum_i P_S^i S^i + \sum_j P_D^j D^j} \end{aligned} \tag{7.9}$$

The dissolved concentrations can be alternately expressed by mass per unit volume of the water phase

$$C_{w:w} = \frac{C_w}{\phi} C_{D:w}^j = \frac{C_D^j}{\phi} D_{:w}^J = \frac{D^j}{\phi} \tag{7.10}$$

with equation (7.9) becoming

$$\begin{aligned}
\frac{C_{w:w}}{C} &= \frac{1}{\phi + \sum_i P_S^i S^i + \sum_j P_D^j \phi D_{:w}^j} \\
\frac{C_{D:w}^j}{C} &= \frac{P_D^j D_{:w}^j}{\phi + \sum_i P_S^i S^i + \sum_j P_D^j \phi D_{:w}^j} \\
\frac{C_S^i}{C} &= \frac{P_S^i S^i}{\phi + \sum_i P_S^i S^i + \sum_j P_D^j \phi D_{:w}^j}
\end{aligned} \tag{7.11}$$

which is a generalization of the Chapra et al. (1997) formulation for absorption to dissolved and particulate organic carbon.

7.2.2 Water Column Transport

The partitioning relationships shown in equation (7.2) and equation (7.3) allows equation (7.1) to be expanded into the transport equation for each contaminant fractions

$$\begin{aligned}
&\frac{\partial}{\partial t}(m_x m_y H C_w) + \frac{\partial}{\partial x}(m_y H u C_w) + \frac{\partial}{\partial y}(m_x H v C_w) + \frac{\partial}{\partial z}(m_x m_y w C_w) \\
&\quad = \frac{\partial}{\partial z}\left[m_x m_y \frac{A_b}{H}\frac{\partial}{\partial z}(C_w)\right] + m_x m_y H\left(\sum_i \left(K_{dS}^j C_S^i\right) + \sum_i \left(K_{dD}^j C_D^i\right)\right) \\
&\qquad - m_x m_y H\left(\sum_i \left(K_{aS}^i S^i\right)(\Psi_w \frac{C_w}{\phi})(\widehat{\chi}_S^i - \chi_S^i)\right. \\
&\qquad\quad \left. + \sum_i \left(K_{aD}^j D^j\right)(\Psi_w \frac{C_w}{\phi})(\widehat{\chi}_D^j - \chi_D^j) + \gamma C_w\right)
\end{aligned} \tag{7.12}$$

$$\begin{aligned}
&\frac{\partial}{\partial t}\left(m_x m_y H C_D^j\right) + \frac{\partial}{\partial x}\left(m_y H u C_D^j\right) + \frac{\partial}{\partial y}\left(m_x H v C_D^j\right) + \frac{\partial}{\partial z}\left(m_x m_y w C_D^j\right) = \\
&\frac{\partial}{\partial z}\left[m_x m_y \frac{A_b}{H}\frac{\partial}{\partial z}(C_D^j)\right] + m_x m_y H\left(K_{sD}^j D^j\right)\left(\psi_w \frac{C_w}{\phi}\right)\left(\widehat{\chi}_D^j - \chi_D^j\right) - m_x m_y H\left(K_{dD}^j + \gamma\right) C_D^j
\end{aligned} \tag{7.13}$$

$$\begin{aligned}
&\frac{\partial}{\partial t}\left(m_x m_y H C_S^i\right) + \frac{\partial}{\partial x}\left(m_y H u C_S^i\right) + \frac{\partial}{\partial y}\left(m_x H v C_S^i\right) + \frac{\partial}{\partial z}\left(m_x m_y w C_S^i\right) + \frac{\partial}{\partial z}\left(m_x m_y w_S^i C_S^i\right) = \\
&\quad \frac{\partial}{\partial z}\left(m_x m_y \frac{A_b}{H}\frac{\partial}{\partial z} C_S^i\right) + m_x m_y H\left(K_{aS}^i S^i\right)\left(\psi_w \frac{C_w}{\phi}\right)\left(\widehat{\chi}_S^i - \chi_S^i\right) - m_x m_y H\left(K_{dS}^i + \gamma\right) C_S^i
\end{aligned} \tag{7.14}$$

Where, equation (7.12) is for the dissolved fraction, equation (7.13) is for the fraction absorbed to the dissolved material and equation (7.14) is for the fraction absorbed to the sediments.

The transport equation for the portion of material *absorbed to a dissolved constituent* D is,

$$\frac{\partial}{\partial t}\left(m_x m_y H D^j \chi_D^j\right)+\frac{\partial}{\partial x}\left(m_y H u D^j \chi_D^j\right)+\frac{\partial}{\partial y}\left(m_x H v D^j \chi_D^j\right)+\frac{\partial}{\partial z}\left(m_x m_y w D^j \chi_D^j\right)= \frac{\partial}{\partial z}\left[m_x m_y \frac{A_b}{H}\frac{\partial}{\partial z}\left(D^j \chi_D^j\right)\right]+m_x m_y H\left(K_{sD}^j D^j\right)\left(\psi_w \frac{C_w}{\phi}\right)\left(\widehat{\chi}_D^j-\chi_D^j\right)-m_x m_y H\left(K_{dD}^j+\gamma\right)\left(D^j \chi_D^j\right) \tag{7.15}$$

The transport equation for the portion of material *absorbed to a suspended constituent* S is,

$$\frac{\partial}{\partial t}\left(m_x m_y H S^i \chi_S^i\right)+\frac{\partial}{\partial z}\left(m_y H u S^i \chi_S^i\right)+\frac{\partial}{\partial y}\left(m_x H v S^i \chi_S^i\right)+ \frac{\partial}{\partial z}\left(m_x m_y w S^i \chi_S^i\right)+\frac{\partial}{\partial z}\left(m_x m_y w_S^i S^i \chi_S^i\right)= \frac{\partial}{\partial z}\left[m_x m_y \frac{A_b}{H}\frac{\partial}{\partial z}\left(S^i \chi_S^i\right)\right]+m_x m_y H\left(K_{aS}^i S^i\right)\left(\psi_w \frac{C_w}{\phi}\right)\left(\widehat{\chi}_S^i-\chi_S^i\right) - m_x m_y H\left(K_{aS}^i+\gamma\right)\left(S^i \chi_S^i\right) \tag{7.16}$$

Adding equations (7.12), (7.13), and (7.14), using the equilibrium partitioning relationship equations (7.4) and (7.5) gives

$$\frac{\partial}{\partial t}\left(m_x m_y H C\right)+\frac{1}{m_x m_y}\frac{\partial}{\partial x}\left(m_y H u C\right)+\frac{1}{m_x m_y}\frac{\partial}{\partial y}\left(m_x v C\right)+\frac{\partial}{\partial z}\left(m_x m_y w C\right)- \frac{\partial}{\partial z}\left(m_x m_y \sum_i w_S^i f_S^i C\right)=\frac{\partial}{\partial z}\left(m_x m_y \frac{A_b}{H}\frac{\partial C}{\partial z}\right)-m_x m_y H \gamma \tag{7.17}$$

the equation for the total concentration C. The boundary condition at the water column-sediment bed interface, $z = 0$ is

$$-\frac{A_b}{H}\frac{\partial C}{\partial z}-\sum_i w_S^i f_S^i C=\sum_i\left(\left(\max\left(J_{SBS}^i\chi_S^i,0\right)+\varepsilon\max\left(\frac{J_{SBS}^i}{\rho_S^i},0\right)\right)\left(\frac{C_w+\sum_j C_D^j}{\phi}\right)\right)_{SB}+$$
$$\sum_i\left(\left(\min\left(J_{SBS}^i\chi_S^i,0\right)+\varepsilon_{dep}\min\left(\frac{J_{SBS}^i}{\rho_S^i},0\right)\right)\left(\frac{C_w+\sum_j C_D^j}{\phi_{dep}}\right)\right)_{WC}+$$
$$\sum_i\left(\left(\varepsilon\max\left(\frac{J_{SBB}^i}{\rho_S^i},0\right)\right)\left(\frac{C_w+\sum_j C_D^j}{\phi}\right)\right)_{SB}+$$
$$\sum_i\left(\left(\varepsilon_{dep}\min\left(\frac{J_{SBB}^i}{\rho_S^i},0\right)\right)\left(\frac{C_w+\sum_j C_D^j}{\phi_{dep}}\right)\right)_{WC}+$$
$$\left(\max\left(q_w,0\right)\left(\frac{C_w+\sum_j C_D^j}{\phi}\right)\right)_{SB}+\left(\min\left(q_w,0\right)\left(\frac{C_w+\sum_j C_D^j}{\phi_{dep}}\right)\right)_{WC}$$
$$-q_{dif}\left(\left(\frac{C_w+\sum_j C_D^j}{\phi_{dep}}\right)_{WC}-\left(\frac{C_w+\sum_j C_D^j}{\phi}\right)_{SB}\right) \quad (7.18)$$

where,

J_{SBS} and J_{SBB} are the suspended load and bedload sediment fluxes between the sediment bed and the water column, defined as positive from the bed,

ρ_2 is the sediment density in g/cm^3,

q_w is the water specific discharge due to bed consolidation and groundwater interaction, defined as positive from the bed, and

q_{dif} is a diffusion velocity incorporating the effects of molecular diffusion, hydrodynamic dispersion, and biological induced mixing.

The subscript SB denotes conditions in the top layer of the sediment bed, while the subscript WC denotes condition in the water column immediately above the bed, with the exception that the specific discharge and diffusion velocity are defined at the water column-bed interface. The subscript dep is used to denote the void ratio and porosity of newly depositing sediment. Equation (7.11) indicates that the contaminant flux between the bed and water column includes a flux of suspended sediment absorbed material; fluxes of water dissolved and absorbed to water dissolved material due to the specific discharge of water associated with consolidation and ground water interaction and water entrainment and expulsion associated with both suspended and bedload sediment deposition and resuspension; and a flux of water dissolved and absorbed to water dissolved material due to diffusion like processes. Transport of bedload sediment absorbed material is represented by direct transport between horizontally adjacent top bed layers and is included in the contaminant mass

conservation equations for the sediment bed. The boundary condition at the water free surface is

$$-\frac{A_b}{H}\frac{\partial C}{\partial z}-\sum_i w_S^i f_S^i C = 0 \;:\; z = 1 \tag{7.19}$$

Using the relationship between the porosity and void ratio

$$\phi = \frac{\varepsilon}{1+\varepsilon} \tag{7.20}$$

and equation (7.3) allows equation (7.18) to be written as

$$\begin{aligned}
-\frac{A_b}{H}\frac{\partial C}{\partial z}-\sum_i w_S^i f_S^i C = \\
\sum_i \left(\left(\max\left(J_{SBS}^i \frac{C_S^i}{S^i}, 0 \right) + (1+\varepsilon)\max\left(\frac{J_{SB}^i}{\rho_S^i}, 0 \right) \right) \left(C_w + \sum_j C_D^j \right) \right)_{SB} \\
+ \sum_i \left(\left(\min\left(J_{SBS}^i \frac{C_S^i}{S^i}, 0 \right) + (1+\varepsilon_{dep})\min\left(\frac{J_{SBS}^i}{\rho_S^i}, 0 \right) \right) \left(C_w + \sum_j C_D^j \right) \right)_{WC} \\
+ \sum_i \left(\left((1+\varepsilon)\max\left(\frac{J_{SBB}^i}{\rho_S^i}, 0 \right) \right) \left(C_w + \sum_j C_D^j \right) \right)_{SB} \\
+ \sum_i \left(\left((1+\varepsilon_{dep})\min\left(\frac{j_{SBB}^i}{\rho_S^i}, 0 \right) \right) \left(C_w + \sum_j C_D^j \right) \right)_{WC} \\
+ \left(\left(\max(q_w, 0) + q_{dif} \right) \frac{1}{\phi} \left(C_w + \sum_j C_D^j \right) \right)_{SB} + \\
\left(\left(\min(q_w, 0) - q_{dif} \right) \frac{1}{\phi} \left(C_w + \sum_j C_D^j \right) \right)_{WC}
\end{aligned} \tag{7.21}$$

The sediment concentration can be expressed in terms of the sediment density and void ratio by

$$S^i = \frac{F^i \rho_s^i}{1+\varepsilon} \tag{7.22}$$

where Fi is the fraction of the total sediment volume occupied by each sediment class

$$F^i = \left(\sum_i \left(\frac{S^i}{\rho_s^i} \right) \right)^{-1} \left(\frac{S^i}{\rho_s^i} \right) \tag{7.23}$$

Introducing equations (7.9) and (7.22) into equation (7.21) gives the final form of the bottom boundary

$$
\begin{aligned}
-\frac{A_b}{H}\frac{\partial C}{\partial z} - \sum_i w_S^i f_S^i C = \\
\sum_i \left(\max\left(\frac{J_{SBS}^i f_S^i}{S^i}, 0 \right) C + \max\left(\frac{F^i J_{SBS}^i}{S^i}, 0 \right) \left(f_w + \sum_j f_D^j \right) C \right)_{SB} \\
+ \sum_i \left(\min\left(\frac{J_{SBS}^i f_S^i}{S^i}, 0 \right) C + \min\left(\frac{F_{dep}^i J_{SBS}^i}{S_{dep}^i}, 0 \right) \left(f_w + \sum_j f_D^j \right) C \right)_{WC} \\
+ \sum_i \left(\left((1+\varepsilon) \max\left(\frac{J_{SBB}^i}{\rho_S^i}, 0 \right) \right) \left(C_w + \sum_j C_D^j \right) \right)_{SB} \\
+ \sum_i \left(\left((1+\varepsilon_{dep}) \min\left(\frac{J_{SBB}^i}{\rho_S^i}, 0 \right) \right) \left(C_w + \sum_j C_D^j \right) \right)_{WC} \\
+ \left(\left(\max(q_w, 0) + q_{dif} \right) \frac{1}{\phi} \left(f_w + \sum_j f_D^j \right) C \right)_{SB} \\
+ \left(\left(\min(q_w, 0) - q_{dif} \right) \frac{1}{\phi} \left(f_w + \sum_j f_D^j \right) C \right)_{WC}
\end{aligned}
\tag{7.24}
$$

Note that the form of the bed flux associated with bedload transport remains unmodified since the sediment concentration in the water column cannot be readily defined for sediment being transported as bedload.

The transport equation (7.17) for the total contaminant concentration in the water column is solved using a fractional step procedure which sequentially treats advection; settling, deposition, and resuspension; pore water advection and diffusion; and reactions. The fractional phase distribution of the contaminant is recalculated between the advection, settling, deposition and resuspension, and pore water advection and diffusion steps using equation (7.9). The advection step is

$$
(HC)^{n+1/4} - (HC)^n + \frac{\theta}{m_x m_y}\frac{\partial}{\partial x}(m_y H u C) + \frac{\theta}{m_x m_y}\frac{\partial}{\partial y}(m_x H v C) + \theta\frac{\partial (wC)}{\partial z} = 0 \tag{7.25}
$$

with the vertical boundary conditions

$$
wC = 0 \ : \ z = 0,\ 1 \tag{7.26}
$$

The fractional time level in equation (7.25) and subsequent equations is used to denote an intermediate result in the fractional step procedure. The spatially discrete form of equation (7.25) is solved using one of the standard high order, flux limited, advective transport solvers in the EFDC+ model.

7.2.3 Settling, Deposition, and Resuspension

The settling, deposition, and resuspension step is

$$(H)^{n+1/2} - (HC)^{n+1/4} = \theta \frac{\partial}{\partial z}\left(\sum_i w_S^i f_S^i C\right) \tag{7.27}$$

with the boundary conditions

$$\begin{aligned} -\sum_i w_S^i f_S^i C = \sum_i \Bigg(\max\left(\frac{J_{SBS}^i f_S^i}{S^i}, 0\right) C + \max\left(\frac{F^i J_{SB}^i}{S^i}, 0\right) \left(f_w + \sum_j f_D^j\right) C \Bigg)_{SB} + \\ \sum_i \Bigg(\min\left(\frac{J_{SBS}^i f_S^i}{S^i}, 0\right) C + \min\left(\frac{F_{dep}^i J_{SBS}^i}{S_{dep}^i}, 0\right) \left(f_w + \sum_j f_D^j\right) C \Bigg)_{WC} + \\ \sum_i \Bigg(\left((1+\varepsilon) \max\left(\frac{J_{SBB}^i}{\rho_S^i}, 0\right) \right) \left(C_w + \sum_j C_D^j\right) \Bigg)_{SB} + \\ \sum_i \Bigg(\left((1+\varepsilon_{de}) \min\left(\frac{J_{SB}^i}{\rho_S^i}, 0\right) \right) \left(C_w + \sum_j C_D^j\right) \Bigg)_{WC} : z = 0 \end{aligned} \tag{7.28}$$

$$w_S^i f_S^i C = 0 \ : \ z = 1 \tag{7.29}$$

Integrating equation (7.27) over a water column layer and using upwind differencing for the settling gives,

$$\begin{aligned} \Delta_k (HC)_k^{n+\frac{1}{2}} - \Delta_k (HC)_k^{n+\frac{1}{4}} = \theta \sum_i \left(\frac{\left(w_S^i S^i\right)_{k+}}{H} \left(\frac{f_S^i}{S^i}\right)_{k+1} \right)^{n+\frac{1}{2}} (HC)_{k+1}^{n+\frac{1}{2}} \\ - \theta \sum_i \left(\frac{\left(w_S^i S^i\right)_{k-}}{H} \left(\frac{f_S^i}{S^i}\right)_{k} \right)^{n+\frac{1}{2}} (HC)_{k}^{n+\frac{1}{2}} \end{aligned} \tag{7.30}$$

for a layer not adjacent to the bed, and,

$$\Delta_1(HC)_1^{n+\frac{1}{2}} - \Delta_1(HC)_1^{n+\frac{1}{4}} =$$

$$\theta\sum_i\left(\left(w_S^i S^i\right)_{1+}\left(\frac{f_S^i}{S^i}\right)_2\right)^{n+\frac{1}{2}} C_2^{n+\frac{1}{2}} +$$

$$\theta\sum_i\left(\max\left(\frac{J_{SBS}^i f_S^i}{S^i},0\right) + \max\left(\frac{J_{SBS}^i F^i}{S^i},0\right)\left(f_w+\sum_j f_D^j\right)\right)_{sb}^{n+\frac{1}{2}} C_{sb}^{n+\frac{1}{2}} +$$

$$\theta\sum_i\left(\min\left(\frac{J_{SBS}^i f_S^i}{S^i},0\right) + \min\left(\frac{J_{SBS}^i F^i}{S^i},0\right)\left(f_w+\sum_j f_D^j\right)\right)_1^{n+\frac{1}{2}} C_1^{n+\frac{1}{2}} +$$

$$\theta\sum_i\left((1+\varepsilon)\max\left(\frac{J_{SBB}^i}{\rho_S^i},0\right)\left(f_w+\sum_j f_D^j\right)\right)_{sb}^{n+\frac{1}{2}} C_{sb}^{n+\frac{1}{2}} +$$

$$\theta\sum_i\left((1+\varepsilon)\min\left(\frac{J_{SBB}^i}{\rho_S^i},0\right)\left(f_w+\sum_j f_D^j\right)\right)_1^{n+\frac{1}{2}} C_1^{n+\frac{1}{2}} \quad (7.31)$$

for the first layer adjacent to the bed. Note that equation (7.31) is also the appropriate form for single layer or depth average application. Since the sediment settling flux is zero at the top of the free surface adjacent layer, equation (7.27) is integrated downward from the top layer to the bottom layer. The bottom layer equation (7.31) is solved simultaneously with a corresponding equation for the top layer of the sediment bed. The settling fluxes $w_S S$, and water column-sediment bed fluxes J_{SB}, in equations (7.30) and (7.31) are known from the preceding solution for sediment settling, deposition and resuspension. Terms containing the sediment absorbed fraction divided by the sediment concentration in equations (7.30) and (7.31)

$$\frac{f_S^i}{S^i} = \frac{P_S^i}{\theta + \sum_i P_S^i S^i + \sum_j P_D^j D^j} \quad (7.32)$$

The diffusion step is given by

$$(HC)^{n+\frac{3}{4}} - (HC)^{n+\frac{1}{2}} = \theta\frac{\partial}{\partial z}\left(\frac{A_b}{H}\partial_z C\right) \quad (7.33)$$

with boundary conditions

$$-\frac{A_b}{H}\frac{\partial C}{\partial z} = \left(\left(\max\left(q_w,0\right) + q_{dif}\right)\frac{1}{\phi}\left(f_w + \sum_j f_D^j\right)C\right)_{SB} + \left(\left(\min\left(q_w,0\right) - q_{dif}\right)\frac{1}{\phi_{dep}}\left(f_w + \sum_j f_D^j\right)C\right)_{WC} \quad : z = 0 \tag{7.34}$$

$$-\frac{A_b}{H}\frac{\partial C}{\partial z} = 0 \ : \ z = 1 \tag{7.35}$$

For the first layer adjacent to the bed

$$(HC)_1^{n+3/4} - (HC)_1^{n+1/2} = \frac{\theta}{\Delta_1}\left(\frac{A_b}{H}\frac{\partial C}{\partial z}\right)_{1+}^{n+\frac{3}{4}} + \frac{\theta}{\Delta_1}\left(\max\left(q_w,0\right) + q_{dif}\right)\left(\left(f_w + \sum_j f_D^j\right)\frac{1}{\phi}\right)_{SB}^{n+\frac{1}{2}} C_{SB}^{n+\frac{3}{4}} + \frac{\theta}{\Delta_1}\left(\min\left(q_w,0\right) - q_{dif}\right)\left(\left(f_w + \sum_j f_D^j\right)\frac{1}{\phi_{dep}}\right)_1^{n+\frac{1}{2}} C_1^{n+\frac{1}{2}} \tag{7.36}$$

It is noted that the bed concentrations are advanced to the $n+3/4$ intermediate time level before the advance of the water column concentrations. While for layers not adjacent to the bed,

$$(HC)_k^{n+\frac{3}{4}} - (HC)_k^{n+\frac{1}{2}} = \frac{\theta}{\Delta_1}\left(\frac{A_b}{H}\frac{\partial C}{\partial z}\right)_{k+}^{n+\frac{3}{4}} - \frac{\theta}{\Delta_1}\left(\frac{A_b}{H}\frac{\partial C}{\partial z}\right)_{k-}^{n+\frac{3}{4}} \tag{7.37}$$

The solution is completed by

$$(HC)_k^{n+1} - (H)_k^{n+3/4} = -\theta\gamma(HC)_k^{n+1} \tag{7.38}$$

an implicit reaction step.

7.2.4 Toxic Bed Processes

Contaminant transport in the sediment bed is represented using the discrete layer formulation developed for bed geomechanical processes. The conservation of mass for the total contaminant concentration in a layer of the sediment bed is given by

$$\frac{\partial}{\partial t}(BC)_k = -\gamma(BC)_k$$
$$- \delta(k,kt)\sum_i \left(\max\left(\frac{J^i_{SBS} f^i_S}{BS^i}, 0\right) + \max\left(\frac{J^i_{SBS} F^i}{BS^i}, 0\right) \left(f_w + \sum_j f^j_D\right)\right)_{kt} (BC)_{kt}$$
$$- \delta(k,kt)\sum_i \left(\min\left(\frac{J^i_{SBS} f^i_S}{S^i}, 0\right) C + \min\left(\frac{J^i_{SBS} F^i_{dep}}{S^i_{dep}}, 0\right) \left(f_w + \sum_j f^j_D\right) C\right)_{WC}$$
$$- \delta(k,kt)\sum_i \left(\left(J^i_{SBB}\partial^i_{SBL}, 0\right)\right) - \delta(k,kt)\sum_i \left((1+e)\max\left(\frac{J^i_{SBB}}{B\partial^i_S}, 0\right) \left(f_w + \sum_j f^j_D\right)\right)_{kt}$$
$$\times (BC)_{kt} - \delta(k,kt)\sum_i \left((1+e_{dep})\min\left(\frac{J^i_{SBB}}{\partial^i_S}, 0\right) \left(f_w + \sum_j f^j_D\right) C\right)_{WC}$$
$$- \left(\left(\max(q_w, 0) + q_{dif}\right)_{k+} - \left(\min(q_w, 0) - q_{dif}\right)_{k-}\right) \left(\frac{1}{\phi B}\left(f_w + \sum_j f^j_D\right)\right)_k$$
$$\times (BC)_k - \delta(k,kt)\left(\min(q_w, 0) - q_{dif}\right)_{kt+} \times \left(\frac{1}{\phi}\left(f_w + \sum_j f^j_D\right) C\right)_{WC}$$
$$- (1\delta(k,kt))\left(\min(q_w, 0) - q_{dif}\right)_{k+} \times \left(\frac{1}{\phi B}\left(f_w + \sum_j f^j_D\right)\right)_{k+1} (BC)_{k+1}$$
$$+ \left(\max(q_w, 0) + q_{dif}\right)_{k-} \times \left(\frac{1}{\phi B}\left(f_w + \sum_j f^j_D\right)\right)_{k-1} (BC)_{k-1} \quad (7.39)$$

where,

$$\delta(k,kt) = \begin{cases} 0 & : \ k = kt1 \\ & : \ k \neq kt \end{cases} \quad (7.40)$$

is used to distinguish processes specific to the top, water column adjacent layer of the bed, kt. Advective fluxes associated with pore water advection in equation (7.40) are represented in upwind form. In the sediment bed, the actual computational variables for sediment, contaminant, and dissolved material are their concentrations times the thickness of the bed layer. Consistent with this formulation, the fractional phase components in the bed are defined by

$$(f_w)_k = \left(\frac{BC_w}{BC}\right)_k =$$
$$\left(\frac{B\phi}{B\phi + \sum_i P_S^i BS^i + \sum_j P_D^j BD^j}\right)_k \left(f_D^j\right)_k = \left(\frac{BC_D^j}{BC}\right)_k = \left(\frac{P_D^j BD^j}{B\phi + \sum_i P_S^i BS^i + \sum_j P_D^j BD^j}\right)_k$$
$$\left(f_S^i\right)_k = \left(\frac{BC_S^i}{BC}\right)_k = \left(\frac{P_S^i BS^i}{B\phi + \sum_i P_S^i BS^i + \sum_j P_D^j BD^j}\right)_k \quad (7.41)$$

7.2.4.0.1 Bedload Transport

The contaminant fluxes associated bedload sediment transport are determined as follows.

$$m_x m_y J_{SBB}^i = \frac{\partial}{\partial x}\left(m_y Q_{SBLx}^i\right) + \frac{\partial}{\partial x}\left(m_x Q_{SBLy}^i\right) \quad (7.42)$$

is used to evaluate the flux associated with pore water entrainment and expulsion in equations (7.25) and (7.40). The transport equation for material absorbed to the bedload is

$$\frac{\partial}{\partial x}\left(m_y Q_{SBLx}^i \chi_{SBL}^i\right) + m_x\left(m_x Q_{SBy}^i \chi_{SBL}^i\right) = m_x m_y J_{SB}^i \chi_{SL}^i \quad (7.43)$$

Since the contaminant mass per sediment mass in the transport divergence corresponds to conditions in the top layer of the sediment bed, equation (7.43) can be written as

$$\frac{\partial}{\partial x}\left(m_y Q_{SBLx}^i \frac{f_S^i}{S^i} C\right) + \frac{\partial}{\partial x}\left(m_x Q_{SBLy}^i \frac{f_S^i}{S^i} C\right) = m_x m_y J_{SBB}^i \chi_{SBL}^i \quad (7.44)$$

and solved using an upwind approximation

$$\begin{aligned} m_x m_y J_{SB}^i \chi_{SBL}^i = {} & \max\left(m_y Q_{SBLx}^i\right)_E \times \left(\frac{f_S^i}{S^i} C\right)_C + \min\left(m_y Q_{SBLx}^i\right)_E \times \left(\frac{f_S^i}{S^i} C\right)_E \\ & - \max\left(m_y Q_{SBLx}^i\right)_W \times \left(\frac{f_S^i}{S^i} C\right)_W - \min\left(m_y Q_{SBLx}^i\right)_W \times \left(\frac{f_S^i}{S^i} C\right)_C \\ & + \max\left(m_x Q_{SBLy}^i\right)_N \times \left(\frac{f_S^i}{S^i}\right)_C + \min\left(m_x Q_{SBy}^i\right)_N \times \left(\frac{f_S^i}{S^i} C\right)_N \\ & - \max\left(m_x Q_{SBLy}^i\right)_S \times \left(\frac{f_S^i}{S^i} C\right)_S - \min\left(m_x Q_{SBLy}^i\right)_S \times \left(\frac{f_S^i}{S^i} C\right)_C \end{aligned} \quad (7.45)$$

to evaluate the transport of bedload absorbed material between horizontally adjacent top layers of the sediment bed.

7.2.4.1 Settling, Depostion and Resuspension

Equation (7.39) is solved using a fractional step procedure consistent with that used for the water column transport. Equation (7.41) is used to update the fractional distribution in the bed between the settling, deposition, and resuspension step and the pore water advection and diffusion step. The settling, deposition, and resuspension step applies only to the top layer of the bed and is

$$
\begin{aligned}
&(BC)_{kt}^{n+\frac{1}{2}} - (BC)_{kt}^{n} \\
&\quad = -\theta \sum_i \left(\max\left(\frac{J_{SBS}^i f_S^i}{BS^i}, 0 \right) + \max\left(\frac{J_{SBS}^i F^i}{BS^i}, 0 \right) \left(f_w + \sum_j f_D^j \right) \right)_{kt}^{n+\frac{1}{2}} (BC)_{kt}^{n+\frac{1}{2}} \\
&\qquad - \theta \sum_i \left(\min\left(\frac{J_{SBS}^i f_S^i}{S^i}, 0 \right) C + \min\left(\frac{J_{SBS}^i F_{dep}^i}{S_{dep}^i}, 0 \right) \left(f_w + \sum_j f_D^j \right) C \right)_{WC}^{n+\frac{1}{2}} \\
&\qquad\qquad - \theta \sum_i \left(J_{SBB}^i \chi_{SBL}^i, 0 \right) \\
&\qquad - \theta \sum_i \left((1+\varepsilon) \max\left(\frac{J_{SBB}^i}{B\rho_S^i}, 0 \right) \left(f_w + \sum_j f_D^j \right) \right)_{kt}^{n+\frac{1}{2}} (BC)_{kt}^{n+\frac{1}{2}} \\
&\qquad\qquad - \theta \sum_i \left((1+\varepsilon_{dep}) \min\left(\frac{J_{SBB}^i}{\rho_S^i}, 0 \right) \left(f_w + \sum_j f_D^j \right) C \right)_{WC}^{n+\frac{1}{2}}
\end{aligned}
\tag{7.46}
$$

This equation is solved simultaneously with equation (7.31) for the bottom layer of the water column. The solution is represented by

$$
\begin{bmatrix} a_{11} & a_{12} \\ a_{21} & a_{22} \end{bmatrix}
\begin{Bmatrix} (BC)_{kt}^{n+\frac{1}{2}} \\ (HC)_1^{n+\frac{1}{2}} \end{Bmatrix}
=
\begin{Bmatrix} (BC)_{kt}^{n} - \theta \sum_{\substack{i \\ i=ib}} \left(J_S^i \chi_{SBL}^i \right)^{n+\frac{1}{2}} \\ \Delta_1 C_1^{n+\frac{1}{4}} + \theta \sum_i \left(\left(w_S^i S^i \right)_{1+} \left(\frac{f_S^i}{S^i} \right)_2 \right)^{n+\frac{1}{2}} C_2^{n+\frac{1}{2}} \end{Bmatrix}
\tag{7.47}
$$

where the coefficients are given by

$$
\begin{aligned}
a_{11} = 1 &+ \theta \sum_i \left(\max\left(\frac{J_{SBS}^i f_S^i}{BS^i}, 0 \right) + \max\left(\frac{J_{SBS}^i F^i}{BS^i}, 0 \right) \left(f_w + \sum_j f_D^j \right) \right)_{kt}^{n+\frac{1}{2}} \\
&+ \theta \sum_i \left((1+\varepsilon) \max\left(\frac{J_{SBB}^i}{B\rho_S^i}, 0 \right) \left(f_w + \sum_j f_D^j \right) \right)_{kt}^{n+\frac{1}{2}}
\end{aligned}
\tag{7.48}
$$

$$a_{12} = \frac{\theta}{H}\sum_i \left(\min\left(\frac{J^i_{SBS} f^i_S}{S^i}, 0\right) C + \min\left(\frac{J^i_{SBS} F^i_{dep}}{S^i_{dep}}, 0\right) \left(f_w + \sum_j f^j_D\right)\right)_1^{n+\frac{1}{2}} + \frac{\theta}{H}\sum_i \left((1+\varepsilon_{dep}) \min\left(\frac{J^i_{SBB}}{\rho^i_S}, 0\right) \left(f_w + \sum_j f^j_D\right)\right)_1^{n+\frac{1}{2}} \quad (7.49)$$

$$a_{21} = -\theta\sum_i \left(\max\left(\frac{J^i_{SBS} f^i_S}{BS^i}, 0\right) + \max\left(\frac{J^i_{SBS} F^i}{BS^i}, 0\right) \left(f_w + \sum_j f^j_D\right)\right)_{kt}^{n+\frac{1}{2}} - \theta\sum_i \left((1+\varepsilon) \max\left(\frac{J^i_{SBB}}{B\rho^i_S}, 0\right) \left(f_w + \sum_j f^j_D\right)\right)_{kt}^{n+\frac{1}{2}} \quad (7.50)$$

$$a_{22} = \Delta_1 - \frac{\theta}{H}\sum_i \left(\min\left(\frac{J^i_{SBS} f^i_S}{S^i}, 0\right) C + \min\left(\frac{J^i_{SBS} F^i}{S^i}, 0\right) \left(f_w + \sum_j f^j_D\right)\right)_1^{n+\frac{1}{2}} - \frac{\theta}{H}\sum_i \left((1+\varepsilon) \min\left(\frac{J^i_{SBB}}{\rho^i_S}, 0\right) \left(f_w + \sum_j f^j_D\right)\right)_1^{n+\frac{1}{2}} \quad (7.51)$$

Adding the two equations in (7.46) gives

$$(BC)^{n+\frac{1}{2}}_{kt} + \Delta_1 (HC)^{+\frac{1}{2}}_1 = (BC)^n_{kt} + \Delta_1 (HC)^{n+\frac{1}{4}}_1 + \theta\sum_i \left(\left(w^i_S S^i\right)_{1+} \left(\frac{f^i_S}{S^i}\right)_2\right)^{n+\frac{1}{2}} C_2^{n+\frac{1}{2}} - \theta\sum_i \left(J^i_S \chi^i_{SBL}\right)^{n+\frac{1}{2}} \quad (7.52)$$

This equation verifies the consistency of the water column-sediment bed exchange since the source and sinks on the right side include only settling into the top of the water column layer, and transfer of bedload sediment absorbed contaminant between horizontal sediment bed cells.

7.2.4.2 Porewater Advection and Diffusion

The pore water advection and diffusion step for the top, water column adjacent, layer is

$$(BC)_{kt}^{n+3/4} = (BC)_{kt}^{n+1/2} - \theta\left(\max\left(q_w,0\right) + q_{dif}\right)_{kt} + \left(\frac{1}{\phi}\left(f_w + \sum_j f_D^j\right)\right)_{kt}^{n+1/2} (BC)_{kt}^{n+3/4} + \theta\left(\min\left(q_w,0\right) - q_{di}\right)_{kt-} \left(\frac{1}{\phi B}\left(f_w + \sum_j f_D^j\right)\right)_{kt}^{+1/2} (BC)_{kt}^{n+3/4} - \theta\left(\min\left(q_w,0\right) - q_{dif}\right)_{kt+} \left(\frac{1}{\phi H}\left(f_w + \sum_j f_D^j\right)\right)_1^{n+1/2} (HC)_1^{n+1/2} + \theta\left(\max\left(q_w,0\right) + q_{dif}\right)_{kt-} \left(\frac{1}{\phi B}\left(f_w + \sum_j f_D^j\right)\right)_{kt-1}^{n+1/2} (BC)_{kt-1}^{n+1/2} \quad (7.53)$$

which is an implicit form. Writing equation (7.36) in the form

$$\Delta_1 (HC)_1^{n+3/4} = \Delta_1 (HC)_1^{n+1/2} + \theta\left(\frac{A_b}{H}\frac{\partial C}{\partial z}\right)_{1+}^{n+3/4} + \theta\left(\max\left(q_w,0\right) + q_{dif}\right)_{kt+} \left(\frac{1}{\phi B}\left(f_w + \sum_j f_D^j\right)\right)_{SB}^{n+1/2} (BC)_{kt}^{n+3/4} + \theta\left(\min\left(q_w,0\right) - q_{dif}\right)_{kt+} \left(\frac{1}{\phi H}\left(f_w + \sum_j f_D^j\right)\right)_1^{n+1/2} (HC)_1^{n+1/2} \quad (7.54)$$

and combining with equation (7.52) gives

$$(BC)_{kt}^{n+3/4} + \Delta_1 (HC)_1^{n+3/4} = (BC)_{kt}^{n+1/2} + \Delta_1 (HC)_1^{n+1/2} + \theta\left(\frac{A_b}{H}\partial_z C\right)_{1+}^{n+3/4} + \theta\left(\min\left(q_w,0\right) - q_{dif}\right)_{kt-} \times \left(\frac{1}{\phi B}\left(f_w + \sum_j f_D^j\right)\right)_{kt}^{n+1/2} (BC)_{kt}^{n+3/4} + \theta\left(\max\left(q_w,0\right) + q_{dif}\right)_{kt-} \times \left(\frac{1}{\phi B}\left(f_w + \sum_j f_D^j\right)\right)_{kt-1}^{n+1/2} (BC)_{kt-1}^{n+1/2} \quad (7.55)$$

This equation verifies the consistency of the representation of pore water advection and diffusion across water column-sediment bed interface since the source and sink terms on the right side of equation (7.55) represent fluxes at the top to the water column cell and the bottom of the bed cell.

The pore water diffusion and advection step for the remaining bed layers is given by

$$
\begin{aligned}
(BC)_k^{n+3/4} = (BC)_k^{n+1/2} - \\
\theta\left(\min\left(q_w,0\right) - q_{dif}\right)_{k+}\left(\frac{1}{\phi B}\left(f_w+\sum_j f_D^j\right)\right)_{k+1}^{n+1/2}(BC)_{k+1}^{n+3/4} - \\
\theta\left(\max\left(q_w,0\right) + q_{dif}\right)_{k+}\left(\frac{1}{\phi B}\left(f_w+\sum_j f_D^j\right)\right)_{k}^{n+1/2}(BC)_{k}^{n+3/4} + \\
\theta\left(\min\left(q_w,0\right) - q_{dif}\right)_{k-}\left(\frac{1}{\phi B}\left(f_w+\sum_j f_D^j\right)\right)_{k}^{n+1/2}(BC)_{k}^{n+3/4} + \\
\theta\left(\max\left(q_w,0\right) + q_{dif}\right)_{k-}\left(\frac{1}{\phi B}\left(f_w+\sum_j f_D^j\right)\right)_{k-1}^{n+1/2}(BC)_{k-1}^{n+3/4}
\end{aligned}
\tag{7.56}
$$

For the bottom layer of the bed $k = 1$, the bottom k_0, specific discharge and diffusion velocity must be specified as well as the total contaminant concentration, C_0. The corresponding thickness of the unresolved layer, $k = 0$, is set to unity without loss of generality. The system of equations represented by equations (7.52) and (7.55) is implicit and is solved using a tri-diagonal linear equation solver. It is noted that the $n+3/4$ time level layer thickness is actually the $n+1$ time level thickness determined by the solution of equation (7.23). The specific discharges in equations (7.52) and (7.55) are given by equation (7.41) and represent those appearing in equation (7.23) and guarantee mass conservation for the pore water advection.

The bed transport solution is completed by

$$(BC)_k^{n+1} - (BC)_k^{n+3/4} = -\theta\gamma(BC)_k^{n+1} \tag{7.57}$$

an implicit reaction step.

7.3. Toxic Contaminant Loss Terms

7.3.1 Bulk Degradation

Bulk degradation can be included in the water column and/or the sediment bed for any toxic constituent. The bulk degradation in the water column follows a first order decay rate

$$\frac{dC_k}{dt} = -KC_k \tag{7.58}$$

where,

C is the toxic concentration in mg/m^3 in layer k,

K is the first order decay rate in $1/s$, and

t is time in seconds.

For bulk degradation there is no temperature effects on the degradation rate.

In the sediment bed, bulk degradation can be applied for sediment thickness up to a maximum sediment depth

$$\frac{dC_{b,k}}{dt} = -KC_{b,k}, \text{ for } \sum_{k}^{kt} H_{bed,k} = D_{max} \tag{7.59}$$

where,

$C_{b,k}$ is the sediment bed toxic contaminant concentration in layer k (mg/g),

K is the bulk decay rate $(1/s)$,

$H_{bed,k}$ is the sediment bed layer thickness (m), and

D_{max} is the maximum depth to use bulk degradation (m).

7.3.2 Biodegradation

Bacterial degradation, sometimes referred to as microbial transformation, biodegradation or biolysis, is the breakdown of a compound by the enzyme systems in bacteria. Although these transformations can detoxify and mineralize toxins and defuse potential toxins, they can also activate potential toxins.

Biodegradation in EFDC+ follows the bulk degradation approach shown previously

$$\frac{dC_k}{dt} = -K_{w,bio}C_k \tag{7.60}$$

and

$$\frac{dC_{b,k}}{dt} = -K_{b,bio}C_{b,k}, \text{for} \sum_{k}^{kt} H_{bed,k} = D_{bio} \tag{7.61}$$

where,

C_k is the toxic concentration in the water column in layer k (mg/m^3),

$C_{b,k}$ is the sediment bed toxic contaminant concentration in layer k (mg/g),

$K_{w,bio}$ is the water column biodegradation rate $(1/s)$,

$K_{b,bio}$ is the sediment bed biodegradation rate $(1/s)$,

$H_{bed,k}$ is the sediment bed layer thickness (m), and

D_{bio} is the maximum depth to apply biodegradation (m).

And where the degradation coefficient be temperature dependent according to

$$K_{bio} = K_{bio,ref} Q_{10}^{(T-20)/10} \tag{7.62}$$

where,

$K_{bio,ref}$ is respective reference biodegradation rate at $20\,^{\circ}C$ $(1/s)$,

Q_{10} is the temperature correction factor for biodegradation, and

T is the relevant current temperature ($^{\circ}C$).

The temperature correction factors represent the increase in the biodegradation rate constants resulting from a 10 °C temperature increase. Values in the range of 1.5 to 2.0 are common.

7.3.3 Volatilization

Volatilization is the movement of chemical across the air-water interface as the dissolved neutral concentration attempts to equilibrate with the gas phase concentration. Equilibrium occurs when the partial pressure exerted by the chemical in solution equals the partial pressure of the chemical in the overlying atmosphere. The rate of exchange is proportional to the gradient between the dissolved concentration and the concentration in the overlying atmosphere and the conductivity across the interface of the two fluids. The conductivity is influenced by both chemical properties (molecular weight, Henry's Law constant) and environmental conditions at the air-water interface (turbulence-controlled by wind speed, current velocity, and water depth).

In EFDC+, volatilization of a dissolved toxic constituent is computed by

$$\left.\frac{\partial C}{\partial t}\right|_{volat} = \frac{K_v}{H_{KC}} \left(f_d C - \frac{C_a}{\frac{H_L}{RT_K}} \right) \tag{7.63}$$

where,

C is the water column concentration in layer,

KC is the top layer number (dimensionless),

K_v is the transfer rate (m/day),

H_{kc} is the water column thickness of the layer KC (m),

f_d is the fraction of the total chemical that is dissolved,

C_a is the atmospheric concentration (mg/m^3),

R is the universal gas constant $8.206 \times 10^{-5} atm - m^3/mole - K$,

T_K is the water temperature in Kelvin ($^{\circ}K$), and

H_L is the Henry's law coefficient for the air-water partitioning of the toxic ($atm - m^3/mole$).

Equilibrium occurs when the dissolved concentration equals the partial pressure divided by the Henry's Law Constant.

The dissolved concentration of a chemical in a surface water column segment can volatilize at a rate determined by the two-layer resistance model Whitman et al. (1923). The two-resistance method assumes that two "stagnant films" are bounded on either side by well mixed compartments. Concentration differences serve as the driving force for the water layer diffusion. Pressure differences drive the diffusion for the air layer. From mass balance considerations, it is obvious that the same mass must pass through both films, thus the two resistances combine in series, so that the conductivity is the reciprocal of the total resistance:

$$K_v = (R_L + R_G)^{-1} = \left[K_L^{-1} + \left(K_G \frac{H_L}{RT_K} \right)^{-1} \right]^{-1} \tag{7.64}$$

where,

R_L is the liquid phase resistance (day/m),

K_L is the liquid phase transfer coefficient (m/day),

R_G is the gas phase resistance (day/m), and

K_G is the gas phase transfer coefficient (m/day).

There is yet another resistance involved, the transport resistance between the two interfaces, but it is assumed to be negligible. This may not be true in two cases: very turbulent conditions and in the presence of surface-active contaminants. Although this two-resistance method, the Whitman model, is rather simplified in its assumption of uniform layers, it has been shown to be as accurate as more complex models.

The value of K_v, the conductivity, depends on the intensity of turbulence in a water body and in the overlying atmosphere. Leinonen and Mackay (1975) have discussed conditions under which the value of K_v is primarily determined by the intensity of turbulence in the water. As the Henry's Law coefficient increases, the conductivity tends to be increasingly influenced by the intensity of turbulence in water. As the Henry's Law coefficient decreases, the value of the conductivity tends to be increasingly influenced by the intensity of atmospheric turbulence.

The computed volatilization rate from equation (7.64) is for a temperature of $20°C$. It is adjusted for water temperature using the equation:

$$K_{v,T} = K_v T^{T-20} \tag{7.65}$$

where,

Θ is the temperature correction factor, and

T is the water temperature ($^{\circ}C$).

The liquid and gas film transfer coefficients computed under this option vary with the type of waterbody. The type of waterbody is specified as one of the volatilization constants and can either be a flowing stream, river or estuary or a stagnant pond or lake. The primary difference is that in a flowing waterbody the turbulence is primarily a function of the stream velocity, while for stagnant waterbodies wind shear may dominate. The formulations used to compute the transfer coefficients vary with the waterbody type as shown below.

EFDC+ automatically determines which flow regime to apply based on the following criteria

$$\left\{ \begin{array}{l} H > H_{max},\ Lake\ conditions \\ H = H_{max},\ River\ conditions \end{array} \right\} \tag{7.66}$$

or

$$\left\{ \begin{array}{l} U = U_{max},\ Lake\ conditions \\ U > U_{max},\ River\ conditions \end{array} \right\} \tag{7.67}$$

where,

H is total depth (m),

H_{max} is maximum depth allowed for river conditions (m),

U is the depth averaged velocity magnitude (m/s), and

U_{max} is the maximum lake velocity magnitude (m/s).

7.3.3.1 Flowing Stream, River or Estuary

For a flowing system the transfer coefficients are controlled by flow induced turbulence. For flowing conditions, the liquid film transfer coefficient (K_L) is computed using the Covar method (Covar, 1976) in which the equation used varies with the velocity and depth of the cell.

For cells with depths less than 0.61 m, the Owens formula is used to calculate the oxygen reaeration rate (7.68).

$$K_L = \frac{5.349}{86400} \frac{U^{0.67}}{H^{1.5}} \tag{7.68}$$

where,

U is the depth averaged water velocity magnitude (m/s), and

H is cell depth (m).

For segments with a velocity less than 0.518 m/s or a depth (m) greater than $13.584U^{2.9135}$ the O'Connor-Dobbins formula is used:

$$K_L = D_w \frac{U^{0.5}}{H^{1.5}} \tag{7.69}$$

where, D_w is the diffusivity of the chemical in water (m^2/s), computed from

$$D_w = \frac{22 \cdot 10^{-9}}{M_w^{0.6667}} \tag{7.70}$$

In all other cases, the Churchill formula is used to calculate reaeration rate:

$$K_L = \frac{5.049}{86400} \frac{U^{0.969}}{H^{1.673}} \tag{7.71}$$

The gas transfer coefficient (K_G) is assumed constant at 100 m/day for flowing systems.

7.3.3.2 Lake or Pond

For more quiescent conditions, the transfer coefficients are controlled by wind induced turbulence. For these systems, the liquid film transfer coefficient (K_L) is computed using either the O'Connor equations or Mackay and Yeun (1983).

7.3.3.2.1 Option 1 O'Connor Approach

$$K_L = u_* \left(\frac{\partial_a}{\partial_w} \right)^{0.5} \frac{\partial^{0.33}}{\partial_2} S_{cw}^{-0.67} \tag{7.72}$$

$$K_G = u_* \frac{\partial^{0.33}}{\partial_2} S_{ca}^{-0.67} \tag{7.73}$$

where, u_* is the shear velocity (m/s) computed from

$$u_* = C_d^{0.5} W_{10} \tag{7.74}$$

where,

C_d is the drag coefficient (0.0011),

W_{10} is wind velocity at 10 m above the water surface (m/s),

ρ_a is density of air, internally calculated from air temperature (kg/m^3),

ρ_w is density of water, internally calculated from water temperature (kg/m^3),

κ is von Karman's constant,

λ_2 is dimensionless viscous sublayer thickness, and

S_{ca} and S_{cw} are air and water Schmidt Numbers, computed from

$$S_{ca} = \frac{\mu_a}{\partial_a D_a} \tag{7.75}$$

$$S_{cw} = \frac{\mu_w}{\partial_w D_w} \tag{7.76}$$

where,

D_a is diffusivity of chemical in air (m^2/s),

D_w is diffusivity of chemical in water (m^2/s),

μ_a is viscosity of air, internally calculated from air temperature ($kg/m-sec$), and

μ_w is viscosity of water, internally calculated from water temperature ($kg/m-sec$).

The diffusivity of the chemical in water is computed using equation (7.70) while the diffusivity of the chemical in air (D_a, m^2/sec) is computed from

$$D_a = \frac{1.9 \cdot 10^{-4}}{M_w^{2/3}} \tag{7.77}$$

This K_G is proportional to wind and inversely proportional to molecular weight to the 4/9 power.

7.3.3.2.2 Option 2 Mackay and Yeun Approach

Under this option, the liquid and gas film transfer coefficients are computed using formulations described by Mackay and Yeun (1983). The Mackay equations are:

$$K_L = \begin{cases} 10^{-6} + 0.00341 u_* S_{cw}^{-0.5}, & u_* > 0.3\text{m/s} \\ 10^{-6} + 0.01441 u_*^{2.2} S_{cw}^{-0.5}, & u_* < 0.3\text{m/s} \end{cases} \tag{7.78}$$

$$K_G = 10^{-3} + 0.0462 u_* S_{ca}^{-0.67} \tag{7.79}$$

7.3.3.2.3 Volatilization Input Data

Although there are many calculations involved in determining volatilization, most are performed internally using a small set of data. Volatilization data specifications are summarized in Table 7.1 Not all of the constants are required. Volatilization is only active for the surface layer.

Table 7.1. Volatilization Input Data

Description	Notation	Range	Units
Measured or calibrated conductance	K_v	0.6 — 25	m/day
Henry's Law Constant	H	10^{-7} — 10^{-1}	$atm-m^3/mole$
Concentration of chemical in atmosphere	C_a	0 — 1000	$\mu g/L$
Molecular weight	M_w	10 — 10^3	$g/mole$
Reaeration coefficient (conductance of oxygen)	K_a	0.6 — 25	m/day
Experimentally measured ratio of volatilization to reaeration	k_{vo}	0 — 1	
Current velocity	u_x	0.2	m/s
Water depth	D	0.1 — 10	m
Water temperature	T	4 — 30	$^\circ C$
Wind speed 10m above surface	W_{10}	0 — 20	m/s

Chapter 8

EUTROPHICATION MODULE

8.1. Introduction

This section summarizes the basic theory of the water quality-eutrophication module of the EFDC+ model.The kinetic processes included in the EFDC+ water quality module are derived from the CE-QUAL-ICM water quality model (Cerco and Cole, 1995) as described in Park et al. (1995). This document describes the current module formulation including comparisons with subsequent published documentation of CE-QUAL-ICM model applications. Table 8.1 lists the model's complete set of state variables, and their interactions are illustrated in Figure 8.1. As opposed to earlier water quality models such as WASP (Ambrose et al., 1993), which use biochemical oxygen demand (BOD) to represent oxygen demanding organic material, the EFDC+ eutrophication module is carbon based. The four algal species are represented in carbon units. The three organic carbon variables play an equivalent role to BOD. Organic carbon, nitrogen and phosphorous can be represented by up to three reactive sub-classes, refractory particulate, labile particulate and labile dissolved. The use of sub-classes allows a more realistic distribution of organic material by reactive classes when data are to estimate distribution factors. The following sub-sections discuss the role of each variable and summarize their kinetic interaction processes. The kinetic processes include the exchange of fluxes at the sediment-water interface, including sediment oxygen demand (SOD). The description of the EFDC+ eutrophication module in this section closely follows Park et al. (1995).

8.2. Water Column Eutrophication Formulation

8.2.1 Model State Variables

8.2.1.1 Algae

Algae are grouped into four model classes: cyanobacteria, diatoms, greens, and stationary. The grouping is based upon the distinctive characteristics of each class and upon the significant role the characteristics play in the ecosystem. Cyanobacteria, commonly

Table 8.1. EFDC+ model water quality state variables

#	Water quality state variable	Acronyms	Units	Group
1	Cyanobacteria	B_c	mg/l C	Algae
2	Diatom algae	B_d	mg/l C	
3	Green algae	B_g	mg/l C	
4	Refractory particulate organic carbon	$RPOC$	mg/l	Organic carbon
5	Labile particulate organic carbon	$LPOC$	mg/l	
6	Dissolved organic carbon	DOC	mg/l	
7	Refractory particulate organic phosphorus	$RPOP$	mg/l	Phosphorus
8	Labile particulate organic phosphorus	$LPOP$	mg/l	
9	Dissolved organic phosphorus	DOP	mg/l	
10	Total phosphate	$PO4$	mg/l	
11	Refractory particulate organic nitrogen	$RPON$	mg/l	Nitrogen
12	Labile particulate organic nitrogen	$LPON$	mg/l	
13	Dissolved organic nitrogen	DON	mg/l	
14	Ammonia nitrogen	$NH4$	mg/l	
15	Nitrate and nitrite nitrogen	$NO3$, $NO2$, NOX	mg/l	
16	Particulate biogenic silica	SU	mg/l	Silica
17	Dissolved available silica	SA	mg/l	
18	Chemical oxygen demand	COD	mg/l	Others
19	Dissolved oxygen	DO	mg/l	
20	Total active metal	TAM	$mole/m^3$	
21	Fecal coliform bacteria	FCB	$MPN/100ml$	
22	Macroalgae/Periphyton	B_m	mg/l C	

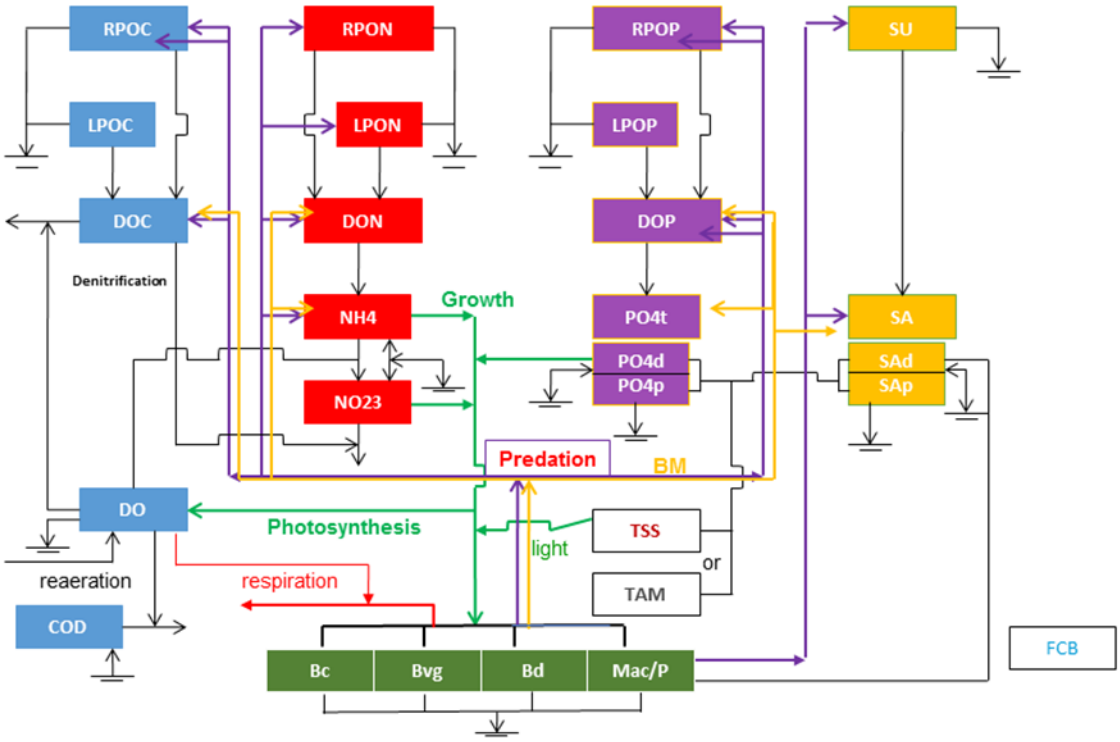

Fig. 8.1. Schematic diagram of EFDC+ Water Quality Model Structure.

called blue-green algae, are characterized by their abundance (as picoplankton) in saline water and by their bloom-forming characteristics in fresh water. Cyanobacteria are unique in that some species fix atmospheric nitrogen, although nitrogen fixers are not believed to be predominant in many river systems. Diatoms are distinguished by their requirement of silica as a nutrient to form cell walls. Diatoms are large algae, characterized by high settling velocities. Settling of spring diatom blooms to the sediments may be a significant source of carbon for sediment oxygen demand. Algae that do not fall into the preceding two groups are lumped into the heading of green algae. Green algae settle at a rate intermediate between cyanobacteria and diatoms, and are subject to greater grazing pressure than cyanobacteria.

A stationary or non-transported algae (constituent 22) variable is included in the model and has been used to simulate macroalgae/periphyton. The stationary algae variable has the same kinetic formulation as the original algae groups, with the exception that it is not transported. The stationary algae group can also be used to represent various types of bottom substrate attached or floating periphyton. It is also noted that, in applications requiring simulation of multiple classes of stationary algae, one or more of the three transported algae groups can be switched to stationary model, under the restriction that the total number

of transport and stationary algae classes remains less than or equal to four. Appendix A provides additional specifics with respect to model configuration simulation of macroalgae and periphyton.

8.2.1.2 Organic Carbon

Three organic carbon state variables are considered: dissolved, labile particulate, and refractory particulate. Labile and refractory distinctions are based upon the time scale of decomposition. Labile organic carbon decomposes on a time scale of days to weeks whereas refractory organic carbon requires more time. Labile organic carbon decomposes rapidly in the water column or the sediments. Refractory organic carbon decomposes slowly, primarily in the sediments, and may contribute to sediment oxygen demand years after deposition.

8.2.1.3 Nitrogen

Nitrogen is first divided into organic and mineral fractions. Organic nitrogen state variables are dissolved organic nitrogen, labile particulate organic nitrogen, and refractory particulate organic nitrogen. Two mineral nitrogen forms are considered: ammonium and nitrate. Both are utilized to satisfy algal nutrient requirements, although ammonium is preferred from thermodynamic considerations. The primary reason for distinguishing the two is that ammonium is oxidized by nitrifying bacteria into nitrate. This oxidation can be a significant sink of oxygen in the water column and sediments. An intermediate in the complete oxidation of ammonium, nitrite, also exists. Nitrite concentrations are usually much less than nitrate, and for modeling purposes, nitrite is combined with nitrate. Hence, the nitrate state variable actually represents the sum of nitrate plus nitrite.

8.2.1.4 Phosphorus

As with carbon and nitrogen, organic phosphorus is considered in three states: dissolved, labile particulate, and refractory particulate. Only a single mineral form, total phosphate, is considered. Total phosphate exists as several states within the model ecosystem: dissolved phosphate, phosphate sorbed to inorganic solids, and phosphate incorporated in algal cells. Equilibrium partition coefficients are used to distribute the total among the three states.

8.2.1.5 Silica

Silica is divided into two state variables: available silica and particulate biogenic silica. Available silica is primarily dissolved and can be utilized by diatoms. Particulate biogenic silica cannot be utilized. In the model, particulate biogenic silica is produced through diatom mortality. Particulate biogenic silica undergoes dissolution to available silica or else settles to the bottom sediments.

8.2.1.6 Chemical Oxygen Demand

In the context of this study, chemical oxygen demand is the concentration of reduced substances that are oxidizable by inorganic means. The primary component of chemical oxygen demand is sulfide released from sediments. Oxidation of sulfide to sulfate may remove substantial quantities of dissolved oxygen from the water column.

8.2.1.7 Dissolved Oxygen

Dissolved oxygen is required for the existence of higher life forms. Oxygen availability determines the distribution of organisms and the flows of energy and nutrients in an ecosystem. Dissolved oxygen is a central component of the water quality model.

8.2.1.8 Total Active Metal

Both phosphate and dissolved silica adsorb to inorganic solids, primarily iron and manganese. Sorption and subsequent settling is one pathway for removal of phosphate and silica from the water column. Consequently, the concentration and transport of iron and manganese are represented in the model. However, limited data do not allow a complete treatment of iron and manganese chemistry. Rather, a single-state variable, total active metal, is defined as the total concentration of metals that are active in phosphate and silica transport. Total active metal is partitioned between particulate and dissolved phases by an oxygen-dependent partition coefficient. Inorganic suspended solids can be used, in lieu of total active metal, as a sorption sited for phosphate and silica. Inorganic suspended solids concentration is provided by the sediment transport component of the EFDC+ modeling system.

8.2.1.9 Salinity

Salinity is a conservative tracer that provides verification of the transport component of the model and facilitates examination of conservation of mass. Salinity also influences the dissolved oxygen saturation concentration and is used in the determination of kinetics constants that differ in saline and fresh water. Salinity is simulated in the hydrodynamic component of the model.

8.2.1.10 Temperature

Temperature is a primary determinant of the rate of biochemical reactions. Reaction rates increase as a function of temperature, although extreme temperatures result in the mortality of organisms. Temperature is simulated in the hydrodynamic component of the model.

8.2.2 Conservation of Mass Equation

The governing mass-balance equation for each of the water quality state variables may be expressed as:

$$\frac{\partial}{\partial t}(m_x m_y HC)+\frac{\partial}{\partial x}(m_y HuC)+\frac{\partial}{\partial y}(m_x HvC)+\frac{\partial}{\partial z}(m_x m_y wC)= \frac{\partial}{\partial x}\left(\frac{m_y HA_x}{m_x}\frac{\partial C}{\partial x}\right)+\frac{\partial}{\partial y}\left(\frac{m_x HA_y}{m_y}\frac{\partial C}{\partial y}\right)+\frac{\partial}{\partial z}\left(m_x m_y \frac{A_z}{H}\frac{\partial C}{\partial z}\right)+m_x m_y HS_c \quad (8.1)$$

The last three terms on the left-hand side (LHS) of equation (8.1) account for the advective transport, and the first three terms on the right-hand side (RHS) account for the diffusive transport. These six terms for physical transport are analogous to, and thus the numerical method of solution is the same as, those in the mass-balance equation for salinity in the hydrodynamic model (Hamrick, 1992). The last term in equation (8.1) represents the kinetic processes and external loads for each of the state variables. The present model solves equation (8.1) using a fractional step procedure which decouples the kinetic terms from the physical transport terms.

$$\frac{\partial}{\partial t_p}(m_x m_y HC)+\frac{\partial}{\partial x}(m_y HuC)+\frac{\partial}{\partial y}(m_x HvC)+\frac{\partial}{\partial z}(m_x m_y wC)= \frac{\partial}{\partial x}\left(\frac{m_y HA_x}{m_x}\frac{\partial C}{\partial x}\right)+\frac{\partial}{\partial y}\left(\frac{m_x HA_y}{m_y}\frac{\partial C}{\partial y}\right)+\frac{\partial}{\partial z}\left(m_x m_y \frac{A_z}{H}\frac{\partial C}{\partial z}\right)+m_x m_y HS_{CP} \quad (8.2)$$

$$\frac{\partial C}{\partial t_K}=S_{CK} \quad (8.3)$$

with

$$\frac{\partial}{\partial t}(m_x m_y HC)=\frac{\partial}{\partial t_p}(m_x m_y HC)+(m_x m_y H)\frac{\partial C}{\partial t_K} \quad (8.4)$$

In equation (8.2) the source sink term has been split into physical sources and sinks which are associated in volumetric inflows and outflows, and kinetic sources and sinks. Since variations in the water column depth are coupled with the divergence of the volume transport field, the kinetic step is made at a constant water column depth corresponding to the depth field at the end for the physical transport step. This allows the depth and scale factors to be eliminated from the kinetic step in equation (8.3) which can be further split into reactive and internal sources and sinks.

$$\frac{\partial C_K}{\partial t}=KC+R \quad (8.5)$$

Where K is kinetic rate ($time^{-1}$) and R represents internal source/sink term ($mass\ volume^{-1} time^{-1}$). Equation (8.5) is obtained by linearizing some terms in the kinetic equations, mostly Monod type expressions. Hence, K and R are known values in equation (8.5). Equation (8.2) is identical to, and thus its numerical method of solution is the same as, the mass-balance equation for salinity (Hamrick, 1992). The solution scheme for both the physical transport (Hamrick, 1992) and the kinetic equations is second-order accurate.

8.2.3 Kinetic Equations for State Variables

The remainder of this chapter details the kinetics portion of the mass-conservation equation for each state variable. Parameters are defined where they first appear. All parameters are listed, in alphabetical order, in an appendix. For consistency with reported rate coefficients, kinetics are detailed using a temporal dimension of days. Within the CE-QUAL-ICM computer code, kinetics sources and sinks are converted to a dimension of seconds before they are used in the mass-conservation equation.

8.2.3.1 Algae

Algae, which occupies a central role in the model, are grouped into three model state variables: cyanobacteria (blue-green algae), diatoms, and green algae. The subscript $\boldsymbol{x}$, is used to denote four algal groups: $\boldsymbol{c}$ for cyanobacteria, $\boldsymbol{d}$ for diatoms, $\boldsymbol{g}$ for green algae, and $\boldsymbol{m}$ for macroalgae. Sources and sinks included in the model are:

1. Growth (production)
2. Basal metabolism
3. Predation
4. Settling
5. External loads

Equations describing these processes are largely the same for the four algal groups with differences in the values of parameters in the equations. The kinetic equation describing these processes is:

$$\frac{\partial B_{\boldsymbol{x}}}{\partial t} = (P_{\boldsymbol{x}} - BM_{\boldsymbol{x}} - PR_{\boldsymbol{x}})\,B_{\boldsymbol{x}} + \frac{\partial}{\partial Z}(WS_{\boldsymbol{x}}B_{\boldsymbol{x}}) + \frac{WB_{\boldsymbol{x}}}{V} \tag{8.6}$$

where,

$B_{\boldsymbol{x}}$ is the algal biomass of algal group $\boldsymbol{x}$ ($g\,C/m^3$),

t is the time ($days$),

$P_{\boldsymbol{x}}$ is the production rate of algal group $\boldsymbol{x}$ ($1/day$),

BM_x is the basal metabolism rate of algal group x $(1/day)$,

PR_x is the predation rate of algal group x $(1/day)$,

WS_x is the positive settling velocity of algal group x (m/day),

WB_x is the external loads of algal group x $(g\,C/day)$, and

V is the cell volume (m^3).

8.2.3.1.1 Production (Algal Growth)

Algal growth depends on nutrient availability, ambient light, and temperature. The effects of these processes are considered to be multiplicative:

$$P_x = PM_x f_1(N) f_2(I) f_3(T) f_4(S) \tag{8.7}$$

where,

PM_x is the maximum growth rate under optimal conditions for algal group x $(1/day)$,

$f_1(N)$ is the effect of suboptimal nutrient concentration $(0 \le f_1 \le 1)$,

$f_2(I)$ is the effect of suboptimal light intensity $(0 \le f_2 \le 1)$,

$f_3(T)$ is the effect of suboptimal temperature $(0 \le f_3 \le 1)$, and

$f_4(S)$ is the effect of salinity on cyanobacteria growth $(0 \le f_4 \le 1)$,

The freshwater cyanobacteria may undergo rapid mortality in saltwater, e.g., freshwater organisms in the Potomac River (Thomann et al., 1985). For the freshwater organisms, the increased mortality is included in the model by the salinity toxicity term in the growth equation for cyanobacteria. Activation of the salinity toxicity term, $f_4(S)$, is an option in the source code.

8.2.3.1.1.1 Effect of Nutrients on Algal Growth

Using Liebig's "law of the minimum" (Odum, 1971) algal growth is determined by the nutrient in least supply, the nutrient limitation for growth of cyanobacteria and green algae is expressed as:

$$f_1(N) = \left(\frac{NH4 + NO3}{KHN_x + NH4 + NO3}, \frac{PO4d}{KHP_x + PO4d}, \frac{SAd}{KHS + SAd} \right) \tag{8.8}$$

where,

$NH4$ is the ammonium nitrogen concentration $(g\,N/m^3)$,

$NO3$ is the nitrate nitrogen concentration $(g\,N/m^3)$,

KHN_x is the half-saturation constant for nitrogen uptake for algal group x $(g\,N/m^3)$,

$PO4d$ is the dissolved phosphate phosphorus concentration ($g\ P/m^3$),

KHP_x is the half-saturation constant for phosphorus uptake for algal group x ($g\ P/m^3$),

SAd is the concentration of dissolved available silica ($g\ Si/m^3$), and

KHS is the half-saturation constant for silica uptake for diatoms ($g\ Si/m^3$).

Some cyanobacteria (e.g., *Anabaena*) can fix nitrogen from atmosphere and thus are not limited by nitrogen. Hence, equation (8.8) is not applicable to the growth of nitrogen fixers. Since diatoms require silica as well as nitrogen and phosphorus for growth, the nutrient limitation for diatoms includes silica limitation.

8.2.3.1.1.2 Effect of Light on Algal Growth

1. Effect of Light on Algal Growth

The light field in the water column is governed by:

$$\frac{\partial I}{\partial Z_*} = -K_{ess}\, I \tag{8.9}$$

where,

I is the light intensity (W/m^2),

K_{ess} is the light extinction coefficient ($1/m$), and

$Z*$ is the depth below the water surface (m).

with the light extinction coefficient being a function of the depth below the water surface. Integration of (8.9) gives:

$$I = I_{ws}\exp\left(-\int_0^{Z_*} K_{ess}\, dZ_*\right) \tag{8.10}$$

The light intensity at the water surface I_{ws}, is given by

$$I_{ws} = I_o \min\left(\exp\left(-Keme\left(H_{RPS} - H\right)\right),\ 1\right) \tag{8.11}$$

where,

I_o is the light is the light intensity at the top of the emergent aquatic plant canopy for emergent shoots or the light intensity at the water surface for submerged shoots (W/m^2),

$Keme$ is the light extinction coefficient for emergent shoots ($1/m$),

H_{RPS} is the rooted plant shoot height (m), and

H is the water column depth (m).

When submerged aquatic plants are simulated, the light extinction coefficient in the water column above the canopy is given by

$$K_{essac} = Ke_b + Ke_{ISS} \cdot ISS + Ke_{VSS} \cdot VSS + Ke_{Chl} \sum_{m=1}^{M} \left(\frac{B_m}{CChl_m} \right) \tag{8.12}$$

and the light extinction coefficient in the water column within the canopy is given by

$$K_{essic} = Ke_b + Ke_{ISS} \cdot SED + Ke_{VSS} \cdot VSS + Ke_{Chl} \sum_{m=1}^{M} \left(\frac{B_m}{CChl_m} \right) + Ke_{RPS} \cdot RPS \tag{8.13}$$

where,

Ke_b is the background light extinction $(1/m)$,

Ke_{ISS} is the light extinction coefficient for inorganic suspended solid $(1/m\ perg/m^3)$,

SED is the inorganic suspended solid concentration (g/m^3) provided from the hydrodynamic model,

Ke_{VSS} is the light extinction coefficient for volatile suspended solid $(1/m\ perg/m^3)$,

VSS is the volatile suspended solid concentration (g/m^3) provided from the water quality model,

$CChl_{RPE}$ is the carbon-to-chlorophyll ratio for epiphytes $(g\ C\ per\ mg\ Chl)$,

Ke_{Chl} is the light extinction coefficient for algae chlorophyll $(1/m\ per\ mg\ Chl/m^3)$,

B_m is the concentration of algae group m $(g\ C\ per\ ml)$,

$CChl_m$ is the carbon-to-chlorophyll ratio in algal group m $(g\ C\ per\ mg\ Chl)$,

Ke_{RPS} is the light extinction coefficient for rooted plant shoots $(1/m\ per\ gm\ C/m^2)$, and

RPS is the concentration of plant shoots $(g\ C\ per\ m^2)$.

The forms of equations (8.12) and (8.13) are quite general and readily allow inclusion of algae biomass into the volatile suspended solids or visa-versa. The form of equation (8.13) assumes that the rooted plant shoots are primarily self-shading and that epiphyte effect are manifested only on the shoot surface.

The solutions of equation (8.10) above and in the rooted plant shoot canopy are

$$I = I_{ws} \exp\left(-K_{essac}\ Z_*\right)\ ;\ 0 \le Z_* \le H - H_{RPS} \tag{8.14}$$

$$I = I_{ct} \exp\left(-Kesic\ \left(Z_* - H + H_{RPS}\right)\right) \tag{8.15}$$

$$I_{ct} = I_{ws} \exp\left(-K_{essac}\ \left(H - H_{RPS}\right)\right) \tag{8.16}$$

$$H - H_{RPS} \le Z_* \le H \tag{8.17}$$

2. Steele's Equation for Light Limitation

The original version of CE-QUAL-ICM (Cerco and Cole, 1995) used Steele's equation

$$f_2(I) = \frac{I}{I_{sx}} \exp\left(1 - \frac{I}{I_{sx}}\right) \tag{8.18}$$

to express light limitation. A daily and vertically integrated form of Steele's equation, in the absences of a plant canopy is:

$$f_2 = \frac{\exp(1)\ FD}{K_{ess}\ (ZB - ZT)} \left(\exp(-\alpha_b)\ - \exp(-\alpha_T)\ \right) \tag{8.19}$$

$$\alpha_B = \left(\frac{I_{wsavg}}{FDI_{sx}}\right) \exp(-K_{ess}\ ZB) \tag{8.20}$$

$$\alpha_T = \left(\frac{I_{wsavg}}{FDI_{sx}}\right) \exp(-K_{ess}\ ZT) \tag{8.21}$$

where,

FD is the fractional day length $(0 \leq FD \leq 1)$,

K_{ess} is the total light extinction coefficient $(1/m)$,

ZT is the distance from water surface to layer top (m),

ZB is the distance from water surface to layer bottom (m),

I_{wsavg} is the daily total light intensity at water surface $(langleys/day)$, and

I_{sx} is the optimal light intensity for algal group x $(langleys/day)$.

Optimal light intensity I_{sx} for photosynthesis depends on algal taxonomy, duration of exposure, temperature, nutritional status, and previous acclimation. Variations in I_{sx} are largely due to adaptations by algae intended to maximize production in a variable environment. Steele (1962) noted the result of adaptations is that the optimal intensity is a consistent fraction (approximately 50 percent) of daily intensity. Kremer and Nixon (1978) reported an analogous finding that maximum algal growth occurs at a constant depth (approximately 1 m) in the water column. Their approach is adopted so that optimal intensity is expressed as:

$$I_{sx} = \min\left(I_{wsavg} \exp(-K_{ess}\ D_{optx})\ ,\ I_{sxmin}\right) \tag{8.22}$$

where,

D_{optx} is the depth of maximum algal growth for algal group x (m),

I_{wsavg} is the adjusted surface light intensity (W/m^2), and

I_{sxmin} is the minimum optimum light intensity (W/m^2).

A minimum I_{sxmin}, in equation (8.22) is specified so that algae do not thrive at extremely low light levels. The time required for algae to adapt to changes in light intensity is recognized by estimating I_{sxmin} based on a time-weighted average of daily light intensity:

$$I_{0avg} = CI_a I_0 + CI_b I_1 + CI_c I_2 \tag{8.23}$$

where,

I_1 is the daily light intensity 1 day preceding model day ($langleys/day$),

I_2 is the daily light intensity 2 days preceding model day ($langleys/day$), and

CI_a, CI_b, C_c are the weighting factors for I_0, I_1 and I_2, respectively: $CI_a + CI_b + CI_c = 1$.

Equations (8.19)-(8.21) can be applied instantaneously by setting the fraction of daylight to unity. It can also be applied within a canopy by replacing I_{ws} with I_{ct} in the equation (8.15).

3. Alternate Formulations for Light Limitation

Figure 8.1 of CE-QUAL-ICM (Bunch et al., 2000) used a Monod type limitation

$$f_2(I) = \frac{I}{KHI + I} \tag{8.24}$$

or a modified Monod limitation (Cerco et al., 2000)

$$f_2(I) = \frac{I}{\sqrt{KHI^2 + I^2}} \tag{8.25}$$

where, KHI is the half saturation for light limitation (W/m^2).

Equation (8.25) was used in the CE-QUAL-ICM Florida Bay water quality modeling study Cerco et al. (2000). Equation (8.24) can be directly averaged over a water column layer to give

$$f_{2avg} = \frac{1}{K_{ess}(ZB - ZT)} \ln\left(\frac{KHI + I_{ws} exp(-K_{ess}\, ZT)}{KHI + I_{ws} exp(-K_{ess}\, ZB)}\right) \tag{8.26}$$

while the average of equation (8.25) is

$$f_{2avg} = \frac{1}{K_{ess}} \frac{1}{ZB - ZT} \left(\begin{array}{c} \sqrt{1 + \left(\frac{I_{ws}}{KHI} \exp(-K_{ess}\, ZT)\right)^2} \\ -\sqrt{1 + \left(\frac{I_{ws}}{KHI} \exp(-K_{ess}\, ZB)\right)^2} \end{array} \right) \tag{8.27}$$

with ZT and ZB defined in the equation (8.15). Equations (8.26) and (8.27) can be applied within a canopy by replacing I_{ws} with I_{ct} and use of the appropriate light extinction coefficient.

8.2.3.1.1.3 Effect of Temperature on Algal Growth

A Gaussian probability curve is used to represent temperature dependency of algal growth:

$$f_3(T) = \begin{cases} \exp\left(-KTG1_x(T - TM1_X)^2\right) & : T \leq TM1_X \\ 1 & : TM1_X < T < TM2_X \\ \exp\left(-KTG2_x(T - TM2_X)^2\right) & : T \geq TM2_X \end{cases} \tag{8.28}$$

where

T is the temperature ($^\circ C$) provided from the hydrodynamic model,

TM_x is the optimal temperature for algal growth for algal group x ($^\circ C$),

$KTG1_x$ is the effect of temperature below $TM1_x$ on growth for algal group x ($1/^\circ C^2$), and

$KTG2_x$ is the effect of temperature above $TM2_x$ on growth for algal group x ($1/^\circ C^2$).

The formulation of equation (8.28) represents a modification to the CE-QUAL-ICM formulation to allow for temperature range specification of optimum growth.

8.2.3.1.1.4 Effect of Salinity on Growth of Freshwater Cyanobacteria

The growth of freshwater cyanobacteria in salt water is limited by:

$$f_4(S) = \frac{STOXS^2}{STOXS^2 + S^2} \tag{8.29}$$

where,

$STOXS$ is the salinity at which Microcystis growth is halved (ppt), and

S is the salinity in water column (ppt) provided from the hydrodynamic model.

8.2.3.1.2 Effect of Temperature on Algal Basal Metabolism

Algal biomass in the present model decreases through basal metabolism (respiration and excretion) and predation. Basal metabolism in the present model is the sum of all internal processes that decrease algal biomass and consists of two parts; respiration and excretion. In basal metabolism, algal matter (carbon, nitrogen, phosphorus, and silica) is returned to organic and inorganic pools in the environment, mainly to dissolved organic and inorganic matter. Respiration, which may be viewed as a reversal of production, consumes dissolved oxygen. Basal metabolism is considered to be an exponentially increasing function of temperature:

$$BM_x = BMR_x \exp\left(KTB_x[T - TR_x]\right) \tag{8.30}$$

where,

BMR_x is the basal metabolism rate at $TR_x$for algal group x $(1/day)$,

KTB_x is the effect of temperature on metabolism for algal group x $(1/^\circ C)$, and

TR_x is the reference temperature for basal metabolism for algal group x $(^\circ C)$.

8.2.3.1.3 Effect of Algal Biomass and Temperature on Algal Predation

The present model does not include zooplankton. Instead, a constant rate can be specified for the algal predation, which implicitly assumes zooplankton biomass is a constant fraction of algal biomass. Alternately, the predation rate can be taken as proportional to the algae biomass. Using a temperature effect similar to that for metabolism, the predation rate is given as

$$PR_x = PRR_x \left(\frac{B_x}{B_{xP}} \right)^{\alpha_P} \exp\left(KTP_x [T - TR_x]\right) \tag{8.31}$$

where,

PRR_x is the reference predation rate at B_xP and TR_x for algal group x $(1/day)$,

B_{xP} is the reference algae concentration for predation $(g\,C/m^3)$,

α_P is the exponential dependence factor, and

KTP_x is the effect of temperature on predation for algal group x $(1/^\circ C)$.

The difference between predation and basal metabolism lies in the distribution of the end products of the two processes. In predation, algal matter (carbon, nitrogen, phosphorus, and silica) is returned to the organic and inorganic pools in the environment, mainly to particulate organic matter. It is also noted that predation in the EFDC+ water quality model follows the original formulation in the CE-QUAL-ICM model (Cerco and Cole, 1995) which uses a predation rate constant with total predation loss being proportional to algae concentration. Subsequent CE- QUAL-ICM documentation Cerco et al. (2000), appear to define predation independent of algae concentration.

8.2.3.1.4 Algal Settling

Settling velocities for four algal groups, WS_c, WS_d, WS_g, and WS_m, are specified as an input. Seasonal variations in settling velocity of diatoms can be accounted for by specifying time-varying WS_d.

8.2.3.2 Organic Carbon

The present model has three state variables for organic carbon: refractory particulate, labile particulate, and dissolved.

8.2.3.2.1 Particulate Organic Carbon

Labile and refractory distinctions are based on the time scale of decomposition. Labile particulate organic carbon with a decomposition time scale of days to weeks decomposes rapidly in the water column or in the sediments. Refractory particulate organic carbon with a longer than weeks decomposition time scale decomposes slowly, primarily in the sediments, and may contribute to sediment oxygen demand years after decomposition. For labile and refractory particulate organic carbon, sources and sinks included in the model are (Figure 8.1):

1. Algal predation,
2. Dissolution to dissolved organic carbon,
3. Settling, and
4. External loads.

The governing equations for refractory and labile particulate organic carbons are:

$$\frac{\partial RPOC}{\partial t} = \sum_{x=c,d,g,m} FCRP_X PR_X B_X - K_{RPOC} RPOC + \frac{\partial}{\partial Z}(WS_{RP} RPOC) + \frac{WRPOC}{V} \tag{8.32}$$

$$\frac{\partial LPOC}{\partial t} = \sum_{x=c,d,g,m} FCLP_X PR_X B_X - K_{LPOC} LPOC + \frac{\partial}{\partial Z}(WS_{LP} LPOC) + \frac{WLPOC}{V} \tag{8.33}$$

where,

$RPOC$ is the concentration of refractory particulate organic carbon ($g\,C/m^3$),

$LPOC$ is the concentration of labile particulate organic carbon ($g\,C/m^3$),

$FCRP$ is the fraction of predated carbon produced as refractory particulate organic Carbon,

$FCLP$ is the fraction of predated carbon produced as labile particulate organic carbon,

K_{RPOC} is the dissolution rate of refractory particulate organic carbon ($1/day$),

K_{LPOC} is the dissolution rate of labile particulate organic carbon ($1/day$),

WS_{RP} is the settling velocity of refractory particulate organic matter (m/day),

W_{LP} is the settling velocity of labile particulate organic matter (m/day),

$WRPOC$ is the external loads of refractory particulate organic carbon ($g\,C/day$), and

$WLPOC$ is the external loads of labile particulate organic carbon ($g\,C/day$.)

8.2.3.2.2 Dissolved Organic Carbon

Sources and sinks for dissolved organic carbon included in the model are (Figure 8.1):

1. Algal excretion (exudation) and predation,
2. Dissolution from refractory and labile particulate organic carbon,
3. Heterotrophic respiration of dissolved organic carbon (decomposition),
4. Denitrification, and
5. External loads.

The kinetic equation describing these processes is:

$$\frac{\partial DOC}{\partial t} = \sum_{x=c,d,g,m} \left[FCD_X + (1 - FCD_X) \left(\frac{KHR_X}{KHR_X + DO} \right) \right] BM_X B_X + FCDP_X PR_X B_X + K_{RPOC} RPOC + K_{LPOC} LPOC - K_{HR} DOC - Denit DOC + \frac{WDOC}{V} \quad (8.34)$$

where,

DOC is the concentration of dissolved organic carbon ($g\,C/m^3$),

FCD_x is the fraction of basal metabolism exuded as dissolved organic carbon at infinite dissolved oxygen concentration for algal group x,

KHR_x is the half-saturation constant of dissolved oxygen for algal dissolved organic carbon excretion for group x ($g\,O_2/m^3$),

DO is the dissolved oxygen concentration ($g\,O_2/m^3$),

$FCDP$ is the fraction of predated carbon produced as dissolved organic carbon,

K_{HR} is the heterotrophic respiration rate of dissolved organic carbon ($1/day$),

$Denit$ is the denitrification rate ($1/day$),

$BFDOC$ is the benthic flux of dissolved organic carbon in bottom layer only ($g\,C/m^2/day$), and

$WDOC$ is the external loads of dissolved organic carbon ($g\,C/day$).

The remainder of this section explains each term in equations (8.32)-(8.34).

8.2.3.2.3 Effect of Algae on Organic Carbon

The terms within summation (Σ) in equations (8.32)-(8.34) account for the effects of algae on organic carbon through basal metabolism and predation.

8.2.3.2.3.1 Basal Metabolism

Basal metabolism, consisting of respiration and excretion, returns algal matter (carbon, nitrogen, phosphorus, and silica) back to the environment. Loss of algal biomass through basal metabolism is:

$$\frac{\partial B_x}{\partial t} = -BM_x B_x \tag{8.35}$$

The equation (8.35) indicates that the total loss of algal biomass due to basal metabolism is independent of ambient dissolved oxygen concentration. In this model, it is assumed that the distribution of total loss between respiration and excretion is constant as long as there is sufficient dissolved oxygen for algae to respire. Under that condition, the losses by respiration and excretion may be written as:

$$(1 - FCD_x)\, BM_x B_x \ : \text{ respiration} \tag{8.36}$$

$$FCD_x BM_x B_x \ : \text{ excretion} \tag{8.37}$$

where, FCD_x is a constant of value between 0 and 1.0.

Algae cannot respire in the absence of oxygen, however. Although the total loss of algal biomass due to basal metabolism is oxygen independent (equation (8.35)), the distribution of total loss between respiration and excretion is oxygen-dependent. When oxygen level is high, respiration is a large fraction of the total. As dissolved oxygen becomes scarce, excretion becomes dominant. Thus, equation (8.36) represents the loss by respiration only at high oxygen levels. In general, equation (8.36) can be decomposed into two fractions as a function of dissolved oxygen availability:

$$(1 - FCD_x) \left(\frac{DO}{KHR_x + DO} \right) BM_x B_x \ : \text{ respiration} \tag{8.38}$$

$$(1 - FCD_x) \left(\frac{KHR_x}{KHR_x + DO} \right) BM_x B_x \ : \text{ excretion} \tag{8.39}$$

where, KHR_x is the metabolic DO coefficient ($g/m^3\ O_2$).

Equation (8.38) represents the loss of algal biomass by respiration, and equation (8.39) represents additional excretion due to insufficient dissolved oxygen concentration. The parameter KHR_x, which is defined as the half-saturation constant of dissolved oxygen for algal dissolved organic carbon excretion in equation (8.34), can also be defined as the half-saturation constant of dissolved oxygen for algal respiration in equation (8.39).

Combining equations (8.37) and (8.39) the total loss due to excretion is:

$$\left[FCD_X + (1 + FCD_X) \left(\frac{KHR_X}{KHR_X + DO} \right) \right] BM_X B_X \tag{8.40}$$

Equations (8.38) and (8.40) combine to give the total loss of algal biomass due to basal metabolism $BM_x AB_x$, equation (8.35). The definition of FCD_x in equation (8.34) becomes

apparent in equation (8.40), (i.e., fraction of basal metabolism exuded as dissolved organic carbon at infinite dissolved oxygen concentration). At zero oxygen level, 100 percent of total loss due to basal metabolism is by excretion regardless of FCD_x. The end carbon product of respiration is primarily carbon dioxide, an inorganic form not considered in the present model, while the end carbon product of excretion is primarily dissolved organic carbon. Therefore, equation (8.40), that appears in equation (8.34), represents the contribution of excretion to dissolved organic carbon, and there is no source term for particulate organic carbon from algal basal metabolism in equations (8.32) and (8.33).

Although this general formulation is incorporated for consistency with the original CE-QUAL-IMC formulation (Cerco and Cole, 1995), most of the subsequent applications of CE-QUAL-ICM have simplified the basal metabolism in the published *DOC* and *DO* equations or specified input parameters which effectively set KHR_x and FCD_x to zero (see Table 8.2), which results in simplifying the *DOC* equation to

$$\frac{\partial DOC}{\partial t} = \sum_{x=c,d,g,m} FCDP_X PR_X B_X + K_{RPOC} RPOC + K_{LPOC} LPOC - K_{HR} DOC - Denit\ DOC + \frac{WDOC}{V} \quad (8.41)$$

8.2.3.2.3.2 Predation

Algae produce organic carbon through the effects of predation. Zooplankton take up and redistribute algal carbon through grazing, assimilation, respiration, and excretion. Since zooplankton are not included in the model, routing of algal carbon through zooplankton predation is simulated by empirical distribution coefficients in equations (8.32) to (8.34); *FCRP*, *FCLP*, and *FCDP*. The sum of these three predation fractions should be unity.

8.2.3.2.4 Heterotrophic Respiration and Dissolution

The refractory and labile particulate organic carbon equations (8.32) and (8.34) contain decay terms that represent dissolution of particulate material into dissolved material. These terms appear in equation (8.34) as sources. The third sink term in the *DOC* equation (8.34) represents heterotrophic respiration of dissolved organic carbon. The oxic heterotrophic respiration is a function of dissolved oxygen; the lower the dissolved oxygen, the smaller the respiration term becomes. Heterotrophic respiration rate, therefore, is expressed using a Monod function of dissolved oxygen:

$$K_{HR} = \left(\frac{DO}{KHOR_{DO} + DO} \right) K_{DOC} \quad (8.42)$$

where,

Table 8.2. Basal Metabolism Formulations and Parameter in CE-QUAL-ICM

Study	FCD_x and KHR_x in DOC Equation	$FCDx$ and KHR_x in from DO Equation
Cerco and Cole (1995) (Chesapeake Bay)	General	General
Bunch et al. (2000) (San Juan Bay, PR)	General (used $FCD = 0$, $KHRx = 0.5$)	General (used $FCD = 0$, $KHRx = 0.5$)
Cerco et al. (2000) (Florida Bay)	No BMx source in equation, implies $FCD_x = 0$, $KHR_x = 0$	Consistent with $FCD_x = 0$, $KHR_x = 0$
Cerco et al. (2002) (Chesapeake Bay, Trib. Refinements)	No BMx source in equation, implies $FCD_x = 0$, $KHR_x = 0$	Consistent with $FCD_x = 0$, $KHR_x = 0$
Cerco et al. (2004) (Lake Washington)	Equation implies $KHR_x = 0$ (used $FCD_x = 0$)	Consistent with $KHR_x = 0$ (used $FCD_x = 0$)
Tillman et al. (2004) (St. Johns River)	No BM_x source in equation, implies $FCD_x = 0$, $KHR_x = 0$	Consistent with $FCD_x = 0$, $KHR_x = 0$

$KHOR_{DO}$ is the oxic respiration half-saturation constant for dissolved oxygen ($g\ O_2/m^3$), and

$KDOC$ is the heterotrophic respiration rate of dissolved organic carbon at infinite dissolved oxygen concentration ($1/day$).

Dissolution and heterotrophic respiration rates depend on the availability of carbonaceous substrate and on heterotrophic activity. Algae produce labile carbon that fuels heterotrophic activity: dissolution and heterotrophic respiration do not require the presence of algae though, and may be fueled entirely by external carbon inputs. In the model, algal biomass, as a surrogate for heterotrophic activity, is incorporated into formulations of dissolution and heterotrophic respiration rates. Formulations of these rates require specification of algal-dependent and algal- independent rates:

$$K_{RPOC} = \left(K_{RC} + K_{RCalg} \sum_{x=c,d,g} B_x \right) \exp\left(KT_{HDR}\left(T - TR_{HDR}\right)\right) \tag{8.43}$$

$$K_{LPOC} = \left(K_{LC} + K_{LCalg} \sum_{x=c,d,g} B_x \right) \exp\left(KT_{HDR}\left(T - TR_{HDR}\right)\right) \tag{8.44}$$

$$K_{DOC} = \left(K_{DC} + K_{DCalg} \sum_{x=c,d,g} B_x \right) \exp\left(KT_{MIN} \left(T - TR_{MIN} \right) \right) \tag{8.45}$$

where,

K_{RC} is the minimum dissolution rate of refractory particulate organic carbon $(1/day)$,

K_{LC} is the minimum dissolution rate of labile particulate organic carbon $(1/day)$,

K_{DC} is the minimum respiration rate of dissolved organic carbon $(1/day)$,

K_{RCalg}, K_{LCalg} are the constants that relate dissolution of refractory and labile particulate organic carbon, respectively, to algal biomass $(1/day;\ per\ g\ C/m^3)$,

K_{DCalg} is the constant that relates respiration to algal biomass $(1/day\ per\ g\ C/m^3)$,

KT_{HDR} is the effect of temperature on hydrolysis of particulate organic matter $(1/^{\circ}C)$,

TR_{HDR} is the reference temperature for hydrolysis of particulate organic matter $(^{\circ}C)$,

KT_{MIN} is the effect of temperature on mineralization of dissolved organic matter $(1/^{\circ}C)$, and

TR_{MIN} is the reference temperature for mineralization of dissolved organic matter $(^{\circ}C)$.

Equations (8.43) to (8.45) have exponential functions that relate rates to temperature.

In the present model, the term "hydrolysis" is defined as the process by which particulate organic matter is converted to dissolved organic form, and thus includes both dissolution of particulate carbon and hydrolysis of particulate phosphorus and nitrogen. Therefore, the parameters KT_{HDR} and TR_{HDR}, are also used for the temperature effects on hydrolysis of particulate phosphorus (equations (8.58) and (8.59)) and nitrogen (equations (8.73) and (8.74)). The term "mineralization" is defined as the process by which dissolved organic matter is converted to dissolved inorganic form, and thus includes both heterotrophic respiration of dissolved organic carbon and mineralization of dissolved organic phosphorus and nitrogen. Therefore, the parameters, KT_{MIN} and TR_{MIN}, are also used for the temperature effects on mineralization of dissolved phosphorus (8.60) and nitrogen (8.75).

8.2.3.2.5 Effect of Denitrification on Dissolved Organic Carbon

As oxygen is depleted from natural systems, organic matter is oxidized by the reduction of alternate electron acceptors. Thermodynamically, the first alternate acceptor reduced in the absence of oxygen is nitrate. The reduction of nitrate by a large number of heterotrophic anaerobes is referred to as denitrification, and the stoichiometry of this reaction is Stumm et al. (1970).

$$4NO_3^- + 4H^+ + 5CH_2O \rightarrow 2N_2 + 7H_2O + 5CO_2 \tag{8.46}$$

The last term in the equation (8.34) accounts for the effect of denitrification on dissolved organic carbon. The kinetics of denitrification in the model are first-order:

$$Denit = \left(\frac{KROR_{DO}}{KROR_{DO}+DO}\right)\left(\frac{NO3}{KHDN_N+NO3}\right)AANOX K_{DOC} \tag{8.47}$$

where,

$KROR_{DO}$ is the denitrification half-saturation constant for dissolved oxygen ($g\ O/m^3$),

$KHDN_N$ is the denitrification half-saturation constant for nitrate ($g\ N/m^3$), and

$AANOX$ is the ratio of denitrification rate to oxic dissolved organic carbon respiration rate.

In equation (8.47), the dissolved organic carbon respiration rate K_{DOC}, is modified so that significant decomposition via denitrification occurs only when nitrate is freely available and dissolved oxygen is depleted. The ratio $AANOX$, makes the anoxic respiration slower than oxic respiration. Note that K_{DOC}, defined in equation (8.45), includes the temperature effect on denitrification.

8.2.3.2.6 Labile and Refractory Splitting of Dissolved Organic Carbon

A number of water quality models, including the CE-QUAL-ICM application to the St. Johns River, Florida (Tillman et al., 2004) split dissolved organic carbon into labile and refractory components. The refractory component equation is

$$\frac{\partial RDOC}{\partial t} = \sum_{x=c,d,g,m} FCRDP_X\ PR_X\ B_X - K_{RDOC}RDOC + \frac{WRDOC}{V} \tag{8.48}$$

where,

$RDOC$ is the concentration of dissolved organic carbon ($g\ C/m^3$),

$FCRDP$ is the fraction of predated carbon produced as dissolved organic carbon,

K_{RDOC} is the respiration rate of refractory dissolved organic carbon ($1/day$), and

$WRDOC$ is the external loads of dissolved organic carbon ($g\ C/day$).

The decay term in (8.48) can include a photoreaction component. The labile component equation retains the general form of the DOC equation

$$\frac{\partial LDOC}{\partial t} = \sum_{x=c,d,g,m} FCLDP\ PR_X\ B_X + K_{RPOC}RPOC + K_{LPOC}LPOC - K_{LDOC}LDOC - Denit\ LDOC + \frac{WLDOC}{V} \tag{8.49}$$

where,

$LDOC$ is the concentration of dissolved organic carbon ($g\,C/m^3$),

$FCLDP$ is the fraction of predated carbon produced as dissolved organic carbon,

K_{LDOC} is the respiration rate of labile dissolved organic carbon ($1/day$), and

$WLDOC$ is the external loads of dissolved organic carbon ($g\,C/day$).

Equations (8.48) and (8.49) follow from Tillman et al. (2004), but are not currently implemented in the EFDC+ water quality model.

8.2.3.3 Phosphorus

The present model has four state variables for phosphorus: three organic forms (refractory particulate, labile particulate, and dissolved) and one inorganic form representing the sum of dissolved and particulate phosphate in the water phase, but exclude phosphate in algae cells.

8.2.3.3.1 Particulate Organic Phosphorus

For refractory and labile particulate organic phosphorus, sources and sinks included in the model are (Figure 8.1);

1. Algal basal metabolism and predation,
2. Dissolution to dissolved organic phosphorus,
3. Settling, and
4. External loads.

The kinetic equations for refractory and labile particulate organic phosphorus are;

$$\frac{\partial RPOP}{\partial t} = \sum_{x=c,d,g,m} (FPR_X\ BM_X + FPRP_X PR_X) APC_X B_X - K_{RPOP} RPOP + \frac{\partial}{\partial Z}(WS_{RP} RPOP) + \frac{WRPOP}{V} \quad (8.50)$$

$$\frac{\partial LPOP}{\partial t} = \sum_{x=c,d,g,m} (FPL_X\ BM_X + FPLP_X\ PR_X) APC_X B_X - K_{LPOP} LPOP + \frac{\partial}{\partial Z}(WS_{RP} LPOP) + \frac{WLPOP}{V} \quad (8.51)$$

where,

$RPOP$ is the concentration of refractory particulate organic phosphorus ($g\ P/m^3$),

$LPOP$ is the concentration of labile particulate organic phosphorus ($g\ P/m^3$),

FPR_x is the fraction of metabolized phosphorus by algal group x produced as refractory particulate organic phosphorus,

FPL_x is the fraction of metabolized phosphorus by algal group x produced as labile particulate organic phosphorus,

$FPRP$ is the fraction of predated phosphorus produced as refractory particulate organic phosphorus,

$FPLP$ is the fraction of predated phosphorus produced as labile particulate organic phosphorus,

APC is the mean algal phosphorus-to-carbon ratio for all algal groups ($g\ P\ per\ g\ C$),

K_{RPOP} is the hydrolysis rate of refractory particulate organic phosphorus ($1/day$),

K_{LPOP} is the hydrolysis rate of labile particulate organic phosphorus ($1/day$),

$WRPOP$ is the external loads of refractory particulate organic phosphorus ($g\ P/day$), and

$WLPOP$ is the external loads of labile particulate organic phosphorus ($g\ P/day$).

8.2.3.3.2 Dissolved Organic Phosphorus

Sources and sinks for dissolved organic phosphorus included in the model are (Figure 8.1);

1. Algal basal metabolism and predation,
2. Dissolution from refractory and labile particulate organic phosphorus,
3. Mineralization to phosphate phosphorus, and
4. External loads.

The kinetic equation describing these processes is:

$$\frac{\partial DOP}{\partial t} = \sum_{x=c,d,g,m} (FPD_X\ BM_X + FPDP_X\ PR_X) APC_X B_X + K_{RPOP} RPOP + K_{LPOP} LPOP - K_{DOP} DOP + \frac{WDOP}{V} \quad (8.52)$$

where

DOP is the concentration of dissolved organic phosphorus ($g\ P/m^3$),

FPD_x is the fraction of metabolized phosphorus by algal group x produced as dissolved organic phosphorus,

$FPDP_x$ is the fraction of predated phosphorus produced as dissolved organic phosphorus,

K_{DOP} is the mineralization rate of dissolved organic phosphorus ($1/day$), and

$WDOP$ is the external loads of dissolved organic phosphorus ($g\ P/day$).

8.2.3.3.3 Total Water Phase Phosphate

For total phosphate that includes both dissolved and sorbed phosphate in the water phase, sources and sinks included in the model are;

1. Algal basal metabolism, predation, and uptake,
2. Mineralization from dissolved organic phosphorus,
3. Settling of sorbed phosphate,
4. Sediment-water exchange of dissolved phosphate for the bottom layer only, and
5. External loads.

The kinetic equation describing these processes is

$$\frac{\partial}{\partial t}(PO4p + PO4d) = \sum_{x=c,d,g,m}(FPI_X\ BM_X + FPIP_X\ PR_X - P_X)APC_X B_X + K_{DOP}DOP + \frac{\partial}{\partial Z}(WS_{TSS}PO4p) + \frac{BFPO4d}{\Delta Z} + \frac{WPO4p}{V} + \frac{WPO4d}{V} \quad (8.53)$$

where,

$PO4t = PO4d + PO4p$ is the total phosphate ($g\ P/m^3$),

$PO4d$ is the dissolved phosphate ($g\ P/m^3$),

$PO4p$ is the particulate (sorbed) phosphate ($g\ P/m^3$),

FPI_x is the fraction of metabolized phosphorus by algal group x produced as inorganic phosphorus,

$FPIP$ is the fraction of predated phosphorus produced as inorganic phosphorus,

WS_{TSS} is the settling velocity of suspended solid (m/day), provided by the hydrodynamic model,

$BFPO4d$ is the sediment-water exchange flux of phosphate ($g\ P/m^2/day$), applied to the bottom layer only, and

$WPO4t$ is the external loads of total phosphate ($g\ P/day$).

In equation (8.53), if the total active metal is chosen as a measure of sorption site, the settling velocity of total suspended solid WS_{TSS}, is replaced by that of particulate metal WS_s. The remainder of this section explains each term in equations (8.50) to (8.53). Alternate forms of the total phosphate equation are discussed in next paragraph.

8.2.3.3.4 Total Phosphate System

Suspended and bottom sediment particles (clay, silt, and metal hydroxides) adsorb and desorb phosphate in river and estuarine waters. This adsorption-desorption process buffers phosphate concentration in the water column and enhances the transport of phosphate away from its external sources (Carritt and Goodgal, 1954; Froelich, 1988). To ease the computational complication due to the adsorption-desorption of phosphate, dissolved and sorbed phosphate are treated and transported as a single state variable. Therefore, the model phosphate state variable total phosphate, is defined as the sum of dissolved and sorbed phosphate (equation (8.53)), and the concentrations for each fraction are determined by equilibrium partitioning of their sum.

In CE-QUAL-ICM, sorption of phosphate to particulate species of metals including iron and manganese was considered based on a phenomenon observed in the monitoring data from the mainstem of the Chesapeake Bay: phosphate was rapidly depleted from anoxic bottom waters during the autumn reaeration event (Cerco and Cole, 1994). Their hypothesis was; reaeration of bottom waters caused dissolved iron and manganese to precipitate, and phosphate sorbed to newly formed metal particles and rapidly settled to the bottom. One state variable total active metal, in CE-QUAL-ICM was defined as the sum of all metals that acts as sorption sites, and the total active metal was partitioned into particulate and dissolved fractions via an equilibrium partitioning coefficient. Then phosphate was assumed to sorb to only the particulate fraction of the total active metal.

In the treatment of phosphate sorption in CE-QUAL-ICM, the particulate fraction of metal hydroxides was emphasized as a sorption site in bottom waters under anoxic conditions. Phosphorus is a highly particle-reactive element, and phosphate in solution reacts quickly with a wide variety of surfaces, being taken up by and released from particles Froelich (1988). The present model has two options, total suspended solids and total active metal, as a measure of a sorption site for phosphate, and dissolved and sorbed fractions are determined by equilibrium partitioning of their sum as a function of total suspended solids or total active metal concentration:

$$PO4p = \left(\frac{K_{PO4p}SORPS}{1+K_{PO4p}SORPS}\right)(PO4p+PO4d)$$
$$PO4p = \left(\frac{1}{1+K_{PO4p}SORPS}\right)(PO4p+PO4d) \quad (8.54)$$
$$SORPS = SED \text{ or } TAM_P$$

where,

$KPO4p$ is the empirical coefficient relating phosphate sorption to total suspended solid ($per\ g/m^3$) or particulate total active metal ($per\ mol/m^3$) concentration,

SED is the inorganic sediment concentration (mg/l), and

$TAMp$ is the particulate total active metal (mol/m^3).

The definition of the partition coefficient alternately follows form (8.54)

$$K_{PO4p} = \frac{PO4p}{PO4d}\frac{1}{TSS} \quad (8.55)$$
$$K_{PO4p} = \frac{PO4p}{PO4d}\frac{1}{TAMp} \quad (8.56)$$

where the meaning of K_{PO4p} becomes apparent, i.e., the ratio of sorbed to dissolved phosphate per unit concentration of total suspended solid or particulate total active metal (i.e., per unit sorption site available).

8.2.3.3.5 Algal Phosphorus-to-Carbon Ratio (APC)

Algal biomass is quantified in units of carbon per volume of water. In order to express the effects of algal biomass on phosphorus and nitrogen, the ratios of phosphorus-to-carbon and nitrogen-to-carbon in algal biomass must be specified. Although global mean values of these ratios are well known (Redfield, 1963), algal composition varies especially as a function of nutrient availability. As phosphorus and nitrogen become scarce, algae adjust their composition so that smaller quantities of these vital nutrients are required to produce carbonaceous biomass (Di Toro, 1980). Examining the field data from the surface of upper Chesapeake Bay, Cerco and Cole (1993) showed that the variation of nitrogen-to-carbon stoichiometry was small and thus used a constant algal nitrogen-to-carbon ratio $ANCx$. Large variations, however, were observed for algal phosphorus-to-carbon ratio indicating the adaptation of algae to ambient phosphorus concentration (Cerco and Cole, 1993); algal phosphorus content is high when ambient phosphorus is abundant and is low when ambient phosphorus is scarce. Thus, a variable algal phosphorus-to-carbon ratio APC, is used in model formulation. A mean ratio for all algal groups APC, is described by an empirical approximation to the trend observed in field data (Cerco and Cole, 1994):

$$APC = \left(CP1_{prm} + CP2_{prm}\exp\left(-CP3_{prmPO4d}\right)\right)^{-1} \tag{8.57}$$

where

$CP1_{prm}$ is the minimum carbon-to-phosphorus ratio ($g\ C\ per\ g\ P$),

$CP2_{prm}$ is the difference between minimum and maximum carbon-to-phosphorus ratio ($g\ C\ per\ g\ P$), and

$CP3_{prm}$ is the effect of dissolved phosphate concentration on carbon-to-phosphorus ratio ($per\ g\ P/m^3$).

8.2.3.3.6 Effect of Algae on Phosphorus

The terms within summation in equations (8.50) to (8.53) account for the effects of algae on phosphorus. Both basal metabolism (respiration and excretion) and predation are considered, and thus formulated, to contribute to organic and phosphate phosphorus. That is, the total loss by basal metabolism (BM_xAB_x) is distributed using distribution coefficients (FPR_x, FPL_x, FPD_x, and FPI_x). The total loss by predation (PR_xAB_x), is also distributed using distribution coefficients ($FPRP$,$FPLP$, $FPDP$, and $FPIP$). The sum of four distribution coefficients for basal metabolism should be unity, and as is the sum for predation. Algae take up dissolved phosphate for growth, and algae uptake of phosphate is represented by ($-3P_xAAPCAB_x$) in equation (8.53).

8.2.3.3.7 Mineralization and Hydrolysis

The third term on the RHS of equations (8.50) and (8.51) represents hydrolysis of particulate organic phosphorus and the last term in equation (8.52) represents mineralization of dissolved organic phosphorus. Mineralization of organic phosphorus is mediated by the release of nucleotidase and phosphatase enzymes by bacteria Chróst and Overbeck (1987) and algae Boni et al. (1989). Since the algae themselves release the enzymes and bacterial abundance is related to algal biomass, the rate of organic phosphorus mineralization is related to algal biomass in model formulation. Another mechanism included in the model formulation is that algae stimulate production of an enzyme that mineralizes organic phosphorus to phosphate when phosphate is scarce (Boni et al., 1989; Chróst and Overbeck, 1987). The formulations for hydrolysis and mineralization rates including these processes are:

$$K_{RPOP} = \left(K_{RP} + \left(\frac{KHP}{KHP + PO4d}\right) K_{RPalg} \sum_{x=c,d,g,m} B_x\right) \exp\left(KT_{HDR}\left(T - TR_{HDR}\right)\right) \tag{8.58}$$

$$K_{LPOP} = \left(K_{LP} + \left(\frac{KHP}{KHP + PO4d} \right) K_{LPalg} \sum_{x=c,d,g,m} B_x \right) \exp\left(KT_{HDR} \left(T - TR_{HDR} \right) \right) \tag{8.59}$$

$$K_{DOP} = \left(K_{DP} + \left(\frac{KHP}{KHP + PO4d} \right) K_{DPalg} \sum_{x=c,d,g,m} B_x \right) \exp\left(KT_{MIN} \left(T - TR_{MIN} \right) \right) \tag{8.60}$$

where

K_{RP} is the minimum hydrolysis rate of refractory particulate organic phosphorus $(1/day)$,

K_{LP} is the minimum hydrolysis rate of labile particulate organic phosphorus $(1/day)$,

K_{DP} is the minimum mineralization rate of dissolved organic phosphorus $(1/day)$,

K_{RPalg} and K_{LPalg} are the constants that relate hydrolysis of refractory and labile particulate organic phosphorus, respectively, to algal biomass $(1/day\ per\ g\ C/m^3)$,

K_{DPalg} is the constant that relates mineralization to algal biomass $(1/day\ per\ g\ C/m^3)$, and

KHP is the mean half-saturation constant for algal phosphorus uptake $(g\ P/m^3)$.

$$KHP = \frac{\sum_{x=c,d,g,m} KHP_X}{\sum_{x=c,d,g,m} x} \tag{8.61}$$

When phosphate is abundant relative to KHP, the rates are close to the minimum values with little influence from algal biomass. When phosphate becomes scarce relative to KHP, the rates increase with the magnitude of increase depending on algal biomass. Equations (8.58) to (8.60) have exponential functions that relate rates to temperature.

8.2.3.3.8 Alternate Forms of the Total Phosphate Equation

In the CE-QUAL-ICM model (Cerco and Cole, 1995), total phosphate is defined to include dissolved phosphate in algae cells. The phosphate in algae cells is given by

$$\frac{\partial PO4a}{\partial t} = \sum_{x=c,d,g,m} (APC\ B_X)$$
$$= \sum_{x=c,d,g,m} (P_X - FPI_X\ BM_X - FPIP\ PR_X)\ APC_X\ B_X$$
$$- \sum_{x=c,d,g,m} (FPR_X\ BM_X + FPRP\ PR_X)\ APC_X\ B_X$$
$$- \sum_{x=c,d,g,m} (FPL_X\ BM_X + FPLP\ PR_X)\ APC_X\ B_X$$
$$- \sum_{x=c,d,g,m} (FPD_X\ BM_X + FPDP\ PR_X)\ APC_X\ B_X$$
$$+ \frac{\partial}{\partial Z}\left(\sum_{x=c,d,g,m} WS_{AlgX}\ APC_X B_X\right) \quad (8.62)$$

Where the first term on the right side represents net uptake of phosphate from the water column, and the subsequent three terms represent loss of organic phosphorous. Noting that the distribution factors for basal metabolism and predation must sum to unity, (8.62) reduces to

$$\frac{\partial PO4a}{\partial t} = \sum_{x=c,d,g,m} (P_X - BM_X - PR_X) APC_X\ B_X + \frac{\partial}{\partial Z}\left(\sum_{x=c,d,g,m} WS_{AlgX}\ APC_X B_X\right) \quad (8.63)$$

which is simply equation (8.6) multiplied by the algae phosphorous to carbon ratio and summed over all algae species. Combining (8.63) with (8.64) gives

$$\frac{\partial}{\partial t}(PO4p + PO4d + PO4a) =$$
$$K_{DOP}DOP - \sum_{x=c,d,g,m} ((1 - FPI_X)BM_X + (1 - FPIP)PR_X) APC_X\ B_X$$
$$+ \frac{\partial}{\partial Z}\left(WS_{TSS}PO4p + \sum_{x=c,d,g,m} WS_{AlgX}\ APC_X B_X\right) +$$
$$\frac{BFPO4d}{\Delta Z} + \frac{WPO4p}{V} + \frac{WPO4d}{V} \quad (8.64)$$

It is noted that this equation differs from Cerco and Cole (1995, equation (3-51)), which is in error, but is identical to the subsequently corrected in Cerco et al. (2000, equation 35) which documents the Florida Bay CE-QUAL-ICM model application. Thus, either equations (8.53) or (8.64) can be used for total phosphate as long as partitioning between particulate and dissolved phosphate in the water phase is appropriately represented by equations (8.54) and (8.66).

8.2.3.3.9 Labile and Refractory Splitting of Dissolve Organic Phosphorous

A number of water quality models, including the CE-QUAL-ICM application to the St. Johns River, Florida (Tillman et al., 2004) split dissolved organic phosphorous into labile and refractory components. The refractory component equation is

$$\frac{\partial RDOP}{\partial t} = \sum_{x=c,d,g,m} (FPRD_X\ BM_X + FPRDP_X\ PR_X)\ APC_X\ B_X - K_{RDOP}RDOP + \frac{WRDOP}{V} \quad (8.65)$$

where,

$RDOP$ is the concentration of refractory dissolved organic phosphorus ($g\ P/m^3$),

$FPRD_x$ is the fraction of metabolized phosphorus by algal group x produced as refractory dissolved organic phosphorus,

$FPRDP$ is the fraction of predated phosphorus produced as refractory dissolved organic phosphorus,

K_{RDOP} is the mineralization rate of refractory dissolved organic phosphorus ($1/day$), and

$WRDOP$ is the external loads of refractory dissolved organic phosphorus ($g\ P/day$).

The labile component equation is

$$\frac{\partial LDOP}{\partial t} = \sum_{x=c,d,g,m} (FPLD_X\ BM_X + FPLDP_X\ PR_X)\ APC_X\ B_X - K_{RDOP}RDOP + K_{LPOP}LPOP - K_{LDOP}LDOP + \frac{WLDOP}{V} \quad (8.66)$$

where,

$LDOP$ is the concentration of dissolved organic phosphorus ($g\ P/m^3$),

$FPLD_x$ is the fraction of metabolized phosphorus by algal group x produced as dissolved organic phosphorus,

$FPLDP$ is the fraction of predated phosphorus produced as dissolved organic phosphorus,

K_{LDOP} is the mineralization rate of dissolved organic phosphorus ($1/day$), and

$WLDOP$ is the external loads of dissolved organic phosphorus ($g\ P/day$).

Equations (8.65) and (8.66) follow from Tillman et al. (2004), but are not currently implemented in the EFDC+ water quality model.

8.2.3.4 Nitrogen

The present model has five state variables for nitrogen: three organic forms (refractory particulate, labile particulate, and dissolved) and two inorganic forms (ammonium and nitrate). The nitrate state variable in the model represents the sum of nitrate and nitrite.

8.2.3.4.1 Particulate Organic Nitrogen

For refractory and labile particulate organic nitrogen, sources and sinks included in the model are (Figure 8.1);

1. Algal basal metabolism and predation,
2. Dissolution to dissolved organic nitrogen,
3. Settling, and
4. External loads.

The kinetic equations for refractory and labile particulate organic nitrogen are:

$$\frac{\partial RPON}{\partial t} = \sum_{x=c,d,g,m} (FNR_X\ BM_X + FNRP_X\ PR_X)\ ANC_X\ B_X - K_{RPON}RPON + \frac{\partial}{\partial Z}(WS_{RP}RPON) + \frac{WRPON}{V} \quad (8.67)$$

$$\frac{\partial LPON}{\partial t} = \sum_{x=c,d,g,m} (FNL_X\ BM_X + FNLP_X\ PR_X)\ ANC_X\ B_X - K_{LPON}LPON + \frac{\partial}{\partial Z}(WS_{LP}LPON) + \frac{WLPON}{V} \quad (8.68)$$

where,

$RPON$ is the concentration of refractory particulate organic nitrogen ($g\,N/m^3$),

$LPON$ is the concentration of labile particulate organic nitrogen ($g\,N/m^3$),

FNR_x is the fraction metabolized nitrogen by algal group x as refractory particulate organic nitrogen,

FNL_x is the fraction of metabolized nitrogen by algal group x produced as labile particulate organic nitrogen,

$FNRP$ is the fraction of predated nitrogen produced as refractory particulate organic nitrogen,

$FNLP$ is the fraction of predated nitrogen produced as labile particulate organic nitrogen,

ANC_x is the nitrogen-to-carbon ratio in algal group x (g; N; $per\ g\ C$),

K_{RPON} is the hydrolysis rate of refractory particulate organic nitrogen ($1/day$),

K_{LPON} is the hydrolysis rate of labile particulate organic nitrogen ($1/day$),

$WRPON$ is the external loads of refractory particulate organic nitrogen ($g\ N/day$), and

$WLPON$ is the external loads of labile particulate organic nitrogen ($g\ N/day$).

8.2.3.4.2 Dissolved Organic Nitrogen

Sources and sinks for dissolved organic nitrogen included in the model are (Figure 8.1);

1. Algal basal metabolism and predation,
2. Dissolution from refractory and labile particulate organic nitrogen,
3. Mineralization to ammonium, and
4. External loads.

The kinetic equation describing these processes is:

$$\frac{\partial DON}{\partial t} = \sum_{x=c,d,g,m} (FND_X\ BM_X + FNDP_X\ PR_X)\ ANC_X\ B_X + K_{RPON}RPON + K_{LPON}LPON - K_{DON}DON + \frac{BFDON}{\Delta Z} + \frac{WDON}{V} \quad (8.69)$$

where

DON is the concentration of dissolved organic nitrogen ($g\ N/m^3$),

FND_x is the fraction of metabolized nitrogen by algal group x produced as dissolved organic nitrogen,

$FNDP$ is the fraction of predated nitrogen produced as dissolved organic nitrogen,

K_{DON} is the mineralization rate of dissolved organic nitrogen ($1/day$),

$BFDON$ is the benthic flux of dissolved organic nitrogen in bottom layer only ($g\ C/m^2/day$), and

$WDON$ is the external loads of dissolved organic nitrogen ($g\ N/day$).

8.2.3.4.3 Ammonium Nitrogen

Sources and sinks for ammonia nitrogen included in the model are (Figure 8.1):

1. Algal basal metabolism, predation, and uptake,
2. Mineralization from dissolved organic nitrogen,
3. Nitrification to nitrate,
4. Sediment-water exchange for the bottom layer only, and
5. External loads.

The kinetic equation describing these processes is:

$$\frac{\partial NH4}{\partial t} = \sum_{x=c,d,g,m} \left(FNI_X\ BM_X + FNIP_X\ PR_X - PN_X\ P_X\right)\ ANC_X\ B_X + K_{DON}DON - KNit\ NH4 + \frac{BFNH4}{\Delta Z} + \frac{WNH4}{V} \quad (8.70)$$

where

FNI_x is the fraction of metabolized nitrogen by algal group x produced as inorganic nitrogen,

$FNIP$ is the fraction of predated nitrogen produced as inorganic nitrogen,

PN_x is the preference for ammonium uptake by algal group x $(0 \le PN_x \le 1)$,

$Knit$ is the nitrification rate $(1/day)$ given in equation (8.77),

$BFNH4$ is the sediment-water exchange flux of ammonium $(g\ N/m^2/day)$, applied to the bottom layer only

$WNH4$ is the external loads of ammonium $(g\ N/day)$

The form of the nitrification sink in (8.70) and the subsequent source in the nitrate equation (8.71) differ from that in CE-QUAL-ICM.

8.2.3.4.4 Nitrate Nitrogen

Sources and sinks for nitrate nitrogen included in the model are:

1. Algal uptake,
2. Nitrification from ammonium,
3. Denitrification to nitrogen gas,
4. Sediment-water exchange for the bottom layer only, and

5. External loads.

The kinetic equation describing these processes is:

$$\frac{\partial NO3}{\partial t} = \sum_{x=c,d,g,m} (PN_X - 1) P_X \, ANC_X \, B_X + KNit \, NH4 - ANDC \, Denit \, DOC + \frac{BFNO3}{\Delta Z} + \frac{WNO3}{V} \quad (8.71)$$

where,

$ANDC$ is the mass of nitrate nitrogen reduced per mass of dissolved organic carbon oxidized (0.933 $g\ N\ per\ g\ C$),

$BFNO3$ is the sediment-water exchange flux of nitrate ($g\ N/m^2/day$), applied to the bottom layer only, and

$WNO3$ is the external loads of nitrate ($g\ N/day$).

The remainder of this section explains each term in equations (8.67)-(8.71).

8.2.3.4.5 Effect of Algae on Nitrogen

The terms within summation in equations (8.67) to (8.71) account for the effects of algae on nitrogen. As in phosphorus, both basal metabolism (respiration and excretion) and predation are considered, and thus formulated to contribute to organic and ammonium nitrogen. That is, algal nitrogen released by both basal metabolism and predation are represented by distribution coefficients (FNR_x, FNL_x, FND_x, FNI_x, $FNRP$, $FNLP$, $FNDP$, and $FNIP$). The sum of the four distribution coefficients for basal metabolism should be unity; the sum of the predation distribution coefficients should also be unity.

Algae take up ammonium and nitrate for growth, and ammonium is preferred from thermodynamic considerations. The preference of algae for ammonium is expressed as

$$PN_X = NH4 \left(\frac{NO3}{(KHN_X + NH4)(KHN_X + NO3)} \right) + NH4 \left(\frac{KHN_X}{(NH4 + NO3)(KHN_X + NO3)} \right) \quad (8.72)$$

This equation forces the preference for ammonium to be unity when nitrate is absent, and to be zero when ammonium is absent.

8.2.3.4.6 Mineralization and Hydrolysis

The third term on the RHS of equations (8.67) and (8.68) represents hydrolysis of particulate organic nitrogen and the last term in equation (8.69) represents mineralization of dissolved organic nitrogen. Including a mechanism for accelerated hydrolysis and mineralization during nutrient-limited conditions, the formulations for these processes are:

$$K_{RPON} = \left(K_{RN} + \left(\frac{KHN}{KHN + NH4 + NO3} \right) K_{RNalg} \sum_{x=c,d,g,m} B_x \right) \exp\left(KT_{HDR} \left(T - TR_{HDR} \right) \right) \tag{8.73}$$

$$K_{LPON} = \left(K_{LN} + \left(\frac{KHN}{KHN + NH4 + NO3} \right) K_{LNalg} \sum_{x=c,d,g,m} B_x \right) \exp\left(KT_{HDR} \left(T - TR_{HDR} \right) \right) \tag{8.74}$$

$$K_{DON} = \left(K_{DN} + \left(\frac{KHN}{KHN + NH4 + NO3} \right) K_{DNalg} \sum_{x=c,d,g,m} B_x \right) \exp\left(KT_{MIN} \left(T - TR_{MIN} \right) \right) \tag{8.75}$$

where,

K_{RN} is the minimum hydrolysis rate of refractory particulate organic nitrogen $(1/day)$,

K_{LN} is the minimum hydrolysis rate of labile particulate organic nitrogen $(1/day)$,

K_{DN} is the minimum mineralization rate of dissolved organic nitrogen $(1/day)$,

K_{RNalg} and K_{LNalg} are the constants that relate hydrolysis of refractory and labile particulate organic nitrogen, respectively, to algal biomass $(1/day \text{ per } g\,C/m^3)$,

K_{DNalg} is the constant that relates mineralization to algal biomass $(1/day \text{ per } g\,C/m^3)$, and

KHN is the mean half-saturation constant for algal nitrogen uptake $(g\,N/m^3)$.

$$KHN = \frac{\sum_{x=c,d,g,m} KHN_X}{\sum_{x=c,d,g,m} x} \tag{8.76}$$

Equations (8.73) to (8.75) have exponential functions that relate rates to temperature.

8.2.3.4.7 Nitrification

Nitrification is a process mediated by autotrophic nitrifying bacteria that obtain energy through the oxidation of ammonium to nitrite and of nitrite to nitrate. The stoichiometry of complete reaction is Bowie et al. (1985):

$$NH_4^+ + 2O_2 \rightarrow NO_3^- + H_2O + 2H^+ \tag{8.77}$$

The first term in the second line of equation (8.68) and its corresponding term in equation (8.71) represent the effect of nitrification on ammonium and nitrate, respectively. The kinetics of the complete nitrification process are formulated as a function of available ammonium, dissolved oxygen and temperature:

$$KNit\ NH4 = fNit\ (T)\left(\frac{DO}{KHNit_{DO}+DO}\right)\left(\frac{NH4}{KHNit_N+NH4}\right)Nit_m \tag{8.78}$$

where,

$KHNit_{DO}$ is the nitrification half-saturation constant for dissolved oxygen ($g\ O_2/m^3$),

$KHNit_N$ is the nitrification half-saturation constant for ammonium ($g\ N/m^3$), and

Nit_m is the maximum nitrification rate at $TNit$ ($g\ N/m^3/day$)

This follows the CE-QUAL-ICM model formulation for nitrification. The Monod function of dissolved oxygen in equation (8.76) indicates the inhibition of nitrification at low oxygen level. The Monod function of ammonium indicates that when ammonium is abundant, the nitrification rate is limited by the availability of nitrifying bacteria.

In the EFDC+ water quality model, a reference value of $KNit$ is input into the model instead of Nitm by writing equation (8.78) as

$$KNit = fNit\ (T)\left(\frac{DO}{KHNit_{DO}+DO}\right)\left(\frac{KHNit_N}{KHNit_N+NH4}\right)KNit_m \tag{8.79}$$

where,

$$KNit_m = \frac{Nit_m}{KHNit_N} \tag{8.80}$$

is interpreted as the linear kinetic rate corresponding to $KHNit_N$ equal to unity, since $NH4$ is always must less than unity, and DO effects eliminated by setting $KHNitDO$ to zero. In certain applications, particularly those having long-term BOD and Nitrogen series test results $KNit_m$ is observable.

The temperature function for nitrification in equation (8.78) is given by

$$fNit\ (T) = \begin{cases} \exp\left(-KNit1(T-TNit1)^2\right) & :\ T \le TNit1 \\ 1 & :\ TNit1 \le T \le TNit2 \\ exp\left(-KNit2(T-TNit12)^2\right) & :\ T \ge TNit2 \end{cases} \tag{8.81}$$

where,

$Tnit1$ is the lower optimum temperature for nitrification ($^\circ C$),

$Tnit2$ is the upper optimum temperature for nitrification ($^{\circ}C$),

$KNit1$ is the effect of temperature below $TNit$ on nitrification rate ($1/^{\circ}C^2$), and

$KNit2$ is the effect of temperature above $TNit$ on nitrification rate ($1/^{\circ}C^2$).

The effect of suboptimal temperature is represented using Gaussian form.

8.2.3.4.8 Denitrification

The effect of denitrification on dissolved organic carbon was described in Section 8.2.3.2. Denitrification removes nitrate from the system in stoichiometric proportion to carbon removal as determined by equation (8.46). The sink term in (8.71) represents this removal of nitrate.

8.2.3.4.9 Labile and Refractory Splitting of Dissolved Organic Nitrogen

A number of water quality models, including the CE-QUAL-ICM application to the St. Johns River, Florida (Tillman et al., 2004) split dissolved organic phosphorous into labile and refractory components. The refractory component equation is

$$\frac{\partial RDON}{\partial t} = \sum_{x=c,d,g,m} (FNRD_X\ BM_X + FNRDP_X\ PR_X)\ ANC_X\ B_X - K_{RDON}RDON + \frac{WRDON}{V} \quad (8.82)$$

where

$RDON$ is the concentration of dissolved organic nitrogen ($g\,N/m^3$),

$FNRD_x$ is the fraction of metabolized nitrogen by algal group x produced as dissolved organic nitrogen,

$FNRDP$ is the fraction of predated nitrogen produced as dissolved organic nitrogen,

K_{RDON} is the mineralization rate of dissolved organic nitrogen ($1/day$), and

$WRDON$ is the external loads of dissolved organic nitrogen ($g\,N/day$).

The equation for the labile component is

$$\frac{\partial LDON}{\partial t} = \sum_{x=c,d,g,m} (FNLD_X\ BM_X + FNLDP_X\ PR_X)\ ANC_X\ B_X + K_{RPON}RPON + K_{LPON}LPON - K_{LDON}LDON + \frac{\partial}{\partial Z}(WS_{LP}LPON) + \frac{WDON}{V} \quad (8.83)$$

where

DON is the concentration of dissolved organic nitrogen ($g\ N/m^3$),

FND_x is the fraction of metabolized nitrogen by algal group x produced as dissolved organic nitrogen,

$FNDP$ is the fraction of predated nitrogen produced as dissolved organic nitrogen,

K_{DON} is the mineralization rate of dissolved organic nitrogen ($1/day$), and

$WDON$ is the external loads of dissolved organic nitrogen ($g\ N/day$).

Equations (8.82) and (8.83) follow from Tillman et al. (2004), but are not currently implemented in the EFDC+ water quality model.

8.2.3.5 Silica

The present model has two state variables for silica; particulate biogenic silica and available silica.

8.2.3.5.1 Particulate Biogenic Silica

Sources and sinks for particulate biogenic silica included in the model are (Figure 8.1):

1. Diatom basal metabolism and predation,
2. Dissolution to available silica,
3. Settling, and
4. External loads.

The kinetic equation describing these processes is:

$$\frac{\partial SU}{\partial t} = (FSP_d\ BM_d + FSPP\ PR_d)ASC_d\ B_d - K_{SUA}SU + \frac{\partial}{\partial Z}(WS_dSU) + \frac{WSU}{V} \quad (8.84)$$

where,

SU is the concentration of particulate biogenic silica ($g\ Si/m^3$),

FSP_d is the fraction of metabolized silica by diatoms produced as particulate biogenic silica,

$FSPP$ is the fraction of predated diatom silica produced as particulate biogenic silica,

ASC_d is the silica-to-carbon ratio of diatoms ($g\ Si\ per\ g\ C$),

K_{SUA} is the dissolution rate of particulate biogenic silica ($1/day$), and

WSU is the external loads of particulate biogenic silica ($g\ Si/day$).

8.2.3.5.2 Available Silica

Sources and sinks for available silica included in the model are:

1. Diatom basal metabolism, predation, and uptake,
2. Settling of sorbed (particulate) available silica,
3. Dissolution from particulate biogenic silica,
4. Sediment-water exchange of dissolved silica for the bottom layer only, and
5. External loads.

The kinetic equation describing these processes is:

$$\frac{\partial SA}{\partial t} = (FSI_d\ BM_d + FSIP\ PR_d - P_d)\,ASC_d\ B_d + K_{SUA}SU + \frac{\partial}{\partial Z}(WS_{TSS}SAp) + \frac{BFSAd}{\Delta Z} + \frac{WSA}{V} \quad (8.85)$$

where,

$SA = SAd + SAp$ is the concentration of available silica ($g\ Si/m^3$),

SAd is the dissolved available silica ($g\ Si/m^3$),

Sap is the particulate (sorbed) available silica ($g\ Si/m^3$),

FSI_d is the fraction of metabolized silica by diatoms produced as available silica,

$FSIP$ is the fraction of predated diatom silica produced as available silica,

$BFSAd$ is the sediment-water exchange flux of available silica ($g\ Si/m^2/day$), applied to bottom layer only, and

WSA is the external loads of available silica ($g\ Si/day$).

In equation (8.85), if total active metal is chosen as a measure of sorption site, the settling velocity of total suspended solid WS_{TSS}, is replaced by that of particulate metal WS_s.

8.2.3.5.3 Available Silica System

Analysis of Chesapeake Bay monitoring data indicates that silica shows similar behavior as phosphate in the adsorption-desorption process (Cerco and Cole, 1993). As in phosphate, therefore, available silica is defined to include both dissolved and sorbed fractions. Treatment of available silica is the same as total phosphate, and the same method to partition dissolved and sorbed phosphate is used to partition dissolved and sorbed available silica:

$$SAp = \left(\frac{K_{SAp} SORPS}{1 + K_{SAp} SORPS} \right) SA \tag{8.86}$$

$$SAd = \left(\frac{1}{1 + K_{SAp} SORPS} \right) SA \tag{8.87}$$

$$SORPS = TSS \text{ or } TAM_p \tag{8.88}$$

$$SA = SAp + SAd \tag{8.89}$$

where, $KSAp$ is the empirical coefficient relating available silica sorption to total suspended solid ($per\ g/m^3$) or particulate total active metal ($per\ mol/m^3$) concentration.

8.2.3.5.4 Effect of Diatoms on Silica

In equations (8.84) and (8.86), those terms expressed as a function of diatom biomass (Bd) account for the effects of diatoms on silica. As in phosphorus and nitrogen, both basal metabolism (respiration and excretion) and predation are considered, and thus formulated, to contribute to particulate biogenic and available silica. That is, diatom silica released by both basal metabolism and predation are represented by distribution coefficients (FSP_d, FSI_d, $FSPP$, and $FSIP$). The sum of two distribution coefficients for basal metabolism should be unity and so is that for predation. Diatoms require silica as well as phosphorus and nitrogen, and diatom uptake of available silica is represented by ($-P_d AASC_d AB_d$) in equation (8.85).

8.2.3.5.5 Dissolution

The term ($-K_{SUA} ASU$) in equation (8.84) and its corresponding term in equation (8.85) represent dissolution of particulate biogenic silica to available silica. The dissolution rate is expressed as an exponential function of temperature

$$K_{SUA} = K_{SU} \exp\left(KT_{SUA} \left(T - TR_{SUS}\right)\right) \tag{8.90}$$

where,

K_{SU} is the dissolution rate of particulate biogenic silica at TR_{SUA} ($1/day$),

KT_{SUA} is the effect of temperature on dissolution of particulate biogenic silica ($1/^\circ C$), and

TR_{SUA} is the reference temperature for dissolution of particulate biogenic silica ($^\circ C$).

8.2.3.6 Chemical Oxygen Demand

In the present model, chemical oxygen demand is the concentration of reduced substances that are oxidizable through inorganic means. The source of chemical oxygen demand in saline water is sulfide released from sediments. A cycle occurs in which sulfate is reduced to sulfide in the sediments and reoxidized to sulfate in the water column. In fresh water, methane is released to the water column by the sediment process model. Both sulfide and methane are quantified in units of oxygen demand and are treated with the same kinetic formulation. The kinetic equation, including external loads, if any, is:

$$\frac{\partial COD}{\partial t} = -\left(\frac{DO}{KH_{COD}+DO}\right) K_{COD} COD + \frac{BFCOD}{\Delta Z} + \frac{WCOD}{V} \tag{8.91}$$

where,

COD is the concentration of chemical oxygen demand ($g\ O_2 - equivalents/m^2/day$),

KH_{COD} is the half-saturation constant of dissolved oxygen required for oxidation of chemical oxygen demand ($g\ O_2/m^3$),

K_{COD} is the oxidation rate of chemical oxygen demand ($1/day$),

$BFCO$ is the sediment flux of chemical oxygen demand ($g\ O_2 - equivalents/m^2/day$), applied to bottom layer only, and

$WCOD$ is the external loads of chemical oxygen demand ($g\ O_2 - equivalents/day$).

An exponential function is used to describe the temperature effect on the oxidation rate of chemical oxygen demand:

$$K_{COD} = K_{CD} \exp\left(KT_{COD}\left(T - TR_{COD}\right)\right) \tag{8.92}$$

where

K_{CD} is the oxidation rate of chemical oxygen demand at $TRCOD$ ($1/day$),

KT_{COD} is the effect of temperature on oxidation of chemical oxygen demand ($1/^{\circ}C$), and

TR_{COD} is the reference temperature for oxidation of chemical oxygen demand ($^{\circ}C$).

8.2.3.7 Dissolved Oxygen

Sources and sinks of dissolved oxygen in the water column included in the model are (Figure 8.1):

1. Algal photosynthesis and respiration,
2. Nitrification,
3. Heterotrophic respiration of dissolved organic carbon,

4. Oxidation of chemical oxygen demand,
5. Surface reaeration for the surface layer only,
6. Sediment oxygen demand for the bottom layer only, and
7. External loads.

The kinetic equation describing these processes is:

$$\frac{\partial DO}{\partial t} = \sum_{x=c,d,g,m} \left((1+0.3\,(1-PN_x))\,P_x - (1-FCD_x)\left(\frac{DO}{KHR_x+DO}\right) BM_x \right) AOCR\,B_x$$
$$- AONT\ Nit\ NH4 - AOCR\,K_{HR}DOC - \left(\frac{DO}{KH_{COD}+DO}\right) K_{COD}COD$$
$$+ K_R\,(DO_S - DO) + \frac{SOD}{\Delta Z} + \frac{WDO}{V} \quad (8.93)$$

where

$AONT$ is the mass of dissolved oxygen consumed per unit mass of ammonium nitrogen nitrified (4.33 $g\ O_2\ per\ g\ N$),

$AOCR$ is the dissolved oxygen-to-carbon ratio in respiration (2.67 $g\ O_2\ per\ g\ C$),

KR is the reaeration coefficient ($1/day$): the reaeration term is applied to the surface layer only,

DO_s is the saturated concentration of dissolved oxygen ($g\ O_2/m^3$),

SOD is the sediment oxygen demand ($g\ O_2/m^2/day$), applied to the bottom layer only; positive is to the water column,

WDO is the external loads of dissolved oxygen ($g\ O_2/day$), and

PN_x is the preference for ammonia uptake by algae group x $(0 < PN_x < 1)$.

The remainder of this section explains the effects of algae, nitrification, and surface reaeration.

8.2.3.7.1 Effect of Algae on Dissolved Oxygen

The first line on the RHS of equation (8.93) accounts for the effects of algae on dissolved oxygen. Algae produce oxygen through photosynthesis and consume oxygen through respiration. The quantity produced depends on the form of nitrogen utilized for growth. Equations describing production of dissolved oxygen are (Morel, 1983);

$$106CO_2 + 16NH_4^+ + H_2PO_4^- + 106H_2O \rightarrow protoplasm + 106O_2 + 15H^+ \quad (8.94)$$

$$106CO_2 + 16NO_3^- + H_2PO_4^- + 122H_2O \rightarrow protoplasm + 138O_2 \quad (8.95)$$

When ammonium is the nitrogen source, one mole of oxygen is produced per mole of carbon dioxide fixed. When nitrate is the nitrogen source, 1.3 moles of oxygen are produced per mole of carbon dioxide fixed. The quantity $(1.3 - 0.3APN_x)$, in the first term of equation (8.93) is the photosynthesis ratio and represents the molar quantity of oxygen produced per mole of carbon dioxide fixed. It approaches unity as the algal preference for ammonium approaches unity.

The last term in the first line of equation (8.93) accounts for the oxygen consumption due to algal respiration. A simple representation of respiration process is:

$$CH_2O + O_2 = CO_2 + H_2O \quad (8.96)$$

from which, $AOCR = 2.67\ g\ O_2\ per\ g\ C$.

8.2.3.7.2 Effect of Nitrification on Dissolved Oxygen

The stoichiometry of nitrification reaction equation (8.77), indicates that two moles of oxygen are required to nitrify one mole of ammonium into nitrate. However, cell synthesis by nitrifying bacteria is accomplished by the fixation of carbon dioxide so that less than two moles of oxygen are consumed per mole ammonium utilized (Wezenak and Gannon, 1968), i.e. $AONT = 4.33\ g\ O_2\ per\ g\ N$.

8.2.3.7.3 Effect of Surface Reaeration on Dissolved Oxygen

The reaeration rate of dissolved oxygen at the air-water interface is proportional to the oxygen gradient across the interface $(DO_s - DO)$, assuming that the air is saturated with oxygen. The saturated concentration of dissolved oxygen, which decreases as temperature and salinity increase, is specified using an empirical formula (Genet et al., 1974);

$$DO_s = 14.5532 - 0.38217T + 5.4258 \times 10^{-3}T^2 - CL\left(1.665 \times 10^{-4} - 5.866 \times 10^{-6}T + 9.796 \times 10^{-8}T^2\right) \quad (8.97)$$

$CL = S/1.80655$ is the chloride concentration (mg/l).

The reaeration coefficient includes the effect of turbulence generated by bottom friction (O'Connor and Dobbins, 1958) and that by surface wind stress (Banks and Herrera, 1977):

$$K_r = \frac{1}{\Delta z}\left(K_{ro}\sqrt{\frac{ueq}{heq}} + W_{rea}\right)(KT_r)^{T-20} \quad (8.98)$$

where,

$Kro = 3.933$ is the proportionality constant in SI unit,

$ueq = \sum(ukVk)/3(Vk)$ is the weighted velocity over cross-section (m/s),

$heq = \sum(Vk)/B$ is the weighted depth over cross-section (m),

B is the width at the free surface (m), and

$Wrea$ is the wind-induced reaeration (m/day).

$$W_{rea} = 0.728\sqrt{U_w} - 0.317U_w + 0.0372U_w^2 \tag{8.99}$$

where,

Uw is the wind speed (m/s) at the height of 10 m above surface, and

KTr is the constant for temperature adjustment of dissolved oxygen reaeration rate.

8.2.3.7.4 Simplified Equation for Dissolved Oxygen

The simplified DO equation for $KHRx$ and $FCDx$ equal to zero is

$$\frac{\partial DO}{\partial t} = \sum_{x=c,d,g,m} ((1.3 - 0.3PN_x)P_x - BM_x)AOCR\,B_x - AONT\;Nit\;NH4 - AOCR\,K_{HR}\,DOC - \left(\frac{DO}{KH_{COD} + DO}\right)K_{COD}COD + K_R(DO_S - DO) + \frac{SOD}{\Delta Z} + \frac{WDO}{V} \tag{8.100}$$

which is consistent with the equation (8.93).

8.2.3.8 Total Active Metal

The present model requires simulation of total active metal for adsorption of phosphate and silica if that option is chosen. The total active metal state variable is the sum of iron and manganese concentrations, both particulate and dissolved. In the model, the origin of total active metal is benthic sediments. Since sediment release of metal is not explicit in the sediment model (see Chapter 6), release is specified in the kinetic portion of the water column model. The only other term included is settling of the particulate fraction. Then the kinetic equation for total active metal, including external loads, if any, may be written as:

$$\frac{\partial TAM}{\partial t} = \left(\frac{KHbmf}{KHbmf + DO}\right)(\exp(Ktam(T - Ttam)))\frac{BFTAM}{\Delta z} + \frac{\partial}{\partial Z}(WS_sTAMp) + \frac{WTAM}{V} \tag{8.101}$$

where,

$TAM = TAMd + TAMp$ is the total active metal concentration (mol/m^3),

$TAMd$ is the dissolved total active metal (mol/m^3),

$TAMp$ is the particulate total active metal (mol/m^3),

$KHbmf$ is the dissolved oxygen concentration at which total active metal release is half the anoxic release rate ($g\ O_2/m^3$),

$BFTAM$ is the anoxic release rate of total active metal ($mol/m^2/day$), applied to the bottom layer only,

$Ktam$ is the effect of temperature on sediment release of total active metal ($1/°C$),

$Ttam$ is the reference temperature for sediment release of total active metal ($°C$),

WS_s is the settling velocity of particulate metal (m/day), and

$WTAM$ is the external loads of total active metal (mol/day).

In estuaries, iron and manganese exist in particulate and dissolved forms depending on dissolved oxygen concentration. In oxygenated water, most of the iron and manganese exist as particulate while under anoxic conditions, large fractions are dissolved, although solid-phase sulfides and carbonates exist and may predominate. The partitioning between particulate and dissolved phases is expressed using a concept that total active metal concentration must achieve a minimum level, which is a function of dissolved oxygen, before precipitation occurs:

$$TAMd = \min\left(TAM_{dmx} exp\left(-K_{dotam}\ DO\right)\ ,\ TAM\right) \tag{8.102}$$

$$TAMp = TAM - TAMd \tag{8.103}$$

where

$TAMdmx$ is the solubility of total active metal under anoxic conditions (mol/m^3), and

K_{dotam} is the constant that relates total active metal solubility to dissolved oxygen ($per\ g\ O_2/m^3$).

8.2.3.9 Fecal Coliform Bacteria

The fecal coliform variable is completely decoupled from the rest of the water quality model and is included in the model for convenience in Total Maximum Daily Load (TMDL) applications. Fecal coliform bacteria are indicative of organisms from the intestinal tract of humans and other animals and can be used as an indicator bacteria as a measure of public health (Thomann and Mueller, 1987). In the present model, fecal coliform bacteria have no interaction with other state variables, and have only one sink term, die-off. The kinetic equation, including external loads, may be written as:

$$\frac{\partial FCB}{\partial t} = KFCB\left(TFCB^{T-20}\right)FCB + \frac{WFCB}{V} \tag{8.104}$$

where,

FCB is the bacteria concentration ($MPN\ per\ 100ml$),

$KFCB$ is the first order die-off rate at 20 $^{\circ}C$ ($1/day$),

$TFCB$ is the effect of temperature on decay of bacteria ($1/^{\circ}C$), and

$WFCB$ is the external loads of fecal coliform bacteria ($MPN\ per\ 100ml\ m^3/day$).

8.2.4 Settling, Deposition and Resuspension of Particulate Matter

The kinetic equations for particulate matter, including particulate organic matter, total phosphate, the two silica state variables, and total active metal contain settling term. A representative generic equation is

$$\frac{\partial PM}{\partial t} = \frac{\partial}{\partial z}\left(WS_{PM}PM\right) + PM_{SS} \tag{8.105}$$

where, PMSS represents the additional terms in the equation. Integration of equation (8.105) over the bottom layer gives

$$\frac{\partial PM_1}{\partial t} = \frac{WS_{PM}}{\Delta Z_1}PM_2 - \frac{WS_{PM}}{\Delta Z_1}PM_1 + PM_{SS1} \tag{8.106}$$

The original CE-QUAL-ICM and EFDC+ water quality models were formulated with settling velocities representing long-term average net settling. In the subsequent application of CE- QUAL-ICM to Florida Bay (Cerco et al., 2000), the resuspension or erosion of particulate material form the sediment bed was added and has also been added to the EFDC+ water quality model.

The EFDC+ model allows the use of the net settling formulation (8.106) and a formulation allowing resuspension with equation (8.106) modified

$$\frac{\partial PM_1}{\partial t} = \frac{WS_{POM}}{\Delta Z_1}PM_2 - \frac{P_{depPM}WS_{PM}}{\Delta Z_1}PM_1 + \frac{E_{PM}}{\Delta Z_1} + PM_{SS1} \tag{8.107}$$

to include a probability of deposition factor and an erosion term E_PM with units of mass per unit time-unit area. For EFDC+ model applications with erosion of a particulate material in the water quality module, sediment transport must be active in the hydrodynamic model. The erosion term is then defined by

$$E_{PM} = \left(\frac{PM_{bed}}{SED_{bed}}\right)\max\left(J_{ERO},\ 0\right) \tag{8.108}$$

where,

PM_{bed} is the particulate material concentration in bed ($g\ PM/m^2$ or $g\ PM/m^3$),

SED_{bed} is the concentration finest sediment class in bed ($g\ PM/m^2$ or $g\ PM/m^3$),

P_{depPM} is the probability of deposition of the specific particulate matter variable ($0 \leq P_{depPM} \leq 1$), and

J_{ERO} is the mass rate of erosion or resuspension of the finest sediment class ($g\ SED/day/m^2$).

Usage of the ratio of the water quality model particulate state variable concentration to the finest sediment size class concentration rather than the total solids concentration is based on the reality that finest sediment class (generally less than $63\mu m$) includes both inorganic and organic material and field observations of settling, deposition and resuspension, when available for model calibration account for this. If simultaneous deposition and erosion are not permitted, the probability of deposition is defined as zero when the sediment erosion flux is greater than zero.

In conclusion, it is noted that in the CE-QUAL-ICM documentation which includes particulate matter resuspension (Cerco et al., 2000), resuspension is explicitly included in various state variable equations, while in this document it is included implicitly as described in the current section.

8.2.5 Method of Solution for Kinetics Equations

The kinetic equations for the 20 state variables, excluding fecal coliform, in the EFDC+ water column water quality model can be expressed in a system of 20×20 partial differential equations in each model cell, after linearizing some terms, mostly Monod type expressions:

$$\frac{\partial \boldsymbol{C}}{\partial t} = \boldsymbol{K}\boldsymbol{C} + \frac{\partial}{\partial z}(\boldsymbol{W}\boldsymbol{C}) + \boldsymbol{R} \tag{8.109}$$

where,

$\boldsymbol{C}$ is the vector of the state variables in $[ML^{-3}]$,

$\boldsymbol{K}$ is a matrix in $[T^{-1}]$,

$\boldsymbol{W}$ is in $[LT^{-1}]$, and

$\boldsymbol{R}$ is a vector in $[ML^{-3}T^{-1}]$.

The ordering of variables follows that in Table 8.1 which results in $\boldsymbol{K}$ being lower triangular. Integrating (8.109) over layer k, gives

$$\frac{\boldsymbol{C}_k}{\partial t} = \boldsymbol{K}1_k\boldsymbol{C}_k + \delta_k\boldsymbol{K}2_k\boldsymbol{C}_{k+1} + \boldsymbol{R}_k$$
$$\boldsymbol{K}1_k = \boldsymbol{K}_k - \frac{1}{\Delta_k}\boldsymbol{W} \tag{8.110}$$
$$\boldsymbol{K}2_k = \frac{1}{\Delta_k}\boldsymbol{W}$$

which indicates that the settling of particulate matter from the overlying cell acts as an input for a given cell. For the layer of cells adjacent to the bed, the erosion term in (8.107) is included in the vector $\boldsymbol{R}$. The matrices and vectors in (8.109) and (8.110) are defined in Appendix A of (Park et al., 1995). The layer index k increases upward with KC vertical layers; $k = 1$ is the bottom layer and $k = KC$ is the surface layer. Then $\delta_k = 0$ for $k = KC$; otherwise, $\delta_k = 1$. The matrix $\boldsymbol{K}2$ is a diagonal matrix, and the non-zero elements account for the settling of particulate matter from the overlying cell.

Equation (8.110) is solved using a generalized trapezoidal scheme over a time step of θ, which may be expressed as:

$$\boldsymbol{C}_k^{n+1} - \boldsymbol{C}_k^n = \lambda\theta\left(\boldsymbol{K}1_k^n\boldsymbol{C}_k^{n+1} + \delta_k\boldsymbol{K}2_k^n\boldsymbol{C}_{k+1}^{n+1} + \boldsymbol{R}_k^{n+1}\right) + (1-\lambda)\,\theta\left(\boldsymbol{K}1_k^n\boldsymbol{C}_k^n + \delta_k\boldsymbol{K}2_k^n\boldsymbol{C}_{k+1}^n + \boldsymbol{R}_k^n\right) \tag{8.111}$$

or

$$\left(\boldsymbol{I} - \lambda\theta\boldsymbol{K}1_k^n\right)\boldsymbol{C}_k^{n+1} = \left(\boldsymbol{I} + (1-\lambda)\,\theta\boldsymbol{K}1_k^n\right)\boldsymbol{C}_k^n + \theta\delta_k\boldsymbol{K}2_k^n\left(\lambda\boldsymbol{C}_{k+1}^{n+1} + (1-\lambda)\,\boldsymbol{C}_{k+1}^n\right) + \theta\left(\lambda\boldsymbol{R}_k^{n+1} + (1-\lambda)\,\boldsymbol{R}_k^n\right) \tag{8.112}$$

where,

λ is an implicitness factor ($0 \le \lambda \le 1$),

$\theta = 2 \cdot m \cdot \Delta t$ is the time step for the kinetic equations and

$\boldsymbol{I}$ is the identity matrix; the superscripts n and $n+1$ designate the variables before and after being adjusted for the relevant kinetic processes. Since equation (8.110) is solved from the surface layer downward, the term with $\boldsymbol{C}_{k+1}^{n+1}$ is known for the k^{th} layer and thus placed on the RHS. In equation (8.111), inversion of a matrix can be avoided when the 20 state variables are solved in the order given in Table 8.1.

8.3. Rooted Aquatic Plants Formulation

Rooted macrophyte beds are commonly observed along the banks of many rivers and the accuracy of a water quality model may be improved by simulating submerged aquatic vegetation (epiphytic algae and macrophytes) if a waterbody has documented macrophyte occurrences. EFDC+'s generic Rooted Aquatic Plant and Epiphyte Algae Sub-Model (RPEM) uses kinetic mass balance equations for rooted plant shoots, roots and epiphyte algae growing on the shoots. The user may enable or disable a variety of combinations for RPEM, including enabling simulation of rooted plants or epiphytes; enabling epiphytes growing on rooted plants; enabling the RPEM – Water Column Nutrient Interaction; and enabling RPEM – Sediment Diagenesis Interaction.

The state variables in the sub-model are rooted plant shoots, roots, epiphyte algae biomass and rooted plant shoot detritus biomass. The kinetic mass balance of these variables depends mainly on production, respiration and non-respiration loss rates. These rates in turn are mainly controlled by nutrients, carbon, oxygen, light field and temperature.

8.3.1 State Variable Equations

The kinetic mass balance equations for rooted plant shoots, roots and epiphyte algae growing on the shoots are

$$\frac{\partial (RPS)}{\partial t} = ((1 - F_{PRPR}) \cdot P_{RPS} - R_{RPS} - L_{RPS}) RPS + JRP_{RS} \tag{8.113}$$

$$\frac{\partial (RPR)}{\partial t} = F_{PRPR} \cdot P_{RPS} \cdot RPS - (R_{RPR} + L_{RPR}) RPR + JRP_{RS} \tag{8.114}$$

$$\frac{\partial (RPE)}{\partial t} = (P_{RPE} - R_{RPE} - L_{RPE}) RPE \tag{8.115}$$

where,

t is the time (day),

$RPS\ (T_a,\ H_a)$ is the Rooted Plant Shoot Biomass ($g\,C/m^2$),

$F_{PRPR}\ (\chi_{Ta},\ \chi_{Ha})$ is the fraction of production directly transferred to roots ($0 < FPGR < 1$),

$P_{RPS}\ (g_{Ta},\ g_{Ha})$ is the production rate for plant shoots ($1/day$),

$R_{RPS}\ (r_T a,\ r_{Ha})$ is the respiration rate for plant shoots ($1/day$),

$L_{RPS}\ (m_{Ta},\ m_{Ha})$ is the non-respiration loss rate for plant shoots ($1/day$),

$JRP_{RS}\ (\chi_{Tb} T_b,\ \chi_{Hb} H_b)$ is the carbon transport positive from roots to shoots ($g\,C/m^2/day$) ,

$RPR\ (T_b,\ H_b)$ is the Rooted Plant Root Biomass ($g\,C/m^2$),

R_{RPR} $(r_{Tb},\ r_{Hb})$ is the respiration rate for plant roots $(1/day)$,

L_{RPR} $(m_{Tb},\ m_{Hb})$ is the non-respiration loss rate for plant roots $(1/day)$,

RPE (E) s the Rooted Plant Epiphyte Biomass $(g\,C/m^2)$,

P_{RPE} (g_E) is the production rate for epiphytes $(1/day)$,

$R_{PRE}(r_E E)$ is the respiration rate for epiphytes $(1/day)$, and

L_{RPE} $(r_{Ta}+m_E)$ is the non-respiration loss rate for epiphytes $(1/day)$.

For comparison, Table 8.3 and Table 8.4 show generic and Florida Bay sea grass model parameters.

Table 8.3. Generic and Florida Bay Sea Grass Model Parameters for Thalassia and Halodule

Parameter	Dimension	Generic	Thalassia	Halodule
F_{PRPR} (χ_{Ta}, χ_{Ha})	none	constant	0.4	0.34
P_{RPS} $(g_{Ta},\ g_{Ha})$	$1/day$	Function of N, P, Light, Temp, Salt	Function of N, P, Light, Temp, Salt	Function of N, P, Light, Temp, Salt
R_{RPS} $(r_{Ta},\ r_{Ha})$	$1/day$	Function of Temperature	0.01 (base) Temperature Function	0.029 (base) Temperature Function
L_{RPS} $(m_{Ta},\ m_{Ha})$	$1/day$	Function of Temperature	0.001 (base) Temperature Function	0.004 (base) Temperature Function
R_{RPR} (r_{Tb}, r_{Hb})	$1/day$	Function of Temperature	0.0025 (base) Temperature Function	0.011(base) Temperature Function
L_{RPR} (m_{Tb}, m_{Hb})	$1/day$	Function of Temperature	0.0001 (base) Temperature Function	0.0004 (base) Temperature Function
JRP_{RS} $(\chi_{Tb}Tb, \chi_{H_b}Hb)$	$g\,C/m^2/day$	$KRP_{RS}\cdot RPR$	$\chi_{Tb}Tb$ $(\chi_{Tb}=0.0005)$	$\chi_{Hb}Hb$ $(\chi_{Hb}=1\times10^{-5})$

An additional state variable is also added to account for shoot detritus at the bottom of the water column

$$\frac{\partial\,(RPD)}{\partial t} = F_{PRSD}\cdot P_{RPS}\cdot RPS - L_{RPD}RPS \tag{8.116}$$

where,

Table 8.4. Generic and Florida Bay Sea Grass Model Parameters for Epiphytes

Parameter	Dimension	Generic	Epiphytes
$P_{RPE}(g_E)$	none	Function of N, P, Light, Temp, Salt	Function of N, P, Light, Temp, Salt
$R_{RPE}(r_E E)$	$1/day$	Function of Temperature	$r_E Er_E = (0.01 m^2/gm - day)$
$L_{RPE}(m_{Ta} + m_E E)$	$1/day$	constant	$m_{Ta} + m_E Er_E = (0.05 m^2/gm - day)$

RP is the Rooted Plant Shoot Detritus Biomass ($g\,C/m^2$),

F_{RPSD} is the fraction of shoot loss to detritus ($0 < FRPSD < 1$), and

L_{RPD} is the decay rate of detritus ($1/day$).

The Florida Bay sea grass model does not include this variable.

8.3.1.1 Production Rate for Plant Shoots

The production or growth rate for plant shoots is given by

$$P_{RPS} = PM_{RPS} \cdot f_{1W}(N) \cdot f_{1B}(N) \cdot f_2(I) \cdot f_3(T) \cdot f_4(S) \cdot f_5(RPS) \tag{8.117}$$

where,

$PM_{RPS}(V_T, V_H)$ is the maximum growth rate under optimal conditions for plant shoots ($1/day$),

$f_1(N)$ is the effect of suboptimal nutrient concentration ($0 \le f_1 \le 1$),

$f_2(I)$ is the effect of suboptimal light intensity ($0 \le f_2 \le 1$),

$f_3(T)$ is the effect of suboptimal temperature ($0 \le f_3 \le 1$),

$f_4(S)$ is the effect of salinity on fresh water plant shoot growth ($0 \le f_4 \le 1$), and

$f_5(RPS)$ is the carrying capacity effect on shoot growth ($0 \le f_5 \le 1$).

Maximum growth rates for the Florida Bay sea grass model are shown in Table 8.5.

Table 8.5. Maximum Growth Rate

Parameter	Units	Generic	Thalassia	Halodule
$PM_{RPS}(V_T,\ V_H)$	$/day$	constant	0.208	0.29

8.3.1.1.1 Effect of Nutrients on Production

Nutrient limitation is specified in terms of both water column and bed nutrient levels by

$$f_{1W}(N) = \min\left(\frac{(NH4+NO3)_w}{KHN_{RPS}+(NH4+NO3)_w}, \frac{PO4d_w}{KHP_{RPS}+PO4d_w}\right)$$
$$f_{1b}(N) = \min\left(\frac{(NH4+NO3)_b}{KHN_{RPS}+(NH4+NO3)_b}, \frac{PO4d_b}{KHP_{RPS}+PO4d_b}\right) \quad (8.118)$$

where,

$NH4$ is the ammonium nitrogen concentration ($g\,N/m^3$),

$NO3$ is the nitrate + nitrite nitrogen concentration ($g\,N/m^3$),

KHN_{RPS} is the half-saturation constant for nitrogen uptake from water column ($g\,N/m^3$),

KHN_{RPR} (K_{TN},K_{HN}) is the half-saturation constant for nitrogen uptake from bed ($g\,N/m^3$),

$PO4d$ is the dissolved phosphate phosphorus concentration ($g\,P/m^3$),

KHP_{RPS} is the half-saturation constant for phosphorus uptake from water column ($g\,P/m^3$), and

KHP_{RPR} (K_{TP}, K_{HP}) is the half-saturation constant for phosphorus uptake from bed ($g\,P/m^3$).

Table 8.6. List of nutrient limitation parameters for the Florida Bay sea grass model

Parameter	Units	Generic	Thalassia	Halodule
KHN_{RPS}	$gm/m^3(mg/l)$	constant	0.0	0.0
KHN_{RPR}	$gm/m^3(mg/l)$	constant	0.04 μM 0.00056 mg/l	0.04 μM 0.00056 mg/l
KHP_{RPS}	$gm/m^3(mg/l)$	constant	0.0	0.0
KHP_{RPR}	$gm/m^3(mg/l)$	constant	0.04 μM 0.0031 mg/l	0.04 μM 0.0031 mg/l

8.3.1.1.2 The Light Field

The light field in the water column is governed by

$$\frac{\partial I}{\partial Z_*} = -K_{ess} \cdot I \tag{8.119}$$

where,

I is the light intensity ($Langley/day$),

K_{ess} is the light extinction coefficient ($1/m$), and

Z_* is the depth below the water surface (m).

With the light extinction coefficient being a function of the depth below the water surface. Integration of (8.119) gives

$$I = I_{ws} \exp\left(-\int_0^{Z_*} K_{ess} \cdot dZ_*\right) \tag{8.120}$$

The light intensity at the water surface Iws, is given by

$$I_{ws} = I_o \min\left(exp\left(-Kesh \cdot (H_{RPS} - H)\right), 1\right) \tag{8.121}$$

where,

I_o is the light intensity at the top of the emergent shoot canopy for emergent shoots or the light intensity at the water surface for submerged shoots (W/m^2),

K_{eme} is the light extinction coefficient for emergent shoots ($1/m$),

H_{RPS} is the shoot height (m), and

H is the water column depth (m).

For submerged shoots, it is assumed that the light extinction coefficient in the water column above the shoot canopy is given by

$$K_{essac} = Ke_b + Ke_{ISS} \cdot ISS + Ke_{VSS} \cdot VSS + Ke_{Chl} \sum_{m=1}^{M} \left(\frac{B_m}{CChl_m}\right) \tag{8.122}$$

And the light extinction coefficient in the water column within the canopy is given by

$$K_{essic} = Ke_b + Ke_{ISS} \cdot ISS + Ke_{VSS} \cdot VSS + Ke_{Chl} \sum_{m=1}^{M} \left(\frac{B_m}{CChl_m}\right) + Ke_{RPS} \cdot RPS \tag{8.123}$$

where,

Ke_b is the background light extinction $(1/m)$,

Ke_{ISS} is the light extinction coefficient for inorganic suspended solid $(1/m\ per\ g/m^3)$,

ISS is the inorganic suspended solid concentration (g/m^3) provided from the hydrodynamic model,

Ke_{VSS} is the light extinction coefficient for volatile suspended solid $(1/m\ per\ g/m^3)$,

VSS is the volatile suspended solid concentration (g/m^3) provided from the water quality model,

$CChl_{RPE}$ is the carbon-to-chlorophyll ratio for epiphytes $(g\ C\ per\ mg\ Chl)$,

Ke_{Chl} is the light extinction coefficient for algae chlorophyll $(1/m\ per\ mg\ Chl/m^3)$,

B_m is the concentration of algae group m $(g\ C\ per\ ml)$,

$CChl_m$ is the carbon-to-chlorophyll ratio in algal group m $(g\ C\ per\ mg\ Chl)$,

Ke_{RPS} is the light extinction coefficient for rooted plant shoots $(1/m\ per\ gm\ C/m^2)$, and

RPS is the concentration of plant shoots $(g\ C\ per\ m^2)$.

The forms of equations (8.122) and (8.123) readily allow for the inclusion of algae biomass into the volatile suspended solids or vice-versa. The form of equation (8.123) assumes that the shoots are primarily self shading and that epiphyte effect are manifest on the shoot surface.

The solutions of equation (8.120) above and in the canopy are

$$I = I_{ws}\exp\left(-K_{essac}\cdot Z_*\right)\ ;\ 0 \le Z_* \le H - H_{RPS} \tag{8.124}$$

$$I = I_{ct}\cdot\exp\left(-K_{essic}\cdot\left(Z_* - H + H_{RPS}\right)\right) \tag{8.125}$$

$$I_{ct} = I_{ws}\cdot\exp\left(-K_{essac}\cdot\left(H - H_{RPS}\right)\right) \tag{8.126}$$

$$H - H_{RPS} \le Z_* \le H \tag{8.127}$$

Since rooted plants are represented as carbon mass per unit area, the average light intensity over the shoot canopy is an appropriate light measure. For emergent shoots, the average of equation (8.124) over the water column depth, noting that $H = H_{RPS}$, is

$$I_{icwa} = \frac{I_{ws}}{K_{essic}\cdot H}\left(1 - \exp\left(-K_{essac}\cdot H\right)\right) \tag{8.128}$$

For submerged shoots, the average over the canopy is

$$I_{icwa} = \frac{I_{ws}}{K_{essic}\cdot H_{RPS}}\exp\left(-K_{essac}\cdot\left(H - H_{RPS}\right)\right)\cdot\left(1 - \exp\left(-K_{essic}\cdot H_{RPS}\right)\right) \tag{8.129}$$

where I_{icwa} in both equation (8.128) and equation (8.129) is the average in canopy water column light intensity.

When epiphytes grow on the shoot surface, the light intensity at the shoot surface is further reduced according to

$$I_{RPS} = I_{icw}\exp\left(-Ke_{RPE}\cdot RPE\right) \tag{8.130}$$

where,

I_{RPS} is the light intensity on the plant shoots (W/m^2),

I_{icw} is the average water column light intensity in the shoot canopy (W/m^2), and

Ke_{RPE} is the light extinction coefficient for epiphyte (m^2 *per gm C*).

For the Florida Bay sea grass model, the epiphyte light extinction coefficient is given by

$$Ke_{RPE} = 0.11\frac{\delta_{RPE}}{\sum_{Nspecies}\left(\frac{2\cdot RPS\cdot\delta_{RPS}}{W_{RPS}}\right)} \tag{8.131}$$

where,

δ_{RPE} is the Epiphyte dry mass to carbon mass ratio,

δ_{RPS} is the rooted plant shoot dry mass to carbon mass ratio, and

W_{RPS} is the rooted plant shoot mass per unit shoot area.

Values of these parameters for the Florida Bay model are listed in the Table 8.7. It is noted that the expression in equation (8.131) is not dimensionally homogeneous with the numerical coefficient 0.11 having implied units of $(cm^2\ leaf\ surfacearea\ )/(\ mg\ dry\ weight)$. Equation (8.131) can be made dimensionally consistent by use of the alternative form

$$Ke_{RPE}\cdot RPE = \frac{RPE}{\sum_{Nspecies}\left(KRPSE\cdot RPS\right)} \tag{8.132}$$

Where the dimensionless parameter *KRPSE* is also defined in Table 8.7

Table 8.7. Epiphyte Light Attenuation Parameter for Florida Bay Sea Grass Model

Parameter	Units	Thalassia	Halodule
δ_{RPE}	Dry mass/ Carbon mass	9	9
δ_{RPS}	Dry mass/ Carbon mass	2.94	2.4
W_{RPS}	Mg dry mass/ C-m^2 leaf area	1.7	2
KRPSE	Dimensionless	3.49	2.42

Using equations (8.130) and (8.124), the light intensity on the shoot surface can be expressed as

$$I_{RPS} = I_{ws} \cdot \exp\left(\begin{array}{c} -K_{essac} \cdot (H - H_{RPS}) \\ -Ke_{RPE} \cdot RPE \end{array} \right) \cdot \exp\left(-K_{essic} \cdot (Z_* - H + H_{RPS})\right) \quad (8.133)$$

While equations (8.130) and (8.129) give the canopy average light intensity on the shoot surface

$$I_{RPSA} = \frac{I_{ws}}{K_{essic} \cdot H_{RPS}} \exp\left(\begin{array}{c} -K_{essac} \cdot (H - H_{RPS}) \\ -Ke_{RPE} \cdot RPE \end{array} \right) \cdot \left(1 - \exp\left(-K_{essic} \cdot H_{RPS}\right)\right) \quad (8.134)$$

8.3.1.1.3 Effects of Light on Growth

The EFDC+ generic rooted plant model includes three options to specify the effect of light on rooted plant growth. The first option is based on Steele's equation (Steele, 1962)

$$f_2(I) = \frac{I}{I_{RSPopt}} \exp\left(1 - \frac{I}{I_{RSPopt}}\right) \quad (8.135)$$

which can be applied in terms of the average light intensity reaching the shoots to give

$$f_2(I) = \frac{I_{RPSA}}{I_{RSPopt}} \exp\left(1 - \frac{I_{RPSA}}{I_{RSPopt}}\right) \quad (8.136)$$

or due to its unique mathematical form directly averaged over the shoot canopy. The average is given by

$$f_{2avg}(I) = \frac{F_2}{H_{RPS}} \int_{H-H_{RPS}}^{H} \exp\left(\begin{array}{c} 1 - K_{essic} \cdot (Z_* - H + H_{RPS}) \\ -F_2 \cdot exp\left(-K_{essic} \cdot (Z_* - H + H_{RPS})\right) \end{array} \right) dZ_* \quad (8.137)$$

With the results being

$$f_{2avg}(I) = \frac{\exp(1)}{K_{essic} \cdot H_{RPS}} \left[\exp\left(-F_2 \cdot exp\left(-K_{essic} \cdot H_{RPS}\right)\right) - \exp(F_2)\right] \quad (8.138)$$

$$F_2 = \frac{I_{ws}}{I_{RSPopt}} \cdot \exp\left(\begin{array}{c} -K_{essac} \cdot (H - H_{RPS}) \\ -Ke_{RPE} \cdot RPE \end{array} \right) PE)\, c\backslash \quad (8.139)$$

The second option for the effect of light on growth or production is a Monod type formulation adapted from the Chesapeake Bay SAV model

$$f_2(I) = \left(\frac{I_{RPS}}{I_{RPS} + KHI_{RPS}}\right) \quad (8.140)$$

where,

I_{RPS} is the light intensity at the shoot surface (W/m^2), and

KHI_{RPS} is the shoot surface light intensity half saturation (W/m^2).

Equation (8.140) can be applied using the average light intensity over the shoot canopy or averaged over the shoot canopy to give

$$f_{2avg}(I) = \frac{1}{K_{essic} \cdot H} \ln\left(\frac{KHI + I_{ws} exp(Ke_{RPE} \cdot RPE)}{KHI + I_{ws} exp(-K_{essic} \cdot H - Ke_{RPE} \cdot RPE)}\right) \tag{8.141}$$

For an emergent canopy and

$$f_{2avg}(I) = \frac{1}{K_{essic} \cdot H_{RSP}} \ln\left(\frac{KHI + I_{ct} exp(-K_{essic} \cdot (H - H_{RSP}) - Ke_{RPE} \cdot RPE)}{KHI + I_{ct} exp(-K_{essic} \cdot H - Ke_{RPE} \cdot RPE)}\right) \tag{8.142}$$

for a submerged canopy.

The final option is adapted from the Florida Bay sea grass model and is

$$f_2(I) = \tanh\left(\frac{I_{RPSavg}}{l_{RSP}}\right) \tag{8.143}$$

where the average intensity is used since a closed analytical average of this equation is not possible. Values for the parameters in equations (8.140) and (8.143) for Florida Bay are listed in Table 8.8.

Table 8.8. Light Limitation Parameters for Equations (8.140) and (8.143)

Parameter	Units	Thalassia	Halodule
KHI_{RPS}	W/m^2	142(444 $\mu moles/m^2 - s$)	82(255 $\mu moles/m^2 - s$)
l_{RPS}	W/m^2	130(407 $\mu moles/m^2 - s$)	102(319 $\mu moles/m^2 - s$)

Note on conversion: the conversion factor for 1 $\mu moles/m^2 - s$ to 0.3 to 0.34 W/m^2. Conversions in table are based on 0.32.

8.3.1.1.4 Effect of Temperature on Shoot Growth

The effect of temperature on shoot growth is given by a Gaussian function

$$f_3(T) = \begin{cases} \exp\left(-KTP1_{RPS}[T - TP1_{RPS}]^2\right) & if\ T \le TP1_{RPS} \\ 1\ if\ TP1_{RPS} < T < TP2_{RPS} \\ \exp\left(-KTP2_{RPS}[T - TP2_{RPS}]^2\right) & if\ T \ge TP1_{RPS} \end{cases} \tag{8.144}$$

where,

T is the temperature ($^{\circ}C$) provided from the hydrodynamic model,

$TP1_{RPS} < T < TP2_{RPS}$ is the optimal temperature range for shoot production ($^{\circ}C$),

$KTP1_{RPS}$ is the effect of temperature below $TM1_{RPS}$ on shoot production ($1/^{\circ}C^2$), and

$KTP2_{RPS}$ is the effect of temperature above $TM2_{RPS}$ on shoot production ($1/^{\circ}C^2$).

or an exponential function.

$$f_3(T) = \exp\left(KTP_{RPS}\left[T - TPREF_{RPS}\right]\right) \tag{8.145}$$

where,

$TPREF_{RPS}$ is the reference temperature for shoot production ($^{\circ}C$), and

KTP_{RPS} is the effect of temperature on shoot production ($1/^{\circ}C$).

With parameters for the Florida Bay sea grass model given in Table 8.9.

Table 8.9. Parameters for Temperature Effect on Growth for Equation (8.145)

Parameter	Units	Thalassia	Halodule
$TPREF_{RPS}$	$^{\circ}C$	28	31
KTP_{RPS}	$1/^{\circ}C$	0.07	0.07

8.3.1.1.5 Effect of Salinity

The effect of salinity on fresh water plant shoot growth is given by

$$f_4(S) = \frac{STOXS^2}{STOXS^2 + S^2} \tag{8.146}$$

where,

$STOXS$ is the salinity at which growth is halved (ppt), and

S is the salinity in water column (ppt) provided from the hydrodynamic model

8.3.1.1.6 Effect of Rooted Plant Density

The effect of rooted plant density on growth is given by

$$f_5(RPS) = 1 - \left(\sum_{species} \frac{RPS}{RPS_{sat}}\right)^2 \tag{8.147}$$

where RPS_{sat} is the density saturation parameter ($g\,C/m^2$).

The summation indicates when multiple species are simulated, the total density of all species affects each individual species

Table 8.10. Parameters for Plant Density Effect on Growth for Equation (8.147)

Parameter	Units	Thalassia	Halodule
RPS_{sat}	$(g\,C/m^2)$	400	667

8.3.1.2 Respiration Rate for Plant Shoots

The respiration rate for plant shoots is assumed to be temperature dependent

$$R_{RPS} = RREF_{RPS} \cdot \exp\left(KTR_{RPS}\left[T - TRREF_{RPS}\right]\right) \tag{8.148}$$

where,

$RREF_{RPS}$ is the reference respiration rate for shoots $(1/day)$,

T is the temperature $(^\circ C)$ provided from the hydrodynamic model,

$TRREF_{RPS}$ is the reference temperature for shoot respiration $(^\circ C)$, and

KTR_{RPS} is the effect of temperature on shoot respiration $(1/^\circ C^2)$.

Table 8.11. Parameters for Shoot Respiration in Equation (8.148)

Parameter	Units	Thalassia	Halodule
$RREF_{RPS}$	$1/day$	0.01	0.029
KTR_{RPS}	dimensionless	0.07	0.07
$TRREF_{RPS}$	$^\circ C$	28	31

8.3.1.3 Non-Respiration Loss Rate for Plant Shoots

The non-respiration loss rate for shoots is assumed to be temperature dependent.

$$L_{RPS} = LREF_{RPS} \cdot \exp\left(KTL_{RPS}\left[T - TLREF_{RPS}\right]\right) \tag{8.149}$$

where,

$LREF_{RPS}$ is the reference loss rate for shoots $(1/day)$,

T is the temperature $(^\circ C)$ provided from the hydrodynamic model,

$TLREF_{RPS}$ is the reference temperature for shoot loss $(^\circ C)$, and

KTL_{RPS} is the effect of temperature on shoot loss $(1/^\circ C^2)$.

Table 8.12. Parameters for Shoot Mortality of non-respiration loss in (8.149)

Parameter	Units	Thalassia	Halodule
$LREF_{RPS}$	$1/day$	0.001	0.004
KLR_{RPS}	dimensionless	0.07	0.07
$TLREF_{RPS}$	$^{\circ}C$	28	28

8.3.1.4 Carbon Transport from Roots to Shoots

The carbon transport from roots to shoots is defined as positive to the shoots. Two formulations can be utilized; the first is based on observed shoot to root biomass ratios

$$JRP_{RS} = KRPO_{RS} \cdot (RPR - RORS \cdot RPS) \tag{8.150}$$

$$RORS = \frac{RPR_{obs}}{RPS_{obs}} \tag{8.151}$$

where,

$KRPO_{RS}$ is the root to shoot transfer rate to follow observed ratio $(1/day)$, and

$RORS$ is the observed ratio of root carbon to shoot carbon (dimensionless).

and the second formulation transfers root carbon to shoot carbon under unfavorable light conditions for the shoots

$$JRP_{RS} = KRP_{RS}\left(\frac{I_{SS}}{I_{SS} + I_{SSS}}\right) RPR \tag{8.152}$$

where,

KRP_{RS} (χ_{Tb}, χ_{Hb}) is the root to shoot transfer rate $(1/day)$,

I_{SS} is the solar ratio at shoot surface (W/m^2),

I_{SSS} is the half-saturation solar ratio at shoot surface (W/m^2).

8.3.1.5 Respiration Rate for Plant Roots

The respiration rate for plant roots is assumed to be temperature dependent

$$R_{RPR} = RREF_{RPR} \cdot \exp\left(KTR_{RPR}\left[T - TRREF_{RPR}\right]\right) \tag{8.153}$$

where,

$RREF_{RPR}$ is the reference respiration rate for roots $(1/day)$,

Table 8.13. Root to Shoot Transport Parameters in Equation (8.152)

Parameter	Dimension	Generic	Thalassia	Halodule
$KRPO_{RS}$	$1/day$	constant	0.0005	0.00001
$RORS$	dimensionless	constant	0.0000	0.00000
KRP_{RS}	$1/day$	constant	0.0005	0.00001
I_{SSS}	W/m^2	constant	0.0000	0.00000

T is the temperature ($^\circ C$) provided from the hydrodynamic model,

$TRREF_{RPR}$ is the reference temperature for root respiration ($^\circ C$), and

KTR_{RPR} is the effect of temperature on shoot respiration (1/$^\circ$C^2).

Table 8.14. Parameters for Root Respiration in Equation (8.153)

Parameter	Units	Thalassia	Halodule
$RREF_{RPR}$	$1/day$	0.0025	0.011
KTR_{RPR}	dimensionless	0.07	0.07
$TRREF_{RPR}$	$^\circ C$	28	31

8.3.1.6 Non-Respiration Loss Rate for Plant Roots

The non-respiration loss rate for shoots is assumed to be temperature dependent.

$$L_{RPR} = LREF_{RPR} \cdot \exp\left(KTL_{RPR}\left[T - TLREF_{RPR}\right]\right) \tag{8.154}$$

Table 8.15. Parameters for Root Mortality in Equation (8.154)

Parameter	Units	Thalassia	Halodule
$LREF_{RPR}$	$1/day$	0.0001	0.0004
KLR_{RPR}	dimensionless	0.07	0.07
$TLREF_{RPR}$	$^\circ$C	28	28

8.3.1.7 Production Rate for Epiphytes

The production or growth rate for epiphytes on plant shoots is given by

$$P_{RPE} = PM_{RPE} \cdot f_w(N) \cdot f_2(I) \cdot f_3(T) \cdot f_4(RPE, RPS) \tag{8.155}$$

where ,

PM_{RPE} is the maximum growth rate under optimal conditions for plant shoots $(1/day)$,

$f_1(N)$ is the effect of suboptimal nutrient concentration $(0 \le f_1 \le 1)$,

$f_2(I)$ is the effect of suboptimal light intensity $(0 \le f_2 \le 1)$,

$f_3(T)$ is the effect of suboptimal temperature $(0 \le f_3 \le 1)$, and

$f_4(RPE, RPS)$ is the effect of epiphyte and host rooted density $(0 \le f_4 \le 1)$.

8.3.1.7.1 Effect of Nutrients on Epiphyte Growth

Nutrient limitation for epiphytes is given by

$$f_1(N) = \min\left(\frac{NH4 + NO3}{KHN_{RPE} + NH4 + NO3}, \frac{PO4d}{KHP_{RPE} + PO4d}\right) \tag{8.156}$$

where,

$NH4$ is the ammonium nitrogen concentration $(g\,N/m^3)$,

$NO3$ is the nitrate + nitrite nitrogen concentration $(g\,N/m^3)$,

KHN_{RPE} is the half-saturation constant for nitrogen uptake for epiphytes $(g\,N/m^3)$,

$PO4d$ is the dissolved phosphate phosphorus concentration $(g\,P/m^3)$, and

KHP_{RPE} is the half-saturation constant for phosphorus uptake for epiphytes $(g\,P/m^3)$.

8.3.1.7.2 Effect of Light on Epiphyte Growth

Light limitation for epiphyte growth is based on a Monod type equation similar to equation (8.140)

$$f_2(I) = \left(\frac{I_{RPE}}{I_{RPE} + KHI_{RPE}}\right) \tag{8.157}$$

where,

KHI_{RPE} is the half-saturation constant for epiphyte light limitation (W/m^2).

The average light intensity over the shoot canopy

$$I_{RPEA} = \frac{I_{ws}}{K_{essic} \cdot H_{RPS}} \exp\left(-K_{essac} \cdot (H - H_{RPS})\right) \cdot \left(1 - \exp\left(-K_{essic} \cdot H_{RPS}\right)\right) \tag{8.158}$$

which follows from equation (8.137) with $K_{eRPE} = 0$, can be used or equation (8.157) can be averaged over the shoot canopy to give

$$f_{2avg}(I) = \frac{1}{K_{essic} \cdot H_{RSP}} \ln\left(\frac{KHI + I_{ct} exp\left(-K_{essic} \cdot (H - H_{RSP})\right)}{KHI + I_{ct} exp\left(-K_{essic} \cdot H\right)}\right) \tag{8.159}$$

$$I_{ct} = I_{ws} \cdot \exp\left(-K_{essic} \cdot (H - H_{RSP})\right) \tag{8.160}$$

which follows from equation (8.142) with $Ke_{RPE} = 0$.

8.3.1.7.3 Effect of Temperature on Epiphyte Growth

The effect of temperature on epiphyte growth is given by

$$f_3(T) = \begin{cases} \exp\left(-KTP1_{RPE}[T - TP1_{RPE}]^2\right) & if\ T \le TP1_{RPE} \\ 1\ if\ TP1_{RPE} < T < TP2_{RPE} \\ \exp\left(-KTP2_{RPE}[T - TP2_{RPE}]^2\right) & if\ T \ge TP1_{RPE} \end{cases} \tag{8.161}$$

where,

T is the temperature ($^\circ C$) provided from the hydrodynamic model,

$TP1_{RPE} < T < TP2_{RPE}$ is the optimal temperature range for epiphyte production ($^\circ C$),

$KTP1_{RPE}$ is the effect of temperature below $TM1RPS$ on epiphyte production ($1/^\circ C^2$), and

$KTP2_{RPE}$ is the effect of temperature above $TM2RPS$ on epiphyte production ($1/^\circ C^2$)

or an exponential function.

$$f_3(T) = \exp\left(KTP_{RPE}[T - TPREF_{RPE}]\right) \tag{8.162}$$

where,

$TPREF_{RPE}$ is the reference temperature for shoot production ($^\circ C$), and

KTP_{RPE} is the effect of temperature on shoot production ($1/^\circ C$).

8.3.1.7.4 Effect of Epiphyte and Rooted Plant Density on Epiphyte Growth

The effect of rooted plant density on growth is give by

$$f_4(RPE, RPS) = 1 - \left(\frac{RPE \cdot \delta_{RPE}}{W_{RPE} \sum_{Nspecies} \left(\frac{2 \cdot RPS \cdot \delta_{RPS}}{W_{RPS}} \right)} \right)^2 \tag{8.163}$$

where

δ_{RPE} is the Epiphyte dry mass to carbon mass ratio

W_{RPE} (κe) is the maximum epiphyte mass per unit shoot area

8.3.1.8 Respiration Rate for Epiphytes

The respiration rate for epiphytes is assumed to be temperature dependent

$$R_{RPE} = RREF_{RPE} \cdot \exp\left(KTR_{RPE}\left[T - TRREF_{RPE}\right]\right) \tag{8.164}$$

where,

$RREF_{RPE}$ is the reference respiration rate for epiphytes $(1/day)$,

T is the temperature $(^{\circ}C)$ provided from the hydrodynamic model,

$TRREF_{RPE}$ is the reference temperature for epiphytes respiration $(^{\circ}C)$, and

KTR_{RPE} is the effect of temperature on epiphytes respiration $(1/^{\circ}C^2)$.

8.3.1.9 Non-Respiration Loss Rate for Epiphytes

The non-respiration loss rate for shoots is assumed to have a temperature dependency

$$L_{RPE} = LREF_{RPE} \cdot \exp\left(KTL_{RPE}\left[T - TLREF_{RPE}\right]\right) \tag{8.165}$$

where,

$LREF_{RPE}$ is the reference non-respiration loss rate for epiphytes $(1/day)$,

T is the temperature $(^{\circ}C)$ provided from the hydrodynamic model,

$TLREF_{RPE}$ is the reference temperature for epiphytes loss $(^{\circ}C)$, and

KTL_{RPE} is the effect of temperature on epiphytes loss $(1/^{\circ}C^2)$.

8.3.1.10 Decay Rate for Shoot Detritus

The decay rate for shoot detritus is assumed to have a temperature dependency

$$L_{RPD} = LREF_{RPD} \cdot \exp\left(KTL_{RPD}\left[T - TLREF_{RPD}\right]\right) \tag{8.166}$$

where,

$LREF_{RPD}$ is the reference non-respiration loss rate for epiphytes ($1/day$),

T is the temperature ($^{\circ}C$) provided from the hydrodynamic model,

$TLREF_{RPD}$ is the reference temperature for epiphytes loss ($^{\circ}C$), and

KTL_{RPD} is the effect of temperature on epiphytes loss ($1/^{\circ}C^2$).

.

8.3.1.11 Coupling with Organic Carbon

The interaction between rooted plants and epiphytes and water column and bed organic carbon species is given by

$$\frac{\partial RPOC_W}{\partial t} = \frac{1}{H}\left(FCR_{RPS} \cdot R_{RPS} + (1 - F_{RPSD}) \cdot FCRL_{RPS} \cdot L_{RPS}\right) RPS + \frac{1}{H}\left(FCR_{RPE} \cdot R_{RPE} + FCRL_{RPE} \cdot L_{RPE}\right) RPE + \frac{1}{H} FCRL_{RPD} \cdot L_{RPD} \cdot RPD \tag{8.167}$$

$$\frac{\partial RPOC_B}{\partial t} = \frac{1}{B}\left(FCR_{RPR} \cdot R_{RPR} + FCRL_{RPR} \cdot L_{RPR}\right) RPR \tag{8.168}$$

$$\frac{\partial LPOC_W}{\partial t} = \frac{1}{H}\left(FCL_{RPS} \cdot R_{RPS} + (1 - F_{RPSD}) \cdot FCLL_{RPS} \cdot L_{RPS}\right) RPS + \frac{1}{H}\left(FCL_{RPE} \cdot R_{RPE} + FCLL_{RPE} \cdot L_{RPE}\right) RPE + \frac{1}{H} FCLL_{RPD} \cdot L_{RPD} \cdot RPD \tag{8.169}$$

$$\frac{\partial LPOC_B}{\partial t} = \frac{1}{B}\left(FCL_{RPR} \cdot R_{RPR} + FCLL_{RPR} \cdot L_{RPR}\right) RPR \tag{8.170}$$

$$\frac{\partial DOC_W}{\partial t} = \frac{1}{H}\left(FCD_{RPS} \cdot R_{RPS} + (1 - F_{RPSD}) \cdot FCDL_{RPS} \cdot L_{RPS}\right) RPS + \frac{1}{H}\left(FCD_{RPE} \cdot R_{RPE} + FCDL_{RPE} \cdot L_{RPE}\right) RPE + \frac{1}{H} FCDL_{RPD} \cdot L_{RPD} \cdot RPD \tag{8.171}$$

$$\frac{\partial DOC_B}{\partial t} = \frac{1}{B}\left(FCD_{RPR} \cdot R_{RPR} + FCDL_{RPR} \cdot L_{RPR}\right) RPR \tag{8.172}$$

where,

$RPOC$ is the concentration of refractory particulate organic carbon ($g\ C/m^3$),

$LPOC$ is the concentration of labile particulate organic carbon ($g\ C/m^3$),

DOC is the concentration of dissolved organic carbon ($g\ C/m^3$),

FCR is the fraction of respired carbon produced as refractory particulate organic carbon,

FCL is the fraction of respired carbon produced as labile particulate organic carbon,

FCD is the fraction of respired carbon produced as dissolved organic carbon,

$FCRL$ is the fraction of non-respired carbon produced as refractory particulate organic carbon,

$FCLL$ is the fraction of non-respired carbon produced as labile particulate organic carbon,

$FCDL$ is the fraction of non-respired carbon produced as dissolved organic carbon,

H is the depth of water column, and

B is the depth of bed.

8.3.1.12 Coupling with Dissolved Oxygen

The interaction between rooted plants and epiphytes and dissolved oxygen is given by

$$\frac{\partial DO_W}{\partial t} = \frac{1}{H}\left(P_{RPS}\cdot RPSOC\cdot RPS + P_{RPE}\cdot RPEOC\cdot RPE\right) \tag{8.173}$$

where,

DO is the concentration of dissolved oxygen ($g\ O_2/m^3$),

$RPSOC$ is the oxygen to carbon ratio for plant shoots ($g\ O_2\ per\ g\ C$), and

$RPEOC$ is the oxygen to carbon ratio for epiphytes ($g\ O_2\ per\ g\ C$).

8.3.1.13 Coupling with Phosphorous

The interaction between rooted plants and epiphytes and water column and bed phosphorous is given by

$$\begin{aligned}\frac{\partial RPOP_W}{\partial t} = {} & \frac{1}{H}\left(FPR_{RPS}\cdot R_{RPS} + (1-F_{RPSD})\cdot FPRL_{RPS}\cdot L_{RPS}\right)\cdot RPSPC\cdot RPS \\ & + \frac{1}{H}\left(FPR_{RPE}\cdot R_{RPE} + FPRL_{RPE}\cdot L_{RPE}\right)\cdot RPEPC\cdot RPE \\ & + \frac{1}{H}FPRL_{RPD}\cdot L_{RPD}\cdot RPSPC\cdot RPD\end{aligned} \tag{8.174}$$

$$\frac{\partial RPOP_B}{\partial t} = \frac{1}{B}\left(FPR_{RPR}\cdot R_{RPR} + FPRL_{RPR}\cdot L_{RPR}\right) RPRPC\cdot RPR \tag{8.175}$$

$$\begin{aligned}\frac{\partial LPOP_W}{\partial t} = {} & \frac{1}{H}\left(FPL_{RPS}\cdot R_{RPS} + (1-F_{RPSD})\cdot FPLL_{RPS}\cdot L_{RPS}\right)\cdot RPSPC\cdot RPS \\ & + \frac{1}{H}\left(FPL_{RPE}\cdot R_{RPE} + FPLL_{RPE}\cdot L_{RPE}\right)\cdot RPEPC\cdot RPE \\ & + \frac{1}{H}FPLL_{RPD}\cdot L_{RPD}\cdot RPSPC\cdot RPD\end{aligned} \tag{8.176}$$

$$\frac{\partial LPOP_B}{\partial t} = \frac{1}{B}\left(FPL_{RPR}\cdot R_{RPR} + FPLL_{RPR}\cdot L_{RPR}\right) RPRPC\cdot RPR \tag{8.177}$$

$$\begin{aligned}\frac{\partial DOP_W}{\partial t} = {} & \frac{1}{H}\left(FPD_{RPS}\cdot R_{RPS} + (1-F_{RPSD})\cdot FPDL_{RPS}\cdot L_{RPS}\right)\cdot RPSPC\cdot RPS \\ & + \frac{1}{H}\left(FPD_{RPE}\cdot R_{RPE} + FPDL_{RPE}\cdot L_{RPE}\right)\cdot RPEPC\cdot RPE \\ & + \frac{1}{H}FCDL_{RPD}\cdot L_{RPD}\cdot RPSPC\cdot RPD\end{aligned} \tag{8.178}$$

$$\frac{\partial DOP_B}{\partial t} = \frac{1}{B}\left(FPD_{RPR}\cdot R_{RPR} + FPDL_{RPR}\cdot L_{RPR}\right) RPRPC\cdot RPR \tag{8.179}$$

$$\begin{aligned}\frac{\partial PO4t_W}{\partial t} = {} & \frac{1}{H}\left(FPI_{RPS}\cdot R_{RPS} + (1-F_{RPSD})\cdot FPIL_{RPS}\cdot L_{RPS}\right)\cdot RPSPC\cdot RPS \\ & + \frac{1}{H}\left(FPI_{RPE}\cdot R_{RPE} + FPIL_{RPE}\cdot L_{RPE}\right)\cdot RPEPC\cdot RPE \\ & + \frac{1}{H}FCIL_{RPD}\cdot L_{RPD}\cdot RPSPC\cdot RPD - \frac{1}{H}F_{RPSPW}\cdot R_{RPS}\cdot RPSPC\cdot RPS \\ & - \frac{1}{H}P_{RPE}\cdot RPEPC\cdot RPE\end{aligned} \tag{8.180}$$

$$\begin{aligned}\frac{\partial PO4t_B}{\partial t} = {} & \frac{1}{B}\left(FPI_{RPR}\cdot R_{RPR} + FPIL_{RPR}\cdot L_{RPR}\right) RPRPC\cdot RPR - \\ & \frac{1}{H}\left(1-F_{RPSPW}\right) P_{RPS}\cdot RPRPC\cdot RPS\end{aligned} \tag{8.181}$$

$$F_{RPSPW} = \frac{KHP_{RPR}P04d_w}{KHP_{RPR}P04d_w + KHP_{RPS}P04d_b} \tag{8.182}$$

where,

$RPOP$ is the concentration of refractory particulate organic phosphorous ($g\ C/m^3$),

$LPOP$ is the concentration of labile particulate organic phosphorous ($g\ C/m^3$),

DOP is the concentration of dissolved organic phosphorous ($g\ C/m^3$),

$PO4t = PO4d + PO4p$ is the total phosphate ($g\ P/m^3$),

$PO4d$ is the dissolved phosphate ($g\ P/m^3$),

$PO4p$ is the particulate (sorbed) phosphate ($g\ P/m^3$),

FPR is the fraction of respired phosphorous produced as refractory particulate organic phosphorous,

FPL is the fraction of respired phosphorous produced as labile particulate organic phosphorous,

FPD is the fraction of respired phosphorous produced as dissolved organic phosphorous,

FPI is the fraction of respired phosphorous produced as total phosphate,

$FPRL$ is the fraction of non-respired phosphorous produced as refractory particulate organic phosphorous,

$FPLL$ is the fraction of non-respired phosphorous produced as labile particulate organic phosphorous,

$FPDL$ is the fraction of non-respired phosphorous produced as dissolved organic phosphorous,

$FPIL$ is the fraction of non-respired phosphorous produced as total phosphate,

$RPSPC$ is the plant shoot phosphorous to carbon ratio ($g\ P\ per\ g\ C$),

$RPRPC$ is the plant root phosphorous to carbon ratio ($g\ P\ per\ g\ C$),

$RPEPC$ is the epiphyte phosphorous to carbon ratio ($g\ P\ per\ g\ C$),

F_{RPSPW} is the fraction of $PO4d$ uptake from water column,

KHP_{RPS} is the half-saturation constant for phosphorus uptake from water column ($g\ P/m^3$), and

KHP_{RPR} is the half-saturation constant for phosphorus uptake from bed ($g\ P/m^3$).

8.3.1.14 Coupling with Nitrogen

The interaction between rooted plants and epiphytes and water column and bed phosphorous is given by

$$\frac{\partial RPON_W}{\partial t} = \frac{1}{H}\left(FNR_{RPS}\cdot R_{RPS} + (1-F_{RPSD})\cdot FNRL_{RPS}\cdot L_{RPS}\right)\cdot RPSNC\cdot RPS + \frac{1}{H}\left(FNR_{RPE}\cdot R_{RPE} + FNRL_{RPE}\cdot L_{RPE}\right)\cdot RPENC\cdot RPE + \frac{1}{H}FNRL_{RPD}\cdot L_{RPD}\cdot RPSNC\cdot RPD \quad (8.183)$$

$$\frac{\partial RPON_B}{\partial t} = \frac{1}{B}\left(FNR_{RPR}\cdot R_{RPR} + FNRL_{RPR}\cdot L_{RPR}\right) RPRNC\cdot RPR \quad (8.184)$$

$$\frac{\partial LPON_W}{\partial t} = \frac{1}{H}\left(FNL_{RPS}\cdot R_{RPS} + (1-F_{RPSD})\cdot FNLL_{RPS}\cdot L_{RPS}\right)\cdot RPSNC\cdot RPS + \frac{1}{H}\left(FNL_{RPE}\cdot R_{RPE} + FNLL_{RPE}\cdot L_{RPE}\right)\cdot RPENC\cdot RPE + \frac{1}{H}FNLL_{RPD}\cdot L_{RPD}\cdot RPSNC\cdot RPD \quad (8.185)$$

$$\frac{\partial LPON_B}{\partial t} = \frac{1}{B}\left(FNL_{RPR}\cdot R_{RPR} + FNLL_{RPR}\cdot L_{RPR}\right) RPRNC\cdot RPR \quad (8.186)$$

$$\frac{\partial DON_W}{\partial t} = \frac{1}{H}\left(FND_{RPS}\cdot R_{RPS} + (1-F_{RPSD})\cdot FNDL_{RPS}\cdot L_{RPS}\right)\cdot RPSNC\cdot RPS + \frac{1}{H}\left(FND_{RPE}\cdot R_{RPE} + FNDL_{RPE}\cdot L_{RPE}\right)\cdot RPENC\cdot RPE + \frac{1}{H}FNDL_{RPD}\cdot L_{RPD}\cdot RPSNC\cdot RPD \quad (8.187)$$

$$\frac{\partial DON_B}{\partial t} = \frac{1}{B}\left(FND_{RPR}\cdot R_{RPR} + FNDL_{RPR}\cdot L_{RPR}\right) RPRNC\cdot RPR \quad (8.188)$$

$$\frac{\partial NH4_W}{\partial t} = \frac{1}{H}\left(FNI_{RPS}\cdot R_{RPS} + (1-F_{RPSD})\cdot FNIL_{RPS}\cdot L_{RPS}\right)\cdot RPSNC\cdot RPS + \frac{1}{H}\left(FNI_{RPE}\cdot R_{RPE} + FNIL_{RPE}\cdot L_{RPE}\right)\cdot RPENC\cdot RPE + \frac{1}{H}FNIL_{RPD}\cdot L_{RPD}\cdot RPSNC\cdot RPD - \frac{1}{H}PN_{RPS}\cdot F_{RPSNW}\cdot R_{RPS}\cdot RPSNC\cdot RPS - \frac{1}{H}PN_{RPE}\cdot P_{RPE}\cdot RPENC\cdot RPE \quad (8.189)$$

$$\frac{\partial NH4_W}{\partial t} = \frac{1}{B}\left(FNI_{RPR}\cdot R_{RPR} + FNIL_{RPR}\cdot L_{RPR}\right) RPRNC\cdot RPR - \frac{1}{H} PN_{RPE}\left(1-F_{RPSPW}\right) P_{RPS}\cdot RPSNC\cdot RPS \quad (8.190)$$

$$\frac{\partial NO3_W}{\partial t} = -\frac{1}{H}\left(1-PN_{RPS}\right) F_{RPSNW}\cdot P_{RPS}\cdot RPSNC\cdot RPS - \frac{1}{H}\left(1-PN_{RPE}\right) P_{RPE}\cdot RPENC\cdot RPE \quad (8.191)$$

$$\frac{\partial NO3_B}{\partial t} = -\frac{1}{H}\left(1-PN_{RPS}\right)\left(1-F_{RPSNW}\right) P_{RPS}\cdot RPSNC\cdot RPS \quad (8.192)$$

$$PN_{RPS} = \frac{NH4\cdot NO3}{\left(KHNP_{RPS}+NH4\right)\left(KHNP_{RPS}+NO3\right)} + \frac{NH4\cdot KHNP_{RPS}}{\left(NH4+NO3\right)\left(KHNP_{RPS}+NO3\right)} \quad (8.193)$$

$$PN_{RPE} = \frac{NH4\cdot NO3}{\left(KHNP_{RPE}+NH4\right)\left(KHNP_{RPE}+NO3\right)} + \frac{NH4\cdot KHNP_{RPE}}{\left(NH4+NO3\right)\left(KHNP_{RPE}+NO3\right)} \quad (8.194)$$

$$F_{RPSNW} = \frac{KHN_{RPR}(NH4+NO3)_w}{KHN_{RPR}(NH4+NO3)_w + KHN_{RPS}(NH4+NO3)_b} \quad (8.195)$$

where,

RPON is the concentration of refractory particulate organic nitrogen ($g\,N/m^3$),

LPON is the concentration of labile particulate organic nitrogen ($g\,N/m^3$),

DON is the concentration of dissolved organic nitrogen ($g\,N/m^3$),

NH4 is the ammonia ($g\,N/m^3$),

NO3 is the nitrate + nitrite nitrogen ($g\,N/m^3$),

FNR is the fraction of respired nitrogen produced as refractory particulate organic nitrogen,

FNL is the fraction of respired nitrogen produced as labile particulate organic nitrogen,

FND is the fraction of respired nitrogen produced as dissolved organic nitrogen,

FNI is the fraction of respired nitrogen produced as ammonia,

$FNRL$ is the fraction of non-respired nitrogen produced as refractory particulate organic nitrogen,

$FNLL$ is the fraction of non-respired nitrogen produced as labile particulate organic nitrogen,

$FNDL$ is the fraction of non-respired nitrogen produced as dissolved organic nitrogen,

$FNIL$ is the fraction of non-respired nitrogen produced as ammonia,

$RPSNC$ is the plant shoot nitrogen to carbon ratio (g; N; $per\ g\ C$),

$RPRNC$ is the plant root nitrogen to carbon ratio (g; N; $per\ g\ C$),

F_{RPSNW} is the plant shoot fraction of $NH4$ and NOX uptake from water column,

PN_{RPS} is the ammonia nitrogen preference fraction for plant shoots,

$KHNP_{RPS}$ is the saturation coefficient for nitrogen preference for plant shoots (g; N; $per\ g\ C$),

PN_{RPE} is the ammonia nitrogen preference fraction for epiphytes,

$KHNP_{RPE}$ is the saturation coefficient for nitrogen preference for epiphytes (g; N; $per\ g\ C$),

KHN_{RPS} is the half-saturation constant for nitrogen uptake from water column ($g\ N/m^3$), and

KHN_{RPR} is the half-saturation constant for nitrogen uptake from bed ($g\ N/m^3$).

8.4. Macroalgae (Periphyton) State Variable

The EFDC+ water quality model was augmented to represent benthic attached algae (often referred to as macroalgae in estuarine waters and periphyton in fresh waters) using the existing framework for phytoplankton growth kinetics. Mathematical relationships based on the impacts of temperature, available light, available nutrients, stream velocity, and density-dependent interactions were incorporated into the algae growth kinetics framework within EFDC+. The major difference between modeling techniques for attached and free-floating algae are as follows; (1) attached algae are expressed in terms of areal densities rather than volumetric concentrations, (2) attached algae growth can be limited by the availability of bottom substrate, (3)the availability of nutrients to the macroalgae matrix can be influenced by stream velocity, and (4) macroalgae are not subject to hydrodynamic transport. A good description of periphyton kinetics as it relates to water quality modeling

can be found in Warwick et al. (1997) and has been used to develop the current section of this document.

A mass balance approach was used to model macroalgae growth with carbon serving as the measure of standing crop size or biomass. For each model grid cell, the equation for macroalgae growth is slightly different than the one for free-floating algae (equation (8.7)):

$$P_m = PM_m \cdot f_1(N) \cdot f_2(I) \cdot f_3(T) \cdot f_4(V) \cdot f_5(D) \tag{8.196}$$

where,

PM_m is the maximum growth rate under optimal conditions for macroalgae,

$f_1(N)$ is the effect of suboptimal nutrient concentration $(0 \leq f_1 \leq 1)$,

$f_2(I)$ is the effect of suboptimal light intensity $(0 \leq f_2 \leq 1)$,

$f_3(T)$ is the effect of suboptimal temperature $(0 \leq f_3 \leq 1)$,

$f_4(V)$ is the velocity limitation factor $(0 \leq f_4 \leq 1)$, and

$f_5(D)$ is the density dependent growth rate reduction factor $(0 \leq f_3 \leq 1)$.

The basic growth kinetics for macroalgae were developed from those supplied by EFDC+ and others developed by Runke (1985). The macroalgae population as a whole is characterized by the total biomass present without considering the different species and their associated environmental processes. The optimum growth for the given temperature is adjusted for light, nutrients, velocity, and density- dependent limitations. Each growth limitation factor can vary from 0 to 1. A value of 1 indicates the factor does not limit growth, and a value of 0 means the factor is so severely limiting that the growth is stopped entirely (Bowie et al., 1985).

Stream velocity has a two-fold effect on periphyton productivity in freshwater streams: velocity increases to a certain level to enhance biomass accrual, but further increases result in substantial scouring (Horner et al., 1990). A benthic algal population is typified as a plant community with an understory and overstory. The entire community is called a matrix. As the matrix develops, the periphyton community is composed of an outer layer of photosynthetically active cells and inner layers of senescent and decomposing cells. Layering can also develop among different species of periphyton. Environmental conditions within the matrix are altered by the physical structure of the periphyton. This influences nutrient uptake and primary production rates of the algae (Sand-Jensen 1983). Above a certain level, current has a simulating effect on periphyton metabolism by mixing the overlying waters with nutrient poor waters that develop around cells (Whitford and Schumacher, 1964). The physical structure of the periphyton community and nutrient uptake by periphyton interfere with nutrient flux through the microbial matrix (Jan Stevenson and Glover, 1993).

Current is constantly scouring periphyton from its substrate. At high enough velocities, shear stress can result in substantial biomass reduction. Even at low velocities, sudden increases in velocity raise instantaneous loss rates substantially, but these high rates persist

only briefly (Horner et al., 1990). An increase in velocity above that to which benthic algae are accustomed, leads to increased loss rates and temporarily reduced biomass. However, recolonization and growth after biomass reduction are usually rapid. The effects of suboptimal velocity upon growth rate are represented in the model by a velocity limitation function. Two options are available in the model for specifying the velocity limitation; (1) a Michaelis-Menton (or Monod) equation (8.197), and (2) a five-parameter logistic function equation (8.198). The Monod equation limits macroalgae growth due to low velocities whereas the five-parameter logistic function can be configured to limit growth due to either low or high velocities.

Velocity limitation option 1, the Michaelis-Menton equation is written as follows:

$$f_4(V) = \frac{U}{KMV + U} \tag{8.197}$$

where,

U is the stream velocity (m/s), and

KMV is the half-saturation velocity (m/s).

Velocity limitation option 2, the five-parameter logistic function is as follows:

$$f_4(V) = d + \frac{a-d}{\left[1 + \left(\frac{U}{c}\right)^b\right]^e} \tag{8.198}$$

where ,

U is the stream velocity (m/s),

a is the asymptote at minimum x,

b is the slope after asymptote a,

c is the x-translation,

d is the asymptote at maximum x, and

e is the slope before asymptote d.

The half-saturation velocity in equation (8.197) is the velocity at which half the maximum growth rate occurs. This effect is analogous to the nutrient limitation because the effect of velocity at suboptimal levels on periphyton growth is due to increasing the exchange of nutrients between the algal matrix and the overlying water (Runke, 1985). However, this formula can be too limiting at low velocities. This function does not allow periphyton growth in still waters, but periphyton does grow in still waters such as lakes. Therefore, the function is applied only at velocities above a minimum threshold level ($KMVmin$). When velocities are at or below this lower level, the limitation function is applied at the minimum level. Above this velocity, the current produces a steeper diffusion gradient around the periphyton (Whitford and Schumacher, 1964). A minimum formulation is used to combine the

limiting factors for nitrogen, phosphorus, and velocity. The most severely limiting factor alone limits periphyton growth. Note that the equation (8.198) can be configured so that low velocities are limiting by setting parameter d greater than parameter a, and vice versa to limit growth due to high velocities. In waters that are rich in nutrients, low velocities will not limit growth. However, high velocities may cause scouring and detachment of the macroalgae resulting in a reduction in biomass. The five-parameter logistic function can be configured to approximate this reduction by limiting growth at high velocities.

Macroalgae (periphyton) growth can also be limited by the availability of suitable substrate (Ross and Ultsch, 1980). Macroalgae communities reach maximum rates of primary productivity at low levels of biomass (McIntire, 1973; Pfeifer and McDiffett, 1975). The relationship between standing crop and production employs the Michaelis-Menton kinetic equation:

$$f_5(D) = \frac{KBP}{KBP + P_m} \tag{8.199}$$

where,

KBP is the half-saturation biomass level ($g\,C/m^2$), and

P_m is the macroalgae biomass level ($g\,C/m^2$).

The half-saturation biomass level (KBP) is the biomass at which half the maximum growth rate occurs. Caupp et al. (1991) used a KBP value of $5.0 g\,C/m^2$ (assuming 50% of ash free dry mass is carbon) for a region of the Truckee River system in California. The function in equation (8.199) allows maximum rates of primary productivity at low levels of biomass with decreasing rates of primary productivity as the community matrix expands.

Table 8.16. Parameters related to algae in water column

Parameter	Value[a]	Equation Number[b]
$*PM_c\ (1/day)$	2.5 (upper Potomac only)	(8.7)
$*PM_d\ (1/day)$	2.25	(8.7)
$*PM_g\ (1/day)$	2.5	(8.7)
$KHN_x\ (g\,N/m^3)$	0.01 (all groups)	(8.8)
$KHP_x\ (g\,P/m^3)$	0.001 (all groups)	(8.8)
$KHS\ (g\,Si/m^3)$	0.05	(8.8)
FD	Temporally-varying input	(8.19)
$I_o\ (langleys/day)$	Temporally-varying input	(8.11)

Continued on next page

Table 8.16 – continued from previous page

Parameter	Value[a]	Equation Number[b]
$*Ke_b$ $(1/m)$	spatially-varying input	(8.12)
Ke_{ISS} $(1/m\ per\ m^3)$	NA[c]	(8.12)
Ke_{Chl} $(1/m\ per\ mg\ Chl/m^3)$	0.017	(8.12)
$CChl_x$ $(g\ C\ per\ mg\ Chl)$	0.06 (all groups)	(8.12)
$(D_{opt})_x$ (m)	1.0 (all groups)	(8.22)
$(I_s)_{min}$ $(langleys/day)$	40.0	(8.22)
CI_a, CI_b and CI_c	0.7, 0.2 & 0.1	(8.23)
TM_c, TM_d and TM_g (^{o}C)	27.5, 20.0 & 25.0	(8.28)
$KTG1_c$ and $KTG2_c$ (^{o}C^{-2})	0.005 & 0.004	(8.28)
$KTG1_d$ and $KTG2_d$ (^{o}C^{-2})	0.004 & 0.006	(8.28)
$KTG1_g$ and $KTG2_g$ (^{o}C^{-2})	0.008 & 0.01	(8.28)
$STOX$ (ppt)	1.0	(8.29)
$*BMR_c$ $(1/day)$	0.04	(8.30)
$*BMR_d$ $(1/day)$	0.01 (0.03 during Jan.-May in saltwater only)	(8.30)
$*BMR_g$ $(1/day)$	0.01	(8.30)
TR_x, (^oC)	20.0 (all groups)	(8.30)
KTB_x $(^oC^{-1})$	0.069 (all groups)	(8.30)
$*PRR_c$ $(1/day)$	0.01	(8.31)
$*PRR_d$ $(1/day)$	0.215 (0.065 during Jan.-May in saltwater only)	(8.31)
$*PRR_g$ $(1/day)$	0.215	(8.31)
$*WS_c$ (m/day)	0.0	(8.6)
$*WS_d$ (m/day)	0.35 (January - May) 0.1 (June - December)	(8.6)
$*WS_g$ (m/day)	0.1	(8.6)

Continued on next page

Table 8.16 – continued from previous page

Parameter	Value[a]	Equation Number[b]

[a] The evaluation of these values are detailed in Chapter IX of (Cerco and Cole, 1994).
[b] The equation number where the corresponding parameter is first shown and defined.
[c] Not available in (Cerco and Cole, 1994) since their formulations do not include these parameters.
* The parameters declared as an array in the source code.

8.5. Sediment Diagenesis and Flux Formulation

The EFDC+ water quality model provides three options for defining the sediment-water interface fluxes for nutrients and dissolved oxygen. The options are; (1) externally forced spatially and temporally constant fluxes, (2) externally forced spatially and temporally variable fluxes, and (3) internally coupled fluxes simulated with the sediment diagenesis model. The water quality state variables that are controlled by diffusive exchange across the sediment-water interface include phosphate, ammonia, nitrate, silica, chemical oxygen demand and dissolved oxygen. The first two options require that the sediment fluxes be assigned as spatial/temporal forcing functions based on either observed site-specific data from field surveys or best estimates based on the literature and sediment bed characteristics. The first two options, although acceptable for model calibration against historical data sets, do not provide the cause-effect predictive capability that is needed to evaluate future water quality conditions that might result from implementation of pollutant load reductions from watershed runoff. The third option, activation of the sediment diagenesis model developed by Di Toro et al. (2001) does provide the cause-effect predictive capability to evaluate how water quality conditions might change with implementation of alternative load reduction or management scenarios.

Living and non-living particulate organic carbon deposition, simulated in the EFDC+ water quality model, is internally coupled with the EFDC+ sediment diagenesis model. The sediment diagenesis model, based on the sediment flux model of Di Toro et al. (2001), describes the decomposition of particulate organic matter in the sediment bed, the consumption of dissolved oxygen at the sediment-water interface (*SOD*) and the exchange of dissolved constituents (ammonia, nitrate, phosphate, silica, *COD*) across the sediment-water interface, state variables of the EFDC+ sediment flux model are sediment bed temperature, sediment bed particulate organic carbon (*POC*), particulate organic nitrogen (PON), particulate organic phosphorus (*POP*), porewater concentrations of phosphate, ammonia, nitrate, silica and sulfide/methane. The sediment diagenesis model computes sediment-water fluxes of chemical oxygen demand (*COD*), sediment oxygen demand (*SOD*), phosphate, ammonium, nitrate, and silica. The state variables modeled for a typical lake sediment flux model are listed in Table 8.23. An overview of the source and sink terms is presented with a description of each state variable group in this section. The details of the state variable

Table 8.17. Parameters related to organic carbon in water column

Parameter	Value[a]	Equation Number[b]
$FCRP$	0.35	(8.32)
$FCLP$	0.55	(8.33)
FCDP	0.10	(8.34)
FCD_x	0.0 (all groups)	(8.34)
$*WS_{RP}$ (m/day)	1.0	(8.32)
$*WS_{LP}$ (m/day)	1.0	(8.33)
KHR_x $(g\ O_2/m^3)$	0.5 (all groups)	(8.34)
$KHOR_{DO}$ $(g\ O_2/m^3)$	0.5	(8.42)
K_{RC} $(1/day)$	0.005	(8.43)
K_{LC} $(1/day)$	0.075	(8.44)
K_{DC} $(1/day)$	0.01	(8.45)
K_{RCalg} $(1/day\ per\ g\ C/m^3)$	0.0	(8.43)
K_{LCalg} $(1/day\ per\ g\ C/m^3)$	0.0	(8.44)
K_{DCalg} $(1/day\ per\ g\ C/m^3)$	0.0	(8.45)
TR_{HDR} $(^O\mathrm{C})$	20.0	(8.43)
TR_{MIN} $(^O\mathrm{C})$	20.0	(8.45)
KT_{HDR} $(^O\mathrm{C}^{-1})$	0.069	(8.43)
KT_{MIN} $(^O\mathrm{C}^{-1})$	0.069	(8.45)
$KHDN_N$ $(g\ N/m^3)$	0.1	(8.47)
$AANOX$	0.5	(8.47)

[a] The evaluation of these values are detailed in Chapter IX of (Cerco and Cole, 1994).
[b] The equation number where the corresponding parameter is first shown and defined.
* The parameters declared as an array in the source code.

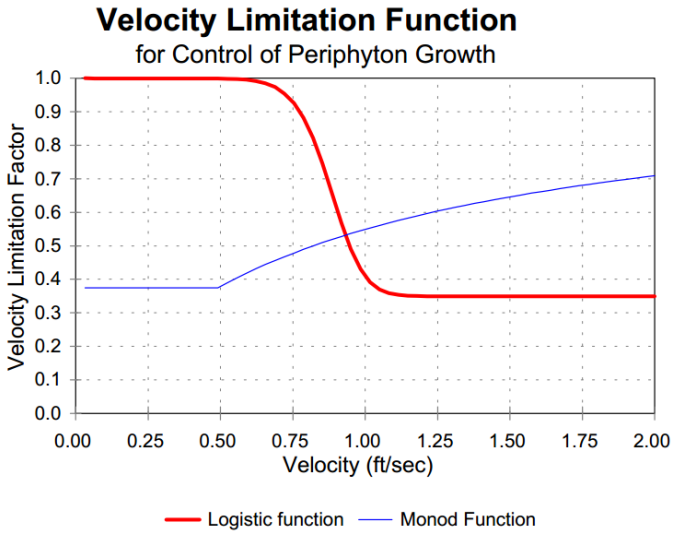

Fig. 8.2. Velocity limitation function for (Option 1) the Monod equation where $KMV = 0.25m/s$ and $KMVmin = 0.15m/s$, and (Option 2) the 5-parameter logistic function where $a = 1.0, b = 12.0, c = 0.3, d = 0.35$, and $e = 3.0$ (high velocities are limiting).

equations, kinetic terms and numerical solution methods for the sediment diagenesis model are presented in Di Toro et al. (2001); Ji (2008); Park et al. (1995).

A sediment process model developed by DiToro and Fitzpatrick (1993) hereinafter referred to as D&F was coupled with CE-QUAL-ICM for Chesapeake Bay water quality modeling (Cerco and Cole, 1994). The sediment process model was slightly modified and incorporated into the EFDC+ water quality model to simulate the processes in the sediment and at the sediment-water interface. The description of the EFDC+ sediment process model in this section is from Park et al. (1995). The sediment process model has 27 water quality related state variables and fluxes (Table 8.24).

The nitrate state variables, numbers (15), (16) and (22) in Table 8.24, in the model represent the sum of nitrate and nitrite nitrogen. The three G classes for particulate organic matter (POM) in Layer 2, and the two layers for inorganic substances are described below.

In the sediment model, benthic sediments are represented as two layers (Figure 8.3). The upper layer (Layer 1) is in contact with the water column and may be oxic or anoxic depending on dissolved oxygen concentration in the overlying water. The lower layer (Layer 2) is permanently anoxic. The upper layer depth, which is determined by the penetration of oxygen into the sediments, is at its maximum only a small fraction of the total depth. Because H_1 ($\sim 0.1cm$) $<< H_2$,

$$H = H_1 + H_2 \approx H_2 \tag{8.200}$$

where,

H is the total depth (approximately $10cm$),

H_1 is the upper layer depth, and

H_2 is the lower layer depth.

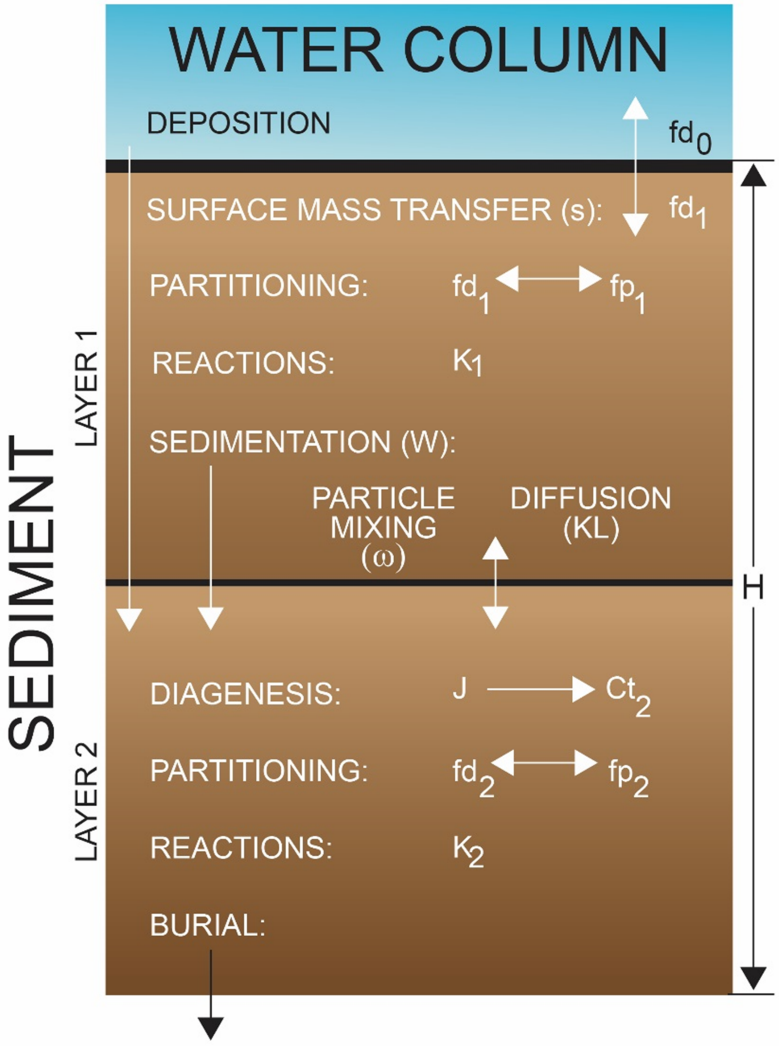

Fig. 8.3. Sediment layers and processes included in sediment process model

The model incorporates three basic processes (Figure 8.4); (1) depositional flux of *POM*, (2) the diagenesis of *POM*, and (3) the resulting sediment flux. The sediment model is driven by the net settling of particulate organic carbon, nitrogen, phosphorus and silica from the overlying water to the sediments (depositional flux). Because of the negligible thickness of the upper layer (equation (8.200)), deposition proceeds from the water column directly to the lower layer. Within the lower layer, the model simulates the diagenesis

(mineralization or decay) of deposited *POM*, which produces oxygen demand and inorganic nutrients (diagenesis flux). The third basic process is the flux of substances produced by diagenesis (sediment flux). Oxygen demand, as sulfide (in saltwater) or methane (in freshwater), takes three paths out of the sediments; (1) oxidation at the sediment-water interface as sediment oxygen demand, (2) export to the water column as chemical oxygen demand, or (3) burial to deep, inactive sediments.

Inorganic nutrients produced by diagenesis take two paths out of the sediments; (1) release to the water column, or (2) burial to deep, inactive sediments (Figure 8.4).

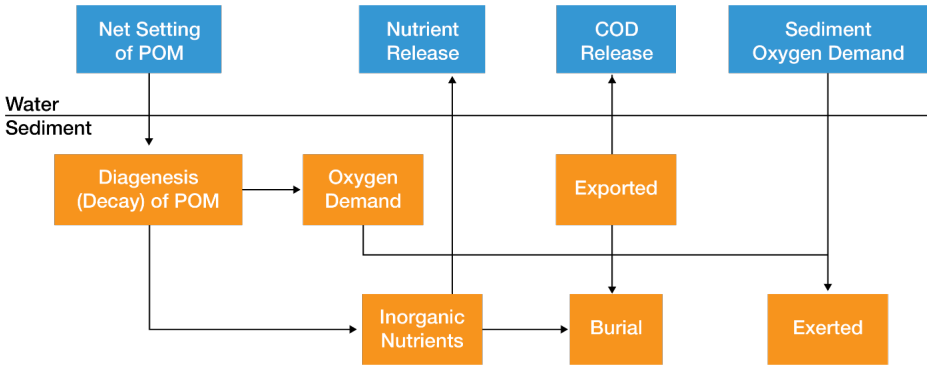

Fig. 8.4. Schematic diagram for sediment process model

This section describes the three basic processes with reactions and sources/sinks for each state variable. The method of solution includes finite difference equations, solution scheme, boundary and initial conditions. Complete model documentation can be found in DiToro and Fitzpatrick (1993).

8.5.1 Depositional Flux

Deposition is one process that couples the water column model with the sediment model. Consequently, deposition is represented in both the water column and sediment models. In the water column model, the governing mass-balance equations for the following state variables contain settling terms, which represent the depositional fluxes:

1. three algal groups, cyanobacteria, diatoms and green algae (equation (8.6))
2. refractory and labile particulate organic carbon (equations (8.32)and (8.33))
3. refractory and labile particulate organic phosphorus (equations (8.50) and (8.51) and total phosphate (equation (8.53))
4. refractory and labile particulate organic nitrogen (equations (8.67) and (8.68))
5. particulate biogenic silica (equation (8.84)) and available silica (equation (8.85))

The sediment model receives these depositional fluxes of particulate organic carbon (*POC*), particulate organic nitrogen (*PON*), particulate organic phosphorus (*POP*) and particulate biogenic silica (*PSi*). Because of the negligible thickness of the upper layer (equation (8.200)), deposition is considered to proceed from the water column directly to the lower layer. Since the sediment model has three G classes of POM, $G;(i = 1,2or3)$, depending on the time scales of reactivity (Section 5.2), the POM fluxes from the water column should be mapped into three G classes based on their reactivity. Then, the depositional fluxes for the i^{th} G class $(i = 1,\ 2\ or\ 3)$ may be expressed as:

$$J_{POC,i} = FCLP_i \cdot WS_{LP} \cdot LPOC^N + FCRP_i \cdot WS_{RP} \cdot RPOC^N + \sum_{x=c,d,g} FCB_{x,i} \cdot WS_x \cdot B_x^N \tag{8.201}$$

$$J_{PON,i} = FNLP_i \cdot WS_{LP} \cdot LPON^N + FNRP_i \cdot WS_{RP} \cdot RPON^N + \sum_{x=c,d,g} FNB_{x,i} \cdot ANC_x \cdot WS_x \cdot B_x^N \tag{8.202}$$

$$J_{POP,i} = FPLP_i \cdot WS_{LP} \cdot LPOP^N + FPRP_i \cdot WS_{RP} \cdot RPOP^N + \sum_{x=c,d,g} FPB_{x,i} \cdot APC \cdot WS_x \cdot B_x^N + \gamma_i \cdot WS_{TSS} \cdot PO4p^N \tag{8.203}$$

$$J_{PSi} = WS_d \cdot SU^N + ASC_d \cdot WS_d \cdot B_d^N + WS_{TSS} \cdot SAp^N \tag{8.204}$$

where,

$J_{POM,i}$ is the depositional flux of POM $(M = C,N$ or $P)$ routed into the i^{th} G class $(g/m^2/day)$,

J_{PSi} is the depositional flux of PSi $(g\ Si/m^2/day)$,

$FCLP_i, FNLP_i$ and $FPLP_i$ are the fraction of water column labile POC, PON and POP respectively, routed into the i^{th} G class in sediment,

$FCRP_i$, $FNRP_i$ and $FPRP_i$ are the fraction of water column refractory POC, PON and POP respectively, routed into the i^{th} G class in sediment,

$FCB_{x,i}$, $FNB_{x,i}$ and $FPB_{x,i}$ are the fraction of POC, PON and POP, respectively, in the algal group x routed into the i^{th} G class in sediment, and

$\gamma_i = 1$ for $i = 1, \gamma_i = 0$ for $i = 2$ or 3.

In the source code, the sediment process model is solved after the water column water quality model, and the calculated fluxes using the water column conditions at $t = t_n$ are used for the computation of the water quality variables at $t = t_n + \theta$. The superscript N

indicates the variables after being updated for the kinetic processes, as defined in equation (8.110).

The settling of sorbed phosphate is considered to contribute to the labile G1 pool in equation (8.203), and settling of sorbed silica contributes to J_{PSi} in equation (8.204) to avoid creation of additional depositional fluxes for inorganic particulates. The sum of distribution coefficients should be unity:

$$\sum_i FCLP_i = \sum_i FNLP_i = \sum_i FPLP_i = \sum_i FCRP_i = \sum_i FNRP_i = \sum_i FPRP_i = \sum_i FCB_{x,i} = \sum_i FNB_{x,i} = \sum_i FPB_{x,i} = 1.$$

The settling velocities, WS_{LP}, WS_{RP}, WS_x, and WS_{TSS}, as defined in the EFDC+ water column model (Section 8.4), are net settling velocities. If total active metal is selected as a measure of sorption site, WS_{TSS} is replaced by WS_s in Equations (8.203) and (8.204).

8.5.2 Diagenesis Flux

Another coupling point of the sediment model to the water column model is the sediment flux. The computation of sediment flux requires that the magnitude of the diagenesis flux be known. The diagenesis flux is explicitly computed using mass-balance equations for deposited *POC*, *PON* and *POP*. Dissolved silica is produced in the sediments as a result of the dissolution of *PSi*. Since the dissolution process is different from the bacterial-mediated diagenesis process, it is presented separately. In the mass-balance equations, the depositional fluxes of *POM* are the source terms and the decay of *POM* in the sediments produces the diagenesis fluxes. The integration of the mass-balance equations for *POM* provides the diagenesis fluxes that are the inputs for the mass-balance equations for ammonium, nitrate, phosphate and sulfide/methane in the sediments.

The difference in decay rates of *POM* is accounted for by assigning a fraction of *POM* to various decay classes (Westrich and Berner, 1984). *POM* in the sediments is divided into three *G* classes, or fractions, representing three scales of reactivity. The G_1 (labile) fraction has a half life of 20 days, and the G_2 (refractory) fraction has a half life of one year. The G_3 (inert) fraction is non-reactive, i.e., it undergoes no significant decay before burial into deep, inactive sediments. The varying reactivity of the *G* classes controls the time scale over which changes in depositional flux will be reflected in changes in diagenesis flux. If the G_1 class would dominate the *POM* input into the sediments, then there would be no significant time lag introduced by *POM* diagenesis and any changes in depositional flux would be readily reflected in diagenesis flux.

As the upper layer thickness is negligible (equation (8.200)) the depositional flux is considered to proceed directly to the lower layer (equations (8.201), to (8.204)), and diagenesis is considered to occur only in the lower layer. The mass-balance equations are similar for *POC*, *PON* and *POP*, and for different *G* classes. The mass-balance equation in the anoxic lower layer for the i^{th} *G* class ($i = 1,\ 2\ or\ 3$) may be expressed as:

$$H_2 \frac{\partial G_{POM,i}}{\partial t} = -K_{POM,i} \cdot \theta_{POM,i}^{T-20} \cdot G_{POM,i} \cdot H_2 - W \cdot G_{POM,i} + J_{POM,i} \tag{8.205}$$

where,

$G_{POM,i}$ is the concentration of $POM (M = C, N \text{ or } P)$ in the i^{th} G class in Layer 2 (g/m^3)

$K_{PMO,i}$ is the decay rate of the i^{th} G class POM at $20°C$ in Layer 2 $(1/day)$

$\theta_{POM,i}$ is the constant for temperature adjustment for $K_{POM,i}$

T is the sediment temperature $(°C)$

W is the burial rate (m/day)

Since the G_3 class is inert $K_{POM,3} = 0$.

Once the mass-balance equations for $G_{POM,1}$ and $G_{POM,2}$ are solved, the diagenesis fluxes are computed from the rate of mineralization of the two reactive G classes:

$$J_M = \sum_{i=1}^{2} K_{POM,i} \cdot \theta_{POM,i}^{T-20} \cdot G_{POM,i} \cdot H_2 \tag{8.206}$$

J_M is the diagenesis flux $(g/m^2/day)$ of carbon $(M = C)$, nitrogen $(M = N)$ or phosphorus $(M = P)$

8.5.3 Sediment Flux

8.5.3.1 Basic Equations

The mineralization of POM produces soluble intermediates, which are quantified as diagenesis fluxes in the previous section. The intermediates react in the oxic and anoxic layers, and portions are returned to the overlying water as sediment fluxes. Computation of sediment fluxes requires mass-balance equations for ammonium, nitrate, phosphate, sulfide/methane and available silica. This section describes the flux portion for ammonium, nitrate, phosphate and sulfide/methane of the model.

In the upper layer, the processes included in the flux portion are:

1. exchange of dissolved fraction between Layer 1 and the overlying water,
2. exchange of dissolved fraction between Layer 1 and 2 via diffusive transport,
3. exchange of particulate fraction between Layer 1 and 2 via particle mixing,
4. loss by burial to the lower layer (Layer 2),
5. removal (sink) by reaction, and
6. internal sources.

Since the upper layer is quite thin ($H_1 \sim 0.1cm$, equation (8.200)) and the surface mass transfer coefficient (s) is on the order of $0.1m/day$, then the residence time in the upper layer is: H/s 10^{-2} $days$. Hence, a steady-state approximation is made in the upper layer. Then the mass-balance equation for ammonium, nitrate, phosphate or sulfide/methane in the upper layer is:

$$H_1\frac{\partial Ct_1}{\partial t} = 0 = s(fd_0\cdot Ct_0 - fd_1\cdot Ct_1) + KL(fd_2\cdot Ct_2 - fd_1\cdot Ct_1) + \omega(fp_2\cdot Ct_2 - fp_1\cdot Ct_1) - W\cdot Ct_1 - \frac{K_1^2}{s}Ct_1 + J_1 \quad (8.207)$$

where,

Ct_1 and Ct_2 are the total concentrations in Layer 1 and 2, respectively (g/m^3),

Ct_0 is the total concentrations in the overlying water (g/m^3),

s is the surface mass transfer coefficient (m/day),

KL is the diffusion velocity for dissolved fraction between Layer 1 and 2 (m/day),

ω is the particle mixing velocity between Layer 1 and 2 (m/day),

fd_0 is the dissolved fraction of total substance in the overlying water ($0 \le fd_0 \le 1$),

fd_1 is the dissolved fraction of total substance in Layer 1 ($0 \le fd_1 \le 1$),

fp_1 is the Particulate fraction of total substance in Layer 1 ($= 1 - fd_1$),

fd_2 is the dissolved fraction of total substance in Layer 2 ($0 \le fd_2 \le 1$),

fp_2 is the Particulate fraction of total substance in Layer 2 ($= 1 - fd_2$),

K_1 is the reaction velocity in Layer 1 (m/day), and

J_1 is the sum of all internal sources in Layer 1 ($g/m^2/day$).

The first term on the RHS of equation (8.207) represents the exchange across sediment-water interface. Then the sediment flux from Layer 1 to the overlying water, which couples the sediment model to the water column model, may be expressed as:

$$J_{aq} = s(fd_1\cdot Ct_1 - fd_0\cdot Ct_0) \quad (8.208)$$

where, J_{aq} is the sediment flux of ammonium, nitrate, phosphate or sulfide/methane to the overlying water ($g/m^2/day$).

The convention used in equation (8.208) is that the positive flux is from the sediment to the overlying water.

In the lower layer, the processes included in the flux portion are (Figure 8.1):

1. exchange of dissolved fraction between Layer 1 and 2 via diffusive transport,

2. exchange of particulate fraction between Layer 1 and 2 via particle mixing,
3. deposition from Layer 1 and burial to the deep inactive sediments,
4. removal (sink) by reaction, and
5. internal sources including diagenetic source.

The mass-balance equation for ammonium, nitrate, phosphate or sulfide/methane in the lower layer is

$$H_2\frac{\partial Ct_2}{\partial t} = -KL(fd_2\cdot Ct_2 - fd_1\cdot Ct_1) - \omega(fp_2\cdot Ct_2 - fp_1\cdot Ct_1) + W(Ct_1 - Ct_2) - K_2\cdot Ct_2 + J_2 \quad (8.209)$$

where,

K_2 is the reaction velocity in Layer 2 (m/day), and

J_2 is the sum of all internal sources including diagenesis in Layer 2 ($g/m^2/day$).

The substances produced by mineralization of *POM* in sediments may be present in both dissolved and particulate phases. This distribution directly affects the magnitude of the substance that is returned to the overlying water. In equations (8.207) to (8.209), the distribution of a substance between the dissolved and particulate phases in a sediment is parameterized using a linear partitioning coefficient.

The dissolved and particulate fractions are computed from the partitioning equations:

$$fd_1 = \frac{1}{1+m_1\cdot\pi_1} \quad fp_1 = 1 - fd_1 \quad (8.210)$$

$$fd_2 = \frac{1}{1+m_2\cdot\pi_2} \quad fp_2 = 1 - fd_2 \quad (8.211)$$

where,

m_1 and m_2 are the solid concentrations in Layer 1 and 2, respectively (kg/l), and

π_1 and π_2 are the partition coefficient in Layer 1 and 2, respectively ($per\ kg/l$).

The partition coefficient is the ratio of particulate to dissolved fraction per unit solid concentration (i.e. per unit sorption site available).

All terms, except the last two terms, in equations (8.207) and (8.209) are common to all state variables and are described in Section 5.3.1. The last two terms represent the reaction and source/sink terms, respectively.

8.5.3.2 Common Parameters for Sediment Flux

Parameters that are needed for the sediment fluxes are s, ω, KL, W,H_2, m_1, m_2, π_1, π_2, κ_1, κ_2, J_1, and J_2 in equations (8.207) to (8.211). Of these, κ_1, κ_2, J_1 and J_2 are variable-specific. Among the other common parameters, W, H_2, m_1 and m_2, are specified as input. The modeling of the remaining three parameters, s, ω, KL, are described in this section.

8.5.3.2.1 Surface mass transfer coefficient

Owing to the observation that the surface mass transfer coefficient s, can be related to the sediment oxygen demand (SOD) (Di Toro et al., 1990) s can be estimated from the ratio of SOD and overlying water oxygen concentration:

$$s = \frac{D_1}{H_1} = \frac{SOD}{DO_0} \tag{8.212}$$

where D is the diffusion coefficient in Layer 1 (m^2/day).

Knowing s, it is possible to estimate the other model parameters.

8.5.3.2.2 Particulate phase mixing coefficient

The particle mixing velocity between Layer 1 and 2 is parameterized as

$$\omega = \frac{D_p \cdot \theta_{D_p}^{T-20}}{H_2} \frac{G_{POC,1}}{G_{POC,R}} \frac{DO_0}{KM_{D_p} + DO_0} \tag{8.213}$$

where,

D_p is the apparent diffusion coefficient for particle mixing (m^2/day),

θ_{Dp} is the constant for temperature adjustment for D_p,

$G_{POC,R}$ is the reference concentration for $G_{POC,1}$ ($g\,C/m^3$), and

KM_{Dp} is the particle mixing half-saturation constant for oxygen ($g\,O_2/m^3$).

The enhanced mixing of sediment particles by macrobenthos (bioturbation) is quantified by estimating D_p. The particle mixing appears to be proportional to the benthic biomass (Matisoff, 1982), which is correlated to the carbon input to the sediment Robbins et al. (1989), This is parameterized by assuming that benthic biomass is proportional to the available labile carbon $G_{POC,1}$, and $G_{POC,R}$ is the reference concentration at which the particle mixing velocity is at its nominal value. The Monod-type oxygen dependency accounts for the oxygen dependency of benthic biomass.

It has been observed that a hysteresis exists in the relationship between the bottom water oxygen and benthic biomass. Benthic biomass increases as the summer progresses. However, the occurrence of anoxia/hypoxia reduces the biomass drastically and also imposes

stress on benthic activities. After full overturn, the bottom water oxygen increases but the population does not recover immediately. Hence, the particle mixing velocity, which is proportional to the benthic biomass, does not increase in response to the increased bottom water oxygen. Recovery of benthic biomass following hypoxic events depends on many factors including severity and longevity of hypoxia, constituent species, and salinity (Diaz et al., 1995).

This phenomenon of reduced benthic activities and hysteresis is parameterized based on the idea of stress that low oxygen imposes on the benthic population. It is analogous to the modeling of the toxic effect of chemicals on organisms (Mancini, 1983). A first order differential equation is employed, in which the benthic stress 1) accumulates only when overlying oxygen is below KM_{Dp} and 2) is dissipated at a first order rate (Figure 8.5a):

$$\frac{\partial ST}{\partial t} = \begin{cases} -K_{ST} \cdot ST + \left(1 - \frac{DO_0}{KM_{Dp}}\right), & \text{if} \quad DO_0 < KM_{Dp} \\ -K_{ST} \cdot ST, & \text{if} \quad DO_0 > KM_{Dp} \end{cases} \tag{8.214}$$

where,

ST is the accumulated benthic stress (day), and

K_{ST} is the first order decay rate for ST ($1/day$).

The behavior of this formulation can be understood by evaluating the steady-state stresses at two extreme conditions of overlying water oxygen, DO_0 as:

$$DO_0 = 0, K_{ST} \cdot ST = 1 \quad f(ST) = (1 - K_{ST} \cdot ST) = 0$$

$$DO_0 \geq KM_{Dp}, K_{ST} \cdot ST = 0 \quad f(ST) = (1 - K_{ST} \cdot ST) = 1$$

The dimensionless expression, $f(ST) = 1 - K_{ST} \cdot ST$, appears to be the proper variable to quantify the effect of benthic stress on benthic biomass and thus particle mixing (Figure 8.5b).

The final formulation for the particle mixing velocity including the benthic stress is:

$$\omega = \frac{D_p \cdot \theta_{Dp}^{T-20}}{H_2} \frac{G_{POC,1}}{G_{POC,R}} \frac{DO_0}{KM_{Dp} + DO_0} f(ST) + \frac{D_{p_{min}}}{H_2} \tag{8.215}$$

where Dp_{min} is the minimum diffusion coefficient for particle mixing (m^2/day).

The reduction in particle mixing due to the benthic stress, f(ST), is estimated by employing the following procedure. The stress ST, is normally calculated with equation (8.214). Once DO_0 drops below a critical concentration $DO_{ST,c}$, for $NC_{hypoxia}$ consecutive days or more, the calculated stress is not allowed to decrease until t_{MBS} days of DO_0 ¿ $DO_{ST,c}$. That is, only when hypoxic days are longer than critical hypoxia days ($NC_{hypoxia}$), the maximum stress, or minimum ($1 - K_{ST} \cdot ST$), is retained for a specified period (t_{MBS} days) after DO_0 recovery (Figure 8.5). No hysteresis occurs if DO_0 does not drop below

$DO_{ST,c}$ or if hypoxia lasts less than $NC_{hypoxia}$ days. When applying maximum stress for t_{MBS} days, the subsequent hypoxic days are not included in t_{MBS}. This parameterization of hysteresis essentially assumes seasonal hypoxia, i.e., one or two major hypoxic events during summer, and might be unsuitable for systems with multiple hypoxic events throughout a year.

Three parameters relating to hysteresis $DO_{ST,c}$, $NC_{hypoxia}$, and t_{MBS} are functions of many factors including severity and longevity of hypoxia, constituent species and salinity, and thus have site-specific variabilities (Diaz et al., 1995). The critical overlying oxygen concentration $DO_{ST,c}$, also depends on the distance from the bottom of the location of DO_0. The critical hypoxia days $NC_{hypoxia}$, depends on tolerance of benthic organisms to hypoxia and thus on benthic community structure (Diaz et al., 1995). The time lag for the recovery of benthic biomass following hypoxic events, tMBS, tends to be longer for higher salinity. The above three parameters are considered to be spatially constant input parameters.

8.5.3.2.3 Dissolved phase mixing coefficient

Dissolved phase mixing between Layer 1 and 2 is via passive molecular diffusion, which is enhanced by the mixing activities of the benthic organisms (bio-irrigation). This is modeled by increasing the diffusion coefficient relative to the molecular diffusion coefficient:

$$KL = \frac{D_d \cdot \theta_{Dd}^{T-20}}{H_2} + R_{BI,BT} \cdot \omega \tag{8.216}$$

where,

D_d is the diffusion coefficient in pore water (m^2/day),

θ_{Dd} is the constant for temperature adjustment for D_d, and

$R_{BI,BT}$ is the ratio of bio-irrigation to bioturbation.

The last term in equation (8.216) accounts for the enhanced mixing by organism activities.

8.5.3.3 Ammonia Nitrogen

Diagenesis is assumed not to occur in the upper layer because of its shallow depth, and ammonium is produced by diagenesis in the lower layer:

$$J_{1,NH4} = 0 \; J_{2,NH4} = J_N \tag{8.217}$$

where J_N is from equation (8.206).

Ammonium is nitrified to nitrate in the presence of oxygen. A Monod-type expression is used for the ammonium and oxygen dependency of the nitrification rate. Then, the oxic layer reaction velocity in equation (8.207) for ammonium may be expressed as:

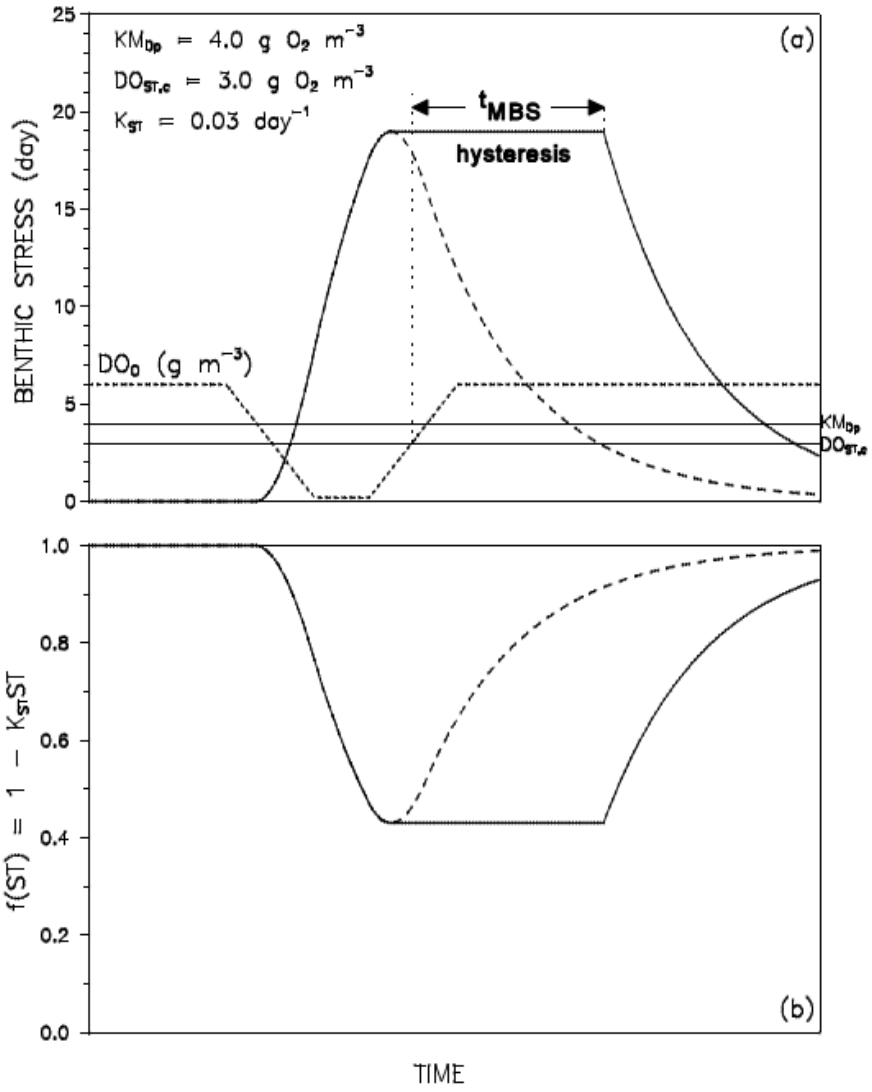

Fig. 8.5. Benthic stress (a) and its effect on particle mixing (b) as a function of overlying water column dissolved oxygen concentration.

$$K^2_{1,NH4} = \frac{DO_0}{2 \cdot KM_{NH4,O2} + DO_0} \frac{KM_{NH4}}{KM_{NH4} + NH4_1} K^2_{NH4} \cdot \theta^{T-20}_{NH4} \tag{8.218}$$

and then the nitrification flux becomes:

$$J_{Nit} = \frac{K^2_{1,NH4}}{s} \cdot NH4_1 \tag{8.219}$$

where,

$KM_{NH4,O2}$ is the nitrification half-saturation constant for dissolved oxygen ($g\ O_2/m^3$),

$NH4_1$ is the total ammonium nitrogen concentration in Layer 1 ($g\ N/m^3$),

KM_{NH4} is the nitrification half-saturation constant for ammonium ($g\ N/m^3$),

K_{NH4} is the optimal reaction velocity for nitrification at $20°C$ (m/day),

θ_{NH4} is the constant for temperature adjustment for K_{NH4}, and

J_{Nit} is the nitrification flux ($g\ N/m^2/day$).

Nitrification does not occur in the anoxic lower layer:

$$K_{2,NH4} = 0 \tag{8.220}$$

Once equations (8.207) and (8.209) are solved for $NH4_1$ and $NH4_2$, the sediment flux of ammonium to the overlying water $J_{aq,NH4}$, can be calculated using equation (8.208). Note that it is not $NH4_1$ and $NH4_2$ that determine the magnitude of $J_{aq,NH4}$ (DiToro and Fitzpatrick (1993, Section X-B-2)), but the magnitude is determined by (1) the diagenesis flux, (2) the fraction that is nitrified, and (3) the surface mass transfer coefficient (s) that mixes the remaining portion.

8.5.3.4 Nitrate Nitrogen

Nitrification flux is the only source of nitrate in the upper layer, given by Equation (8.219), and there is no diagenetic source for nitrate in both layers:

$$\begin{aligned} J_{1,NO3} &= J_{Nit} \\ J_{2,NO3} &= 0 \end{aligned} \tag{8.221}$$

Nitrate is present in sediments as dissolved substance, i.e., $\pi_{1,NO3} = \pi_{2,NO3} = 0$, making $fd_{1,NO3} = fd_{2,NO3} = 1$ (Equations (8.210) and (8.211)): it also makes R meaningless, hence $R = 0$. Nitrate is removed by denitrification in both oxic and anoxic layers with the carbon required for denitrification supplied by carbon diagenesis. The reaction velocities in equations (8.207) and (8.209) for nitrate may be expressed as:

$$K^2_{1,NO3} = K^2_{NO3,1} \cdot \theta^{T-20}_{NO3} \tag{8.222}$$

$$K_{2,NO3} = K^2_{NO3,2} \cdot \theta^{T-20}_{NO3} \tag{8.223}$$

and the denitrification flux out of sediments as a nitrogen gas becomes:

$$J_{N2(g)} = \frac{K^2_{1,NO3}}{s} NO3_1 + K_{2,NO3} \cdot NO3_2 \tag{8.224}$$

where,

$K_{NO3,1}$ is the reaction velocity for denitrification in Layer 1 at $20°C$ (m/day),

$K_{NO3,2}$ is the reaction velocity for denitrification in Layer 2 at $20°C$ (m/day),

θ_{NO3} is the constant for temperature adjustment for $K_{NO3,1}$ and $K_{NO3,2}$,

$J_{N2(g)}$ is the denitrification flux $(g\,N/m^2/day)$,

$NO3_1$ is the total nitrate nitrogen concentration in Layer 1 $(g\,N/m^3)$, and

$NO3_2$ is the total nitrate nitrogen concentration in Layer 2 $(g\,N/m^3)$.

Once equations (8.207) and (8.209) are solved for $NO3_1$ and $NO3_2$, the sediment flux of nitrate to the overlying water $J_{aq,NO3}$, can be calculated using equation (8.208). The steady-state solution for nitrate showed that the nitrate flux is a linear function of $NO3_0$ (DiToro and Fitzpatrick, 1993, equation III-15): the intercept quantifies the amount of ammonium in the sediment that is nitrified but not denitrified (thus releases as $J_{aq,NO3}$), and the slope quantifies the extent to which overlying water nitrate is denitrified in the sediment. It also revealed that if the internal production of nitrate is small relative to the flux of nitrate from the overlying water, the normalized nitrate flux to the sediment $-J_{aq,NO3}/NO3_0$, is linear in s for small s and constant for large s (DiToro and Fitzpatrick, 1993, Section III-C). For small s ($\sim 0.01 m/day$), H is large (equation (8.212)) so that oxic layer denitrification predominates and $J_{aq,NO3}$ is essentially zero independent of $NO3_0$ (DiToro and Fitzpatrick, 1993, Figure III-4).

8.5.3.5 Phosphate Phosphorus

Phosphate is produced by the diagenetic breakdown of POP in the lower layer:

$$\begin{aligned} J_{1,PO4} &= 0 \\ J_{2,PO4} &= J_P \end{aligned} \tag{8.225}$$

where J_P is from equation (8.206). A portion of the liberated phosphate remains in the dissolved form and a portion becomes particulate phosphate, either via precipitation of

phosphate-containing minerals (Troup, 1974) (e.g. vivianite, $Fe_3(PO_4)_2(s)$), or by partitioning to phosphate sorption sites (Barrow, 1983; Giordani and Astorri, 1986; Lijklema, 1980). The extent of particulate formation is determined by the magnitude of the partition coefficients $\pi_{1,PO4}$ and $\pi_{2,PO4}$ in equations (8.210) and (8.211). Phosphate flux is strongly affected by DO_0, the overlying water oxygen concentration. As DO_0 approaches zero, the phosphate flux from the sediments increases. This mechanism is incorporated by making $\pi_{1,PO4}$ larger, under oxic conditions, than $\pi_{2,PO4}$. In the model, when DO_0 exceeds a critical concentration $(DO_0)_{crit,PO4}$, sorption in the upper layer is enhanced by an amount $\pi_{PO4,1}$:

$$\pi_{1,PO4} = \pi_{2,PO4} \cdot (\Delta\pi_{PO4,1})\ DO_0 > (DO_0)_{crit,PO4} \tag{8.226}$$

When oxygen falls below $(DO_0)_{crit,PO4}$, then:

$$\pi_{1,PO4} = \pi_{2,PO4} \cdot \left(\Delta\pi_{PO4,1}\right)^{DO_0/(DO_0)_{crit,PO4}}\ DO_0 \leq (DO_0)_{crit,PO4} \tag{8.227}$$

which smoothly reduces $\pi_{1,PO4}$ to $\pi_{2,PO4}$ as DO_0 goes to zero. There is no removal reaction for phosphate in both layers:

$$\kappa_{1,PO4} = \kappa_{2,PO4} = 0 \tag{8.228}$$

Once equations (8.207) and (8.209) are solved for $PO4_1$ and $PO4_2$, the sediment flux of phosphate to the overlying water $J_{aq,PO4}$, can be calculated using equation (8.208).

8.5.3.6 Sulfide/Methane and Oxygen Demand

8.5.3.6.1 Sulfide

No diagenetic production of sulfide occurs in the upper layer. In the lower layer, sulfide is produced by carbon diagenesis (equation (8.206)) decremented by the organic carbon consumed by denitrification (equation (8.224)). Then:

$$J_{1,H2S} = 0 \quad J_{2,H2S} = a_{O2,C} \cdot J_C - a_{O2,NO3} \cdot J_{N2(g)} \tag{8.229}$$

where,

$a_{O2,C}$ is the stoichiometric coefficient for carbon diagenesis consumed by sulfide oxidation ($2.6667 g\ O_2 - equivalents\ per\ g\ C$), and

$a_{O2,NO3}$ is the stoichiometric coefficient for carbon diagenesis consumed by denitrification ($2.8571 g\ O_2 - equivalents\ per\ g\ N$).

A portion of the dissolved sulfide that is produced in the anoxic layer reacts with the iron to form particulate iron monosulfide ($FeS(s)$) (Morse et al., 1987). The particulate fraction is mixed into the oxic layer where it can be oxidized to ferric oxyhydroxide ($Fe_2O_3(s)$). The remaining dissolved fraction also diffuses into the oxic layer where it is oxidized to sulfate. Partitioning between dissolved and particulate sulfide in the model represents the

formation of $FeS(s)$, which is parameterized using partition coefficients $\%_{1,H2S}$ and $\%_{2,H2S}$, in Equations (8.210) and (8.211).

The present sediment model has three pathways for sulfide, the reduced end product of carbon diagenesis: (1) sulfide oxidation, (2) aqueous sulfide flux, and (3) burial. The distribution of sulfide among the three pathways is controlled by the partitioning coefficients and the oxidation reaction velocities (Section V-E in DiToro and Fitzpatrick (1993)). Both dissolved and particulate sulfide are oxidized in the oxic layer, consuming oxygen in the process. In the oxic upper layer, the oxidation rate that is linear in oxygen concentration is used (Boudreau, 1991; Cline and Richards, 1969; Millero, 1986). In the anoxic lower layer, no oxidation can occur. Then, the reaction velocities in equations (8.207) and (8.209) may be expressed as:

$$K^2_{1,H2S} = \left(K^2_{H2S,d1} \cdot fd_{1,H2S} + K^2_{H2S,p1} \cdot fp_{1,H2S}\right) \theta^{T-20}_{H2S} \frac{DO_0}{2 \cdot KM_{H2S,O2}} \tag{8.230}$$

$$K^2_{2,H2S} = 0 \tag{8.231}$$

where,

$K_{H2S,d1}$ is the reaction velocity for dissolved sulfide oxidation in Layer 1 at $20°C$ (m/day),

$K_{H2S,p1}$ is the reaction velocity for particulate sulfide oxidation in Layer 1 at $20°C$ (m/day),

θ_{H2S} is the constant for temperature adjustment for $K_{H2S,d1}$ and $K_{H2S,p1}$, and

$KM_{H2S,O2}$ is the constant to normalize the sulfide oxidation rate for oxygen $(g\ O_2/m^3)$.

The constant $KM_{H2S,O2}$, which is included for convenience only, is used to scale the oxygen concentration in the overlying water. At $DO_0 = KM_{H2S,O2}$, the reaction velocity for sulfide oxidation rate is at its nominal value.

The oxidation reactions in the oxic upper layer cause oxygen flux to the sediment, which exerts *SOD*. By convention, *SOD* is positive: $SOD = -J_{aq,O2}$. The *SOD* in the model consists of two components, carbonaceous sediment oxygen demand (*CSOD*) due to sulfide oxidation and nitrogenous sediment oxygen demand (*NSOD*) due to nitrification:

$$SOD = CSOD + NSOD = \frac{K^2_{1,H2S}}{s} H2S_1 + a_{O2,NH4} \cdot J_{Nit} \tag{8.232}$$

where,

$H2S_1$ is the total sulfide concentration in Layer 1 $(g\ O_2 - equivalents/m^2/day)$, and

$a_{O2,NH4}$ is the stoichiometric coefficient for oxygen consumed by nitrification $(4.33\ g\ O_2\ per\ g\ N)$.

Equation (8.229) is nonlinear for SOD because the RHS contains $s = SOD/DO_0$) so that SOD appears on both sides of the equation: note that J_{Nit} (equation (8.219)) is also a function of s. A simple back substitution method is used.

If the overlying water oxygen is low, then the sulfide that is not completely oxidized in the upper layer can diffuse into the overlying water. This aqueous sulfide flux out of the sediments, which contributes to the chemical oxygen demand in the water column model, is modeled using

$$J_{aq,H2S} = s(fd_{1,H2S} \cdot H2S_1 - COD) \tag{8.233}$$

The sulfide released from the sediment reacts very quickly in the water column when oxygen is available, but can accumulate in the water column under anoxic conditions. The COD, quantified as oxygen equivalents, is entirely supplied by benthic release in the water column model (equation (8.91)). Since sulfide also is quantified as oxygen equivalents, COD is used as a measure of sulfide in the water column in equation (8.233).

8.5.3.6.2 Methane

When sulfate is used up, methane can be produced by carbon diagenesis and methane oxidation consumes oxygen (Di Toro et al., 1990). Owing to the abundant sulfate in the saltwater, only the aforementioned sulfide production and oxidation are considered to occur in the saltwater. Since the sulfate concentration in the freshwater is generally insignificant, methane production is considered to replace sulfide production in the freshwater. In the freshwater, methane is produced by carbon diagenesis in the lower layer decremented by the organic carbon consumed by denitrification, and no diagenetic production of methane occurs in the upper layer (equation (8.229)):

$$J_{1,CH4} = 0 \; J_{2,CH4} = a_{O2,C} \cdot J_C - a_{O2,NO3} \cdot J_{N2(g)} \tag{8.234}$$

The dissolved methane produced takes two pathways; (1) oxidation in the oxic upper layer causing CSOD, or (2) escape from the sediment as aqueous flux or as gas flux:

$$J_{2,CH4} = CSOD + J_{aq,CH4} + J_{CH4(g)} \tag{8.235}$$

where,

$J_{aq,CH4}$ is the aqueous methane flux ($g\ O_2 - equivalents/m^2/day$), and

$J_{CH4(g)}$ is the gaseous methane flux ($g\ O_2 - equivalents/m^2/day$).

A portion of dissolved methane that is produced in the anoxic layer diffuses into the oxic layer where it is oxidized. This methane oxidation causes CSOD in the freshwater sediment (Di Toro et al., 1990) :

$$CSOD = CSOD_{max} \cdot \left(1 - \text{sech} \left[\frac{K_{CH4} \cdot \theta_{CH4}^{T-20}}{s} \right] \right) \tag{8.236}$$

$$CSOD_{max} = minimum\left\{\sqrt{2 \cdot KL \cdot CH4_{sat} \cdot J_{2,CH4}},\ J_{2,CH4}\right\} \tag{8.237}$$

$$CH4_{sat} = 100\left(1 + \frac{h + H_2}{10}\right) 1.024^{20-T} \tag{8.238}$$

where,

$CSOD_{max}$ is the maximum CSOD occurring when all the dissolved methane transported to the oxic layer is oxidized,

K_{CH4} is the reaction velocity for dissolved methane oxidation in Layer 1 at 20°C (m/day),

θ_{H2S} is the constant for temperature adjustment for K_{CH4} , and

$CH4_{sat}$ is the saturation concentration of methane in the pore water $(g\ O_2 - equivalents/m^3)$.

The term, $(h + H_2)/10$ where h and H_2 are in meters, in equation (8.238) is the depth from the water surface that corrects for the in situ pressure. Equation (8.238) is accurate to within 3% of the reported methane solubility between 5 and 20°C (Yamamoto et al., 1976).

If the overlying water oxygen is low, the methane that is not completely oxidized can escape the sediment into the overlying water either as aqueous flux or as gas flux. The aqueous methane flux, which contributes to the chemical oxygen demand in the water column model, is modeled using (Di Toro et al., 1990):

$$J_{aq,CH4} = CSOD_{max} \cdot \text{sech}\left[\frac{K_{CH4} \cdot \theta_{CH4}^{T-20}}{s}\right] = CSOD_{max} - CSOD \tag{8.239}$$

Methane is only slightly soluble in water. If its solubility $CH4_{sat}$ given by equation (8.238) is exceeded in the pore water, it forms a gas phase that escapes as bubbles. The loss of methane as bubbles, i.e. the gaseous methane flux, is modeled using equation (8.235) with $J_{2,CH4}$ from equation (8.234), $CSOD$ from equation (8.236) and $J_{aq,CH4}$ from equation (8.239) (Di Toro et al., 1990).

8.5.4 Silica

The production of ammonium, nitrate and phosphate in sediments is the result of the mineralization of POM by bacteria. The production of dissolved silica in sediments is the result of the dissolution of particulate biogenic or opaline silica, which is thought to be independent of bacterial processes.

The depositional flux of particulate biogenic silica from the overlying water to the sediments is modeled using equation (8.204). With this source, the mass-balance equation for particulate biogenic silica may be written as:

$$H_2 \frac{\partial PSi}{\partial t} = -S_{Si} \cdot H_2 - W \cdot PSi + J_{PSi} + J_{DSi} \tag{8.240}$$

where,

Psi is the concentration of particulate biogenic silica in the sediment ($g\ Si/m^3$),

S_{Si} is the dissolution rate of PSi in Layer 2 ($g\ Si/m^3/day$),

J_{Psi} is the depositional flux of PSi ($g\ Si/m^3/day$) given by the equation (8.204), and

J_{DSi} is the detrital flux of PSi ($g\ Si/m^3/day$) to account for PSi settling to the sediment that is not associated with the algal flux of biogenic silica.

The processes included in equation (8.240) are dissolution (i.e., production of dissolved silica), burial, and depositional and detrital fluxes from the overlying water. Equation (8.240) can be viewed as the analog of the diagenesis equations for POM (equation (8.205)). The dissolution rate is formulated using a reversible reaction that is first order in silica solubility deficit and follows a Monod-type relationship in particulate silica:

$$S_{Si} = K_{Si} \cdot \theta_{Si}^{T-20} \frac{PSi}{PSi + KH_{PSi}} (Si_{sat} - fd_{2,Si} \cdot Si_2) \tag{8.241}$$

where,

K_{Si} is the first order dissolution rate for PSi at $20°C$ in Layer 2 ($1/day$),

θ_{Si} is the constant for temperature adjustment for K_{Si},

KM_{PSi} is the silica dissolution half-saturation constant for PSi ($g\ Si/m^3$), and

Si_{sat} is the saturation concentration of silica in the pore water ($g\ Si/m^3$).

The mass-balance equations for mineralized silica can be formulated using the general forms, equations (8.207) and (8.209). There is no source/sink term and no reaction in the upper layer:

$$J_{1,Si} = \kappa_{1,Si} = 0 \tag{8.242}$$

In the lower layer, silica is produced by the dissolution of particulate biogenic silica, which is modeled using equation (8.241). The two terms in equation (8.241) correspond to the source term and reaction term in equation (8.209):

$$J_{2,Si} = K_{Si} \cdot \theta_{Si}^{T-20} \frac{PSi}{PSi + KM_{PSi}} Si_{sat} \cdot H_2 \tag{8.243}$$

$$\kappa_{2,Si} = K_{Si} \cdot \theta_{Si}^{T-20} \frac{PSi}{PSi + KM_{PSi}} f_{d2,Si} \cdot H_2 \tag{8.244}$$

A portion of silica dissolved from particulate silica sorbs to solids and a portion remains in the dissolved form. Partitioning using the partition coefficients $\pi_{1,Si}$ and $\pi_{2,Si}$, in Equations (8.210) and (8.211) controls the extent to which dissolved silica sorbs to solids. Since silica shows similar behavior as phosphate in the adsorption-desorption process, the same partitioning method as applied to phosphate is used for silica. That is, when DO_0 exceeds a critical concentration $(DO_0)_{crit,Si}$, sorption in the upper layer is enhanced by an amount $\Delta\pi_{Si,1}$:

$$\pi_{1,Si} = \pi_{2,Si} \cdot (\Delta\pi_{Si,1}) DO_0 > (DO_0)_{crit,Si} \tag{8.245}$$

When oxygen falls below $(DO_0)_{crit,Si}$, then:

$$\pi_{1,Si} = \pi_{2,Si} \cdot \left(\Delta\pi_{Si,1}\right)^{DO_0/(DO_0)_{crit,Si}} DO_0 \leq (DO_0)_{crit,Si} \tag{8.246}$$

which smoothly reduces $\pi_{1,Si}$ to $\pi_{2,Si}$ as DO_0 goes to zero.

Once equations (8.207) and (8.209) are solved for Si_1 and Si_2, the sediment flux of silica to the overlying water $J_{aq,Si}$, can be calculated using equation (8.208).

8.5.5 Sediment Temperature

All rate coefficients in the aforementioned mass-balance equations are expressed as a function of sediment temperature T. The sediment temperature is modeled based on the diffusion of heat between the water column and sediment:

$$\frac{\partial T}{\partial t} = \frac{D_T}{H^2}(T_W - T) \tag{8.247}$$

where,

D_T is the heat diffusion coefficient between the water column and sediment (m^2/s), and

T_W is the temperature in the overlying water column ($^\circ C$) calculated by equation (8.110).

The model application in (Di Toro and Fitzpatrick, 1993) and (Cerco and Cole, 1994) used $D = 1.8 \times 10^{-7}\ m^2/s$.

8.5.6 Method of Solution

8.5.6.1 Finite-Difference Equations and Solution Scheme

An implicit integration scheme is used to solve the governing mass-balance equations. The finite difference form of equation (8.207) may be expressed as:

$$0 = s\left(fd_0 \cdot Ct_o^{'} - fd_1 \cdot Ct_1^{'}\right) + KL\left(fd_2 \cdot Ct_2^{'} - fd_1 \cdot Ct_1^{'}\right) + \omega\left(fp_2 \cdot Ct_2^{'} - fp_1 \cdot Ct_1^{'}\right) - W \cdot Ct_1^{'} - \frac{K_1^2}{s} Ct_1^{'} + J_1^{'} \quad (8.248)$$

where the primed variables designate the values evaluated at $t+$ and the unprimed variables are those at t, where θ is defined in equation (8.110). The finite difference form of equation (8.209) may be expressed as:

$$0 = -KL\left(fd_2 \cdot Ct_2^{'} - fd_1 \cdot Ct_1^{'}\right) - \omega\left(fp_2 \cdot Ct_2^{'} - fp_1 \cdot Ct_1^{'}\right) + W\left(Ct_1^{'} - Ct_2^{'}\right) - \left(K_2 + \frac{H_2}{\theta}\right) Ct_2^{'} + \left(J_2^{'} + \frac{H_2}{\theta} Ct_2\right) \quad (8.249)$$

The two terms $-(H_2/\theta)Ct_2^{'}$ and $(H_2/\theta)Ct_2$, are from the derivative term $H_2(\partial Ct_2/\partial t)$ in equation (8.209). Each of these terms simply add to the Layer 2 removal rate and the forcing function, respectively. Setting these two terms equal to zero results in the steady-state model. The two unknowns $Ct_1^{'}$ and $Ct_2^{'}$, can be calculated at every time step using:

$$\begin{bmatrix} s \cdot fd_1 + a_1 + \frac{K_1^2}{s} & -a_2 \\ -a_1 & a_2 + W + K_2 + \frac{H_2}{\theta} \end{bmatrix} \begin{bmatrix} Ct_1^{'} \\ Ct_2^{'} \end{bmatrix} = \begin{bmatrix} J_1^{'} + s \cdot fd_0 \cdot Ct_0^{'} \\ J_2^{'} + \frac{H_2}{\theta} Ct_2 \end{bmatrix} \quad (8.250)$$

$$\begin{aligned} a_1 &= KL \cdot fd_1 + \omega \cdot fp_1 + W \\ a_2 &= KL \cdot fd_2 + \omega \cdot fp_2 \end{aligned} \quad (8.251)$$

The solution of equation (8.250) requires an iterative method since the surface mass transfer coefficient s, is a function of the SOD (equation (8.212)), which is also a function of s (equation (8.232)). A simple back substitution method is used:

1. Start with an initial estimate of SOD, for example, $SOD = a_{O2,C} J_C$ or the previous time step SOD.
2. Solve equation (8.250) for ammonium, nitrate, and sulfide/methane.
3. Compute the SOD using equation (8.232).
4. Refine the estimate of SOD : a root finding method (Brent's method in Press et al. (1986) is used to make the new estimate.
5. Go to (2) if no convergence.
6. Solve equation 8.250 for phosphate and silica.

For the sake of symmetry, the equations for diagenesis, particulate biogenic silica and sediment temperature are also solved in implicit form. The finite difference form of the diagenesis equation (equation (8.205)) may be expressed as:

$$G'_{POM,i} = \left(G_{POM,i} + \frac{\theta}{H_2} J_{POM,i}\right)\left(1 + \theta \cdot K_{POM,i} \cdot \theta_{POM,i}^{T-20} + \frac{\theta}{H_2} W\right)^{-1} \tag{8.252}$$

The finite difference form of the *PSi* equation (equation (8.240)) may be expressed as:

$$PSi' = \left(PSi + \frac{\theta}{H_2}(J_{PSi} + J_{DSi})\right)\left(1 + \theta \cdot K_{Si} \cdot \theta_{Si}^{T-20} \frac{Si_{sat} - f_{d2,Si} \cdot Si_2}{PSi + KM_{PSi}} + \frac{\theta}{H_2} W\right)^{-1} \tag{8.253}$$

using equation (8.235) for the dissolution term, in which *PSi* in the Monod-type term has been kept at time level t to simplify the solution. The finite difference form of the sediment temperature, shown in equation (8.247), may be expressed as:

$$T' = \left(T + \frac{\theta}{H^2} D_T \cdot T_W\right)\left(1 + \frac{\theta}{H^2} D_T\right)^{-1} \tag{8.254}$$

8.5.6.2 Boundary and Initial Conditions

The above finite difference equations constitute an initial boundary-value problem. The boundary conditions are the depositional fluxes ($J_{POM,i}$ and J_{PSi}) and the overlying water conditions (Ct_0 and T_W) as a function of time, which are provided from the water column water quality model. The initial conditions are the concentrations at $t = 0$, $G_{POM,i}(0)$, $PSi(0)$, $Ct_1(0)$, $Ct_2(0)$ and $T(0)$, to start the computations. Strictly speaking, these initial conditions should reflect the past history of the overlying water conditions and depositional fluxes, which is often impractical because of lack of field data for these earlier years.

Table 8.18. Parameters related to phosphorus in water column

Parameter	Value[a]	Equation Number[b]
$FPLP$	0.2	(8.51)
$FPDP$	0.5	(8.52)
$FPIP$	0.2[c]	(8.53)
FPR_x	0.0 (all groups)	(8.50)
FPL_x	0.0 (all groups)	(8.51)
FPD_x	1.0 (all groups)	(8.52)
FPI_x	0.0[c] (all groups)	(8.53)
$*WS_s$ (m/day)	1.0	(8.53)
K_{PO4p} $(per\ g/m^3)$ for TSS	NA[c]	(8.54)
K_{PO4p} $(per\ mol/m^3)$ for TAM	6.0	(8.54)
CP_{prm1} $(g\ C\ per\ g\ P)$	42.0	(8.57)
CP_{prm2} $(g\ C\ per\ g\ P)$	85.0	(8.57)
CP_{prm3} $(per\ g\ P/m^3)$	200.0	(8.57)
K_{RP} $(1/day)$	0.005	(8.58)
K_{LP} $(1/day)$	0.075	(8.59)
K_{DP} $(1/day)$	0.1	(8.60)
K_{RPalg} $(1/day\ per\ g\ C/m^3)$	0.0	(8.58)
K_{LPalg} $(1/day\ per\ g\ C/m^3)$	0.0	(8.59)
K_{DPalg} $(1/day\ per\ g\ C/m^3)$	0.2	(8.60)

[a] The evaluation of these values are detailed in Chapter IX of (Cerco and Cole, 1994).
[b] The equation number where the corresponding parameter is first shown and defined.
[c] Not available in (Cerco and Cole, 1994) since their formulations do not include these parameters.
: FPI_x is estimated from $FPR_x + FPL_x + FPD_x + FPI_x = 1$.
* The parameters declared as an array in the source code.

Table 8.19. Parameters related to nitrogen in water column

Parameter	Value[a]	Equation Number[b]
$FNLP$	0.55	(8.68)
$FNDP$	0.1	(8.69)
$FNIP$	0.0[c]	(8.70)
FNR_x	0.0 (all groups)	(8.67)
FNL_x	0.0 (all groups)	(8.68)
FND_x	1.0 (all groups)	(8.69)
FNI_x	0.0 (all groups)	(8.70)
ANC_x $(g;\ N;\ per\ g\ C)$	0.167 (all groups)	(8.67)
$ANDC$ $(g;\ N;\ per\ g\ C)$	0.933	(8.71)
K_{RN} $(1/day)$	0.005	(8.73)
K_{LN} $(1/day)$	0.075	(8.74)
K_{DN} $(1/day)$	0.015	(8.75)
K_{RNalg} $(1/day\ per\ g\ C/m^3)$	0.0	(8.73)
K_{LNalg} $(1/day\ per\ g\ C/m^3)$	0.0	(8.74)
K_{DNalg} $(1/day\ per\ g\ C/m^3)$	0.2	(8.75)
Nit_m $(g\ N/m^3/day)$	0.07	(8.78)
$KHNit_{DO}$ $(g\ N/m^3)$	1.0	(8.78)
$KHNit_N$ $(g\ O_2/m^3)$	1.0	(8.78)
$TNit$ (^oC)	27.0	(8.81)
$KNit$ $(^oC^{-2})$	0.0045	(8.81)
$KNit$ $(^oC^{-2})$	0.0045	(8.81)

[a] The evaluation of these values are detailed in Chapter IX of (Cerco and Cole, 1994).
[b] The equation number where the corresponding parameter is first shown and defined.

Table 8.20. Parameters related to silica in water column

Parameter	Value[a]	Equation Number[b]
$FSPP$	1.0[c]	(8.84)
$FSIP$	0.0[c]	(8.85)
FSP_d	1.0[c]	(8.84)
FSI_d	0.0[c]	(8.85)
ASC_d $(g\ Si\ per\ g\ C)$	0.5	(8.84)
K_{SAp} $(per\ g/m^3)$ for TSS	NA[c]	(8.86)
K_{SAp} $(per\ mol/m^3)$ for TAM	6.0	(8.86)
K_{SU} $(1/day)$	0.03	(8.90)
TR_{SUA} (^{o}C)	20.0	(8.90)
KT_{SUA} (^{o}C^{-1})	0.092	(8.90)

[a] The evaluation of these values are detailed in Chapter IX of (Cerco and Cole, 1994).
[b] The equation number where the corresponding parameter is first shown and defined.
[c] Not available in (Cerco and Cole, 1994) since their formulations do not include these parameters.
: FSPP and FSIP are estimated from FSPP+FSIP = 1.
: FSPd and FSId are estimated from FSPd+FSId = 1.

Table 8.21. Parameters related to chemical oxygen demand and dissolved oxygen in water column

Parameter	Value[a]	Equation Number[b]
KH_{COD} $(g\ O_2/m^3)$	1.5	(8.91)
K_{CD} $(1/day)$	20.0	(8.92)
TR_{COD} (^{o}C)	20.0	(8.92)
KT_{COD} (^{o}C^{-1})	0.041	(8.92)
$AOCR$ $(g\ O_2\ per\ g\ C)$	2.67	(8.93)
$AONT$ $(g\ O_2\ per\ g\ N)$	4.33	(8.92)
K_R (in MKS unit)	3.933[c]	(8.93)
KT_r	1.024[c] (1.005-1.030)	(8.98)

[a] The evaluation of these values are detailed in Chapter IX of Cerco and Cole (1994).
[b] The equation number where the corresponding parameter is first shown and defined.
[c] Not available in (Cerco and Cole, 1994) since their formulations do not include these parameters.
: Kro is from O'Connor & Dobbins O'Connor and Dobbins (1958).
: KTr is from Thomann & Mueller Thomann and Mueller (1987).

Table 8.22. Parameters related to total active metal and fecal coliform bacteria in water column

Parameter	Value[a]	Equation Number[b]
$KHbmf$ $(g\ O_2/m^3)$	0.5	(8.101)
$BFTAM$ $(mol/m^2/day)$	0.01	(8.101)
$Ttam$ (^{o}C)	20.0	(8.101)
$Ktam$ (^{o}C^{-1})	0.2	(8.101)
$TAMdmx$ (mol/m^3)	0.015	(8.102)
$Kdotam$ (per g O_2/m^3)	1.0	(8.102)
$KFCB$ $(1/day)$	0.0-6.1[c] (seawater)	(8.104)
$TFCB$ $(^oC^{-1})$	1.07[c]	(8.104)

[a] The evaluation of these values are detailed in Chapter IX of Cerco and Cole (1994).
[b] The equation number where the corresponding parameter is first shown and defined.
[c] Not available in Cerco and Cole (1994) since their formulations do not include these parameters.
: $KFCB$ and $TFCB$ are from Thomann and Mueller (1987).

Table 8.23. EFDC+ sediment diagenesis model state variables

No.	Name	Bed Layer	Units
1	POC-G1	Layer-2	g/m^3
2	POC-G2	Layer-2	g/m^3
3	POC-G3	Layer-2	g/m^3
4	PON-G1	Layer-2	g/m^3
5	PON-G2	Layer-2	g/m^3
6	PON-G3	Layer-2	g/m^3
7	POP-G1	Layer-2	g/m^3
8	POP-G2	Layer-2	g/m^3
9	POP-G3	Layer-2	g/m^3
10	Partic-Biogenic-Silica	Layer-2	g/m^3
11	Sulfide/Methane	Layer-1	g/m^3
12	Sulfide/Methane	Layer-2	g/m^3
13	Ammonia-N	Layer-1	g/m^3
14	Ammonia-N	Layer-2	g/m^3
15	Nitrate-N	Layer-1	g/m^3
16	Nitrate-N	Layer-2	g/m^3
17	Phosphate-P	Layer-1	g/m^3
18	Phosphate-P	Layer-2	g/m^3
19	Available-Silica	Layer-1	g/m^3
20	Available-Silica	Layer-2	g/m^3
21	Ammonia-N-Flux		$g/m^2 - day$
22	Nitrate-N-Flux		$g/m^2 - day$
23	Phosphate-P-Flux		$g/m^2 - day$
24	Silica Flux		$g/m^2 - day$
25	SOD		$g/m^2 - day$
26	*COD* Flux		$g/m^2 - day$
27	Bed Temperature		$^\circ C$

Table 8.24. EFDC+ sediment process model state variables and flux terms

Number	Description
(1)	particulate organic carbon G1 class in layer 2
(2)	particulate organic carbon G2 class in layer 2
(3)	particulate organic carbon G3 class in layer 2
(4)	particulate organic nitrogen G1 class in layer 2
(5)	particulate organic nitrogen G2 class in layer 2
(6)	particulate organic nitrogen G3 class in layer 2
(7)	particulate organic phosphorus G1 class in layer 2
(8)	particulate organic phosphorus G2 class in layer 2
(9)	particulate organic phosphorus G3 class in layer 2
(10)	particulate biogenic silica in layer 2
(11)	sulfide/methane in layer 1
(12)	sulfide/methane in layer 2
(13)	ammonia nitrogen in layer 1
(14)	ammonia nitrogen in layer 2
(15)	nitrate nitrogen in layer 1
(16)	nitrate nitrogen in layer 2
(17)	phosphate phosphorus in layer 1
(18)	phosphate phosphorus in layer 2
(19)	available silica in layer 1
(20)	available silica in layer 2
(21)	ammonia nitrogen flux
(22)	nitrate nitrogen flux
(23)	phosphate phosphorus flux
(24)	silica flux
(25)	sediment oxygen demand
(26)	release of chemical oxygen demand
(27)	sediment temperature

Table 8.25. Assignment of water column particulate organic matter (POM) to sediment G classes used in (Cerco and Cole, 1994)

WCM Variable	Carbon & Phosphorus			Nitrogen		
	G1	G2	G3	G1	G2	G3
A. "stand alon" model	0.65	0.20	0.15	0.65	0.25	0.10
B. coupled model Labile Particulate	1.0	0.0	0.0	1.0	0.0	0.0
Refractory Particulate[a]						
: Bay and Tributary Zones 1	0.0	0.11	0.89	0.0	0.26	0.74
: Bay Zones 2 and 10	0.0	0.43	0.57	0.0	0.54	0.46
: All Other Zones	0.0	0.73	0.27	0.0	0.82	0.18
Algae	0.65	0.255	0.095	0.65	0.28	0.07

[a] See (Cerco and Cole, 1994, Figure 10-6) for the Zones definition.

Table 8.26. Sediment burial rates (W) used in (Cerco and Cole, 1994)

Bay Zonesa[a]	Rate (cm/yr)	Tributary Zonesa[a]	Rate (cm/yr)
1, 2, 10	0.50	1	0.50
3, 6, 9	0.25	2, 3	0.25
7, 8	0.37		

[a] See (Cerco and Cole, 1994, Figure 10-6) for the definition of Zones.

Chapter 9

LAGRANGIAN PARTICLE TRACKING MODULE

9.1. Introduction

The section presents a module coded with FORTRAN 90/95 for Lagrangian particle tracking coupled to EFDC+ (DSI, 2009). The module of Lagrangian particle tracking is developed as an effective tool for solving numerous problems in fluid dynamics related to the simulation and prediction of the trajectory of objects traveling in rivers, lakes and marine systems. The model has been calibrated by using a simple analytical calculation for quasi-steady state and uniform flow in an open channel. In addition, several tests with different hydrodynamic regimes and geometries were performed. The soundness of the model was also demonstrated in a variety of applications. In particular, the test involving a hypothetical situation in the movement of insects at Caloosahatchee River Basin was simulated. From the model results, the drift tendency of insects and their locations corresponding to time moments were determined qualitatively and quantitatively. Through the simulations it was demonstrated that not only the velocity field, but also the randomness and diffusion due to turbulence also considerably impacts the dispersion of the cluster and behavior of drifter trajectories.

9.2. Basic Equations

Study of the trajectories of movement of solid particles in a fluid environment appeared very early in mechanics and was considered as a movement in a Lagrangian approach. The advantage of this method is that it is possible to track the process of movement for each specific particle in more detail and more accurately in comparison with the method of determining average concentration for grid cells. However, the solution was too difficult to implement in practice when the number of particles was very large because of computation costs. With the reduction in computing costs it is now easier to implement the solutions to these problems. The movement of solid particles is decided by a field of fluid velocity,

therefore it is necessary to couple it to a fluid flow model.

9.3. Random Walk

The governing equations used in EFDC+ are Navier-Stokes for fluid flow, the advection-diffusion equations for salinity, temperature, dye, toxic substances and suspended sediment transport (Hamrick and Wu, 1997; Hamrick, 1992, 1996). The equations are presented in curvilinear coordinate system for 2DH and Sigma coordinates for the vertical direction. They are discretized with the finite difference method with explicit scheme. It should be noted that the hypothesis of hydrostatic pressure is used in EFDC+. However, the effect of non-hydrostatic pressure is not important when the vertical velocity of flow is not very large in comparison with the horizontal components as mentioned in Huu Chung and Eppel (2008).

The advection-diffusion equation for mass transport in a three dimensional curvilinear orthogonal coordinate system is:

$$\frac{\partial C}{\partial t}+\frac{\partial (uC)}{\partial x}+\frac{\partial (vC)}{\partial y}+\frac{\partial (wC)}{\partial z}=\frac{\partial}{\partial x}\left(A_H\frac{\partial C}{\partial x}\right)+\frac{\partial}{\partial y}\left(A_H\frac{\partial C}{\partial y}\right)+\frac{\partial}{\partial z}\left(A_b\frac{\partial C}{\partial z}\right) \quad (9.1)$$

where,

t is time,

(x,y,z) are Lagrangian coordinates of a particle,

C is concentration,

(u,v,w) are velocity components of fluid flow, and

A_H and A_b are the horizontal and vertical diffusion coefficients, respectively.

The differential equations for the Lagrangian movement of particles is consistent with the equation (9.1) and are as follows:

$$dx=\left(u+\frac{\partial A_H}{\partial x}\right)dt+(2p-1)\sqrt{2A_H dt} \quad (9.2)$$

$$dy=\left(v+\frac{\partial A_H}{\partial y}\right)dt+(2p-1)\sqrt{2A_H dt} \quad (9.3)$$

$$dz=\left(w+\frac{\partial A_b}{\partial z}\right)dt+(2p-1)\sqrt{2A_b dt} \quad (9.4)$$

In which dt is the time step and p is a random number from a uniformly distributed random variable generator having mean of 0.5. When transformed using the $2p-1$ the random component has a mean of zero and a range from -1 to 1. The transformed random

value allows the diffusion term to move particles $+/-$ about the advected position. Equations (9.2) to (9.4) follow the 3D random walk approach used by Dunsbergen and Stelling (1993).

In order to determine the Lagrangian trajectory of the particle, the equations (9.2) to (9.4) were incorporated into EFDC+ model. The numerical solution was separately divided into the advective transport and random components as described above. This approach allows the user to enable (i.e. turn on random walk) or disable (advective transport only) the random components for either the horizontal and/or the vertical directions.

The Fortran90 module, DRIFTER.F90, has been developed and merged into EFDC+ to solve the equation (9.2)-(9.4). The module contains the following subroutines and functions:

- DRIFTERC: Solves the equations (9.2)-(9.4) using one of three numerical options
- DRIFTER.INP: Reading the input parameters
- READSTR: Reading the comment lines
- CONTAINER: Determining the cell containing the drifter
- AREACAL: Calculating the area of polygons
- DRIFVELCAL: Interpolating the velocity components at the previous location of the drifter
- RANDCAL: Calculating the random movement
- EDGEMOVE: Dealing with the drifter hitting the land boundary or internal walls
- INSIDECELL: Determining if the drifter is inside a cell
- DRIFTERWDEP: Interpolating the bathymetry and total water depth at the location of drifter
- DRIFTERLAYER: Determining the layer containing the drifter

Three options are available for the solution of the differential equations (9.2) to (9.4). They are explicit Euler, predictor-corrector Euler, and forth order Runge-Kutta. Their discretization for the equations are as follows:

Explicit Euler method: This method is very simple with the approximation of $O(\Delta t)$

$$x_{n+1} = x_n + u\left(t_n, x_n, y_n, z_n\right)\Delta t \tag{9.5}$$

$$y_{n+1} = y_n + v\left(t_n, x_n, y_n, z_n\right)\Delta t \tag{9.6}$$

$$z_{n+1} = z_n + w\left(t_n, x_n, y_n, z_n\right)\Delta t \tag{9.7}$$

Predictor-corrector Euler method: This method has the advantage of explicit and implicit features with the approximation of $O(\Delta t^2)$

$$x_{n+1} = x_n + \frac{1}{2}\left[u\left(t_n, x_n, y_n, z_n\right) + u\left(t_{n+1}, x^p_{n+1}, y^p_{n+1}, z^p_{n+1}\right)\right]\Delta t \tag{9.8}$$

$$y_{n+1} = y_n + \frac{1}{2}\left[v\left(t_n, x_n, y_n, z_n\right) + v\left(t_{n+1}, x^p_{n+1}, y^p_{n+1}, z^p_{n+1}\right)\right]\Delta t \tag{9.9}$$

$$z_{n+1} = z_n + \frac{1}{2}\left[w\left(t_n, x_n, y_n, z_n\right) + w\left(t_{n+1}, x^p_{n+1}, y^p_{n+1}, z^p_{n+1}\right)\right]\Delta t \tag{9.10}$$

where ,$\left(x^p_{n+1}, y^p_{n+1}, z^p_{n+1}\right)$ are calculated by equations (9.4) to (9.6)

Runge-Kutta 4 method: This method has the approximation of $O(\Delta t^4)$ and has been shown in the testing for this project that it is best option of the three solution techniques provided

$$x_{n+1} = x_n + \frac{1}{6}\left(\Delta x_1 + 2\Delta x_2 + 2\Delta x_3 + \Delta x_4\right) \tag{9.11}$$

$$y_{n+1} = y_n + \frac{1}{6}\left(\Delta y_1 + 2\Delta y_2 + 2\Delta y_3 + \Delta y_4\right) \tag{9.12}$$

$$z_{n+1} = z_n + \frac{1}{6}\left(\Delta z_1 + 2\Delta z_2 + 2\Delta z_3 + \Delta z_4\right) \tag{9.13}$$

in which

$$\Delta x_1 = u\left(t_n, x_n, y_n, z_n\right)\Delta t \tag{9.14}$$

$$\Delta y_1 = v\left(t_n, x_n, y_n, z_n\right)\Delta t \tag{9.15}$$

$$\Delta z_1 = w\left(t_n, x_n, y_n, z_n\right)\Delta t \tag{9.16}$$

$$\Delta x_2 = u\left(t_n + \frac{1}{2}\Delta t, x_n + \frac{1}{2}\Delta x_1, y_n + \frac{1}{2}\Delta y_1, z_n + \frac{1}{2}\Delta z_1\right)\Delta t \tag{9.17}$$

$$\Delta y_2 = v\left(t_n + \frac{1}{2}\Delta t, x_n + \frac{1}{2}\Delta x_1, y_n + \frac{1}{2}\Delta y_1, z_n + \frac{1}{2}\Delta z_1\right)\Delta t \tag{9.18}$$

$$\Delta z_2 = w\left(t_n + \frac{1}{2}\Delta t, x_n + \frac{1}{2}\Delta x_1, y_n + \frac{1}{2}\Delta y_1, z_n + \frac{1}{2}\Delta z_1\right)\Delta t \tag{9.19}$$

$$\Delta x_3 = u\left(t_n + \frac{1}{2}\Delta t, x_n + \frac{1}{2}\Delta x_2, y_n + \frac{1}{2}\Delta y_2, z_n + \frac{1}{2}\Delta z_2\right)\Delta t \tag{9.20}$$

$$\Delta y_3 = v\left(t_n + \frac{1}{2}\Delta t, x_n + \frac{1}{2}\Delta x_2, y_n + \frac{1}{2}\Delta y_2, z_n + \frac{1}{2}\Delta z_2\right)\Delta t \tag{9.21}$$

$$\Delta z_3 = w\left(t_n + \frac{1}{2}\Delta t, x_n + \frac{1}{2}\Delta x_2, y_n + \frac{1}{2}\Delta y_2, z_n + \frac{1}{2}\Delta z_2\right)\Delta t \tag{9.22}$$

$$\Delta x_4 = u\left(t_n + \Delta t, x_n + \Delta x_3, y_n + \Delta y_3, z_n + \Delta z_3\right)\Delta t \tag{9.23}$$

$$\Delta y_4 = v\left(t_n + \Delta t, x_n + \Delta x_3, y_n + \Delta y_3, z_n + \Delta z_3\right)\Delta t \tag{9.24}$$

$$\Delta z_4 = w\left(t_n + \Delta t, x_n + \Delta x_3, y_n + \Delta y_3, z_n + \Delta z_3\right)\Delta t \tag{9.25}$$

9.4. Oil Spill Model

EFDC+ version allows the simulation of oil spill based on drifters. Oil is maintained at the surface layer and is moved along with the hydrodynamic impacts similar to Lagrangian particles and broken down by evaporation and biodegradation.

EFDC+ will cause the drifter to disappear when the oil per drifter is less than $1.0mm^3$. When configuring an oil spill model, it should be noted that use of the "Vertical Movement Option" is ignored for groups that are designated as simulating oil. If the density of oil is less than that of water then the particles are always in the surface layer. If the oil is heavier than water, then the fully 3D option is enabled.

For simulation on the oil evaporation process, the theory of surface evaporation presented in the paper of Mackin and Aller (1984) is used. EFDC+ also simulates the effect of biodegradation of the oil based on user defined biodegradation rate with a simple first order decay approach based on Stewart et al. (1993). A biodegradation rate of 0.011 *per day* is approximately equal to the half-life of two months. If temperature of an oil drifter is provided by the modeler then this is used as the reference rate for the optimal biodegradation.

In order to simulate a conservative oil, the user would set the degradation rate and the vapor pressure as zero.

Chapter 10

MARINE HYDROKINETICS MODULE

10.1. Introduction

Marine hydrokinetic (MHK) devices extract energy from ocean currents and tides, thereby altering water velocities and currents in the project sites. These hydrodynamic changes can potentially affect the ecosystem, both near the MHK installation and in surrounding (i.e., far field) regions. In both marine and freshwater environments, devices will remove energy (momentum) from the system, potentially altering water quality and sediment dynamics. In estuaries, tidal ranges and residence times could change (either increasing or decreasing depending on system flow properties and where the effects are being measured). Effects will be proportional to the number and size of structures installed, with large MHK projects having the greatest potential effects and requiring the most in-depth analyses. The theory and implementation of MHK in SNL-EFDC+ is presented by James et al. (2010).

10.2. Theory of Marine Hydrokinetics

MHK devices remove momentum from a system, but also alter the turbulent kinetic energy K, and turbulent kinetic energy dissipation rate ε. These effects are captured with appropriate sink terms. S_Q (m^4/s^2) is the volumetric momentum extraction rate by the MHK device due to energy removal, as well as due to form and viscous drag from the MHK structure. S_K (m^5/s^3) represents the volumetric change in net turbulent kinetic energy in the appropriate model cell due to the MHK device (support), with S_ε (m^5/s^3) as its analogous term for the volumetric kinetic energy dissipation rate equation (Poggi et al., 2004). These quantities are advected and dispersed downstream of the MHK device according to the standard conservation equations used in EFDC+. The standard calculation for S_Q neglects viscous drag relative to energy removal and form drag by the MHK device, thereby resulting in

$$S_Q = -\frac{1}{2} C_T A_M U^2 \tag{10.1}$$

where,

- C_T is the MHK thrust coefficient (drag coefficient, C_D, for the support) (dimensionless),
- A_M is the MHK-device flow-facing area (support flow-facing area) (m^2), and
- U is the local flow speed in a cell $\sqrt{(u^2+v^2)}$ (m/s).

Here, MHK-device power P_M (kgm^2/s^3) is defined as

$$P_M = \frac{1}{2} C_T A_M \rho U^3 \tag{10.2}$$

where ρ (kg/m^3) is the water density.

The term S_K arises because MHK devices break up the mean flow motion and generate wake turbulence ($\approx \frac{1}{2} C_T A_M U^3$). However, such wakes dissipate fairly rapidly, speculatively within about 30 MHK device lengths (turbine diameters). Preliminary MHK CFD models have showed overly persistent wakes, perhaps in part because this term was not taken into account. The canonical (or physics-based) form for S_K reflecting the effects of a momentum sink (or partial flow obstruction) is (Sanz, 2003):

$$S_K = \frac{1}{2} C_T A_M \left(\beta_p U^3 - \beta_d U K \right) \tag{10.3}$$

where,

- K is the wake-generated turbulent kinetic energy (m^2/s^2),
- β_p (≈ 1.0) is the fraction of mean flow kinetic energy converted to K by drag (i.e., a source term in the K budget) (dimensionless), and
- β_d ($\approx 1.0 - 5.0$) is the fraction of K dissipated by conversion to kinetic energy (i.e., a sink term in the K budget) (dimensionless).

The most obvious weakness of the $K-\varepsilon$ approaches is its least understood term S_ε (Wilson et al., 1998). Over the last decade or so, various models have been proposed for S_ε (Green, 1992; Katul et al., 2004; Liu et al., 1996), but the simplest is used in this model:

$$S_e = C_{e4} \frac{e}{K} S_K \tag{10.4}$$

where $C_{\varepsilon 4}$ is a closure constant (Katul et al., 2004).

The formulation for equation (10.4) is based on standard dimensional analysis common to all $K-\varepsilon$ approaches. Upon adding equations (10.1) to (10.4) to the momentum and $K-\varepsilon$ equations, it is possible to solve for momentum K, and ε if appropriate upper and lower boundary conditions are specified. For this implementation, $C_{\varepsilon 4} = 0.9$, $\beta_p = 1.0$ and $\beta_d =$

5.1. In SNL-EFDC+, momentum is defined as the product of flow depth H, and velocity u and v); conservation of kinetic energy is solved in terms of $\frac{1}{2}HQ^2$, where q is the turbulent intensity, and conservation of turbulent energy dissipation rate takes the form HQ^2l, where l is the turbulence length scale.

10.3. Implementation into EFDC+

The simplified kinetic energy equation for an MHK device in a model σ layer is

$$\frac{\partial}{\partial t}\left(m_x m_y \rho H \Delta_k \frac{u^2+v^2}{2}\right) = -\frac{1}{2}\rho C_T A_M \left(u^2+v^2\right)^{\frac{3}{2}} = -P_M \tag{10.5}$$

$$A_M = W_M H \Delta_k \tag{10.6}$$

where,

m_x, m_y are the (horizontal) x and y dimensions of a model cell (m),

Δ_k , which is the fraction of total water depth assigned to the $k^{th}0$ layer,

A_M is the frontal flow area of the device (m^2),

W_M is the device or support width (m), and

$H\Delta_k$ is the layer thickness (m).

The corresponding components of the momentum equations, simplified to exclude advective and diffusive terms, are (Galperin and Orszag, 1993).

$$\frac{\partial}{\partial t}\left(m_x m_y H \Delta_k u\right) = -g m_y H \Delta_k \frac{\partial \zeta}{\partial x} - \frac{1}{2} C_T A_M \left(u^2+v^2\right)^{\frac{1}{2}} u \tag{10.7}$$

$$\frac{\partial}{\partial t}\left(m_x m_y H \Delta_k v\right) = -g m_x H \Delta_k \frac{\partial \zeta}{\partial y} - \frac{1}{2} C_T A_M \left(u^2+v^2\right)^{\frac{1}{2}} v \tag{10.8}$$

where,

g is acceleration due to gravity (m/s^2),

ζ is the free-surface potential (m), or the difference between the hydrostatic water level and the flow depth (this is how water elevation or pressure head drives flow)

Solutions of the x- and y-momentum equations in EFDC+ use the form,

$$\frac{\partial}{\partial t}\left(Hu\right) = -g\frac{H}{m_x}\frac{\partial \zeta}{\partial x} - \frac{1}{2m_x m_y \Delta_k} C_T A_M \left(u^2+v^2\right)^{\frac{1}{2}} u \tag{10.9}$$

$$\frac{\partial}{\partial t}\left(Hv\right) = -g\frac{H}{m_y}\frac{\partial \zeta}{\partial y} - \frac{1}{2m_x m_y \Delta_k} C_T A_M \left(u^2+v^2\right)^{\frac{1}{2}} v \tag{10.10}$$

which can be written in terms of MHK device power (and equivalently for support-structure momentum removal) as

$$\frac{\partial}{\partial t}(Hu) = -g\frac{H}{m_x}\frac{\partial \zeta}{\partial x} - \frac{1}{m_x m_y \Delta_k}\frac{P_M}{\rho\left(u^2+v^2\right)}u \tag{10.11}$$

$$\frac{\partial}{\partial t}(Hv) = -g\frac{H}{m_y}\frac{\partial \zeta}{\partial y} - \frac{1}{m_x m_y \Delta_k}\frac{P_M}{\rho\left(u^2+v^2\right)}v \tag{10.12}$$

The solution procedure begins by introducing the σ layer notation based on Δk:

$$\frac{\partial}{\partial t}(\Delta_k H u_k) = -g\Delta_k\frac{H}{m_x}\frac{\partial \zeta}{\partial x} - \left[\frac{1}{m_x m_y \Delta_k}\frac{P_M}{\rho\left(u^2+v^2\right)}\right]_k \Delta_k u_k \tag{10.13}$$

$$\frac{\partial}{\partial t}(\Delta_k H v_k) = -g\Delta_k\frac{H}{m_y}\frac{\partial \zeta}{\partial y} - \left[\frac{1}{m_x m_y \Delta_k}\frac{P_M}{\rho\left(u^2+v^2\right)}\right]_k \Delta_k v_k \tag{10.14}$$

The momentum conservation equations are

$$\frac{\partial}{\partial t}(\Delta_k H u_k) = -g\Delta_k\frac{H}{m_x}\frac{\partial \zeta}{\partial x} - \Delta_k\left(Q_k - \hat{Q}\right)u_k - \Delta_k\hat{Q}u_k \tag{10.15}$$

$$\frac{\partial}{\partial t}(\Delta_k H v_k) = -g\Delta_k\frac{H}{m_y}\frac{\partial \zeta}{\partial y} - \Delta_k\left(Q_k - \hat{Q}\right)v_k - \delta_k\hat{Q}v_k \tag{10.16}$$

where volumetric fluxes Q are

$$Q_k = \left[\frac{1}{m_x m_y \Delta_k}\frac{P_M}{\rho\left(u^2+v^2\right)}\right]_k \tag{10.17}$$

$$\hat{Q} = \sum_{k=1}^{KC}\Delta_k Q_k \tag{10.18}$$

From this point, the solution procedure is illustrated using only the u equation, which is summed over all KC layers to give

$$\frac{\partial}{\partial t}(H\hat{u}) = -g\frac{H}{m_x}\frac{\partial \zeta}{\partial x} - \sum_{k=1}^{KC}\Delta_k\left(Q_k - \hat{Q}\right)u_k - \hat{Q}\hat{u} \tag{10.19}$$

$$\hat{u} = \sum_{k=1}^{KC}\Delta_k u_k \tag{10.20}$$

which is the simplified external mode equation. This equation is solved with the continuity equation for the depth-averaged velocity components, $\hat{u}$ and v^{-}, and the water surface elevation H, using the time-differenced form

$$\left(1+\frac{\hat{Q}}{H}\Delta t\right)(H\hat{u})^{n+1}+\frac{\Delta t}{2}g\frac{H}{m_x}\frac{\partial\zeta^{n+1}}{\partial x}=$$
$$(H\hat{u})^{n}-\frac{\Delta t}{2}g\frac{H}{m_x}\frac{\partial\zeta^{n}}{\partial x}-\Delta t\sum_{k=1}^{KC}\left[\Delta_k\left(Q_k-\hat{Q}\right)u_k\right]^n \quad (10.21)$$

where Δt is the time step.

The internal-mode equation solution is based on considering the difference between equations for two adjacent layers

$$\frac{\partial}{\partial t}(Hu_{k+1})=-g\frac{H}{m_x}\frac{\partial\zeta}{\partial x}-\left(Q_{k+1}-\hat{Q}\right)u_{k+1}-\hat{Q}u_{k+1} \quad (10.22)$$

$$\frac{\partial}{\partial t}(Hu_{k})=-g\frac{H}{m_x}\frac{\partial\zeta}{\partial x}-\left(Q_{k}-\hat{Q}\right)u_{k}-\hat{Q}u_{k} \quad (10.23)$$

which has remainder

$$\frac{\partial}{\partial t}(Hu_{k+1}-Hu_k)+\frac{\hat{Q}}{H}(Hu_{k+1}-Hu_k)=-\left(Q_{k+1}-\hat{Q}\right)u_{k+1}+\left(Q_k-\hat{Q}\right)u_k \quad (10.24)$$

Time differencing yields

$$\left(1+\Delta t\frac{\hat{Q}}{H}\right)(Hu_{k+1}-Hu_k)^{n+1}=$$
$$(Hu_{k+1}-Hu_k)^{n}-\Delta t\left[\left(Q_{k+1}-\hat{Q}\right)u_{k+1}-\left(Q_k-\hat{Q}\right)u_k\right]^n \quad (10.25)$$

The system of $KC-1$ layer-interface equations can be solved for the velocity differences across the layer and used with the definition of the depth-averaged velocity to determine the actual layer velocities.

The MHK device effect in the turbulent kinetic energy (turbulent intensity) equation is given by

$$\frac{\partial}{\partial t}\left(H\frac{q^2}{2}\right)=\beta_p\left(\frac{1}{2}\frac{1}{m_x m_y\Delta_k}C_T A_M\right)\left(u^2+v^2\right)^{\frac{1}{2}}\left(u^2+v^2\right)-$$
$$\beta_d\left(\frac{1}{2}\frac{1}{m_x m_y\Delta_k}C_T A_M\right)\left(u^2+v^2\right)^{\frac{1}{2}}\frac{q^2}{2}-\frac{H}{B_1 l}q^3 \quad (10.26)$$

where dimensionless $B_1=16.6$ is a turbulence closure coefficient from Mellor and Yamada (1982).

The dissipation effect of the device is combined with the standard flow dissipation term to give

$$\frac{\partial}{\partial t}\left(H\frac{q^2}{2}\right)+\left[\beta_d\left(\frac{1}{2}\frac{C_TA_M}{m_xm_y\Delta_k}\right)\frac{\left(u^2+v^2\right)^{\frac{1}{2}}}{H}+\frac{q}{B_1l}\right]Hq^2=$$
$$\beta_p\left(\frac{1}{2}\frac{C_TA_M}{m_xm_y\Delta_k}\right)\left(u^2+v^2\right)^{\frac{1}{2}}\left(u^2+v^2\right) \quad (10.27)$$

where the total dissipation has been moved to the left side of the equation to emphasize that it must be treated implicitly in the numerical solution procedure given by

$$\left\{1+\Delta t\left[\beta_d\left(\frac{C_TA_M}{m_xm_y\Delta_k}\right)\frac{\left(u^2+v^2\right)^{\frac{1}{2}}}{H}+\frac{2q}{B_1l}\right]\right\}\left(Hq^2\right)^{n+1}=$$
$$\left(Hq^2\right)^n+\Delta t\beta_p\left(\frac{C_TA_M}{m_xm_y\Delta_k}\right)\left(u^2+v^2\right)^{\frac{1}{2}}\left(u^2+v^2\right) \quad (10.28)$$

The turbulent length scale equation (turbulent kinetic energy dissipation rate) is

$$\frac{\partial}{\partial t}\left(Hq^2l\right)+\left[C_{e4}\beta_d\left(\frac{1}{2}\frac{C_TA_M}{m_xm_y\Delta_k}\right)\frac{\left(u^2+v^2\right)^{\frac{1}{2}}}{H}+\frac{q}{B_1l}\right]Hq^2l=$$
$$C_{e4}\beta_p\left(\frac{1}{2}\frac{C_TA_M}{m_xm_y\Delta_k}\right)\left(u^2+v^2\right)^{\frac{1}{2}}\left(u^2+v^2\right)l \quad (10.29)$$

which is solved similar to the turbulent kinetic energy equation using

$$\left\{1+\Delta t\left[C_{e4}\beta_d\left(\frac{1}{2}\frac{C_TA_M}{m_xm_y\Delta_k}\right)\frac{\left(u^2+v^2\right)^{\frac{1}{2}}}{H}+\frac{q}{B_1l}\right]\right\}\left(Hq^2l\right)^{n+1}=$$
$$\left(Hq^2l\right)^n+\Delta tC_{e4}\beta_p\left(\frac{1}{2}\frac{C_TA_M}{m_xm_y\Delta_k}\right)\left(u^2+v^2\right)^{\frac{1}{2}}\left(u^2+v^2\right)l \quad (10.30)$$

For completeness, vegetative resistance effects on $K-\varepsilon$ were also included in the SNL-EFDC+ coding.

Chapter 11

SHELLFISH MODULE

11.1. Introduction

This section summarizes the basic theory of the water shellfish module implemented in the EFDC+ code. DSI appreciates ongoing collaboration with the Marine Environment Research Division of Korea's National Institute of Fisheries Science for developing this module.

Shellfish filter feeders occupy a central role in the model ecosystem and interact with multiple components of the eutrophication model. These organisms remove particulate organic matter (POM) from the water column for ingestion and assimilation and deposit a portion of it in the bottom sediments as feces (Cerco and Noel, 2005). In the model, the kinetic processes of the shellfish include filtering, ingestion, assimilation, respiration, mortality, and spawning. A shellfish individual is quantified as the organic carbon incorporated in soft tissue which is computed as a function of food availability, respiration, and mortality. The environmental effects on shellfish life processes are considered by its interactions with the water quality model.

11.2. Governing Equation

For each shellfish individual, the change of its weight with time is the result of changes in net production. Therefore, a fundamental growth equation for filter feeder biomass can be written as:

$$\frac{dW_d}{dt} = NP \tag{11.1}$$

where

t is the time (s)

W_d is the dry meat weight (g C) and

NP is the net production (g C).

According to White et al. (1988) and Kobayashi et al. (1997), the net production is the sum of somatic and reproductive tissue production, which is assumed to be the difference between assimilation and respiration:

$$NP = P_g + P_r = A - R \tag{11.2}$$

where

P_g is the somatic production (g C)

P_r is the reproductive tissue production (g C)

A is the assimilation (g C) and R is the respiration (g C).

11.3. Length - Weight Relation

The relationship between shell length and live weight is routinely used as an index of oyster growth. It is well known with an equation of the form:

$$L = A \cdot {W_d}^B \tag{11.3}$$

where

L is the shell length (cm)

A, B are constants parameters.

By fitting this equation to the experimental measurements, Kobayashi et al. (1997) gave A = 77.9 and B = 0.291 for the Japanese oyster, *Crassostrea gigas*.

11.4. Filtration Rate

Shellfish filtration rate is quantified as water volume cleared of particles per individual per unit time. It is the major determinant of growth that in turn affects changes in shellfish biomass. In the model, filtration rate is represented as a maximum or optimal rate that is modified by ambient temperature, suspended solids, salinity, and dissolved oxygen:

$$FR = FR_W \cdot f_1(T) \cdot f_2(S) \cdot f_3(TSS) \cdot f_4(DO) \tag{11.4}$$

where

FR is the filtration rate (l filtered per individual h^{-1});

FR_W is the maximum filtration rate (l filtered per individual h^{-1});

$f_1(T)$ is the effect of temperature on filtration rate ($0 < f_1(T) \leq 1$);

$f_2(S)$ is the effect of salinity on filtration rate ($0 < f_2(S) \leq 1$);

$f_3(TSS)$ is the effect of suspended solids on filtration rate ($0 < f_3(TSS) \leq 1$); and

$f_4(DO)$ is the effect of dissolved oxygen on filtration rate ($0 < f_4(DO) \leq 1$).

11.4.1 Maximum Filtration Rate

The maximum filtration rate is commonly estimated from the dry meat weight W_d. Coughlan and Ansell (1964) provides the following relationship for siphonate bivalves:

$$FR_W = 2.59 \cdot W_d^{0.73} \tag{11.5}$$

Another formulation was used by Cloern (1982) for studying of bivalves in South San Francisco Bay:

$$FR_W = 7.0 \cdot W_d^{0.67} \tag{11.6}$$

For the Japanese oyster, *Crassostrea gigas*, Kobayashi et al. (1997) proposed the following formula for the maximum filtration rate:

$$FR_W = \begin{cases} 2.51 \cdot {W_d}^{0.279}, & W_d \geq 2\text{g} \\ 0.117 \cdot {W_d}^3 - 1.05 \cdot {W_d}^2 + 3.09 \cdot W_d + 0.133, & W_d < 2\text{g} \end{cases} \tag{11.7}$$

Cerco and Noel (2007) used a constant factor for the maximum filtration rate while studying the native oysters, *Crassostrea virginica* in Chesapeake Bay:

$$FR_W = 0.55 \cdot \frac{1000}{24} \cdot W_d = 22.917 \cdot W_d \tag{11.8}$$

On the other hand, Officer et al. (1982) determined the maximum filtration rate from the total weight W:

$$FR_W = 0.76 \cdot W^{0.60} \tag{11.9}$$

The temperature effect on the maximum filtration rate can be also included as (Doering and Oviatt, 1986):

$$FR_W = \frac{60}{1000} \frac{L^{0.96} T^{0.95}}{2.95} \tag{11.10}$$

11.4.2 Temperature Effect

From Kobayashi et al. (1997), the effect of temperature on filtration rate is modeled as:

$$f_1(T) = \begin{cases} \frac{T^{0.5}}{4.47}, & T \geq 7\,^\circ\text{C} \\ 0.59, & T < 7\,^\circ\text{C} \end{cases} \tag{11.11}$$

Cerco and Noel (2007) considered the temperature effect as an exponentially increasing function of temperature :

$$f_1(T) = \exp(-K_{tg} \cdot (T - T_{opt})^2) \tag{11.12}$$

where T is the temperature (°C), T_{opt} is the temperature for optimal filtration (°C) and K_{tg} is the coefficient for the effect of temperature on filtration.

11.4.3 Salinity Effect

According to Loosanoff (1958), the filtration rate decreases below 7.5 ppt and ceases at 3.5 ppt. A linear relationship was also introduced for the salinity effect between these threshold values:

$$f_2(S) = \begin{cases} 1, & S \geq 7.5\,\text{ppt} \\ \frac{S-3.5}{7.5-3.5}, & 3.5 < S < 7.5\,\text{ppt} \\ 0, & S \leq 3.5\,\text{ppt} \end{cases} \tag{11.13}$$

where S is the ambient salinity (ppt).

A similar mathematical formulation for the salinity effect was reported by Quayle (1988) and Mann et al. (1991) but different threshold salinity values:

$$f_2(S) = \begin{cases} 1, & S \geq 20\,\text{ppt} \\ \frac{S-10}{20-10}, & 10 < S < 20\,\text{ppt} \\ 0, & S \leq 10\,\text{ppt} \end{cases} \tag{11.14}$$

In Cerco and Noel (2005), the authors proposed a tanh functional from for the effect of salinity on filtration rate:

$$f_2(T) = 0.5 \cdot (1 + \tanh(S - S_{KH})) \tag{11.15}$$

with S_{KH} is the the salinity at which the filtration rate is halved (ppt).

Fulford et al. (2007) adjusted the salinity effect as a linear function salinity based on data measurement for oyster *Crassostrea virginica* in Chesapeake Bay, USA:

$$f_2(T) = 0.0926 \cdot S - 0.139 \tag{11.16}$$

Buzzelli et al. (2015) included the effect of salinity on filtration rate simulation of oyster in south Florida estuaries as:

$$f_2(T) = -0.0017 \cdot S^2 + 0.0084 \cdot S - 0.1002 \tag{11.17}$$

11.4.4 Suspended Solids Effect

The effect of high suspended solids concentrations on oyster filtration rate has been long recognized through experiments by Loosanoff and Tommers (1948). From the given data, Hofmann et al. (1992) deduced a formulation as follows:

$$f_3(TSS) = 1 - 0.001. \frac{\log_{10}(TSS) + 3.38}{0.418} \tag{11.18}$$

Cerco and Noel (2005) applied a piecewise function, obtained though visual fit to the data from Jordan (1987) and supplement with the results from Loosanoff and Tommers (1948):

$$f_3(TSS) = \begin{cases} 0.1, & TSS < 5\,\text{mg/l} \\ 1.0, & 5 < TSS < 25\,\text{mg/l} \\ 0.2, & 25 < TSS < 100\,\text{mg/l} \\ 0.0, & TSS \geq 100\,\text{mg/l} \end{cases} \tag{11.19}$$

Fulford et al. (2007) modeled the effect of suspended solid as a power function derived from the data measured by the EPA Chesapeake Bay Monitoring Program:

$$f_3(TSS) = 10.364 \cdot \ln(TSS)^{-2.0477}, \quad TSS > 25\,\text{mg/l} \tag{11.20}$$

11.4.5 Dissolved Oxygen Effect

The model formulation incorporates DO effects on filtration rate which are expressed as proposed in Cerco and Noel (2005):

$$f_4(DO) = \frac{1}{1 + \exp(1.1 \times \dfrac{DO_{hx} - DO}{DO_{hx} - DO_{qx}})} \tag{11.21}$$

where DO is the dissolved oxygen concentration (mg/l); DO_{hx} and DO_{qx} are the dissolved oxygen concentrations (mg/l) at which the filtration rates are 50% and 25% of maximum, respectively.

11.5. Ingestion and Assimilation

Shellfish ingestion capacity is given by multiplying the filtration rate by the food concentration:

$$I = \frac{24}{1000} \times f \times FR \tag{11.22}$$

where I is the ingestion (g dry weight per individual day^{-1}) and f is the food concentration (measured food value) (mg dry weight l^{-1}).

Shellfish assimilation is obtained from ingestion using an assimilation efficiency. It is noted that the fraction of ingested carbon assimilated by shellfish depends on the carbon source.

$$A = \alpha \times I \tag{11.23}$$

in which A is the assimilation rate (g dry weight per individual day^{-1}) and α is the assimilation efficiency.

Shellfish assimilation can be converted into energy via:

$$E_A = C_E \times A \tag{11.24}$$

where E_A is the assimilation energy (calories per individual day^{-1}) and C_E is the caloric conversion factor (5210 calories per g dry weight).

11.6. Respiration

Shellfish respiration is commonly represented as a function of temperature and the dry meat weight :

$$R = B_M \cdot W_d \tag{11.25}$$

where B_M is the dependency of respiration on temperature.

Several mathematical formulations of B_M have been proposed in literature and implemented in the EFDC+ code. According to the Korean National Institute of Fisheries Science (NIFS, 2020):

$$B_M = \begin{cases} K_R \cdot \theta^{T-T_B}, & T > T_B \\ 0, & T \leq T_B \end{cases} \tag{11.26}$$

T_B is the base temperature for respiration (°C),

K_R metabolism rate at reference temperature (day^{-1}),

θ is a temperature coefficient for respiration.

Cerco and Noel (2007) considered basal metabolism to be an exponentially increasing function of temperature

$$B_M = K_R \cdot \exp(K_{Tb} \cdot (T - T_r)) \tag{11.27}$$

where

T_r is the reference temperature for specification of metabolism (°C),

K_R metabolism rate at reference temperature (day^{-1}),

K_{Tb} is a constant that relates metabolism to temperature (°C^{-1}).

For *C. virginica* oyster, respiration rate as a function of temperature and shellfish dry meat weight can be also obtained from Dame (1972):

$$R = (12.6 \cdot T + 69.7) \cdot {W_d}^{-0.25} \tag{11.28}$$

According to Hofmann et al. (1992), salinity effects on oyster respiration over a range of temperature, were parameterized using data given in (Shumway and Koehn, 1982):

$$R_R = \begin{cases} 0.007 \cdot T + 2.099, & T < 20\,^{\circ}\mathrm{C} \\ 0.0915 \cdot T + 1.324, & T \geq 20\,^{\circ}\mathrm{C} \end{cases} \tag{11.29}$$

Where R_R is the ratio of respiration at 10 ppt to respiration at 20 ppt: $R_R = R_{10\text{ppt}}/R_{20\text{ppt}}$. Equations (11.28) and (11.29) were combined to obtain respiration over a range of salinity as follows:

$$R = \begin{cases} R, & S \geq 15\,\text{ppt} \\ R(1+(R_R-1)\frac{15-S}{5}), & 10 < S < 15\,\text{ppt} \\ RR_R, & S \leq 10\,\text{ppt} \end{cases} \tag{11.30}$$

Shumway and Koehn (1982) identified effects of salinity on respiration at 20 ppt.

Finally, the energy consumed by respiration is given by:

$$E_R = \frac{24}{1000} \times C_R \times R \times W_d \tag{11.31}$$

where

E_R is the respiration energy (calories per individual day^{-1}),

C_R is the caloric conversion factor (calories per ml oxygen),

R is the respiration rate (μl oxygen per g dry weight h^{-}).

11.7. Reproduction

For adult shellfish greater or equal to a certain size, net production was apportioned into growth and reproduction by using a temperature-dependent reproduction efficiency of the form:

$$P_r = R_{eff} \cdot NP \tag{11.32}$$

where R_{eff} is the temperature-dependent reproduction efficiency.

A formulation of R_{eff}, derived empirically from observations, was reported in Kobayashi et al. (1997):

$$R_{eff} = \begin{cases} 0.8, & T \geq 27\,^{\circ}\text{C} \\ 0.2 \cdot T - 4.6, & 23 < T < 27\,^{\circ}\text{C} \\ 0, & T \leq 23\,^{\circ}\text{C} \end{cases} \tag{11.33}$$

In cases where $NP < 0$, a preferential resorption of gonadal tissue is assumed to cover the deficit.

11.8. Spawning

Spawning occurs when the environmental conditions (temperature and salinity) are in the suitable ranges and the cumulative production biomass exceeds a certain fraction of

shellfish total biomass. Once spawning occurs, the total reproductive biomass is apportioned into male and female biomass. The ratio of females to males is calculated as e.g., (Powell et al., 1994):

$$f_{ratio} = 0.021 \cdot L_b - 0.62 \tag{11.34}$$

where f_{ratio} is the ratio of females to males and L_b is the shell length in mm. Then, the female portion of reproductive biomass can be calculated and converted into eggs spawned as follows:

$$n_{eggs} = R_f \cdot \frac{1}{E_{egg}} \cdot \frac{1}{W_{egg}} \tag{11.35}$$

where n_{eggs} is the number of eggs spawned, R_f is the female portion of reproductive biomass, W_{eggs} is the egg weight, and E_{eggs} is the egg's caloric content (cal. g dry weight^{-1}). For oysters, the egg weight can be estimated from egg volume as:

$$W_{eggs} = 2.14 \times 10^{-14} \cdot V_{egg} \tag{11.36}$$

where V_{egg} is the oyster egg volume (μm^3).

References

Milton Abramowitz. Handbook of mathematical functions, national bureau of standards. *Applied Mathematics Series*, (55), 1964.

Peter Ackers and William R White. Sediment transport: new approach and analysis. *Journal of the Hydraulics Division*, 99(hy11), 1973.

Robert B Ambrose, Tim A Wool, James L Martin, et al. The water quality analysis simulation program, wasp5, part a: Model documentation. *Environmental Research Laboratory, US Environmental Protection Agency, Athens, GA*, 1993.

ER Anderson et al. Water loss investigations: Lake hefner studies. *US Department of the Interior, Geol*, 1954.

Akio Arakawa and Vivian R Lamb. Computational design of the basic dynamical processes of the ucla general circulation model. *General circulation models of the atmosphere*, 17 (Supplement C):173–265, 1977.

Ralph Alger Bagnold. The flow of cohesionless grains in fluids. *Philosophical Transactions of the Royal Society of London. Series A, Mathematical and Physical Sciences*, 249(964): 235–297, 1956.

Robert B Banks and Francisco Flores Herrera. Effect of wind and rain on surface reaeration. *Journal of the Environmental Engineering Division*, 103(3):489–504, 1977.

NJ Barrow. A mechanistic model for describing the sorption and desorption of phosphate by soil. *Journal of soil science*, 34(4):733–750, 1983.

Alan F Blumberg and George L Mellor. A description of a three-dimensional coastal ocean circulation model. *Three-dimensional coastal ocean models*, 4:1–16, 1987.

L Boni, E Carpene, D Wynne, and M Reti. Alkaline phosphatase activity in protogonyaulax tamarensis. *Journal of plankton research*, 11(5):879–885, 1989.

Bernard P Boudreau. Modelling the sulfide-oxygen reaction and associated ph gradients in porewaters. *Geochimica et Cosmochimica Acta*, 55(1):145–159, 1991.

George L Bowie, William B Mills, Donald B Porcella, Carrie L Campbell, James R Pagenkopf, Gretchen L Rupp, Kay M Johnson, PWH Chan, Steven A Gherini, Charles E Chamberlin, et al. Rates, constants, and kinetics formulations in surface water quality modeling. *EPA*, 600:3–85, 1985.

Derek K Brady, Willard L Graves, and John Charles Geyer. Surface heat exchange at power plant cooling lakes. Technical report, 1969.

Barry W Bunch, Carl F Cerco, Mark S Dortch, Billy H Johnson, and Keu W Kim. Hydrodynamic and water quality model study of san juan bay estuary. Technical report, Army Engineer Waterways Experiment Station Vicksburg Ms Engineer Research, 2000.

Pierre-Yves Burban, Wilbert Lick, and James Lick. The flocculation of fine-grained sediments in estuarine waters. *Journal of Geophysical Research: Oceans*, 94(C6):8323–8330, 1989.

Pierre-Yves Burban, Yao-Jun Xu, Joe McNeil, and Wilbert Lick. Settling speeds of floes in fresh water and seawater. *Journal of Geophysical Research: Oceans*, 95(C10):18213–18220, 1990.

C. Buzzelli, P. Gorman, P.H. Doering, Z. Chen, and Y. Wan. The application of oyster and seagrass models to evaluate alternative inflow scenarios related to everglades restoration. *Ecological Modelling*, 297:154–170, 2015.

Dayton E Carritt and Sol Goodgal. Sorption reactions and some ecological implications. *Deep Sea Research (1953)*, 1(4):224–243, 1954.

Craig L Caupp, James T Brock, and Henry M Runke. *Application of the dynamic stream simulation and assessment model (DSSAM III) to the Truckee River below Reno, Nevada: Model formulation and program description*. Raipd Creek Water Works, 1991.

Carl F Cerco and Thomas Cole. Three-dimensional eutrophication model of chesapeake bay. *Journal of Environmental Engineering*, 119(6):1006–1025, 1993.

Carl F Cerco and Thornas Cole. Users guide to the ce-qualicm three-dimensional eutrophication model. *US Army Corps of Engineers, Waterways Experiment Station, Technical report EL-95-15, Vicksburg, Mississippi*, 1995.

Carl F Cerco, Barry W Bunch, Allen M Teeter, and Mark S Dortch. Water quality model of florida bay. Technical report, Engineer Research and Development Center Vicksburg MS Environmental Lab, 2000.

Carl F Cerco, Lewis Linker, Jeffrey Sweeney, Gary Shenk, and Arthur J Butt. Nutrient and solids controls in virginias chesapeake bay tributaries. *Journal of Water Resources Planning and Management*, 128(3):179–189, 2002.

Carl F Cerco, Mark R Noel, and Sung-Chan Kim. Three-dimensional eutrophication model of lake washington, washington state. Technical report, Engineer Research And Development Center Vicksburg Ms Environmental Lab, 2004.

CF Cerco and TM Cole. Three-dimensional model of cheasapeake bay. *Vicksburg: US Army Corps of Engineers Technical Report EL-94-4*, 1994.

C.F. Cerco and M.R. Noel. Assessing a ten-fold increase in the chesapeake bay native oyster population - a report to the epa chesapeake bay program. Technical report, US Army Engineer Research and Development Center, Vicksburg MS, 07 2005.

C.F. Cerco and M.R. Noel. Can oyster restoration reverse cultural eutrophication in chesapeake bay? *Estuaries and Coasts*, 30(2):43–61, 2007.

Steven C Chapra, Raymond P Canale, and Gary L Amy. Empirical models for disinfection by-products in lakes and reservoirs. *Journal of Environmental Engineering*, 123(7):714–715, 1997.

Nian-Sheng Cheng. Simplified settling velocity formula for sediment particle. *Journal of hydraulic engineering*, 123(2):149–152, 1997.

Ryszard J Chróst and Jürgen Overbeck. Kinetics of alkaline phosphatase activity and phosphorus availability for phytoplankton and bacterioplankton in lake plusee (north german eutrophic lake). *Microbial ecology*, 13(3):229–248, 1987.

Terry L Clark. A small-scale dynamic model using a terrain-following coordinate transformation. *Journal of Computational Physics*, 24(2):186–215, 1977.

Terry L Clark and William D Hall. Multi-domain simulations of the time dependent navier-stokes equations: Benchmark error analysis of some nesting procedures. *Journal of Computational Physics*, 92(2):456–481, 1991.

Joel D Cline and Francis Asbury Richards. Oxygenation of hydrogen sulfide in seawater at constant salinity, temperature and ph. *Environmental Science & Technology*, 3(9): 838–843, 1969.

J.E. Cloern. Does the benthos control phytoplankton biomass in south san francisco bay? *Marine Ecology - Progress Series*, 9:191–202, 1982.

John Coughlan and Alan D. Ansell. A direct method for determining the pumping rate of siphonate bivalves. *ICES Journal of Marine Science*, 29(2):205–213, 1964.

Andrew P Covar. Selecting the proper reaeration coefficient for use in water quality models. In *Proceedings of the Conference on Environmental Modeling and Simulation. Cincinnati, OH, EPA-600/9-76-016, Environmental Protection Agency, Washington, DC*, pages 340–3, 1976.

Daniel T Cox, Nobuhisa Kobayashi, and Akio Okayasu. Bottom shear stress in the surf zone. *Journal of Geophysical Research: Oceans*, 101(C6):14337–14348, 1996.

PM Craig, DH Chung, NT Lam, PH Son, and NX Tinh. Sigma-zed: A computationally efficient approach to reduce the horizontal gradient error in the efdcs vertical sigma grid. In *Proceedings of the 11th International Conference on Hydrodynamics, Singapore*, 2014.

R. F Dame. The ecological energies of growth, respiration, and assimilation in the intertidal american oyster crassostrea virginica. *Marine Biology*, 17:243–250, 1972.

DM Di Toro and JJ Fitzpatrick. Chesapeake bay sediment flux model. final report. Technical report, Hydroqual, Inc., Mahwah, NJ (United States), 1993.

Dominic M Di Toro. Applicability of cellular equilibrium and monod theory to phytoplankton growth kinetics. *Ecological Modelling*, 8:201–218, 1980.

Dominic M Di Toro, Paul R Paquin, Karupannan Subburamu, and David A Gruber. Sediment oxygen demand model: methane and ammonia oxidation. *Journal of Environmental Engineering*, 116(5):945–986, 1990.

Dominic M Di Toro et al. *Sediment flux modeling*, volume 116. Wiley-Interscience New York, 2001.

Robert J Diaz, Rutger Rosenberg, et al. Marine benthic hypoxia: a review of its ecological effects and the behavioural responses of benthic macrofauna. *Oceanography and marine biology. An annual review*, 33:245–03, 1995.

Timothy H Diehl, Melissa A Harris, Jennifer C Murphy, Susan S Hutson, and David E Ladd. *Methods for estimating water consumption for thermoelectric power plants in the United States*. US Department of the Interior, US Geological Survey, 2013.

Nathan Dill, editor. *Modeling Hydraulic Control Structures in Estuarine Environments with EFDC*, 11 2011. International Conference on Estuarine and Coastal Modeling, The name of the publisher.

DM DiToro and JJ Fitzpatrick. Chesapeake bay sediment flux model. prepared for the us army corps of engineer waterways experiment station. vicksburg, ms. *Contract Report EL-93-2. Mahwah, New Jersey*, 1993.

P.H. Doering and C.A. Oviatt. Application of filtration rate models to field populations of bivalves: an assessment using experimental mesocosms. *Marine Ecology - Progress Series*, 31:265–275, 1986.

Daniel Willem Dunsbergen and G Stelling. A 3d particle model for transport problems in transformed coordinates. *Communications on hydraulic and geotechnical engineering, No. 1993-07*, 1993.

Herbert Bristol Dwight. Tables of integrals and other mathematical data. *New York: The MacMillan Company,— c1947, Revised Edition*, 1947.

JE Edinger, DK Brady, and JC Geyer. Heat exchange and transport in the environment. report no. 14. Technical report, Johns Hopkins Univ., Baltimore, MD (USA). Dept. of Geography and, 1974.

Hans Albert Einstein. The bed-load function for sediment transportation in open channel flows. Technical report, Soil Conservation Service, 1950.

EPRI. Evaluating thermoelectric, agricultural, and municipal water consumption in a national water resources framework. Technical report, Electric Power Research Institute, 04 2014.

C Fletcher. *AJ. Computational Techniques for Fluid Dynamics. Fundamental and general techniques*. Springer-Verlag, Berlin, Berlin, Germany, 1988.

Philip N Froelich. Kinetic control of dissolved phosphate in natural rivers and estuaries: a primer on the phosphate buffer mechanism 1. *Limnology and oceanography*, 33(4part2): 649–668, 1988.

Janice M Fulford and Terry W Sturm. Evaporation from flowing channels. *Journal of Energy Engineering*, 110(1):1–9, 1984.

R.S. Fulford, D.L. Breitburg, R.I. E. Newell, W. M. Kemp, and M. Luckenbach. Effects of oyster population restoration strategies on phytoplankton biomass in chesapeake bay: a flexible modeling approach. *Marine Ecology Progress Series*, 336:43–61, 2007.

B Galperin, LH Kantha, S Hassid, and A Rosati. A quasi-equilibrium turbulent energy model for geophysical flows. *Journal of the Atmospheric Sciences*, 45(1):55–62, 1988.

Boris Galperin and Steven A Orszag. *Large eddy simulation of complex engineering and geophysical flows*. Cambridge University Press, 1993.

Marcelo Garcia and Gary Parker. Entrainment of bed sediment into suspension. *Journal of Hydraulic Engineering*, 117(4):414–435, 1991.

L Genet, D Smith, and M Sonnen. Computer program documentation for the dynamic estuary model. *US Environmental Protection Agency, Systems Development Branch, Washington, DC*, 1974.

J Gessler. The beginning of bedload movement of mixtures investigated as natural armoring in channels (translated by ea prych, california institute of technology), swiss federal institute of technology, zurich, laboratory of hydraulic research and soil mechanics, 1967.

Ronald J Gibbs. Estuarine flocs: their size, settling velocity and density. *Journal of Geophysical Research: Oceans*, 90(C2):3249–3251, 1985.

P Giordani and M Astorri. Phosphate analysis of marine sediments. *Chemistry in Ecology*, 2(2):103–111, 1986.

Matthew D Grace, Phi Hung X Thanh, and Scott Carlton James. Sandia national laboratories environmental fluid dynamics code: sediment transport user manual. Technical report, Sandia National Laboratories, 2008.

SR Green. Modeling turbulent air flow in a stand of widely spaced trees. *PHOENICS Journal Computational Fluid Dynamics and its Applications*, 5:294–312, 1992.

John S Gulliver and Heinz G Stefan. Stream productivity analysis with dormi: Development of computational model. *Water Research*, 18(12):1569–1576, 1984.

Harold P Guy, Daryl B Simons, and Everett V Richardson. *Summary of alluvial channel data from flume experiments, 1956-61*, volume 462. US Government Printing Office, 1966.

L Hageman and M Young. Applied iterative methods academic. *New York*, 1981.

George J Haltiner and Roger Terry Williams. Numerical prediction and dynamic meteorology. Technical report, 1980.

JM Hamrick and TS Wu. Computational design and optimization of the efdc/hem3d surface water hydrodynamic and eutrophication models. In *Next generation environmental models and computational methods*, pages 143–161. Society for Industrial and Applied Mathematics Pennsylvania, 1997.

John M Hamrick. Long-term dispersion in unsteady skewed free surface flow. *Estuarine, Coastal and Shelf Science*, 23(6):807–845, 1986.

John M Hamrick. A three-dimensional environmental fluid dynamics computer code: Theoretical and computational aspects. Technical report, 1992.

John M Hamrick. User's manual for the environmental fluid dynamics computer code. 1996.

John M Hamrick and William B Mills. Analysis of water temperatures in conowingo pond as influenced by the peach bottom atomic power plant thermal discharge. *Environmental Science & Policy*, 3:197–209, 2000.

GE Harbeck Jr. Estimating forced evaporation from cooling ponds. *J. Power Div., Am. Soc. Civ. Eng.;(United States)*, 90, 1964.

Hans Hersbach. Sea surface roughness and drag coefficient as functions of neutral wind speed. *Journal of Physical Oceanography*, 41(1):247–251, 2011.

E.E. Hofmann, E.N. Powell, J.M. Klinck, and E.A. Wilson. Modeling oyster populations iii. critical feeding periods, growth and reproduction. *Shellfish Res.*, 11(2):399–416, 1992.

Richard R Horner, Eugene B Welch, Marguerite R Seeley, and Jean M Jacoby. Responses of periphyton to changes in current velocity, suspended sediment and phosphorus concentration. *Freshwater biology*, 24(2):215–232, 1990.

John N Hunt. Direct solution of wave dispersion equation. *Journal of the Waterway, Port, Coastal and Ocean Division*, 105(4):457–459, 1979.

Dang Huu Chung and Dieter P Eppel. Effects of some parameters on numerical simulation of coastal bed morphology. *International Journal of Numerical Methods for Heat & Fluid Flow*, 18(5):575–592, 2008.

Kyu-Nam Hwang and Ashish Jayant Mehta. *Fine sediment erodibility in Lake Okeechobee, Florida*. Coastal & Oceanographic Engineering Department, University of Florida, 1989.

Scott C James, Eddy Seetho, Craig Jones, and Jesse Roberts. Simulating environmental

changes due to marine hydrokinetic energy installations. In *OCEANS 2010 MTS/IEEE SEATTLE*, pages 1–10. IEEE, 2010.

R Jan Stevenson and R Glover. Effects of algal density and current on ion transport through periphyton communities. *Limnology and Oceanography*, 38(6):1276–1281, 1993.

Zhen-Gang Ji. *Hydrodynamics and water quality: modeling rivers, lakes, and estuaries*. John Wiley & Sons, 2008.

CA Jones and W Lick. Sedzlj: A sediment transport model. *Final Report. University of California, Santa Barbara, California*, 2001.

Craig Jones and Wilbert Lick. Effects of bed coarsening on sediment transport. In *Estuarine and Coastal Modeling*, pages 915–930. ASCE, 2000.

S.J. Jordan. *Sedimentation and Remineralization Associated with Biodeposition by the American Oyster Crassostrea Virginica (Gmelin)*. University of Maryland, College Park, 1987.

Lakshmi H. Kantha. On an Improved Model for the Turbulent PBL. *Journal of the Atmospheric Sciences*, 60(17):2239–2246, September 2003. ISSN 0022-4928. doi: 10.1175/1520-0469(2003)060⟨2239:OAIMFT⟩2.0.CO;2. URL https://journals.ametsoc.org/doi/full/10.1175/1520-0469(2003)060%3C2239:OAIMFT%3E2.0.CO%3B2.

Lakshmi H. Kantha and Carol Anne Clayson. An improved mixed layer model for geophysical applications. *Journal of Geophysical Research: Oceans*, 99(C12):25235–25266, 1994. doi: 10.1029/94JC02257. URL https://agupubs.onlinelibrary.wiley.com/doi/abs/10.1029/94JC02257.

Gabriel G Katul, Larry Mahrt, Davide Poggi, and Christophe Sanz. One-and two-equation models for canopy turbulence. *Boundary-Layer Meteorology*, 113(1):81–109, 2004.

James T Kirby, Robert A Dalrymple, and Fengyan Shi. Combined refraction/diffraction model. *CACR Report No. 92–04. University of Delaware, Newark*, 1994.

M. Kobayashi, E.E. Hofmann, E.N. Powell, J.M.Klinck, and K. Kusaka. A population dynamics model for the japanese oyster, crassostrea gigas. *Aquaculture*, 149(34):285–321, 1997.

JN Kremer and SW Nixon. A coastal marine ecosystem, 217 pp, 1978.

Ray Beyers Krone. Flume studies of transport of sediment in estrarial shoaling processes. *Final Report, Hydr. Engr. and Samitary Engr. Res. Lab., Univ. of California*, 1962.

Emmett M Laursen. The total sediment load of streams. *Journal of the Hydraulics Division*, 84(1):1–36, 1958.

Joseph HW Lee and Valiant Cheung. Generalized lagrangian model for buoyant jets in current. *Journal of environmental engineering*, 116(6):1085–1106, 1990.

PJ Leinonen and D Mackay. A mathematical model of evaporation and dissolution from oil spills on ice, land, water and under ice. *Water Quality Research Journal*, 10(1):132–141, 1975.

Wilbert Lick and James Lick. Aggregation and disaggregation of fine-grained lake sediments. *Journal of Great Lakes Research*, 14(4):514–523, 1988.

Lambertus Lijklema. Interaction of orthophosphate with iron (iii) and aluminum hydroxides. *Environmental Science & Technology*, 14(5):537–541, 1980.

J Liu, JM Chen, TA Black, and MD Novak. E-ε modelling of turbulent air flow downwind of a model forest edge. *Boundary-Layer Meteorology*, 77(1):21–44, 1996.

Michael S Longuet-Higgins and RW Stewart. Radiation stresses in water waves; a physical discussion, with applications. In *Deep Sea Research and Oceanographic Abstracts*, volume 11, pages 529–562. Elsevier, 1964.

V.L. Loosanoff. Some aspects of behavior of oysters at different temperatures. *Biol. Bull.*, 114:57–70, 1958.

V.L. Loosanoff and F.D. Tommers. Effect of suspended silt and other substances on rate of feeding of oysters. *Science*, 107(2768):69–70, 1948.

Donald Mackay and Andrew TK Yeun. Mass transfer coefficient correlations for volatilization of organic solutes from water. *Environmental Science & Technology*, 17(4):211–217, 1983.

James E Mackin and Robert C Aller. Ammonium adsorption in marine sediments 1. *Limnology and Oceanography*, 29(2):250–257, 1984.

Rangarao V Madala and Steve A Piacseki. A semi-implicit numerical model for baroclinic oceans. *Journal of Computational Physics*, 23(2):167–178, 1977.

John L Mancini. A method for calculating effects, on aquatic organisms, of time varying concentrations. *Water Research*, 17(10):1355–1362, 1983.

Roger Mann, Eugene M. Burreson, and Patrick K. Baker. The decline of the virginia oyster fishery in chesapeake bay considerations for introduction of a non-endemic species, crassostrea gigas (thunberg, 1793). *Journal of Shellfish Research*, 10(2):379–388, 1991.

Gerald Matisoff. Mathematical models of bioturbation. In *Animal-sediment relations*, pages 289–330. Springer, 1982.

C David McIntire. Diatom associations in yaquina estuary, oregon: A multivariate analysis 1. *Journal of Phycology*, 9(3):254–259, 1973.

AJ Mehta, TM Parchure, JG Dixit, and R Ariathurai. Resuspension potential of deposited cohesive sediment beds. In *Estuarine comparisons*, pages 591–609. Elsevier, 1982.

Ashish J Mehta, Earl J Hayter, W Reginald Parker, Ray B Krone, and Allen M Teeter. Cohesive sediment transport. i: Process description. *Journal of Hydraulic Engineering*, 115(8):1076–1093, 1989.

George L Mellor. An equation of state for numerical models of oceans and estuaries. *Journal of Atmospheric and Oceanic Technology*, 8(4):609–611, 1991.

George L Mellor and Alan F Blumberg. Modeling vertical and horizontal diffusivities with the sigma coordinate system. *Monthly Weather Review*, 113(8):1379–1383, 1985.

George L Mellor and Tetsuji Yamada. Development of a turbulence closure model for geophysical fluid problems. *Reviews of Geophysics*, 20(4):851–875, 1982.

George L Mellor, Tal Ezer, and Lie-Yauw Oey. The pressure gradient conundrum of sigma coordinate ocean models. *Journal of atmospheric and oceanic technology*, 11(4):1126–1134, 1994.

Li Mengguo and Qin Chongren. Numerical simulation of wave-induced nearshore current. In *Proceedings of the International Conference on Estuaries and Coasts*. Citeseer, 2003.

Eugen Meyer-Peter and R Müller. Formulas for bed-load transport. In *IAHSR 2nd meeting,*

Stockholm, appendix 2. IAHR, 1948.

Frank J Millero. The thermodynamics and kinetics of the hydrogen sulfide system in natural waters. *Marine Chemistry*, 18(2-4):121–147, 1986.

François MM Morel. Principles of aquatic chemistry. *John Wiley and Sons, New York NY. 1983. 446*, 1983.

John W Morse, Frank J Millero, Jeffrey C Cornwell, and David Rickard. The chemistry of the hydrogen sulfide and iron sulfide systems in natural waters. *Earth-science reviews*, 24(1):1–42, 1987.

Iehisa Nezu. Turbulence in open-channel flows. *IAHR-monograph*, 1993.

NIFS. National institute of fisheries science, korea. 2020.

Donald J O'Connor and William E Dobbins. Mechanism of reaeration in natural streams. *Transactions of the American Society of Civil Engineers*, 123(1):641–666, 1958.

Eugene P Odum. Fundamentals of ecology–wb saunders company. *Philadelphia, London, Toronto*, 1971.

C. B. Officer, T. J. Smayda, and R. Mann. Benthic filter feeding: A natural eutrophication control. *Marine Ecology - Progress Series*, 9:203–210, 1982.

Kyeong Park, Albert Y Kuo, Jian Shen, and John M Hamrick. A three-dimensional hydrodynamic-eutrophication model (hem-3d): Description of water quality and sediment process submodels. Technical report, Virginia Institute of Marine Science, 1995.

Gary Parker, Chris Paola, and Suzanne Leclair. Probabilistic exner sediment continuity equation for mixtures with no active layer. *Journal of Hydraulic Engineering*, 126(11): 818–826, 2000.

Roger Peyret and T.D. Taylor. *Computational Methods for Fluid Flow*. Springer-Verlag, 1983.

RF Pfeifer and WF McDiffett. Some factors affecting primary productivity of stream riffle communities. *Archiv Fur Hydrobiologie*, 1975.

Davide Poggi, Amilcare Porporato, Luca Ridolfi, JD Albertson, and GG Katul. The effect of vegetation density on canopy sub-layer turbulence. *Boundary-Layer Meteorology*, 111(3):565–587, 2004.

Eric Powell, John Klinck, Eileen Hofmann, and Sammy Ray. Modeling oyster populations. iv: Rates of mortality, population crashes, and management. *Fishery Bulletin*, 92, 01 1994.

WH Press, BP Flannery, SA Teukolsky, WT Vetterling, and JR Chipperfield. *Numerical recipes: the art of scientific computing*. Cambridge University Press, 1986.

D.B. Quayle. *Pacific oyster culture in British Columbia*. Department of Fisheries and Oceans, 1988.

Alfred C Redfield. The influence of organisms on the composition of seawater. *The sea*, 2: 26–77, 1963.

I Reid and LE Frostick. Fluvial sediment transport and deposition. *Sediment transport and depositional processes*, pages 89–155, 1994.

Leo C van Rijn. Sediment transport, part ii: suspended load transport. *Journal of hydraulic engineering*, 110(11):1613–1641, 1984.

JA Robbins, T Keilty, DS White, and DN Edgington. Relationships among tubificid abundances, sediment composition, and accumulation rates in lake erie. *Canadian Journal of Fisheries and Aquatic Sciences*, 46(2):223–231, 1989.

Jesse Roberts, Rich Jepsen, Doug Gotthard, and Wilbert Lick. Effects of particle size and bulk density on erosion of quartz particles. *Journal of Hydraulic Engineering*, 124(12): 1261–1267, 1998.

Martha J Ross and Gordon R Ultsch. Temperature and substrate influences on habitat selection in two pleurocerid snails (goniobasis). *American Midland Naturalist*, pages 209–217, 1980.

HM Runke. *Simulation of the lotic periphyton community of a small mountain stream by digital computer*. PhD thesis, Thesis presented to Utah State University, Logan, Utah, in partial fulfill, 1985.

Patrick J Ryan, Donald RF Harleman, and Keith D Stolzenbach. Surface heat loss from cooling ponds. *Water resources research*, 10(5):930–938, 1974.

Lawrence P Sanford and Jerome P-Y Maa. A unified erosion formulation for fine sediments. *Marine Geology*, 179(1-2):9–23, 2001.

Christophe Sanz. A note on k-ε modelling of vegetation canopy air-flows. *Boundary-Layer Meteorology*, 108(1):191–197, 2003.

AJ Semtner Jr. An oceanic general circulation model with bottom topography. Technical report, 1974.

Albert Shields. Application of similarity principles and turbulence research to bed-load movement. Technical report, 1936.

Parmeshwar L Shrestha and Gerald T Orlob. Multiphase distribution of cohesive sediments and heavy metals in estuarine systems. *Journal of Environmental Engineering*, 122(8): 730–740, 1996.

S.E. Shumway and R.K. Koehn. Oxygen consumption in the american oyster crassostrea virginica. *Marine Ecology - Progress Series*, 9(1):59–68, 1982.

Theodore J Simons et al. Development of three-dimensional numerical models of the great lakes. In *IWD Scientific Series*, volume 12. Inland Waters Directorate, 1973.

Joseph Smagorinsky. General circulation experiments with the primitive equations: I. the basic experiment. *Monthly weather review*, 91(3):99–164, 1963.

J Dungan Smith and SR McLean. Spatially averaged flow over a wavy surface. *Journal of Geophysical research*, 82(12):1735–1746, 1977.

Jane M Smith, Ann R Sherlock, and Donald T Resio. Stwave: Steady-state spectral wave model user's manual for stwave, version 3.0. Technical report, Engineer Research And Development Center Vicksburg Ms Coastal And Hydraulics Lab, 2001.

Piotr K Smolarkiewicz and Terry L Clark. The multidimensional positive definite advection transport algorithm: Further development and applications. *Journal of Computational Physics*, 67(2):396–438, 1986.

Piotr K Smolarkiewicz and Wojciech W Grabowski. The multidimensional positive definite advection transport algorithm: Nonoscillatory option. *Journal of Computational Physics*, 86(2):355–375, 1990.

RL Soulsby, RJS Whitehouse, et al. Threshold of sediment motion in coastal environments. In *Pacific Coasts and Ports' 97: Proceedings of the 13th Australasian Coastal and Ocean Engineering Conference and the 6th Australasian Port and Harbour Conference; Volume 1*, page 145. Centre for Advanced Engineering, University of Canterbury, 1997.

Miodrag Spasojevic and Forrest M Holly Jr. Three-dimensional numerical simulation of mobile-bed hydrodynamics. Technical report, Iowa Institute Of Hydraulic Research Iowa City, 1994.

John H Steele. Environmental control of photosynthesis in the sea. *Limnology and oceanography*, 7(2):137–150, 1962.

Philip S Stewart, Dante J Tedaldi, Aaron R Lewis, and Eugene Goldman. Biodegradation rates of crude oil in seawater. *Water environment research*, 65(7):845–848, 1993.

Humbert Chu Stuart Churchill. Correlating equations for laminar and turbulent free convection from a vertical plate. *International Journal of Heat and Mass Transfer*, 18(11): 1323–1329, 1975. doi: http://dx.doi.org/10.1016/0017-9310(75)90243-4.

Werner Stumm, James J Morgan, et al. *Aquatic chemistry; an introduction emphasizing chemical equilibria in natural waters*. Wiley-Interscience, 1970.

K Suzuki, H Yamamoto, and A Kadota. Mechanism of bedload fluctuations of sandgravel mixture in a steep slope channel. *EU Department of Civil and Environmental engineering, Matsuyama, Japan, editor*, page 10, 1998.

Dirk Hermanus Swart. Offshore sediment transport and equilibrium beach profiles. 1974.

SWAN Team. *Implementation Manual Swan Cycle III*. Delft University of Technology, Department of Civil Engineering, 41.31 edition, 2019.

Tetra Tech. Users manual for environmental fluid dynamics code. *Tetra Tech, Inc*, 1, 2002.

Tetra Tech et al. Theoretical and computational aspects of sediment and contaminant transport in the efdc model. Technical report, US Environmental Protection Agency, 2002.

Tetra Tech et al. The environmental fluid dynamics code theory and computation volume 3: Water quality module. *Technical report, Tetra Tech, Inc., Fairfax, VA*, 2007.

Robert V Thomann and John A Mueller. *Principles of surface water quality modeling and control*. Harper & Row Publishers, 1987.

RV Thomann, NJ Jaworski, SW Nixon, HW Paerl, and Jay Taft. The 1983 algal bloom in the potomac estuary. *Prepared for the Potomac Strategy State/EPA Management Committee by the Algal Bloom Expert Panel, Washington, DC*, 1985.

Dottie H Tillman, Carl F Cerco, Mark R Noel, James L Martin, and John Hamrick. Three-dimensional eutrophication model of the lower st. john river, florida. Technical report, Engineer Research And Development Center Vicksburg Ms Environmental Lab, 2004.

Bruce Neil Troup. *The interaction of iron with phosphate, carbonate and sulfide in Chesapeake Bay interstitial waters: A thermodynamic interpretation*. PhD thesis, Johns Hopkins University, 1974.

Cheng-Han Tsai, Sam Iacobellis, and Wilbert Lick. Flocculation of fine-grained lake sediments due to a uniform shear stress. *Journal of Great Lakes Research*, 13(2):135–146, 1987.

Andre van Niekerk, Koen R Vogel, Rudy L Slingerland, and John S Bridge. Routing of

heterogeneous sediments over movable bed: Model development. *Journal of Hydraulic Engineering*, 118(2):246–262, 1992.

C Villaret and M Paulic. Experiments on the erosion of deposited and placed cohesive sediments in an annular flume and a rocking flume. report ufl/coel-86/007. 1986.

James R Villemonte. Submerged weir discharge studies. *Engineering News-Record*, 139 (26):54–56, 1947.

Marcel Vinokur. Conservation equations of gasdynamics in curvilinear coordinate systems. *Journal of Computational Physics*, 14(2):105–125, 1974.

George H Ward. Hydrography and circulation processes of gulf estuaries. In *Estuarine and Wetland Processes*, pages 183–215. Springer, 1980.

JJ Warwick, D Cockrum, and M Horvath. Estimating non-point-source loads and associated water quality impacts. *Journal of Water Resources Planning and Management*, 123(5): 302–310, 1997.

Ian T Webster and Bradford S Sherman. Evaporation from fetch-limited water bodies. *Irrigation Science*, 16(2):53–64, 1995.

Scott A Wells and Thomas M Cole. Ce-qual-w2, version 3. Technical report, Army Engineer Waterways Experiment Station Vicksburg Ms Engineer Research, 2000.

Joseph T Westrich and Robert A Berner. The role of sedimentary organic matter in bacterial sulfate reduction: The g model tested 1. *Limnology and oceanography*, 29(2):236–249, 1984.

Chester T Wezenak and John J Gannon. Evaluation of nitrification in streams. *Journal of the Sanitary Engineering Division*, 94(5):883–896, 1968.

M.E. White, E.N. Powell, and S.M. Ray. Effect of parasitism by the pyramidellid gastropod boonea impressa on the net productivity of oysters (crassostrea virginica). *Estuarine, Coastal and Shelf Science*, 26(4):359 – 377, 1988. ISSN 0272-7714. doi: https://doi.org/10.1016/0272-7714(88)90018-2. URL http://www.sciencedirect.com/science/article/pii/0272771488900182.

LA Whitford and GJ Schumacher. Effect of a current on respiration and mineral uptake in spirogyra and oedogonium. *Ecology*, 45(1):168–170, 1964.

WG Whitman, RP Russell, CM Welling, and JD Cochrane. The effect of velocity on the corrosion of steel in sulfuric acid. *Industrial & Engineering Chemistry*, 15(7):672–677, 1923.

John D Wilson, John J Finnigan, and Michael R Raupach. A first-order closure for disturbed plant-canopy flows, and its application to winds in a canopy on a ridge. *Quarterly Journal of the Royal Meteorological Society*, 124(547):705–732, 1998.

Lawrence D Winiarski and Walter F Frick. *Cooling tower plume model*. US Environmental Protection Agency, Office of Research and Development, 1976.

Sachio Yamamoto, James B Alcauskas, and Thomas E Crozier. Solubility of methane in distilled water and seawater. *Journal of Chemical and Engineering Data*, 21(1):78–80, 1976.

Chih Ted Yang. Incipient motion and sediment transport. *Journal of the hydraulics division*, 99(10):1679–1704, 1973.

Chih Ted Yang and Albert Molinas. Sediment transport and unit stream power function. *Journal of the Hydraulics Division*, 108(6):774–793, 1982.

C Kirk Ziegler and Bradley Nisbet. Fine-grained sediment transport in pawtuxet river, rhode island. *Journal of Hydraulic Engineering*, 120(5):561–576, 1994.

C Kirk Ziegler and Bradley S Nisbet. Long-term simulation of fine-grained sediment transport in large reservoir. *Journal of Hydraulic Engineering*, 121(11):773–781, 1995.

Carl Kirk Ziegler and Wilbert Lick. The transport of fine-grained sediments in shallow waters. *Environmental Geology and Water Sciences*, 11(1):123–132, 1988.

Carl Kirk Ziegler and Wilbert J Lick. *A numerical model of the resuspension, deposition and transport of fine-grained sediments in shallow water*. Department of Mechanical & Environmental Engineering, University of California, 1986.